Developing a *Drosophila* model of radiation induced toxicity to identify risk loci

A thesis submitted in candidature for the degree of

Doctor of Philosophy (PhD)

By

Terrence Matthew Trinca

February 2022

Acknowledgments

Table of content

Table of tables

Table of figures

Table of Abbreviations

8-oxogaunine	8-oxo-G
Adipose system	AS
Anlage/primordium	A/P
Audio Video Interleave	AVI
Auxin-inducible degradation system	AID
Bovine serum albumin	BSA
Bromophenol blue	BPB
cap-n-collar	*cnc*
Catalase	*Cat*
Circulatory system	CS
Cox proportional hazard	CoxPH
Differential expressed	DE
Differential expressed genes	DEGs
Digestive system	DS
Double strand breaks	DSB
Drosophila genetic reference panel	DGRP
Dual oxidase	*Duox*
egg/oocyte	E/O
Endocrine system	EndoS
Entereoblast	EB
Entereocyte	EC
Entereoendocrine	EE
Excretory system	ExcS
Extracellular matrix	ECM
Frames per second	FPS
Gene ontology	GO
Genome wide association study	GWAS
Glutathione S-transferase D1	*GstD1*
Gray	Gy
Growth arrest and DNA damage-inducible 45	*Gadd45*
Hazard ratio	HR
Human phenotype ontology	HP
Hydrogen peroxide	H2O2
Hydroxyl radicals	OH
Hyper-fractionation	HF
Imaginal tissue	IT
Indole-3-acetic acid	IAA
Integumentary system	IS
Intestinal stem cell	ISC
Inverted repeat-bind protein	*Irbp*
Jafrac1	*Jafrac*
Kaplan-Meir	KM
Kyoto ecyclopaedia of genes and genomes	KEGG
Low-earth orbit	LEO

meiotic 9	*mei-9*
Muscle system	MS
N-acetyl cysteine	NAC
Naphthaleneacetic acid	NAA
National aeronautics and space administration	NASA
Nervous system	NS
Nullsoft Scriptable Install System	NSIS
Other anatomical entity	Other
Overall survival	OS
PBS containing 0.1% Triton-X100	PBT
Polylactic acid	PLA
Principle component analysis	PCA
Radiotherapy	RT
Rapid iterative negative geotaxis	RING
Reactive oxygen species	ROS
Reads per kilobase per million	RPKM
Reproductive system	RS
Sensory system	SS
Serine/threonine kinase ATM	ATM
Single nucleotide polymorphism	SNP
Single strand breaks	SSB
Standard deviation	SD
Stem cell	SC
Stereolithography	STL
Superoxide dismutase 1	*SOD*
Tracheal system	TS
TRANSFAC	TF
Transforming Growth Factor beta 1	TGFβ
Traumatic brain injury	TBI
Viking	*Vkg*
Visceral muscle	VM
WikiPathways	WP
X-ray repair cross complementation 1	*XRCC1*

Summary

Humans are becoming increasingly more exposed to radiation through medical treatment such as radiotherapy, occupational hazard, environmental exposure, and travel at high-altitude or space flight. The long-term consequences of radiation exposure/treatment are poorly understood, with the field of radiobiology currently lacking any pre-clinical models. *Drosophila melanogaster* offers to be an enticing *in vivo* pre-clinical model to better understand the radiation response, largely due to its short lifespan, genetic tractability and affordability of research. The work presented here highlights efforts to develop a *Drosophila* model for long-term radiation-induced tissue toxicity. Initial work involved characterising *Drosophila* response to radiation using various metric of overall health such as lifespan, fertility and movement assaying. Subsequent work identified tissue specific sensitivity to radiation treatment, as observed in humans, in particular the midgut was identified as a sensitive organ. Further, it was shown that the midgut underwent systemic remodelling and sustained oxidative stress which persists long-term *post* radiation treatment.

Drosophila were then used to identify genetic loci associated with the radiation response. To do this, an RNA-seq experiment was performed which quantified the transcriptome of various adult tissues (e.g. midgut, brain, muscle and fat body) *post* irradiation. For each tissue there were many differentially expressed genes, and subsequent analysis identified a subset of 19 genes which were differentially expressed in all tissues – a conserved signature of irradiation. Additional to employing genome-wide approaches, a candidate approached was performed on a select number of genes, to try and functionally validate their role in modulating radiation sensitivity in *Drosophila*.

This work highlights the need and the success of a *Drosophila* radiation response model. RNA-seq analysis has identified many loci that have yet to be functionally validated, and as majority of these loci have human orthologues, their functional validation may help to elucidate the underlying mechanisms of long-term radiation-induced tissue toxicity in humans.

Chapter 1: Introduction

1.1 Cancer incidence, mortality and survival rates

Worldwide in 2020, it was estimated that there were 19.3 million newly reported cases of cancer, and 10 million cancer-related deaths (Ferlay *et al.*, 2020). These large incidence and mortality rates represent a huge burden on global healthcare to treat and care for patients. Additionally, incidence rates have increased over time and so has the cancer care burden. For example, within Europe in 2012, there were 3.45 million new cases and 1.75 million cancer deaths, and in 2018 there were 3.91 million new cases and 1.93 million deaths (Ferlay et al., 2018, 2013). Lastly, mortality rates are decreasing overall for most cancer types, this has resulted an increase in the number of patients that survive long-term, in particular 5-year overall survival (OS). When comparing data collected in the United Kingdom for cancers of the colon, the 5 year OS in 1995 was 44.4% of patients, and in 2014 was 59% (Arnold *et al.*, 2019). Therefore, not only is the overall incidence of cancer increasing but also the number of patients surviving is increasing, both adding to the healthcare burden associated with cancer (Bentzen, 2006). Globally, the burden of cancer will only increase with the incidence rate estimated to be at >20 million by 2025 (Zugazagoitia et al., 2016). The steady increase in cancer incidence and number of deaths means we need to develop better ways of treating cancer.

1.2 Cancer treatment

There are currently various treatment options available to cancer patients and depending on the cancer type and patient history an optimum treatment regime can be designed which may include multiple treatment types (National Cancer Institute, 2019). Treatment types include chemotherapy, hormone therapy, immunotherapy, radiotherapy (RT), and surgical resection. From the mentioned treatments, the most commonly used treatments are surgical resection, chemotherapy and RT, which can be used independently, or concurrently to improve their effectiveness. Despite improvements in cancer therapy, no regime is currently 100% effective at treating cancer, hence it is an area of active and extensive research.

1.3 Developing new cancer treatments

The development of new pharmaceuticals to combat cancer is becoming more difficult with rising cost being a significant factor, and this is in spite of advancements in knowledge of cancer biology and improvements and accessibility

of various technologies such as whole-genome sequencing and screening platforms (Lacombe et al., 2014). It is now estimated to cost ~£1.8 billion to develop and test a new pharmaceutical, as opposed to ~£200 million 20 years ago (Catapult, 2018). Further, new pharmaceuticals are now being designed to treat smaller cohorts of patients, either to treat specific types of cancers, or to treat specific sub-types of cancers depending on biomarkers expressed by patient and/or cancer. This approach of treating cancers depending on expressed biomarkers has begun to be integrated into clinical trials with patients being screened *prior* to selection in trials (Lacombe et al., 2014). Due to this increase in cost, time and selectivity of pharmaceuticals under development, some researchers believe it to be more advantageous to try refining existing therapies such as RT.

1.4 Radiotherapy

Radiation was first used in medicine in the late 1900s to treat various conditions, such as lupus, bacterial infections and cancer, and has since gone through extensive improvement in its application and selectivity of use (Pusey, 1983; Donya *et al.*, 2014). Radiation has a wide variety of applications in modern medicine, and it has been estimated that RT, in the form of external beam therapy, should be administer to approximately 52% of all cancer patients (Delaney, Jacob, Featherstone, & Barton, 2005). RT involves the delivery of either high-energy subatomic particles or rays to cancer cells which leads to molecular damage, specifically DNA strand breaks. If enough damage accumulates cell death ensues with highly proliferative cancer tissues being greater affected by treatment (Mettler & Voelz, 2002). However, healthy tissue within a close proximity to the targeted tissue absorbs a dose of radiation, albeit less than the cancerous tissue. To reduce healthy tissue damage there have been two major advances in RT administration. Firstly, fractionated dosages were introduced which split the dose into multiple treatments to allow time for healthy tissue to repair. Secondly, improved precision due to imaging technology, used to focus the dose to the cancerous tissue, minimising the dose received by peripheral healthy tissue. These improvements have led to a reduction in side effects and have improved the curative rate (Bentzen, 2006). However, despite these advances, healthy peripheral tissue still receives a dose of radiation and therefore insult, leading to the development of side effects (Kerns et al., 2015).

1.4.1 Side effects of radiotherapy

The effects of radiation can be split into transient (immediate) and late side effects, and their severity depends on multiple variables e.g. dose rate, total dose, type of radiation and parts of body exposed (Bushberg, 2020). The immediate effects of exposure to ionizing radiation are ubiquitous amongst patients and act to reduce their quality of life (Bentzen, 2006). Collectively known as 'radiation sickness', side effects include fatigue, bleeding, dehydration, vomiting and diarrhoea, fever, hair loss and inflammation. Depending on the dose, these side effects can manifest within hours and potentially last for weeks, however, they can be well managed in a modern healthcare system (Mettler & Voelz, 2002; Bentzen, 2006).

The late side effects include but are not limited to; fibrosis, secondary malignancies, tissue atrophy, vascular and neuronal damage (Bushberg, 2020). These late effects can present months to years after treatment and can lead to lifelong suffering by the patient (Mettler & Voelz, 2002; Bentzen, 2006; Bergom *et al.*, 2019). There is high inter-patient variation in severity of late effects, with severity currently impossible to predict. To minimise late side effects, clinicians administer suboptimal dosages of RT, which in turn reduces curative potential of treatment (Kerns et al., 2015). The ability of predicting predisposition of patients to RT would allow for patient-tailored dosages, improving either quality of life in radiosensitive patients or improving curative rate of treatment in radioresistant patients (Bentzen, 2006).

1.5 Radiogenomics - predicting patient sensitivity

Despite its reasonable success rate (40% curative rate), RT dosages are suboptimal due to a small proportion of cancer patients that express high sensitivity to treatment (Andreassen, 2005; Kerns et al., 2015). The radiation response is a polygenic trait and some of the risk loci that modulate the response have already been identified (Andreassen, 2005). Patients with genetic disorders such as ataxia-telangiectasia, which impairs the mechanisms of DNA repair, have been shown to be extremely sensitive to RT (Gatti, 2001; Bergom *et al.*, 2019). Ataxia-telangiectasia is a rare condition present in individuals homozygous for mutant *serine/threonine kinase ATM* (*ATM*) (Taylor et al., 1975). Under physiological conditions, *ATM* is recruited and activated by DNA double-strand breaks, phosphorylating several targets involved in cell cycle regulation, DNA repair and apoptosis (Zgheib *et al.*, 2005). There is a general consensus amongst oncologists and radiologists that sufferers of disorders that compromise DNA repair should not undergo RT (Bergom et al., 2019). It is also worth mentioning that the risk loci for

radiation sensitivity are not limited to DNA repair genes. For example, *Transforming Growth Factor beta 1* (*TGFβ*) has been associated with radiation-induced fibrosis and is under active research as a potential therapeutic target to alleviate late symptoms of irradiation (Ewan *et al.*, 2002; Andreassen, 2005; Bentzen, 2006, Lan *et al.*, 2021).

It is thought that the majority of loci associated with the radiation response are unknown and this has been attributed to the high variability in the radiation response and the difficulty in measuring clinical outcomes (Bentzen, 2006). The successful identification of more risk harbouring loci could lead to the development of a single nucleotide polymorphism (SNP) predictive assay, allowing clinicians to tailor RT regimes accordingly, and with a better understanding of the genetic architecture of the radiation response, clinicians can better treat and manage over-responders (Andreassen, 2005; Bentzen, 2006; Kerns *et al.*, 2015). Further, *prior* knowledge of sensitivity of patients would allow clinicians to give higher doses to resistant patients, thus improving their chances of eliminating cancer, whereas those more sensitive to treatment, would have a better quality of life by receiving a smaller radiation dose.

1.5.1 Approaches to identifying risk associated loci/variants

To identify risk loci that are predictive of radiation sensitivity, two approaches have been used by the radiogenomics community: candidate and genome-wide studies (Hirschorn *et al.*, 2005; Bahlo *et al.*, 2006). Regarding candidate gene studies, excluding loci involved in DNA repair mechanisms, there has yet to be a successfully identified locus that has also been validated in subsequent independent investigation (Andreassen, 2005). Candidate work has largely been *in vitro* research dissecting the genetic causes of cellular radiation sensitivity, with a typical phenotypic assay being the clonogenic (colony formation) survival assay performed on cell cultures which have received large dosages (1-10 Gy). One study which employed the clonogenic assay on patient-derived fibroblast successfully identified a significant correlation between *in vitro* sensitivity and more severe long-term skin reactions to treatment (Ho et al., 2006; Oppitz, Baier, Wulf, Schakowski, & Flentje, 2001). Another example showed a correlation between increased *in vitro* survival of fibroblasts and increased severity of subcutaneous fibrosis (Johansen, Bentzen, Overgaard, & Overgaard, 1994). However, a subsequent study which explored the diagnostic value of using skin fibroblasts for predicting the onset of fibrosis in breast cancer patients did not identify a significant correlation between *in*

vitro and *in vivo* sensitivity to irradiation (Russell et al., 1998). The examples mentioned above though were not specifically dissecting the genetic architecture of the radiation response but were rather attempts by researchers and clinicians to develop a diagnostic test to identify the predisposition of patients to RT. They highlight the innate difficultly of applying such an approach to identify risk loci, loci identified via *in vitro* assays may not have any *in vivo* relevance or prognostic value for clinicians.

Due to the difficulties and lack of success using the candidate approach, significant efforts at broader approaches such as genome wide association studies (GWAS) have been used. To date, there have been multiple GWAS performed by the radiogenomics community, however they themselves suffer the same problem as the previous approach – each new study despite identifying some new loci, does not corroborate the results of previous studies. The reason for these apparent failures is thought to be an attribute of the trait - the radiation response is highly polygenic with each locus only conveying a small level of risk which is difficult to identify in small cohort sized GWAS studies. If this is correct, then the solution is to increase cohort sizes to gain statistical power to identify low risk loci. To this end, the radiogenomics community has been slowly increasing cohort sizes in its clinical trials, however this adds additional difficulty and cost to the research (Kerns et al., 2015).

1.6   *Drosophila melanogaster* as a preclinical model

Drosophila melanogaster is an enticing model system to introduce to the radiogenomics and radiobiology fields as it is genetically tractable, has a short lifespan, affordable to rear, and the majority of the genes associated with human disease have *Drosophila* orthologues. In addition, *Drosophila* offers additional advantages that can address issues faced by the radiogenomics community. For example, GWAS are cheap and are routinely performed using *Drosophila* in various fields of study (Vaisnav *et al.*, 2014; Wangler, Hu & Shulman, 2017; Sharma *et al.*, 2020). Whereas the cost of human GWAS for the radiogenomics community is a limiting factor, and as a result, few have been performed (Barnett et al., 2009). Another example of an issue that has burdened the radiogenomics field, is the difficulty in interpreting data derived from patients who received RT from different institutions. The development of RT regimes by clinicians and radiologists is constrained by a number of factors which include patient history, state of tumour, standards of practice of local healthcare system, and availability of irradiation equipment. These factors have the potential of drastically altering the administration

of RT, leading to additional variation to clinical outcome, and regarding clinical research, making the stratification of data obtained from different institutions very difficult. *Drosophila* is an appealing model system because large cohorts can be irradiated simultaneously, thus eliminating any potential institutional bias.

1.6.1 Radiation and *Drosophila*

Insects have generally been thought of as radio-resistant when compared against radio-sensitive mammals, and this has been attributed to their respective life-histories, with most insect adult tissues being *post* mitotic and therefore more resistant to the genotoxic effect of treatment (Koval *et al.*, 1978; Paithankar, Deeksha & Patil, 2017; Paithankar, Ghodke & Patil, 2020; Sharma *et al.*, 2020). *Drosophila* has a long history within radiation research, with Muller receiving a Nobel prize in 1946 for his work demonstrating that X-ray radiation induces mutations (Muller, 1930). Since then, *Drosophila* radiobiology research has been sparce, but it has been shown that at the organism level, there are reductions in multiple health metrics: lifespan reduction (Sudmeier, Howard & Ganetzky, 2015; Sharma *et al.*, 2020), movement impairment (Sudmeier *et al.*, 2015; Sharma *et al.*, 2020) and infertility (Sudmeier *et al.*, 2015; Paithankar *et al.*, 2017). This is true for both larvae and adult *Drosophila*.

1.6.2 Candidates identified through *Drosophila* GWAS

There have been two *Drosophila* GWAS to date and both used the *Drosophila* genetic reference panel (DGRP) to characterise the genetic architecture of the radiation response (Sharma et al., 2020; Vaisnav et al., 2014). The DGRP is a community resource of over 200 highly inbred and closely related *Drosophila* strains which have been selected to represent the natural variation of a typical WT population. DGRP lines were established via collection of WT gravid females from a farmer's market in Raleigh (North Carline, United States) they were subsequently inbred >20 generations, and then sequenced (MacKay *et al.*, 2012). There is publicly available sequence data for every strain of the panel, allowing *Drosophila* researchers to perform large GWAS of polygenic traits without the need of expensive genotyping.

The first study subjected adult males from 154 members of the DGRP to a large dose of radiation (1382 Gy, γ-rays) and quantified their ability to fly 24 hours *post* treatment (Vaisnav et al., 2014). This study was not successful in identifying any significant loci associated with the radiation response. The second study focussed on the adult midgut's ability to withstand damage after radiation treatment (Sharma,

et al., 2019). This study assayed midgut permeability (smurf assay) two weeks *post* irradiation, and identified a number of loci significantly associated with reduced midgut health *post* irradiation (**Table 1.1**). Though this study identified risk loci, no biological processes were enriched in the list of associated genes. Therefore, this study also was under powered with only a few significant hits passing the pre-determined *p*-value threshold which accounts for false positive associated with multiple testing.

The problems associated with these studies would need to be addressed before another GWAS is attempted. Particularly increasing panel size and designing a more appropriate assay which better reflects overall health. These are issues that human studies have also struggled with addressing: low sample size and poor characterisation of clinical outcome.

Table 1.1: Significant hits reported from GWAS performed by Sharma. *et al*., (2019). * Data acquired from FlyBase consortium.

Gene Symbol	Human orthologue	Biological process*
Ddr	*DDR2*	Development, response to stimulus, signalling, protein metabolism and other biological process.
CG42324	*Begain*	N/A
msi	*MSI2*	Other biological process
CG1824	*ABCB8*	Transport/localisation
Cka	*STRN3*	Cell cycle/proliferation, development, reproduction, response to stimulus and signaling

1.7 Other sources of radiation exposure

A better understanding of the radiation response does not simply have implications and relevance to medical research. The maturing of radiobiology field can have a wide array of implications and applications from environmental procedure of clearing radioactive waste and contamination to help with the screening of personal for space flight.

Environmental contamination

Within the past ~80 years that humans have had nuclear technology there have been numerous incidents of environmental contamination either from nuclear waste, power plant accidents (Mayak/Kyshtym, Chernobyl & Fukushima Daiichi) or from atomic bomb detonations (Hiroshima, Nagasaki, Bikini Atolls, & Nevada desert). The damage to these areas is long-lasting and the effects on biological systems and organisms are poorly understood. For instance the Chernobyl incident that occurred in 1986 led to increased mutation rates in WT populations of *Drosophila* (estimated <1 Gy exposure) which persisted at least until 1989 (last reported year) (Zainullin, Shevchenko, Mjasnjankina, Generalova, & Rakin, 1992).

A better understanding of the radiation response of *Drosophila* would help us to better understand the long-term effects to invertebrate populations in these contaminated areas, which form crucial links and chains within the majority of food chains and thus having important economic and environmental impact (Paithankar *et al.*, 2020). Additionally, it has been suggested that *Drosophila* can be used as a 'canary' to detect and quantify levels of radiation exposure in a particular environment. Regarding the treatment of irradiated individuals, it is critical to know total received dose as it can dictate treatment regimes, however it can be difficult to quantify received dose, particularly long-term after the radiation event occurred. In *Drosophila*, a number of genes have been identified that are differentially expressed long-term *post* exposure, such as *Inverted repeat-bind protein* (*Irbp*) a orthologue of human XRCC6 that facilitates double strand break (DSB) repair (Shrestha, Vanasse, Cooper, & Antosh, 2017). Therefore, *Drosophila* makes for an appealing dosimetry tool due to its cosmopolitan distribution around the globe and its quantifiable sustained response to irradiation.

Space flight

On Earth and in low-earth orbit (LEO), life is protected from harmful ionising radiation (cosmic radiation & solar flares) by the magnetosphere of Earth, however beyond LEO astronauts will require protection, and as current protection is not

enough, the national aeronautics and space administration (NASA) limits the time that astronauts can stay in space (Chancellor et al., 2018; Shang et al., 2020). Worldwide, space agencies and corporations have stated clear intention of travelling past the protection of the magnetosphere within the next decade, either to the Moon, Mars or deep space. NASA has initiated the Artemis programme, an international effort to take humans back to the Moon and to maintain a permanent human presence. Additionally, Gateway will be a station in lunar orbit which will eventually be staffed (NASA, 2020; Smith et al., 2020). The private company SpaceX is also preparing missions beyond LEO (Moon and Mars) (Buchanan, 2017; Musk, 2017).

On the surface of the Moon, which lacks a magnetosphere, the typical radiation exposure from cosmic-rays would range from 0.06 to 0.195 Gy, within a 190 day mission-span (Hellweg & Baumstark-Khan, 2007; Chancellor *et al.*, 2018). Simultaneous measurements in LEO and on the Moon have shown that the dose rate on the moon is approximately 2.6 larger than in LEO (Zhang et al., 2020). For perspective, a received dose of 1 Gy is sufficient to reduce human life expectancy by ~4 months (Cologne & Preston, 2000). Therefore, for long-term missions it would be prudent for these organisations to screen potential astronauts/personnel based-off their radiation sensitivity. However, no such diagnostic test exists, as of yet.

Drosophila radiation research has shown long-term effects from prolonged radiation exposure on WT populations (Mosse & Lyakh, 1994). This particular experiment exposed *Drosophila* to low dosages of radiation for 115 consecutive generations, and found that exposure changed the population genetic structure leading to an increase in mutations that led to a decrease in viability. Identifying the genetic architecture of the *Drosophila* radiation response would prove invaluable to the efforts of developing genetic diagnostic tests to be used clinically or commercially.

1.8   Aims and objectives

Overall **aims** and **objectives** of this thesis are as follows:

Aim 1 - Develop a method to expedite *Drosophila* lifespan assaying

Objectives:

- Develop hardware that facilitates the handling of multiple vials of *Drosophila* simultaneously

- Create a statistical analysis software specific to *Drosophila* lifespan datasets
- Compare the new method of lifespan assaying to conventional method
- Use the new method to generate useful scientific data as proof of principle

Aim 2 – Develop a *Drosophila* model for long-term radiation toxicity

Objectives:

- Assess the *Drosophila* response to irradiation through various health metrics
- Understand the aetiology of late radiation toxicity by focusing on the role of chronic oxidative stress
- Recapitulate human RT regimes to assess the radiation of *Drosophila*

Aim 3 – Identify risk loci associated with radiation induced late toxicity in *Drosophila*

Objectives:

- Perform a literature review of *Drosophila* radiation research to collate a list of risk genes
- Functionally validate genes identified from either literature search or human radiation research
- Design and perform an RNA-seq experiment to identify individual genes and processes involved in the radiation response

Chapter 2: Developing tools for higher through-put assaying of *Drosophila* health

2.1 Introduction

The aim of this chapter was to develop methods that facilitate higher throughput assaying of overall *Drosophila* health. Characterising the effects of radiation on *Drosophila* health is crucial in identifying genetic loci that are involved in the radiation response. The radiation response is a highly polygenic trait and to identify the genetic loci associated with this trait would require large quantitative studies, such as the GWAS employed by the radiogenomics community. To measure changes in health status associated with radiation treatment, multiple phenotypes have been assayed such as: fertility, lifespan/survival, faecal (frass) quantification, movement impairment, and various histological assays. Two of these assays (survival and frass quantification) have been identified as requiring optimisation and this will be discussed in this chapter.

2.1.1 Measuring overall health of *Drosophila* – Lifespan assaying

Survival analysis of *Drosophila* is commonly employed in many fields such as in ageing, immunology, stem cell biology, metabolism, physiology and evolutionary biology, to gauge survivorship and overall health (Mair *et al.*, 2003; Flatt, 2011; Tatar, Post & Yu, 2014; Galenza *et al.*, 2016; Strilbytska *et al.*, 2020). The broad use of *Drosophila* is due to the advantages it conveys such as short lifespan, cheap rearing and genetic tractability - making it an appealing model for survival analysis (Linford, Bilgir, Ro, & Pletcher, 2013). These advantages allow for the lifespan assaying of large cohorts (>1,000 individuals), as seen in the evolutionary/ageing literature (Mair et al., 2003).

However, the conventional method of lifespan assaying *Drosophila* is labour-intensive and time-consuming. Typically, experimental cohorts are housed in standard culturing vials that are replaced with fresh vials/media 2-3 times weekly, whilst recording the number of dead, censored, and carried over *Drosophila*. There has been little innovation or change regarding the manual handling of *Drosophila* since its initial culturing within laboratories (Bangham, 2019). The only alternative to manual handling is the stock-changing robots employed by the Janelia neurobiological research facility (Bangham, 2019). These robots eliminate the need for manual handling but are not commercially available, expensive, and are not appropriate for lifespan assaying because they cannot record data. Additionally, these robots anaesthetize (CO_2) *Drosophila every* transfer thus introducing a

confounding variable (video). There is a gap between conventional and automated handling, and with this gap in mind a novel system of lifespan assaying has been developed throughout this PhD.

2.1.2 Measuring midgut health – Frass assaying

Across metazoans the functions of the gastrointestinal tract are highly conserved and are as follows: (1) to digest and absorb nutrients, (2) to maintain hydrostatic balance of the soma, and (3) to act as a mechanical barrier to protect the soma from biotic and abiotic insults (Apidianakis & Rahme, 2011; Wijtten, Meulen & Verstegen, 2011). Dysfunction of the intestine can pose significant risk to any animal, and if not corrected, can affect overall fitness and survival.

Quantification of faecal output can be used to gauge the functional status of the *Drosophila* midgut by measuring multiple characteristics, e.g. pH change, size and shape of depositions and quantity. To keep with *Drosophila* nomenclature and for the rest of this thesis, faeces will be referred to as frass when referencing *Drosophila* faeces. An assay has already been developed that allows for the quantification of *Drosophila* frass by the addition of the pH indicator Bromophenol Blue (BPB) to their diet (Cognigni, Bailey & Miguel-Aliaga, 2011). This assay has successfully shown that frass composition is affected by a number of variables such as: reproductive status, sex, age and microbiota composition (Cognigni *et al.,* 2011; Clark *et al.*, 2015).

This assay requires the transfer of *Drosophila* to a filter paper-lined enclosure in which frass is deposited and collected (Cognigni *et al.,* 2011; Clark *et al.*, 2015). However, this method relies on CO_2 anesthetizing for transferring of adult *Drosophila* from standard rearing tubes to filter paper-lined petri dishes. Exposure to high CO_2 concentrations in insects has been shown to have numerous effects on both behaviour and physiology (reviewed by Nicolas & Sillans, 1989). Specifically the CO_2 anaesthetisation of *Drosophila* induces changes in metabolism (glycolysis and oxidative phosphorylation), perturbations in pH of haemolymph, and reduced functioning of the neuromuscular junction which induces muscle relaxation (Nicolas & Sillans, 1989; Colinet & Renault, 2012). The dysregulation of metabolism persists for at least 24 hr after anaesthetisation resulting in relaxation of gastrointestinal muscles, in particular the anal sphincter, inducing premature *Drosophila* defecation (Colinet & Renault, 2012). This introduces a confounding variable when trying to quantify frass. To eliminate this variable, a modified version of the frass assay has been developed that eliminates the need for CO_2 anesthetization.

2.1.3 Aims and Objectives

As mentioned, both lifespan and frass assaying have their limitations and currently there are no viable alternative methods commercially available nor published that were appropriate to be used in the context of this PhD. Therefore, novel methods were developed with the aim of being scalable, timesaving and introduce standardisation to experimentation.

Aim 1 - Develop a method to expedite *Drosophila* lifespan assaying

Objectives:

- Develop hardware that allows for the handling of multiple vials of *Drosophila* simultaneously
- Create a statistical analysis software specific to *Drosophila* lifespan datasets
- Compare the new method of lifespan assaying to conventional method
- Use the new method to generate useful scientific data as proof of principle

Aim 2 – Modify the frass assay to eliminate the need for CO_2 anesthetization

Objectives:

- Design an adaptor funnel to allow for the direct transfer of *Drosophila* from rearing vials to a modified petri dish
- Determine if the use of the frass 'chamber' can give consistent results under various experimental conditions

2.2 Materials and Methods

2.2.1 *Drosophila* strains

All stocks were maintained at 25 °C with a 12 hr:12 hr light:dark photocycle and on standard *Drosophila* cornmeal medium (**Table 2.1**).

Table 2.1: Wildtype *Drosophila* stocks used for chapter 2. Including source and if available reference number.

Stock	Source (reference)
w^{1118}	BDSC # 5905
Oregon R	BDSC # 25211
Vallecas	Gift from José Félix de Celis
DGRP 21	BDSC # 28154
DGRP 304	BDSC # 25177
Samarkand	BDSC # 4270
Swedish C	BDSC # 4271

2.2.2   Preparation of standard cornmeal food

Drosophila cornmeal medium was prepared a maximum of two to three weeks in advance and the recipe (per litre) was as follows: agar 6.74 g, maize 72.4 g, dextrose 75 g, yeast 35 g, hydroxybenzoic acid methyl ester 2.22 g, absolute ethanol 26 ml, propionic acid 3.5 ml, and H_2O 970 ml.

2.2.3   Preparation of drug supplemented food

Prior to food dispensing, drugs were supplemented - plant auxins: 1-Naphthaleneacetic acid (NAA) and Indole-3-acetic acid (IAA). Due to the viscosity of the standard media and to ensure equal distribution within media, both IAA and NAA were dissolved in ethanol (50 mg/ml). Note control media was prepared by adding equal volume of ethanol prior to dispensing. Once the media was prepared, adult *Drosophila* were reared on auxin supplemented food as an *ad libitum* diet for the duration of their lifespan/survival.

2.2.4   3D modelling and printing

All models were designed in the freely available Fusion[360] software (under student or small business licence). Stereolithography (STL) files were exported to the freely available slicer Cura and converted to 3D printing compatible gcode. Recommended print settings were used except all components were printed at 35 mm/min speed, and support was generated for the MultiFlipper and box. Printing was performed on an AnyCubic I3 mega using polylactic acid (PLA) 1.75 mm filament.

2.2.5   Lifespan assay

All cohorts were age synchronised (purped) (Linford *et al*, 2013; Clancy, David & Kennington, 2001). Upon eclosion, *Drosophila* were transferred to fresh media and allowed to mate for 48 hr, followed by deposition within MultiFlipper housing rack. Lifespan was performed 10 *Drosophila* of either sex per vial were transferred to fresh media using the MultiFlipper 2-3 times weekly, during each transfer deaths/carried over/censored were recorded using experiment specific data acquisition sheets.

2.2.6   Lifespan statistical analysis

Lifespan survival datasets were visualised with Kaplan-Meir (KM) plots using the R package Survival [1.2] (Therneau & Lumley, 2015). Survival curves were visually inspected to check data distribution and for potential outliers which would violate subsequent modelling (Bradburn, Clark, Love, & Altman, 2003). As *Drosophila* were

kept 10 – 15 per rearing vial the effect of replicate was checked, and this was done via visual inspection of KM plots and through checking of median survival times for each vial, with 95% confidence interval reported to indicate likelihood that true median survival lies within indicated range. All datasets underwent log-rank testing and Cox Proportional hazard (CoxPH) modelling using the R package Survminer [1.0] (Kassambara, Kosinski & Biecek, 2017). When multiple variables were under study as well as potential interactions, only CoxPH modelling was performed. CoxPH modelling relies on the assumption that hazard risk is proportional i.e independent of time, Schoenfeld residuals test was used to check this assumption (Bradburn et al., 2003). CoxPH models were visualised with forest plots using R Survminer package. For each independent variable the significance (p value) and hazard ratio (HR) were reported. HR can be described as a comparison of the probabilities of events (deaths) between experimental groups (T. G. Clark, Bradburn, Love, & Altman, 2003). For example, a HR of 0.75 would mean a 25% lower risk of death. An example of an automated statistical analysis can be found in **Appendix 2**.

2.2.7 Frass assay

Housing chambers were constructed and consisted of standard 90 mm petri dish, 3D printed hardware and rubber bands. Media was prepared with the pH indicator BPB salt (B5525, Sigma-Aldrich) that was added to standard *Drosophila* culturing media (**Section 2.2.2**) just prior to dispensing (60-65 °C).

Briefly, *Drosophila* were purped (**Section 2.2.5**) and deposited in replicates of 30 *Drosophila* per vial and fed BPB supplemented media for at least 48 hr prior to assaying. *Drosophila* were then transferred to modified petri dishes via standard manual transfer technique (tipping) without anaesthetisation and enclosed in with a moistened cotton ball.

2.2.8 Frass composition statistical analysis

Statistical analysis of frass datasets was performed in base R. For total output, t-test were performed to compare different treatments, followed by Shapiro-Wilk testing for normality and homogeny of variance testing, and for data with cohorts >2 Tukey's multiple comparison testing was performed.

2.2.9 Lifespan analyser software development

The Lifespan Analyser was designed in Python (version 3.6) within both the PyCharm interpreter and Jupiter notebooks, and the GUI within the PyQt5 designer.

Programme was compiled and made into an executable programme using the Nullsoft Scriptable Install System (NSIS) software (version 3.05). Script was designed and written with help from Dr Joaquin de Navascues.

2.3 Medium through-put lifespan assaying - The MultiFlipper System

2.3.1 Components of the MultiFlipper System

The MultiFlipper system is a combination of both physical components (**Figures 2.1 – 2.5**) and software (**Figures 2.6 – 2.7**). The physical components were designed to allow for faster handling of *Drosophila* lifespan cohorts. This is achieved by allowing the handling of 12 vials simultaneously which reduces maintenance time. A vial housing rack was designed and optimised to house 12 vials, with a slot on the back spine for a label to keep track of stored cohort (**Figure 2.2**), and a lid (**Figure 2.3**). During each subsequent transfer, the MultiFlipper is used by quickly replacing the lid with the MultiFlipper (**Figure 2.1**). The cohort is then temporarily transferred and stored within the MultiFlipper whilst old vials within the rack are replaced with fresh vials. Old vials are checked for dead *Drosophila* and data recorded using coloured markers on experiment specific datasheets which are subsequently scanned and analysed by a software (The Lifespan Analyser) to automatically compile data for statistical analysis. The Lifespan Analyser software was designed to be as simple as possible whilst having useful functionality (**Figure 2.6**). This software has multiple functions with each contained within a specific window that can be accessed from the main window (**Figure 2.7**). Lifespan Analyser functions include:

- Checking colour compatibility of marker for data recording – colour check window (**Figure 2.8**)
- Storing of experimental metadata – datasheet window (**Figure 2.9**)
- Anonymisation of lifespan experiments – datasheet window (**Figure 2.9**)
- Experiment specific datasheet generation – datasheet window (**Figure 2.9**)
- Digitisation of lifespan datasets – main window (**Figure 2.10**)
- Statistical analysis of lifespan datasets – main window (**Figure 2.11**)

The programme is soon to be under MIT creative licence and will be freely available for download from GitHub along with accompanying 3D printable files, construction guides and detailed stepwise protocols (https://github.com/Trincatalyst/MultiFlipper).

2.3.1.1 Physical components of the MultiFlipper system
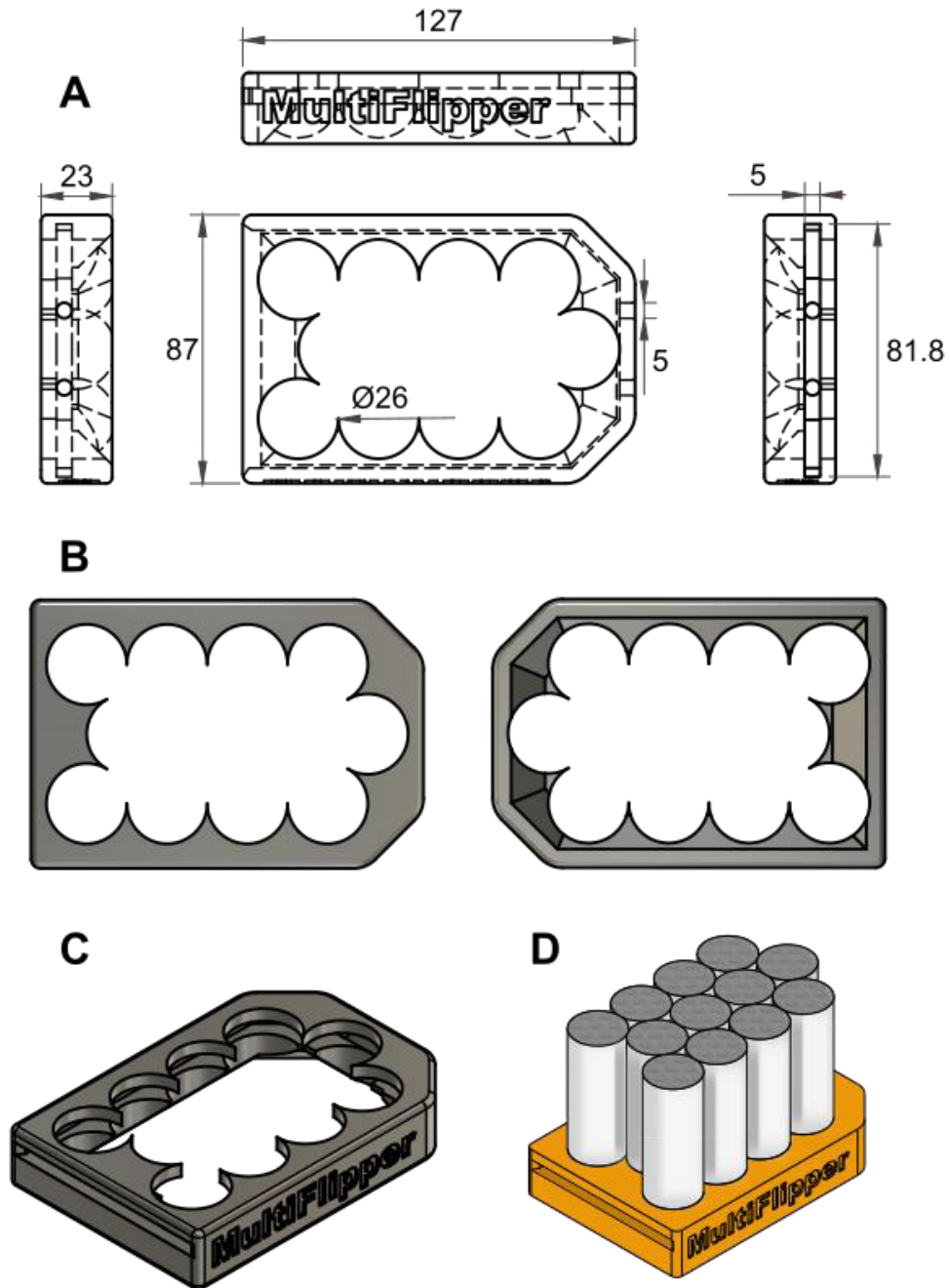
Figure 2.1: Design schematics of the temporary housing and transfer (MultiFlipper) component. Designed in Fusion[360] software. Compatible with vials of a 25 mm diameter. (**A**) Schematics showing key measurements (mm) of MultiFlipper. (**B**) top and bottom views of the MultiFlipper, respectively. (**C**) side angle view of the MultiFlipper, and (**D**) side angle view of a MultiFlipper with *post* print modifications.
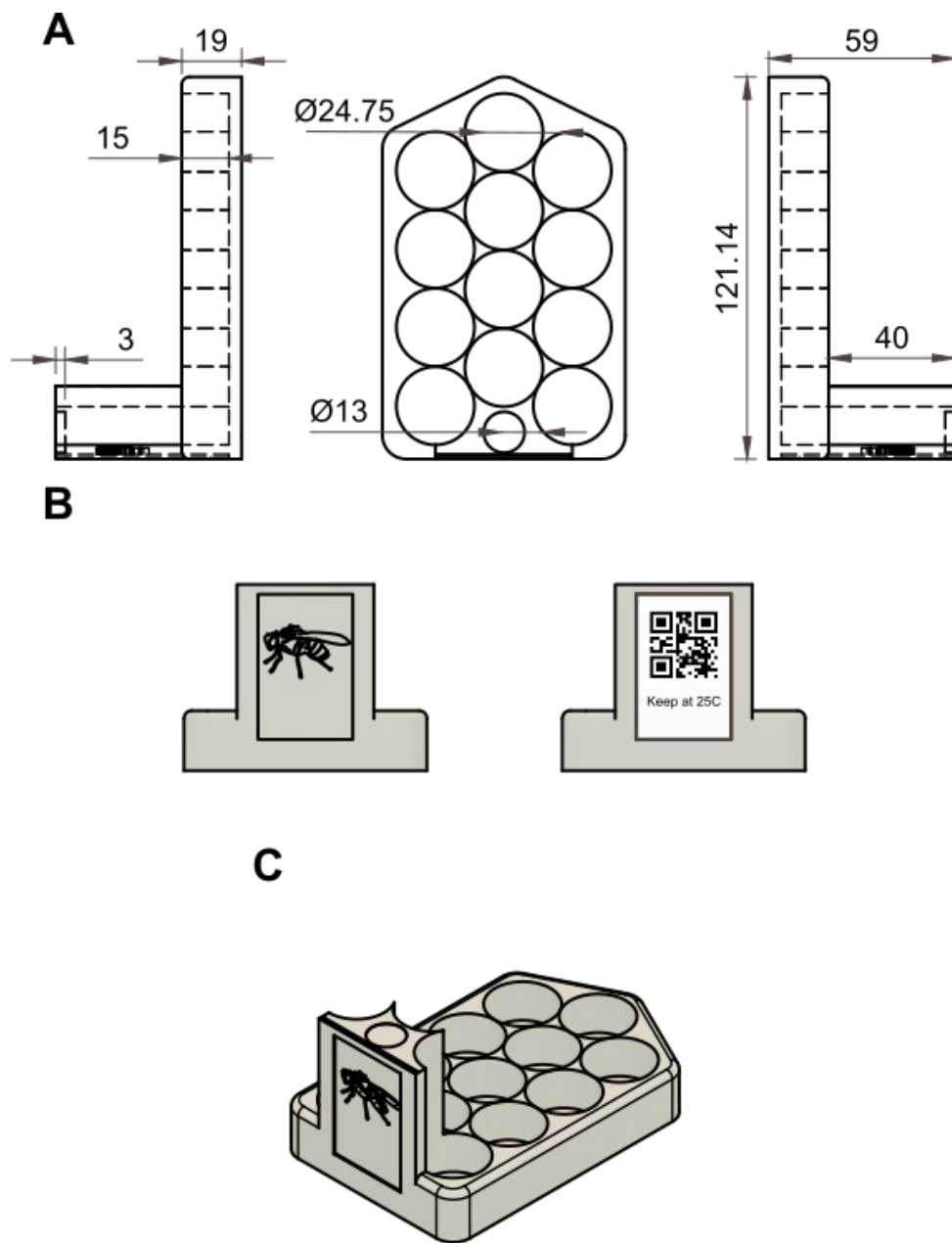
Figure 2.2: Design schematics of the cohort housing (Rack) component. Designed in Fusion[360] software. Compatible to house up to 12 vials of a 25 mm diameter. (**A**) Schematics showing key measurements (mm) of housing Rack. (**B**) Spine of Rack showing window to display QR code (generated in Lifespan Analyser) containing all cohort specific information. (**C**) Side angle view of the housing Rack to be used in conjunction with the Lid (**Figure 2.3**).
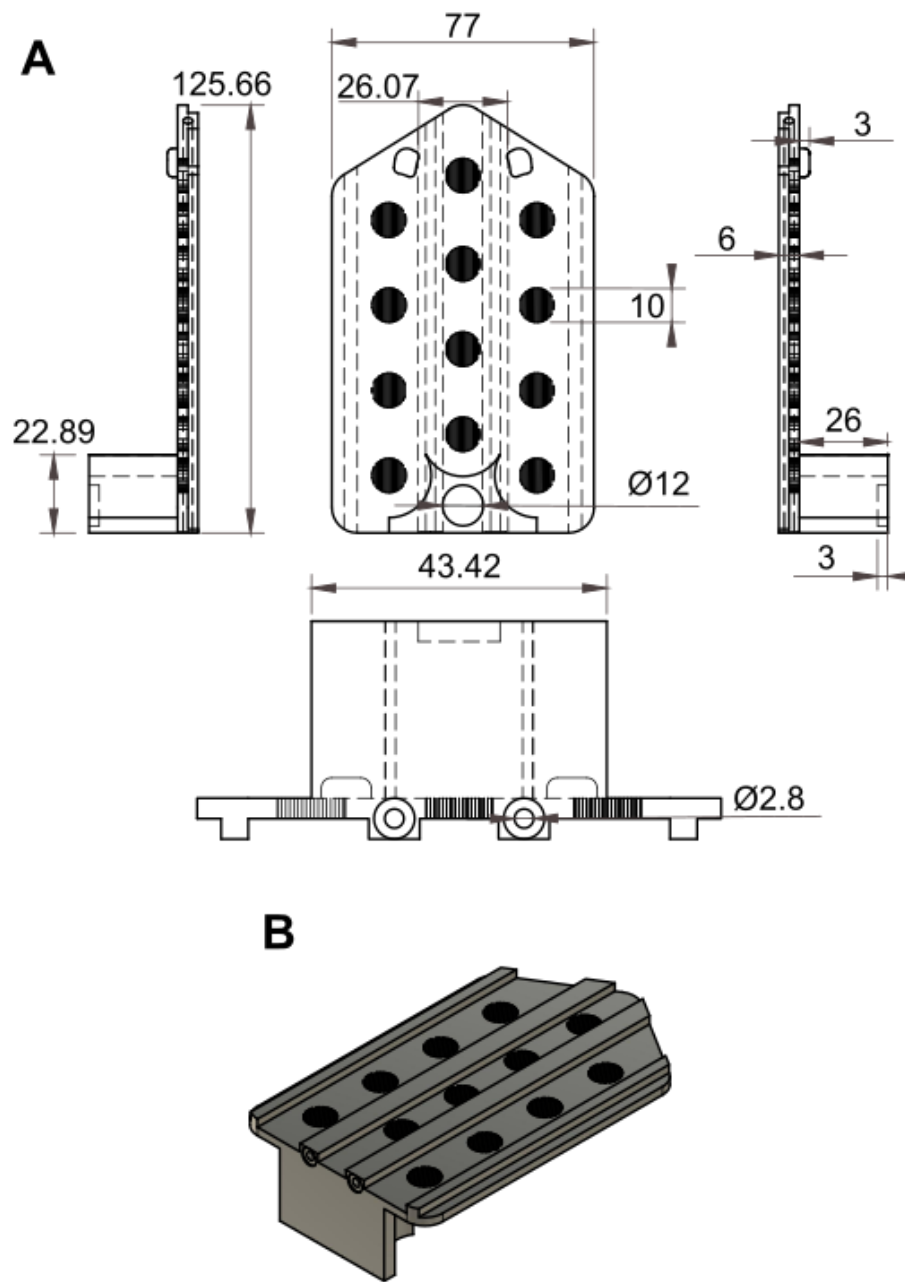
Figure 2.3: Design schematics of the cohort housing (Lid) component. Designed in Fusion[360] software. Compatible to house up to 12 vials of a 25 mm diameter. (**A**) Schematics showing key measurements (mm) of housing Lid. (**B**) Side angle view of the housing Lid to be used in conjunction with the Rack (**Figure 2.2**).
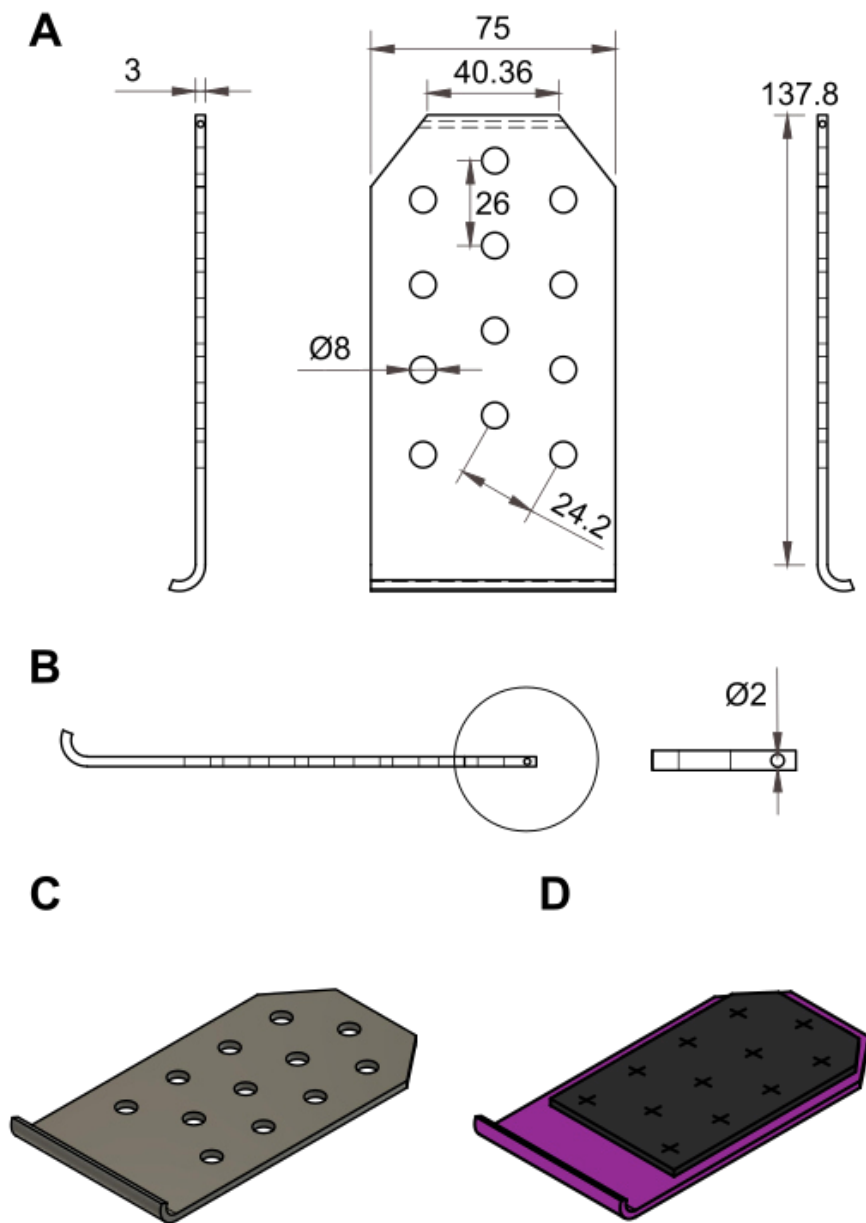
Figure 2.4: Design schematics of the Depositor to help with the initial deposition of cohorts within the MultiFlipper. (**A**) Schematics showing key measurements (mm) of slider. Designed in Fusion[360] software. (**B**) Side view of Depositor showing hole for ferrous metal nail. (**C**) side angle view of slider, and (**D**) side angle view of a Depositor with *post* print modification.
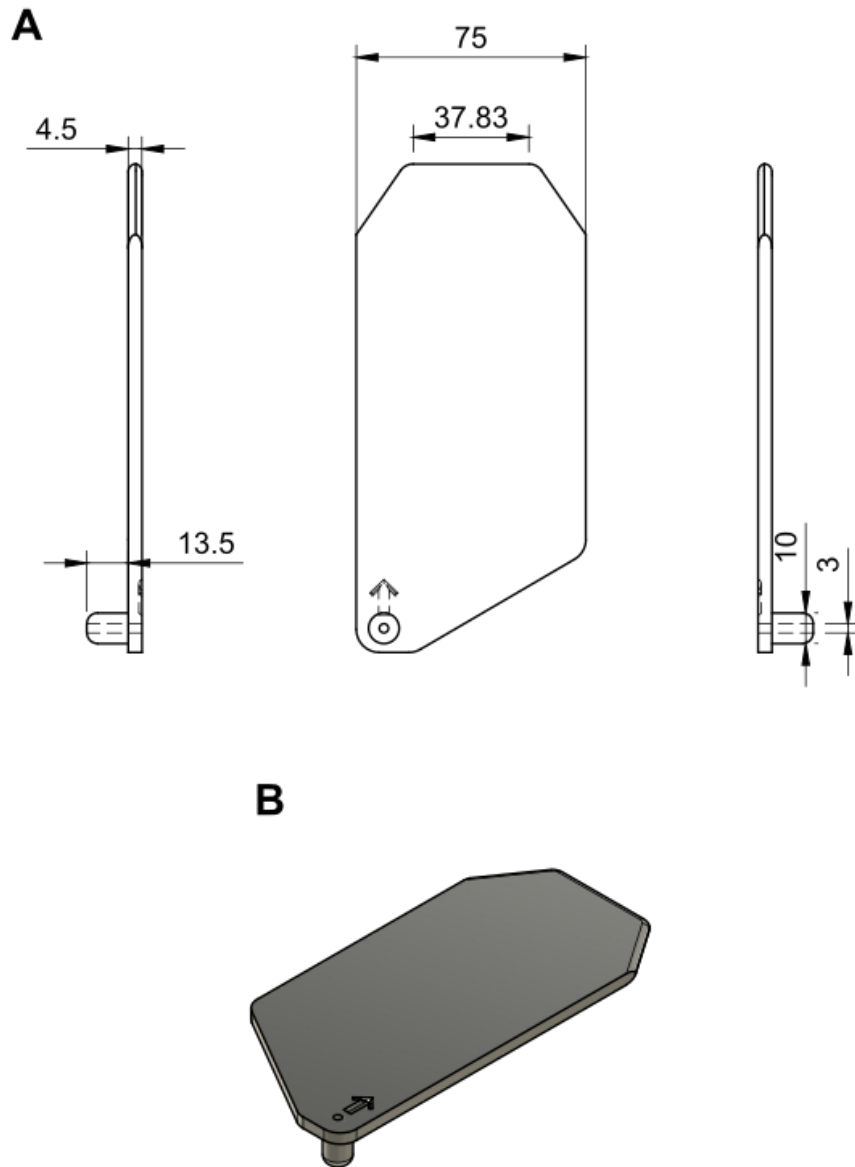
Figure 2.5: Design schematics of the Slider to help store cohorts within the MultiFlipper during transfers. Designed in Fusion[360] software.

2.3.1.2 Software component of the MultiFlipper system
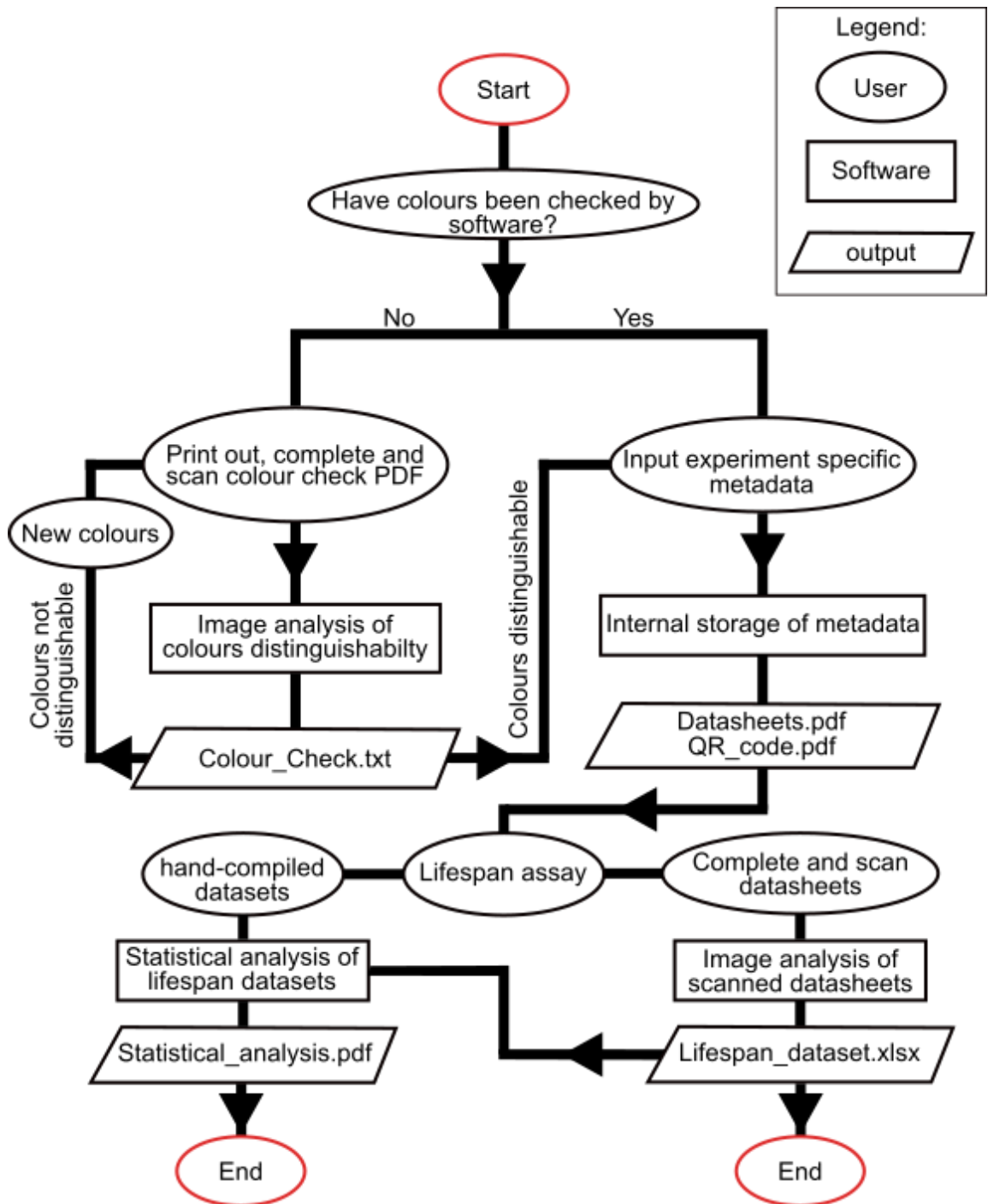
Figure 2.6: Chronological order of user and Lifespan Analyser software interaction.
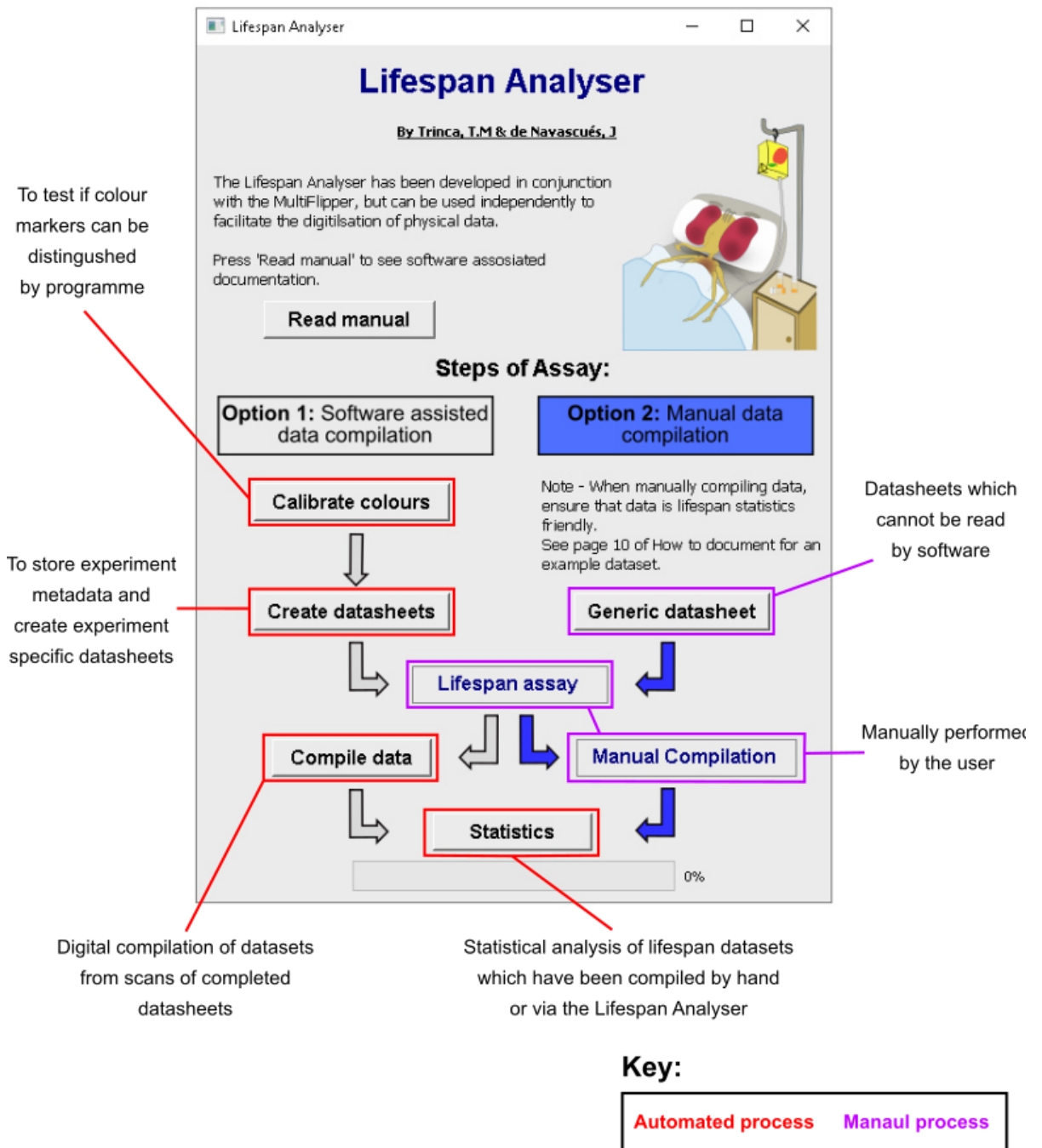
Figure 2.7: Main window of Lifespan Analyser graphical user interface. Version 0.1 taken from windows OS.
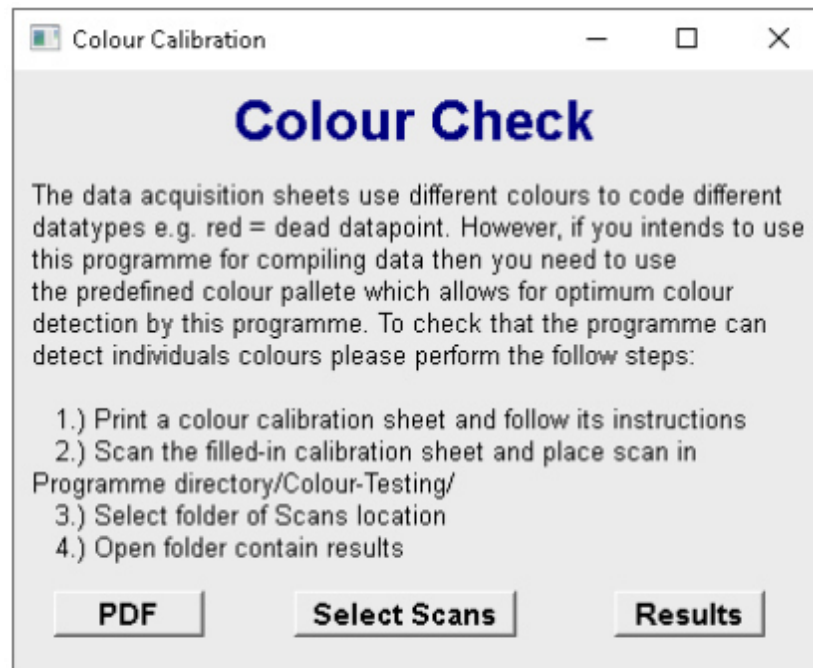
Figure 2.8: Colour calibration window of Lifespan Analyser graphical user interface.

Figure 2.9: Experiment specific metadata storage and datasheet generation window of Lifespan Analyser graphical user interface. (**A**) digital storage of metadata pertinent to ongoing lifespan experiment. (**B**) Continuation of digital storage of metadata but a dynamically generated window based of how racks are being using in lifespan experiment.
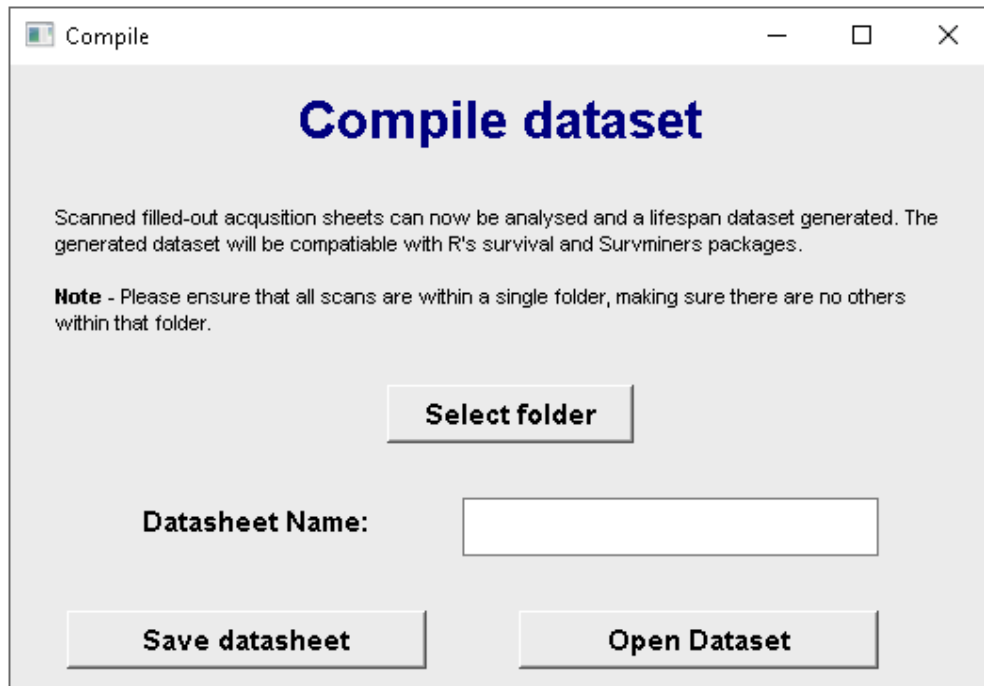
Figure 2.10: Dataset compilation window of Lifespan Analyser graphical user interface.
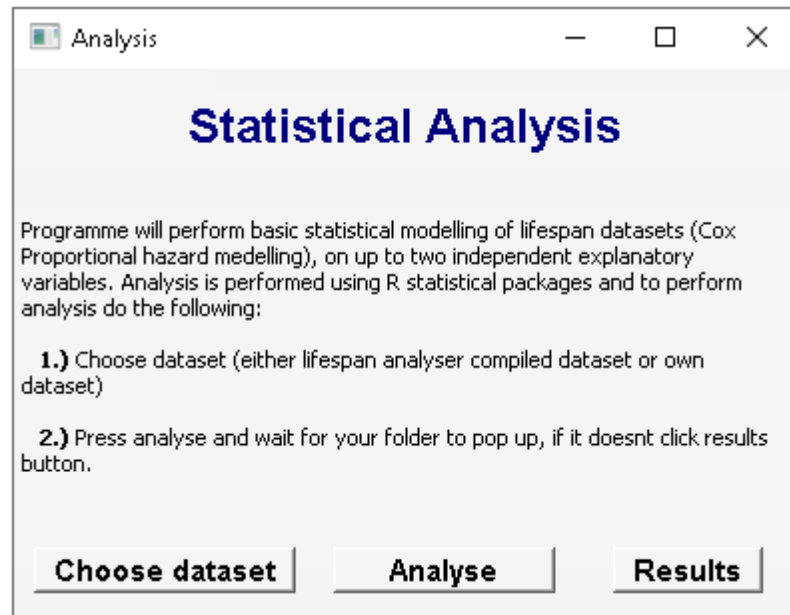
Figure 2.11: Dataset statistical analysis window of Lifespan Analyser graphical user interface.

2.3.2 Validation of the MultiFlipper System

To validate the hardware components of the MultiFlipper system as a time-saving alternative to conventional transfer method, the cumulative time taken to transfer a cohort of *Drosophila* for an entire lifespan assay was measured, for both a novice and intermediate Drosophilist. Both novice and intermediate Drosophilists showed a consistent reduction in time taken to transfer cohorts when using the MultiFlipper (**Figure 2.12 A** & **C**). Accumulated handling time was reduced by 85% and 83% for novice and intermediate, respectively (**Figure 2.12 B** & **D**).

The mean transfer times for both methods were compared to determine if using the MultiFlipper led to consistently reduced transfer time. This was achieved by recording the time taken to maintain *Drosophila* cohorts for the duration of their lifespan either through use of the MultiFlipper or via conventional transfer method. For a novice Drosophilist, the mean transfer time using the MultiFlipper (44 sec) was significantly faster than conventional transfer (282 sec). Transfer times were determined to be significantly different via Welch' two sample t-test ($p = 3.5 \times 10^{-15}$). For an intermediate Drosophilist, the mean transfer time using the MultiFlipper (39 sec) was significantly faster than conventional transfer (228 sec), which was determined to be significantly different via Welch' two sample t-test ($p < 0.0001$) (**Figure 2.12 E**).

Drosophilists ($N = 11$) with various experience levels (1 – 20 years) were asked to use the MultiFlipper to further confirm speed reduction (**Figure 2.13**). Participants were asked to transfer *Drosophila* once and their time taken was recorded. When comparing speed between methods and disregarding experience level, the mean transfer time for all 11 participants with the MultiFlipper was faster (31 sec) compared to conventional transfer (162 sec). For novices (<= 1 year *Drosophila* experience), transfer with the MultiFlipper (28 sec) was faster compared to conventional transfer (198 sec). For intermediates (1 - 4 year *Drosophila* experience), transfer with the MultiFlipper (42 sec) was faster compared to conventional transfer (116 sec). For experts (>4 year *Drosophila* experience), transfer with the MultiFlipper (23 sec) was faster compared to conventional transfer (123 sec). Both method of transfer ($p < 2.55 \times 10^{-9}$) and experience level ($p = 0.0158$) were determined via Two-way ANOVA test to significantly influence transfer time. Additionally, there was a significant negatively correlated interaction between experience level and transfer method ($p = 0.0047$).

Once it was established that the MultiFlipper system facilitates faster transfer, I investigated whether its use had a negative effect on lifespan (**Figure 2.14**). The lifespan of *Drosophila* when maintained by a novice Drosophilist using the MultiFlipper (median survival: 49 days) was significantly lower by 14% when compared to conventional transfer (median survival: 57 days) (**Figure 2.14 A**). Log-rank testing was used to determine significance ($p = 0.0053$). Whereas, lifespan of *Drosophila* maintained by intermediate Drosophilist when using the MultiFlipper (median survival: 61 days) was signficantly higher by 9% when compared to conventional transfer (median survival: 56 days) (**Figure 2.14 B**). Log-rank testing was used to determine significance ($p = 0.04$).

The conventionally transferred cohorts from both lifespan datasets (novice and intermediate) were compared to determine if direct comparisons could be made between datasets but they were found to be significantly different ($p < 0.05$), attributed to batch effect. Therefore, CoxPH modelling was performed on the individual datasets, with replicates and transfer method as potential explanatory catagorical variables (**Figure 2.14 C**). The variable of replicate (individual vials) did not signficantly influence lifespan for either the novice or intermediate Drosophilist ($p = 0.334$ & 0.559, respectively). For the novice, method was a signficant vairable influencing lifespan ($p = 0.0278$) with a hazard ratio (HR) of 1.6465 with low confidence in this HR due to the large amount of censoring that occurred early on in the lifespan experiment. For the intermediate Drosophilist, method was not a signficant variable influencing lifespan ($p = 0.719$).
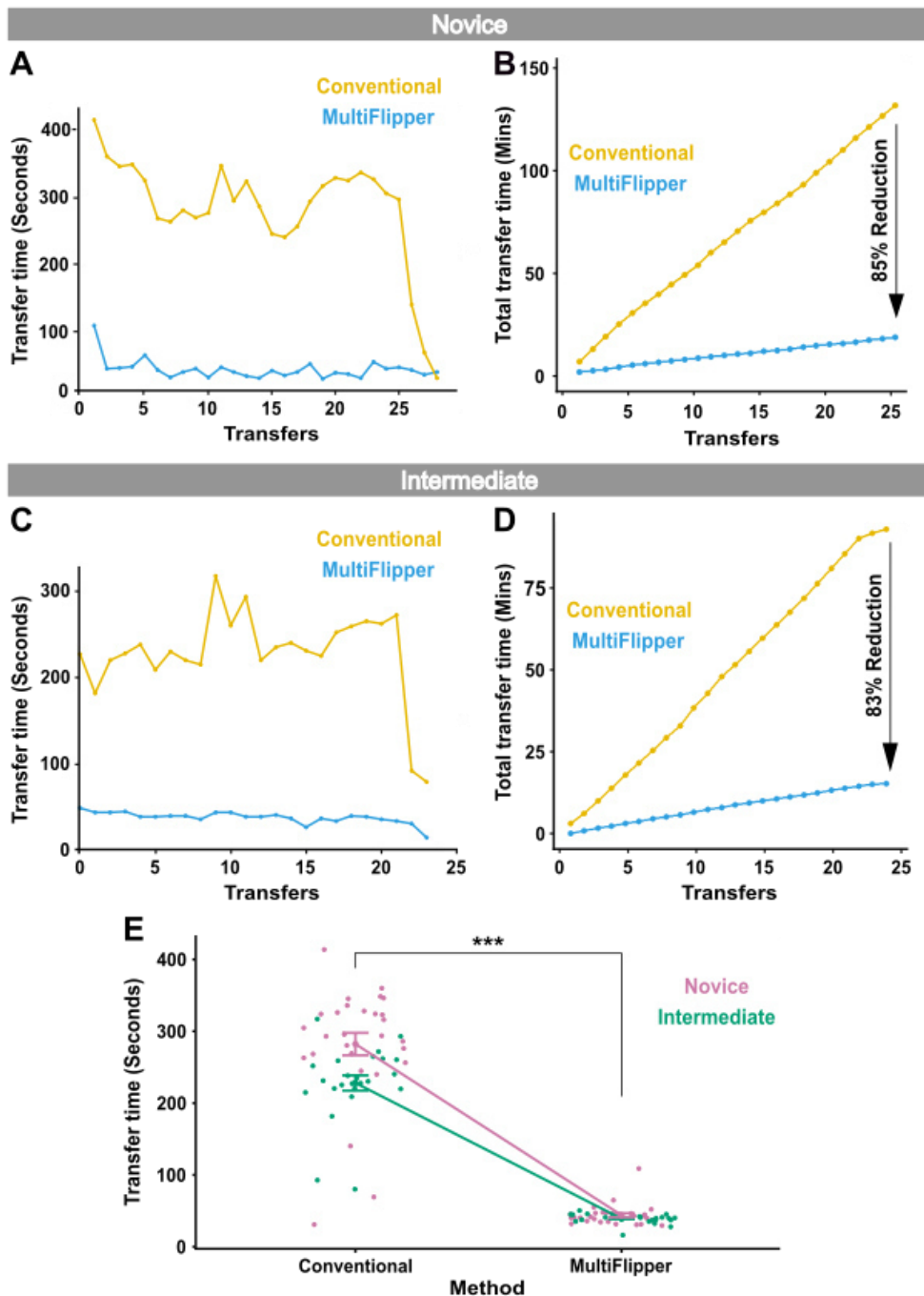
Figure 2.12: Using the MultiFlipper consistently reduces manual handling time of lifespan cohorts for both novice and intermediate Drosophilists. (**A**) Comparing the time taken for a novice to transfer 120 *Drosophila* with the MultiFlipper, over the course of an entire lifespan experiment. (**B**) Accumulated time taken to maintain lifespan experiment for novice Drosophilist. (**C**) Comparing the time taken for an intermediate to transfer 120 *Drosophila* with the MultiFlipper, over the course of an entire lifespan experiment. (**D**) Accumulated time taken to maintain lifespan experiment for intermediate Drosophilist. (**E**) Comparison of transfer speed between experience levels. Dataset was derived from w^{1118} 48 hr mated female *Drosophila*.
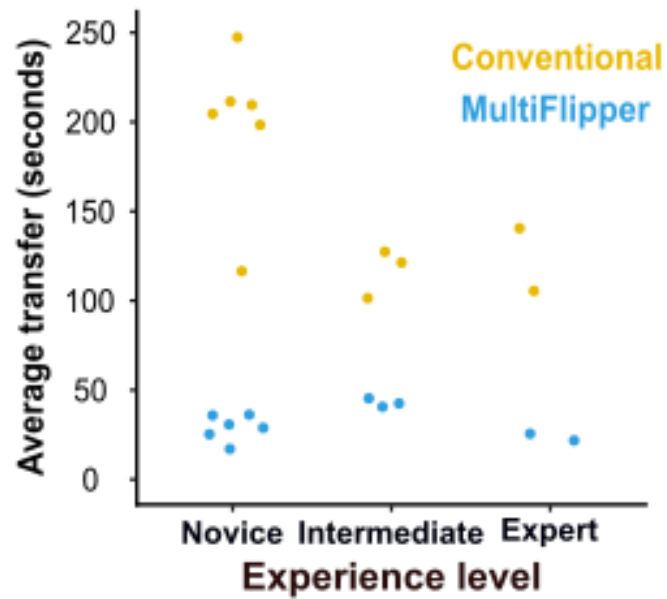
Figure 2.13: Every experience background showed a reduction in time taken to transfer Drosophila when using the MultiFlipper. A novice was < 1 year' experience, intermediate 1 – 4 years' experience and expert was >4 years' experience handling *Drosophila*. Datasets was derived from w^{1118} female *Drosophila*. Ethical approval to measure participants' transfer times was given by School of Biosciences, Cardiff University, and each participant signed a study consent form.
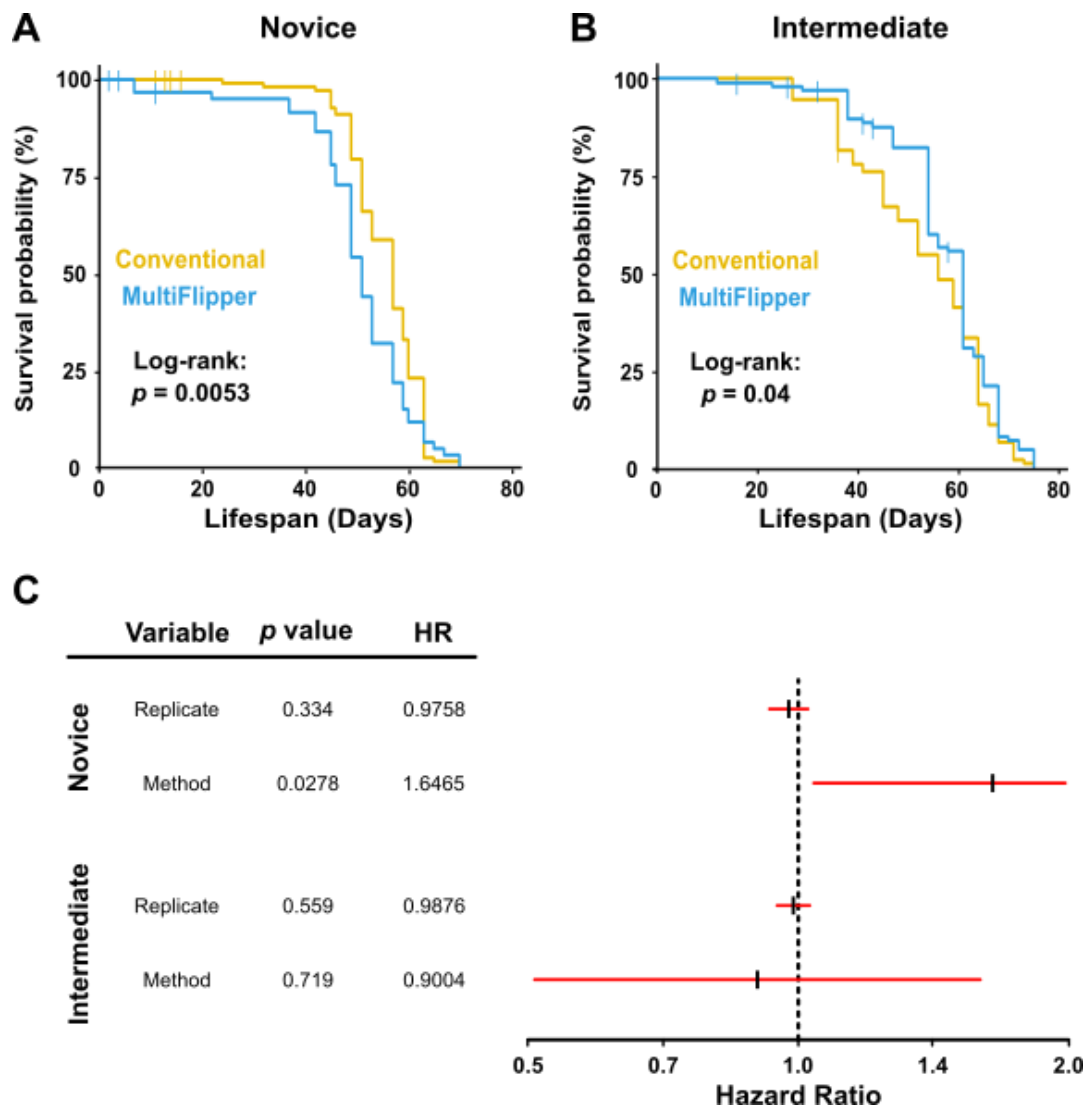
Figure 2.14: Comparison of lifespan of male *w^1118* adults maintained through different transfer methods. (**A**) Lifespan of *Drosophila* when maintained by a novice Drosophilist with ~two months experience. (**B**) Lifespan of Drosophila when maintained by an intermediate Drosophilist with ~two-year experience handling *Drosophila*. (**C**) Predicted hazard ratios derived from two independent CoxPH models.

2.3.3 Proof of principle experiments

As proof of principle that the MultiFlipper can be used to answer novel biological questions, it was used to assay the effects on lifespan of continuous feeding (*ad libitum* diet) of two plant auxins – IAA and NAA. These chemical were chosen as they are currently being considered as inducers of gene transcription systems but it is unknown if long-term exposure is toxic to *Drosophila*. Auxins have been fed to *Drosophila* in concentrations ranging from 0.3 – 1 mM, therefore it was decided to expose *Drosophila* to a high concentration of 10 mM to ensure best possible chance of observing auxin associated lifespan modulation (Trost *et al.*, 2016; Bence *et al.*, 2017).

When transferred conventionally, continuous feeding of IAA (10 mM) resulted in a reduction in lifespan for both sexes. For males, median lifespan was reduced by 8.3% from 48 (95% CI: 46 – 50) to 44 (95% CI: 42 – 48) days. For females, median lifespan significantly reduced by 11.4% from 70 (95% CI: 68 – 70) to 62 (95% CI: 58 – 68) days (**Figure 2.15 A** & **B**). When transferred with the MultiFlipper, continuous feeding of IAA (10 mM) resulted in insignificant changes to lifespan for both sexes. For males, median lifespan increased by 2% from 49 (95% CI: 49 – 49) to 50 (95% CI: 46 – 52) days. For females, median lifespan increased by 5.9% from 68 (95% CI: 49 – 71) to 72 (95% CI: 68 – 72) days (**Figure 2.15 C** & **D**).

To determine if both datasets could be combined, the effect of batch was determined by comparing lifespan of the non-exposed control cohorts for both sexes and transfer method. For unexposed males, median lifespan when transferred conventionally and with the MultiFlipper was not significantly different (48 and 49 days, respectively) (Log-rank: p = 0.19) (**Figure 2.16 A**). For unexposed females median lifespan when transferred conventionally and with the MultiFlipper was not significantly different (70 & 68 days, respectively) (Log-rank: p = 0.56) (**Figure 2.16 B**). As control cohorts between transfer methods showed indistinguishable lifespans, transfer method was disregarded as a potential explanatory variable and a combined dataset underwent CoxPH modelling.

A CoxPH model was generated with the explanatory variables: sex, IAA treatment and a potential interaction of both. Method was not modelled to reduce the risk of over modelling and because it was shown not be a significant variable between the unexposed cohorts (**Figure 2.16 B**). When compared to females, males had significantly ($p < 2x10^{-16}$) reduced lifespan and a high calculated HR of 6.79 (95% CI: 4.98 – 9.26). Both drug treatment and an interaction between treatment and sex

were insignificant ($p = 0.15$ & $= 0.808$, respectively). Testing for proportional hazards that are independent of time determined that both sex, treatment and their interaction did not violate proportional hazards assumption ($p = 0.17$, $= 0.43$ & $= 0.59$, respectively). Therefore, continuous feeding of IAA was determined not to significantly influence lifespan.

As the MultiFlipper reduces transfer time and does not influence survival, it was decided to investigate the effects of the second plant auxin NAA on lifespan with the MultiFlipper alone. Continuous feeding of NAA (10 mM) resulted in a reduction in lifespan for both sexes. For males, median lifespan significantly reduced by 14% from 43 (95% CI: 39 – 49) to 37 (95% CI: 35 – 39) days. For females, median lifespan significantly reduced by 8% from 62 (95% CI: 60 – 65) to 57 (95% CI: 55 – 60) days (**Figure 2.17 A** & **B**). A CoxPH model was generated with the explanatory variables: sex, NAA treatment and a potential interaction of both. When compared to females, males had significantly ($p < 8.82 \times 10^{-16}$) reduced lifespan and a high calculated HR of 5.54 (95% CI: 3.65 – 8.41). *Drosophila* exposed to NAA (10 mM) had a significantly ($p = 0.003$) reduced lifespan and a HR of 1.81 (95% CI: 1.22 – 2.7). A significant interaction ($p = 0.047$) was identified between treatment and sex, with exposed males having a HR of 1.77 (95% CI: 1.01 – 3.12). Testing for proportional hazards that are independent of time determined that both sex, treatment and their interaction violated proportional hazards assumption ($p = 0.04$, $= 0.01$ & $= 0.02$, respectively). Though the modelling violated the proportional hazard assumption, it suggested that NAA treatment had a negative effect on survival for both sexes, with possibly males being more sensitive to treatment.
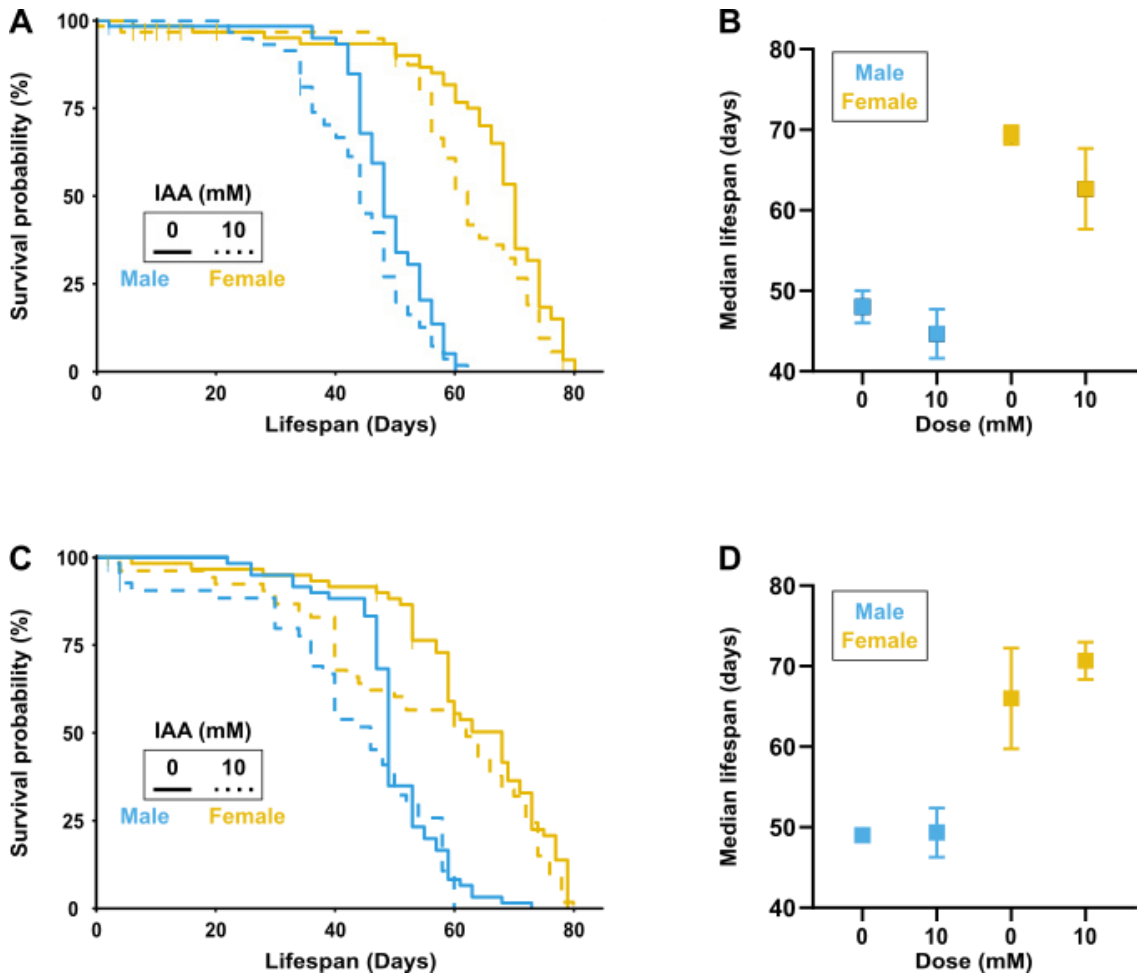
Figure 2.15: Continuous feeding of IAA show comparable results when maintained using the MultiFlipper. All experiments were performed on cohorts of 60 *w1118 Drosophila* per sex *w1118* housed 10 per vial. Lifespan when continuously exposed to IAA and transferred conventionally (**A**) and median lifespan with error bars representing 95% CI of the average median lifespan for all replicate vials (**B**). Lifespan when continuously exposed IAA and transferred with the MultiFlipper (**C**) and median lifespan with error bars representing 95% CI of the average median lifespan for all replicate vials (**D**).
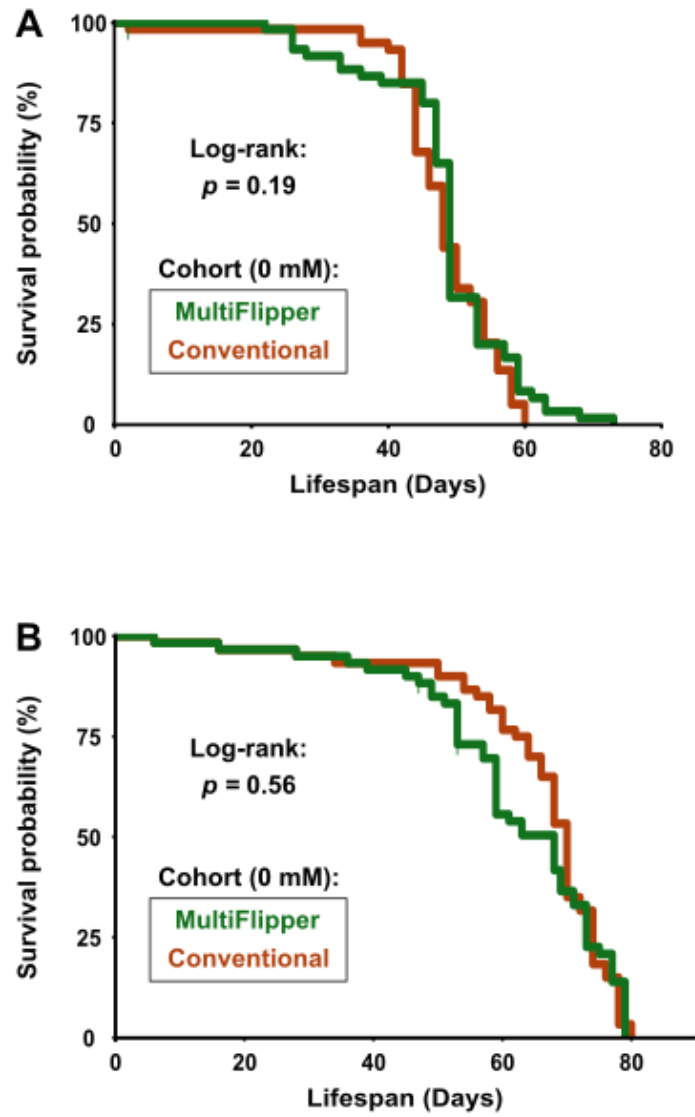
Figure 2.16: The effect of transfer methods on lifespan of unexposed IAA cohorts. All experiments were performed on cohorts of 60 w^{1118} *Drosophila* per condition with 10 housed per vial. Methods effect on lifespan for unexposed males (**A**) and females (**B**).
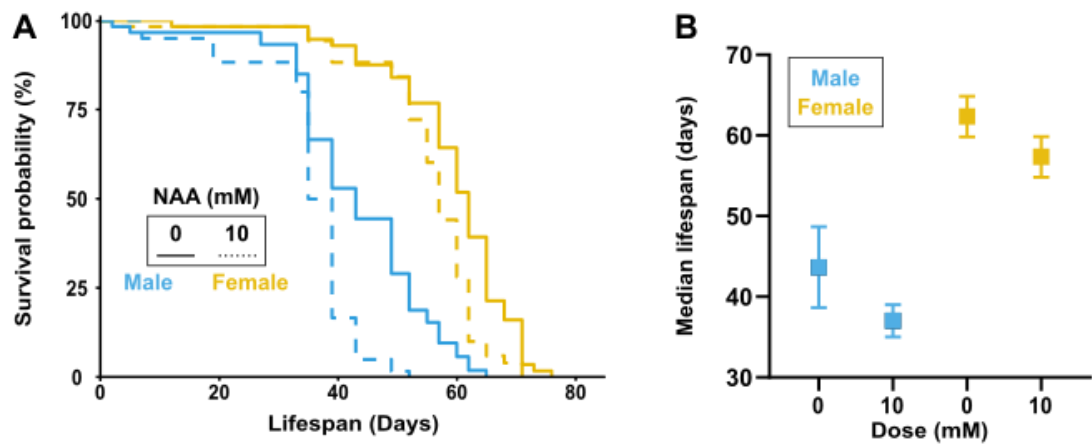
Figure 2.17: Continuous feeding of NAA show comparable results when maintained using the MultiFlipper. All experiments were performed on cohorts of 60 *Vallecas Drosophila* per sex housed 10 per vial. Lifespan when continuously fed of NAA and transferred conventionally (**A**) and median lifespan for each cohort with error bars representing 95% CI of the average median lifespan for all replicate vials (**B**).

2.4 Measuring Midgut Fitness - Frass Quantification

2.4.1 Developing hardware for quantifying frass

A funnel was designed to improve frass quantification assay by acting as an adaptor between a 25 mm diameter housing tube and a petri dish, eliminating the need to anesthetize *Drosophila* when transferring (**Figure 2.18**). Adaptor funnel and the media bowl were designed in Fusion[360] and printed using an Anycubic i3 Mega 3D printer (ANYCUBIC[TM]). Adapter was designed to be either glued or held on top of a petri dish lid using either an elastic band or glue (**Figure 2.18**). To ensure it remains in a place a 14 mm diameter extrusion was designed which would fit within a 15 mm drilled hole within the petri dish hole (**Figure 2.18 C**). The assay was optimised to collect frass output from *Drosophila* over a 24 hr period, and therefore a media bowl was designed to be glued into the petri dish base and to be filled with food, to ensure *Drosophila* have a source of food for the duration of assaying (**Figure 2.18 D**). To use the adaptor funnel, a brief working protocol was developed and optimised by undergraduate student Alex Bartlett, under my supervision.
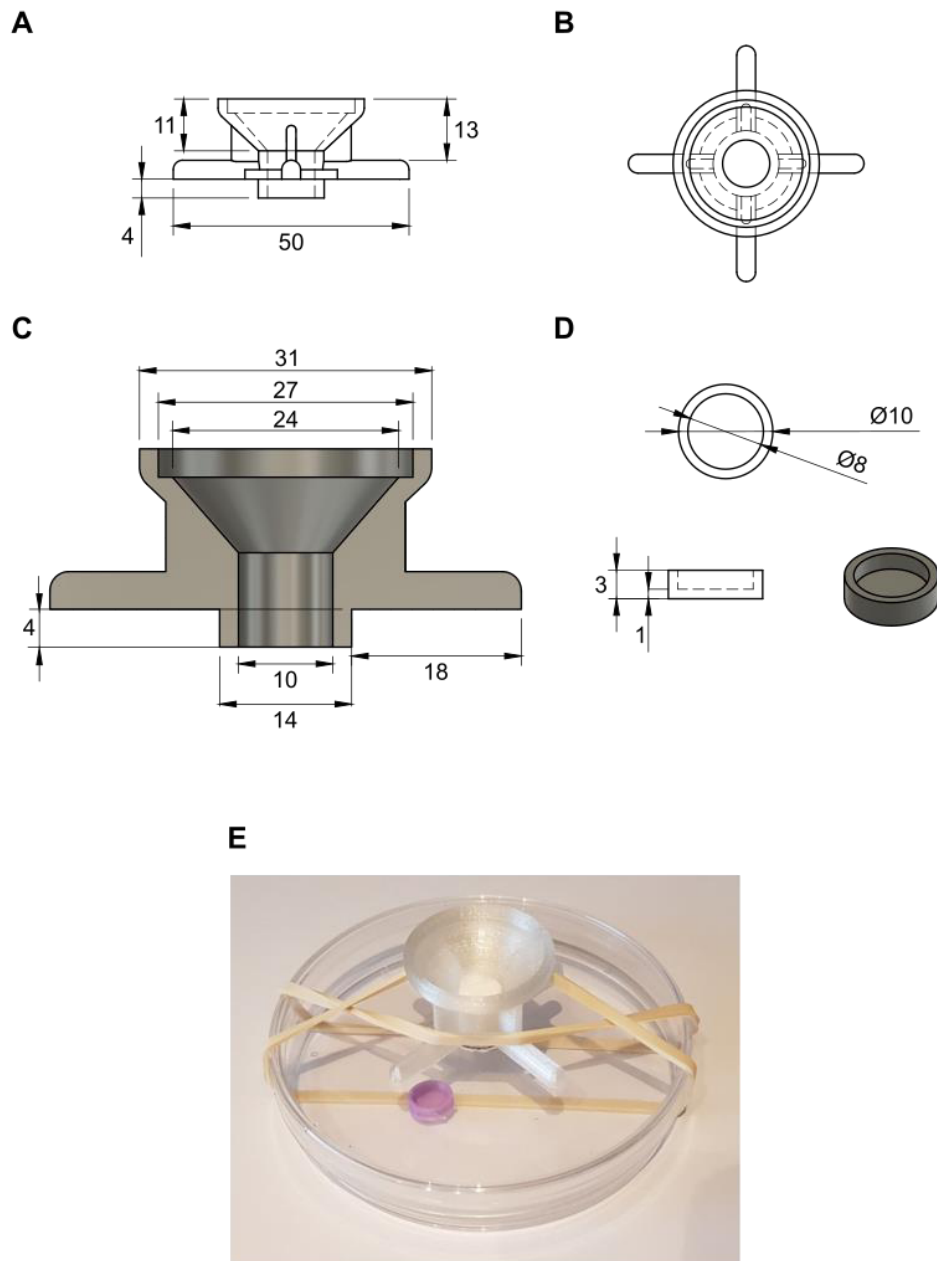
Figure 2.18: Frass assay purpose designed housing chamber. Schematics showing key measurements (mm) of adaptor funnel, media bowl and petri dish. (**A**) Side view of the adaptor funnel. (**B**) top -side view of the adaptor funnel. (**C**) 2:1 Cross-section view of adaptor funnel. (**D**) Key measure measurements of the media bowl. (**E**) Completed set-up of the frass assaying. Designed in Fusion[360] software. Compatible with vials of a 25 mm diameter.

2.4.2 Validation of Modified Frass Assay

Once hardware was optimised and functional, its use was validated to determine that it could be used to reliably give consistent results both internally (within lab) and results that corroborate data published in recent literature. To do so, the quantity of frass produced by both sexes and by young and old *Drosophila* was investigated. As well as the pH composition of frass using the pH indicator BPB.

To measure internal consistency, independent replicates under same experimental conditions were analysed to determine standard deviation and distribution of data (**Figure 2.19 A** & **C**). At day four, males had a mean 24 hr output of 6 frass (SD = 0.62), compared to females 24 hr output of 6 frass (SD = 0.44) (**Figure 2.19 A**). The means were determined not to be significantly different ($p = 0.8492$) via Welch two sample t-test, and data was shown to follow a standard distribution ($p = 0.0674$) via the Shapiro-Wilk test, and had homogeny of variance ($p = 0.6573$) via Bartlett's test. At day 11, males had a mean 24 hr output of 3 frass (SD = 0.58), compared to females 24 hr output of 10 frass (SD = 0.38) and these means were determined to be significantly different ($p = 0.00035$) via Welch two sample t-test (**Figure 2.19 C**). Replicate values from male and female were shown to be derived from a normal distribution via Shapiro-Wilk testing ($p = 0.846$, $p = 0.172$, respectively), and homogeny of variance ($p = 0.6121$) via Bartlett's test. Therefore, within each cohort, replicates showed no significant difference with standard deviations being <1 frass for all treatments, indicating consistency of results and therefore of experimental method. Similar to frass output, there was consistency within cohorts for pH composition of frass. Interestingly the composition of female frass became more acidic with age, whereas male frass pH composition remained the same (**Figure 2.19 B** & **D**).

Five wildtype strains were assayed to determine if the assay was sensitive enough to detect differences in frass composition between strains under the same experimental and physiological conditions (**Figure 2.20**). Strains showed variability in frass output with strain *DGRP-21* having the highest output of 10 frass per 24 hr period, compared to 3 frass for *Oregon R* (**Figure 2.20 A**). Data was determined to be normally distributed via Shapiro-Wilk test ($p > 0.05$), and Multiple t-test was performed to determine which genotypes were significantly different from each other. Regarding pH composition of frass, all strains apart from *Samarkand* had similar composition levels (**Figure 2.20 B**).
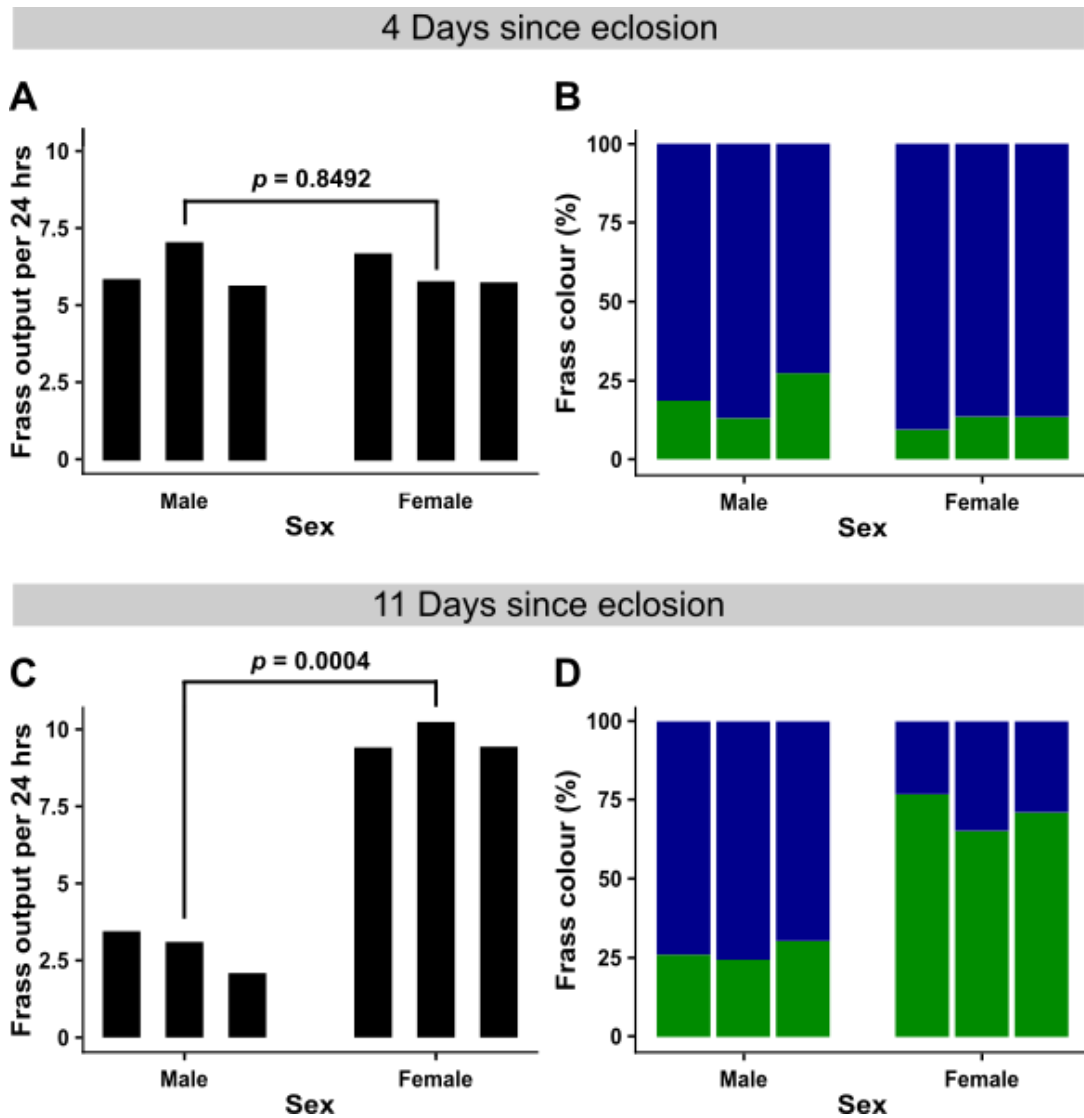
Figure 2.19: Differences in frass output between sexes and with age. (**A**) and (**C**) normalised to per *Drosophila* frass output in 24 hr period. (**B**) and (**D**) percentage (%) of either green (acidic) or blue (basic) frass deposited on petri dishes after *Drosophila* were fed BPB supplemented media. Mated *Drosophila w^1118* were purped and reared at 25 ˚C. Data was acquired from three replicates with each replicate consisting of 30 *Drosophila* per petri dish.
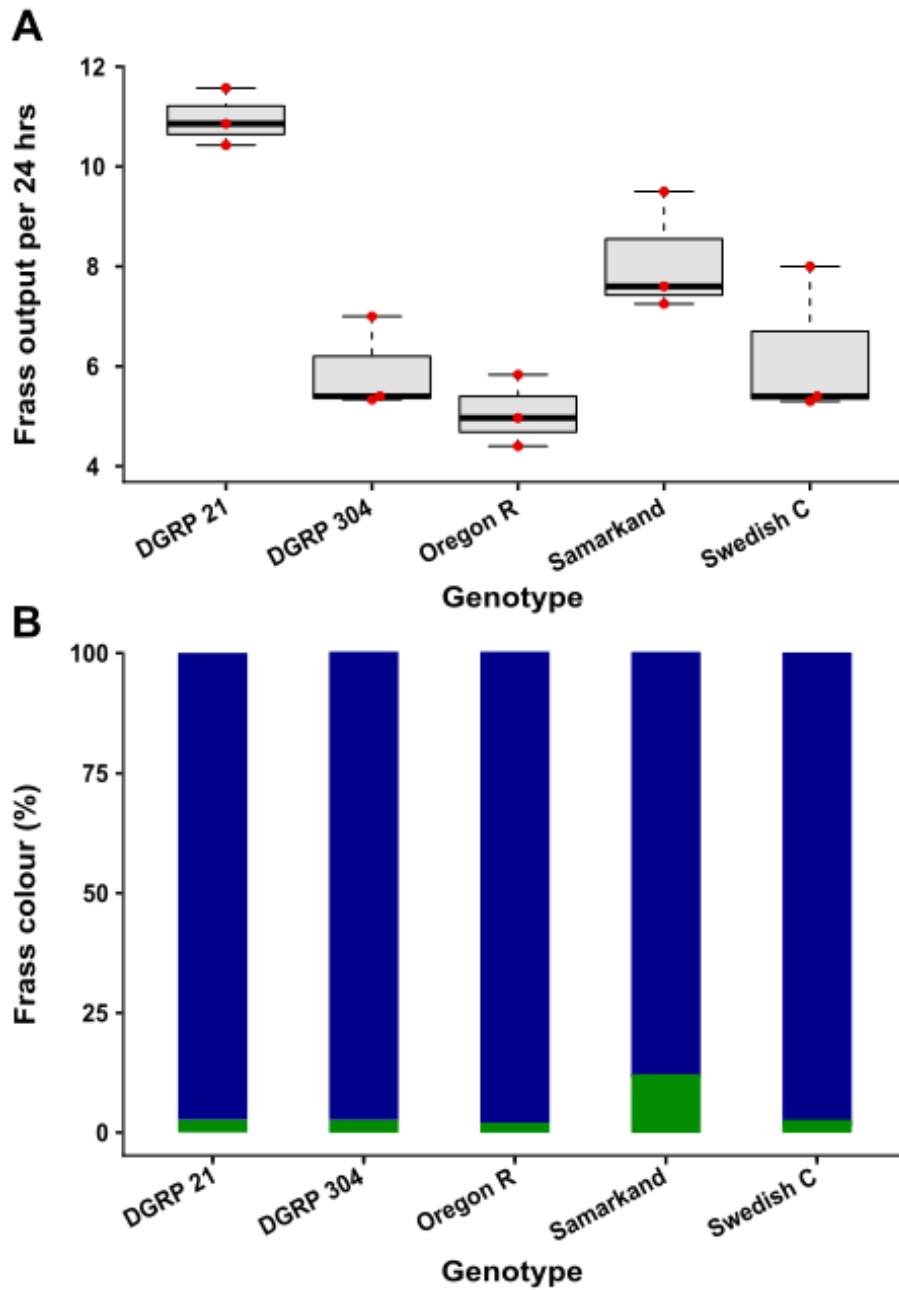
Figure 2.20: Comparison of frass output between WT isogenic strains. (**A**) normalised frass output per *Drosophila* frass in 24 hr period. (**B**) percentage of either green (acidic) or blue (basic) frass. Data was collected from 48 hr mated male *Drosophila* of various genotypes reared at 25 ˚C. Data was acquired from three replicates for each genotype and treatment with each replicate consisting of 30 *Drosophila* per petri dish.

2.5 Discussion

2.5.1 MultiFlipper System

The conventional method of lifespan assaying *Drosophila* is time consuming, repetitive, and not scalable. As stated, I aimed to develop a standardised system to expedite this process.

Components of the MultiFlipper system

The physical components can all be 3D printed and were benchmarked on the commercially available AnyCubic I3 Mega printer (ANYCUBIC^{TM}). The hardware was designed to be ergonomic and its ease of use was confirmed when all participants involved in its testing were able to use it correctly with minimal explanation (**Figure 2.13**). The software was also designed to be easy to use and deployable on all operating systems as a standalone programme. Currently the Lifespan Analyser has been successfully launched on both Windows and Mac operating systems. There has been minimum debugging of the Lifespan Analyser and the software will be published on GitHub, an online repository of software. This platform allows for the community to test, submit, and offer corrections to any software published (Padhye, Mani & Sinha, 2014). Therefore, any anticipated issues or bugs with software are anticipated to be highlighted quickly and corrected.

Effectiveness of the MultiFlipper system

It was decided that in order for the MultiFlipper to be an effective alternative to conventional manual transfer, it would have to (1) reduce time taken maintaining experimental cohorts and (2) its use must not introduce an additional experimental variable. Transfer speed was recorded in a longitudinal experiment in which both novice and intermediate Drosophilists showed significant reductions in accumulated transfer time (**Figure 2.12**). Further, a cohort of 11 participants, with varying levels of *Drosophila* experience, all showed significant reductions in transfer time when using the MultiFlipper (**Figure 2.13**).

Lifespan data generated from the novice and intermediate Drosophilists was analysed to determine if the use of the MultiFlipper was a confounding variable. CoxPH modelling of the novice dataset generated a HR of 1.65 associated with MultiFlipper use (p = 0.0278) (**Figure 2.14**). This HR indicates that *Drosophila* have a higher risk of dying at any timepoint when transferred with the MultiFlipper, relative to conventionally transferred *Drosophila*. This increased risk of death has been associated with excessive banging by the novice during each transfer.

However, the CI associated with HR is large and was attributed to multiple early censoring events. It is anticipated that repeating this experiment would reduce the HR as visual inspection of the curve shows a modest reduction in lifespan (**Figure 2.14 A**). The intermediate Drosophilist who was gentler when transferring experimental cohort, as their experience helped them to better gauge the minimum force necessary to transfer *Drosophila*, produced a dataset which when modelled showed no significant difference in risk associated with MultiFlipper use (p = 0.719).

To further show that excessive banging was the cause of the increased risk associated with MultiFlipper use, the novice dataset was tested for proportional hazards. Schoenfeld residual testing determined that as time went on the risk of dying from MultiFlipper use increased i.e. there was no proportional hazards (p = 9×10^{-4}). This fits with the hypothesis that excessive and accumulated banging was the cause of the *Drosophila* premature deaths – as banging accumulates with each consecutive transfer, risk of dying associated with MultiFlipper use increases. Traumatic brain injury (TBI) occurs when a strong jolt induces damage to the brain, resulting immediate and long-term consequences including ataxia, memory loss and death. Currently in *Drosophila*, TBI can be induced, with detrimental effects on mortality and lifespan, with a single percussive strike (Katzenberger et al., 2013). A dose/strike dependent decrease in lifespan was reported, this corroborates the novice lifespan dataset which violates the proportional hazards assumption.

Continuous feeding of auxins induces changes in lifespan

Currently, the *Drosophila* community is interested in developing alternative tools that give researchers temporal control of transcriptional expression systems. An example of a developing system is the auxin-inducible degradation system (AID) which relies on an exogenous application of auxins to facilitate the degradation of transcription inhibitors (Trost, Blattner & Lehner, 2016; Bence *et al.*, 2017). Depending on the design of a potential experiment, *Drosophila* could be exposed to auxins for days and yet auxin associated toxicity to *Drosophila* has not been fully elucidated. To show that the MultiFlipper system can be used to answer novel and useful scientific hypotheses, the effect of prolonged exposure to two auxins on *Drosophila* lifespan was assayed. The first auxin IAA was tested and repeated for both transfer methods. With unexposed cohorts showing similar lifespans it was decided to combine datasets. CoxPH modelling of the IAA dataset showed that exposure to IAA had no significant effect on lifespan (p = 0.15) for both sexes, indicating that continuous feeding of IAA is not toxic. In addition, proportional hazard

testing determined that the risk of death associated with IAA feeding was independent of time, therefore toxicity did not increase over time, as is typically expected with accumulated exposure to toxins.

 In contrast, continuous feeding of NAA resulted in a reduction in lifespan for both sexes. CoxPH modelling determined that exposure to NAA resulted in a HR of 1.81 (p = 0.003). This relatively high HR indicates that *Drosophila* exposed to NAA die 1.8 times faster than unexposed *Drosophila*. There was also a significant interaction (p = 0.047) between dose and sex – males exposed to NAA showed a greater reduction in lifespan than females (**Figure 2.17 A**). Additionally, median lifespan further demonstrates this trend, male lifespan was reduced by 14% and females 8% (**Figure 2.17 B**). Both dose and the interaction between dose and sex violated the proportional hazard assumption, p = 0.04 & = 0.02, respectively. This indicates that the risk associated with exposure is not independent of time and that NAA toxicity is accumulative.

The MultiFlipper has been successfully used to identify that NAA is toxic and IAA is not, at 10 mM. This is very important because the AID degradation system is still in development, and so future work should be focussed on optimising the system with IAA. It is worth noting that the dose of 10 mM was identified as being a high dose, with reported doses ranging from 0.3 – 1 mM (Trost *et al.*, 2016; Bence *et al.*, 2017). Assuming that NAA toxicity is dose dependent, a lower dose could mitigate lifespan reduction whilst still being functionally effective at transcriptional regulation. Auxin feeding for days is sufficient to induce gene expression, which is not likely to effect lifespan when you consider that feeding for months (**Figure 2.17 A**) results in a modest reduction in lifespan.

2.5.2   Frass quantification

Modification of frass assay to eliminate CO_2 anesthetization

Due to the physiological effects associated with CO_2 exposure, hardware was designed to eliminate the need to anesthetize *Drosophila* when performing frass assays. A funnel was designed that acted as an adaptor between a 25 mm diameter housing tube and a petri dish, allowing for direct transfer of *Drosophila* without the use of CO_2 (**Figure 2.18**). This is important because CO_2-induced premature evacuation of the *Drosophila* rectum could influence results.

Validation of modified assay

Modified hardware was determined to give internal consistency of results via inspection of SD within each cohort. Replicates showed no significant differences, indicating consistency of results and therefore hardware. The sexes showed similar frass output early in adult life which diverged later in life with females producing more frass compared to younger females and males at both timepoints. The literature reports similar findings, and this has been attributed to females requiring more nutrients to support egg production (Cognigni *et al.*, 2011). This increased demand would translate to increased nutrient intake and increased frass output. Therefore, the data produced from using the modified frass assay is internally consistent when comparing replicates and corroborates findings already published.

Further to ensure the suitability of the modified assay for future work, five randomly selected wildtype strains were assayed to determine if the assay was sensitive enough to detect differences in frass composition between strains under the same experimental and physiological conditions (**Figure 3.20**). The observations of inter-strain variability and intra-strain consistency led to concluding that the modified frass assay was suitable for future work.

2.5.3   General Conclusion

The methods developed in this chapter were chosen as they are good measures of overall health of adult *Drosophila*, however there was technical issues associated with their typical execution. For each assay issues were identified, and new methods were developed to overcome those issues. A number of advantages are now conveyed when using the modified methods/protocols which include: 1) reduced manual handling time, 2) reproducibility of results and analysis, 3) elimination of confounding variables and finally all modifications are affordable, simple to implement and accessible to others via 3D printing. These methods were subsequently used to measure their respective phenotypes upon irradiation treatment, this being one of the main aims of my PhD, to characterise the *Drosophila* radiation response. As stated, the radiation response is a highly polygenic trait and to identify the genetic loci associated with this trait would require large quantitative studies, such as GWAS employed by the radiogenomics community. In this chapter I have shown that lifespan assay and frass quantification can be used to detect changes between strain which are closely related.

Chapter 3: Developing a *Drosophila* model for radiation toxicity

3.1 Introduction

In humans, the long-term side effects from radiation exposure are poorly understood, with patients that have received RT developing side effects months to years after initial treatment (Bentzen, 2006; Straub *et al*., 2015). The radiogenomics community currently lacks a preclinical model that has a short lifespan, genetically tractable and affordable to use in large studies (**Section 1.5**). These are all characteristics of *Drosophila*, however the *Drosophila* response to radiation is currently less understood than the human response.

Most *Drosophila* research has focussed on DNA repair mechanisms, and measuring general health metrics such as fertility, survival and movement (**Section 1.6**). Additionally, excluding research demonstrating general health reduction, there has been little work that highlights a chronic response to radiation exposure in *Drosophila*. One study characterised the radiation-induced transcriptome of whole *Drosophila* 20 days *post* treatment (Shrestha et al., 2017). It showed that changes in the transcriptome persist till the last timepoint quantified, however the study did not publish generated genes list nor was gene ontology (GO) analysis performed, making the evaluation of the effects of irradiation difficult. It is not clear what are the underlying mechanisms that are maintaining this chronicity. Trying to understand the aetiological cause of long-term side effects associated with irradiation, is an area of active research for clinicians (Bentzen, 2006).

It is currently thought that in humans the aetiological cause of long-term radiation toxicity is due to persistent perturbations of the redox state in irradiated cells (Azzam, Jay-Gerin & Pain, 2012). However, work has largely been limited to *in vitro* studies due to the difficultly associated with studying reactive oxygen species (ROS), such as their short half-life (Wang *et al*., 2010). *Drosophila* makes for an appealing model due to shared redox biochemistry and genes involved in redox biology (e.g. *superoxide dismutase 1* and *catalase*) being highly conserved between *Drosophila* and humans (Radyuk, Klichko & Orr, 2004).

A *Drosophila* radiation model would be a valuable tool to the radiogenomics community but first the *Drosophila* response to irradiation needs to be better characterised, followed by confirmation that this model is a relevant preclinical system to model human long-term radiation toxicity. Lastly, this model will then be

used to characterise the genetic architecture that governs the radiation response (**Figure 3.1**).
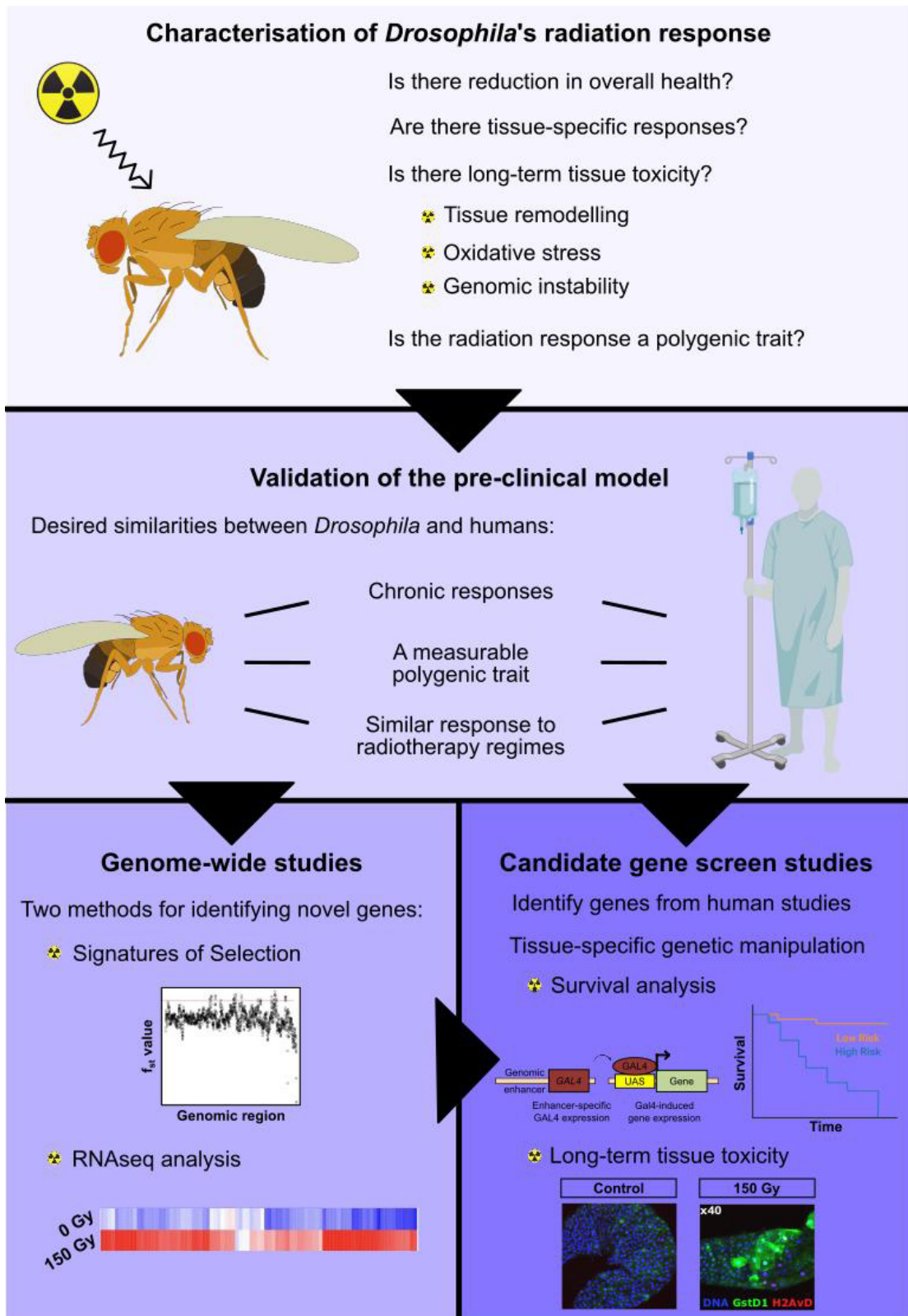
Figure 3.1: Projected workflow of developing a *Drosophila* radiation injury model: from characterisation to novel gene identification and functional analysis.

3.1.1. Aims and objectives

This chapter discusses the development of a novel *Drosophila* long-term model for radiation toxicity and the use of the model to try and elucidate the role of oxidative stress as the aetiological cause of long-term toxicity.

Aim 1 – Develop a *Drosophila* long-term model for radiation-induced toxicity

Objectives:

- Determine dose response for subsequent experimentation.
- Use standard phenotypic measures of health to assess *Drosophila* response to irradiation.
- Identify which tissues are sensitive to radiation treatment.
- Focus on a particular tissue for histological analysis of long-term tissue toxicity.
- Validate the model by exposing *Drosophila* to radiation regimes similar to clinical regimes.

Aim 2 – Use the developed model to explore outstanding research questions within the radiobiology field

Objectives:

- Investigate whether oxidative stress is involved in the radiation response within *Drosophila.*
- Investigate if radiation-induced oxidative stress in *Drosophila* can be recovered through pharmacological intervention.

3.2 Materials and Methods

3.2.1 *Drosophila* strains

All stocks (**Table 3.1**) were maintained at 25°C with a 12 hr:12 hr light:dark photocycle and on standard *Drosophila* cornmeal medium, see **Section 2.2.2** for recipe.

Table 3.1: *Drosophila* stocks used for Chapter 3.

Stock	Source (reference)
*w*¹¹¹⁸	BDSC # 5905
Samarkand	BDSC # 4270
Swedish C	BDSC # 4271
Oregon R	BDSC # 25211
Vallecas	José Félix de Celis
Urbana S	BDSC # 4272
DGRP-21	BDSC # 28122
DGRP-304	BDSC # 25177
w;GstD1::GFP	Marco Milán (FBtp0069371)
w;Viking-GFP	Ernesto Sánchez Herrero (FBal0286155)

3.2.2   Irradiation of *Drosophila*

Drosophila were irradiated using a γ-rays generated from a Caesium[137] source at an estimated dose rate of 0.43 Gy/min, during long irradiation sessions (>4 hr), *Drosophila* were moved within irradiation chamber to ensure homogenous absorbed dose between replicates.

3.2.3   Lifespan assay and analysis

Lifespan assay of *Drosophila* was performed as described in **Section 2.2.5**. Datasets were analysed as described in **Section 2.2.6**.

3.2.4   Starvation assay

Adult *Drosophila* were age synchronised as previously described (Clancy, David & Kennington, 2001; Linford *et al.*, 2013). Upon eclosion *Drosophila* were transferred to fresh rearing media (**Section 2.2.2**) and allowed to mate for 48 hr. Desired *Drosophila* were selected and housed without standard media in rearing vials (25 mm diameter). Strips of filter paper (10 mm X 50 mm) were placed in vials with 500 ml of dH_2O for *Drosophila* to drink. Each vial housed between 10 and 15 *Drosophila* and were periodically checked every 2 – 5 hrs, and number of alive and dead *Drosophila* recorded.

3.2.5   Measuring egg laying capacity and hatching rate

Female *Drosophila* were purped as described in **Section 2.2.5**, allowed to mate for 48 hr and irradiated (150 Gy). They were reared on apple juice agar plates with additional yeast paste (~1 ml). *Drosophila* were transferred to fresh plates daily, and the old plates were counted for number of eggs. Plates containing eggs were kept for a maximum of seven days and hatching rates were measured. Number of individuals left alive in each replicate were recorded daily to normalise egg counts per female.

To measure male fertility, male *Drosophila* were irradiated and allowed to mate with non-irradiated virgin females for 48 hr. Plates were collected before, during and after mating, with plates kept for a maximum of seven days to measure hatching rates. Normality was tested using Shapiro-Wilks' test, followed by Student's T-test.

3.2.6   Weight measurements

To measure whole-body wet-weight, *Drosophila* were anaesthetised with CO_2, transferred to weighing boats and weighed using a MS Semi-Micro Balance (Mettler Toledo) in groups of 30. To measure whole-body dry-weight, sachets of silica crystals were heated up for 5 min using a microwave to evaporate any accumulated

moisture. CO_2 anaesthetised *Drosophila* were placed into small 200 ml glass beakers and heated sachets placed gently on top with tinfoil used to close the beaker. *Drosophila* were desiccated for at least 24 hr and weighed.

3.2.7 Dissection, immunohistofluoresence and imaging of *Drosophila*

Tissues were dissected in ice-cold PBS, dissection sessions lasting no longer than 8 minutes. Tissues were fixed in a formaldehyde (3.7%) and covered with an equal volume of heptane for 15 min whilst rocking. Formaldehyde was replaced with methanol (100%) for a further 15 min to permeabilise tissue and was washed with PBS containing 0.1% Triton-X100 (PBT). Blocking consisted of 3x rinses and 3x 15-minute washes in PBT containing 2% bovine serum albumin (BSA). Tissue was stained with primary antibodies overnight (~16 hr) at 4°C with mild rocking (**Table 3.2**), followed by 15 min washing in PBT (3x rinses and 3x washes). Tissue was stained with secondary antibodies for 2 hr at room temperature with mild rocking (**Table 3.3**). DNA was stained with Hoescht 33342 (Sigma Aldrich, B2261) at 1:10,000 (10 μg/ml) which was added alongside secondary antibodies. Tissue was washed as before and mounted in home-made mounting medium (Glycerol: PBS 80:20 with added propyl gallate 4%).

Images were obtained with a Zeiss LSM 710, and unless stated otherwise, using an EC Plan-Neofluar 40x oil immersion objective (numerical aperture 1.3). All midgut images were acquired from the posterior midgut and in practice three positions were imaged for each replicate.

Table 3.2: Primary antibodies used for Chapter 3.

Antigen	Host/type	Dilution	Source (reference)
GFP	Chicken/Polyclonal	1:3000	Abcam (ab13970)
RFP	Rabbit/Polyclonal	1:500	Takara (632496)
Armadillo	Mouse/Monoclonal	1:50	DSHB (N2 7A1)
γpH2AvD	Rabbit/Polyclonal	1:200	Rockland (pS137)
Delta	Mouse/Monoclonal	1:100	DSHB (C594.9B)
Prospero	Mouse/Monoclonal	1:200	DSHB (MR1A)

Table 3.3: Secondary antibodies used for Chapter 3. All were used at a working dilution of 1:500. All secondary antibodies were purchased from Sigma-Aldrich.

Host	Species reactivity	Alexa fluorophores (reference)
Donkey	Rabbit	594 (A21207)
	Mouse	594 (A21203)
Goat	Rabbit	488 (A11032), 633 (A21071)
	Chicken	488 (A11042), 633 (A21103)
	Mouse	633 (A21052)

3.2.8 Paraffin sectioning and immunohistofluoresence of whole *Drosophila*

Whole *Drosophila* were fixed in Carnoy's solution (absolute ethanol, chloroform and glacial acetic acid, 6:3:1), at 4°C for 6 hr with mild rocking. Carnoy's was washed with PBS (3x rinses and washes) and samples were placed in PBS agar (1%). Agar blocks containing samples were pre-treated with ethanol (70%) for at least 2 hr prior to paraffin embedding and sectioning which were performed by Cardiff University Histology Unit using a cryostat microtome (Leica CM1900) at a thickness of 5 μm.

Sectioned tissue needed to be de-paraffinised before staining, this involved a series of progressive washes – two washes in xylene (5 min each), absolute ethanol (3 min), 95% ethanol (1 min), 80% ethanol (1 min), and a final antigen retrieval using citrate buffer (citric acid 10 mM, Tween 0.05%, pH 6) for 20 min at 95-98°C. Sections were blocked for 30 min using PBT:BSA 2%. Primary and secondary staining was performed as described in **Section 3.2.7**.

3.2.9 Image analysis

All quantitative image analyses were performed using Python 3.9.1 with the following modules [version] being extensively used: matplotlib [3.3.2], numpy [1.19.5], openpyxl [3.0.6], pandas [1.1.5], scikit-image [0.17.2], scipy [1.5.2], statsmodels [0.12.1], xlrd [2.0.1] and XlsxWriter [1.3.7].

Automated estimation of cell density via Delaunay's triangulation

To quantify cell density of midgut tissue, the centroid pixel of each nucleus needed to be identified. Nuclei were segmented by generating a maximum projection in the 405 nm channel which was binarized using an Otsu threshold, and small objects removed via an arbitrary size threshold of 10 pixels. Then a watershed was applied to separate nuclei that shared a border, followed by identification of centroid location for each nucleus.

Delaunay's triangulation was used on the centroid coordinate set to determine the vertices between nuclei and their neighbours. These vertices were then filtered to generate a convex hull of the tissue which was used to determine the size of the tissue in pixels, which was subsequently converted to microns through using image stack metadata. Tissue density was determined by dividing number of centroids by convex hull area, and number of cells per 10 μm^2 was decided as being a convenient quantification (**Appendix 4**).

Determining cell closeness with 3D coordinates and Euclidean calculations

XYZ coordinates for each nuclei were determined via identifying centroid pixels on the global XY and local XZ maximum projections. First XY projections were binarized using an Otsu threshold and small objects removed via an arbitrary size threshold of 10 pixels. A watershed was applied to separate nuclei that shared a border, followed by, for all nuclei, the generation of nuclear-spanning bounding box and identification of centroid location. To identify the nuclear centroid on the Z axis, the XY bounding box for each nucleus was used to crop the original stack and a XZ maximum projection in the 405 channel was generated. This XZ projection was processed as described above (Otsu threshold, size threshold, watershed), it was assumed that the biggest object in this cropped projection was the nucleus of interest, and its Z position was recorded. Finally, each cell's absolute distance to all other cells within a tissue was calculated by accounting for XYZ coordinates and using the Euclidean calculation for 3D coordinates ($d = \sqrt{(x_1 - x_0)^2 + (y_1 - y_0)^2 + (z_1 - z_0)^2}$). For each cell, its closeness to all other nuclei was ordered (closest to furthest), and the average distance from five closest neighbours was determined (**Appendix 4**).

3.2.10 Movement assaying

Assay

Rapid iterative negative geotaxis (RING) assay was performed to assess perturbations in movement associated with radiation treatment. RING assay was performed following standard practice (Nichols, Becnel & Pandey, 2012).

Data manipulation

Videos were recorded using a Galaxy S8 mobile telephone (4032x2268 pixels), and were converted into Audio Video Interleave (AVI) format using the freely available ffmpeg command line software. To improve subsequent software performance during analysis, sound was removed and number of frames per second (fps) were limited to 30, reducing overall video size.

Data analysis

Videos were analysed in ImageJ to measure height reached for each *Drosophila* for each second after banging. Both X and Y coordinates (pixels) were recorded and converted into true distance (mm). Euclidean calculations were used to determine absolute distance traversed for each *Drosophila* at each second, similar to

calculations used when cell distances were determined within confocal stacks (**Section 3.2.9**).

Statistical analysis

Two metrics were analysed: total distance travelled after 10 seconds and velocity. Regarding distance travelled after 10 seconds, T-tests were performed and normality checked using Shapiro-Wilks test. Velocity datasets were determined to be non-normally distributed, therefore Man-Whitney U testing was performed taking into account of both irradiation status and time since irradiation.

3.2.11 Frass assay

Frass assay was performed as described in **Section 2.2.7**.

3.2.12 Statistical Analysis

All statistical analyses were performed using either R [4.0.2] or Python [version 3.6], and each analysis has been explicitly specified for each dataset.

Time-to-event tests

Statistical analysis of lifespan and survival datasets was performed as described in **Section 2.2.6**.

Analysis of variance

The normality of datasets was assessed using the Shapiro-Wilks test. For normally distributed datasets, parametric testing was performed using either T-test (N<15) or ANOVA (N>15). For non-normally distributed datasets, the non-parametric Wilcoxon signed-rank testing was performed. If an independent variable had >2 levels multiple comparison testing was performed using the Tukey's test.

3.3 Overall effects on health from lethal radiation exposure

First, I wanted to determine the optimum dose of radiation required to irradiate *Drosophila* for subsequent experimentation. The criteria for an optimum dose was one that significantly reduced lifespan but allowed *Drosophila* to survive long enough to study any potential long-term side effects. To do this, three doses of 50, 100 and 150 Gy were studied on different *Drosophila* strains and sexes. Once optimum conditions and variables were identified, work to characterise *Drosophila* response to radiation exposure began, which included assaying various phenotypes with emphasis on midgut functioning.

3.3.1 Dose effect of irradiation on *Drosophila*
Radiation treatment reduces survival of males

The effect of various dosages on the lifespan of adult w^{1118} *Drosophila* for both sexes was assayed (**Figure 3.2**). Within the dose range assayed, females did not show a dose dependent response to radiation exposure. The smaller dosages of 50 and 100 Gy showed similar survival curves to the non-irradiated control arm. The largest dose of 150 Gy showed an increase in survival when compared to control (**Figure 3.2 A** & **C**). In contrast, males showed a dose dependent response to radiation exposure with each larger dose further reducing survival compared to control (**Figure 3.2 B** & **D**).

A CoxPH model was generated with the explanatory variables: dose, sex and a potential interaction of both (**Figure 3.2 E**). Dose was determined to be a significant modulator of survival, however, the associated HR of 0.993 (0.991–0.995, 95% CI) was close to 1 ($p = 1.56 \times 10^{-9}$) meaning little difference in survival odds between cohorts. Sex was determined be a significant modulator of lifespan with males having an associated HR of 0.075 (0.051–0.109, 95% CI) indicating longer lifespan irrespective of treatment ($p = 2 \times 10^{-16}$). An interaction between sex:male and dose was identified as being significant with a HR of 1.020 (1.016-1.024, 95% CI) indicating reduced survival for exposed males ($p = 2 \times 10^{-16}$). Testing for proportional hazards that are independent of time determined that dose did not violate proportional hazards assumption ($p = 0.397$). Whereas sex and an interaction between sex and dose did violate proportional hazards assumption ($p = 0.0004$ & = 0.001 respectively). The violation of the proportional hazard assumption means the model is invalid, possibly due to the opposing directional effect of dose between the sexes.

Radiation treatment induces systemic midgut DNA damage

Since radiation treatment is known to induce DNA damage (**Section 1.6.1**), it was investigated whether the levels of DNA damage were also dosage-dependent. This was performed by quantifying the levels of phosphorylated histone 2 - γH2AvD (H2AvD) which is phosphorylated by *ATM* when a DSB are detected (Redon et al., 2002). Dose dependent changes were also observed at the DNA level with persistent DNA damage (H2AvD staining) occurring in female midguts 7 days *post* irradiation (**Figure 3.3**). There was a positive correlation between increased dose and increased H2AvD signal per nuclei (**Figure 3.3 A**). ANOVA testing determined that H2AvD intensity was dependent on the dose received ($p = 2X10^{-16}$). Nuclei from non-irradiated midguts had significantly less H2AvD intensity than irradiated nuclei (150 Gy) (**Figure 3.3 B**).

From the doses tested, 150 Gy was sufficient to induce significant changes in survival for both sexes. However, females appear to have a complex response to irradiation as evident by the lack of dosage response and positive effect of radiation on survival, possibly an indication of an interaction between fertility, lifespan and treatment.
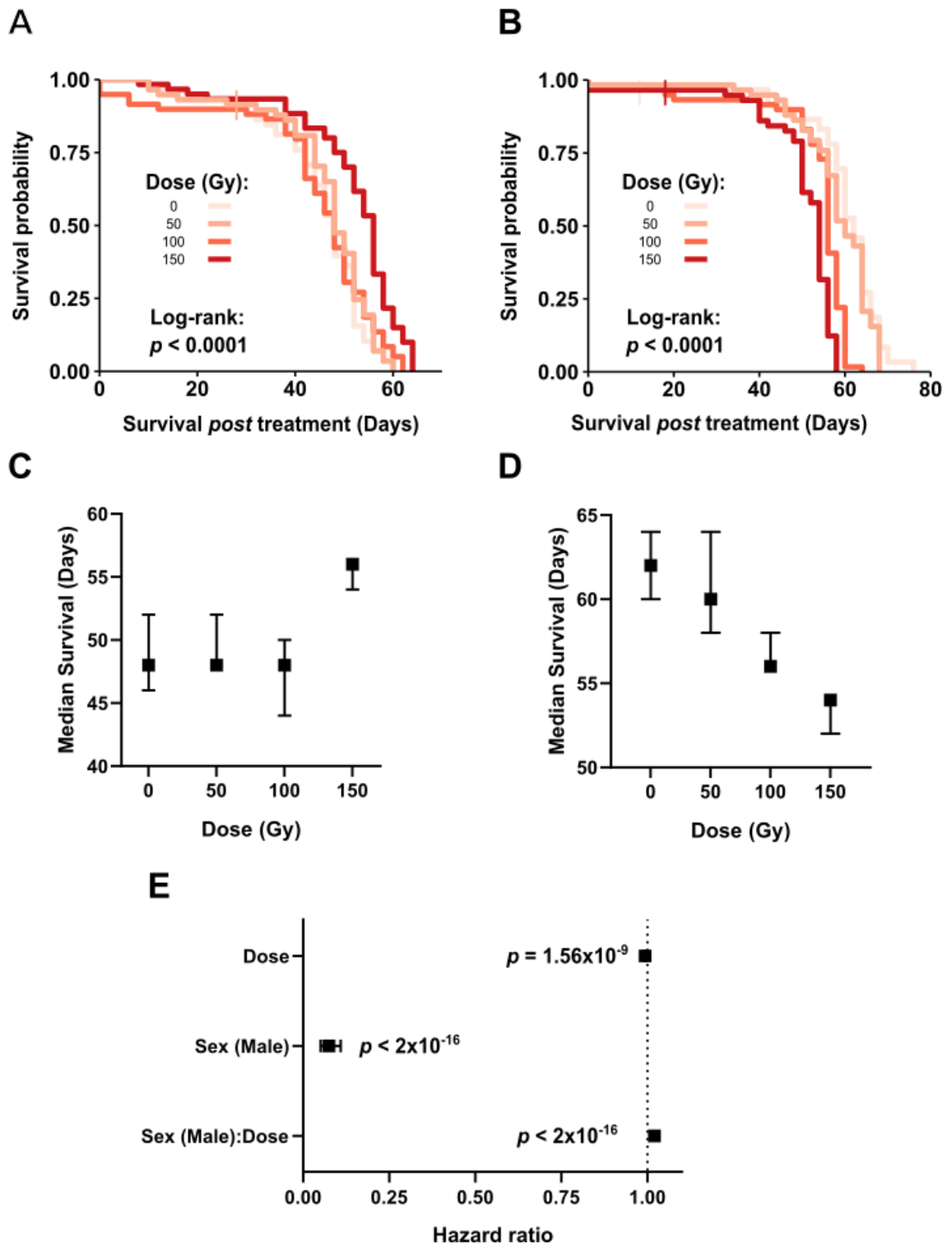
Figure 3.2: Dosage dependent changes in survival associated with radiation exposure in adult male and female *w^1118* Drosophila. (**A**) and (**B**) are KM curves for females and males, respectively. For KM curves a pipe **I** represents censored *Drosophila*. (**C**) and (**D**) median survival from each technical replicate (vial) for various dosages for females and males, respectively. Error bars representing 95% CI, *N* = 240 with 60 *Drosophila* in each arm. (**E**) combined CoxPH model for both female and male datasets.
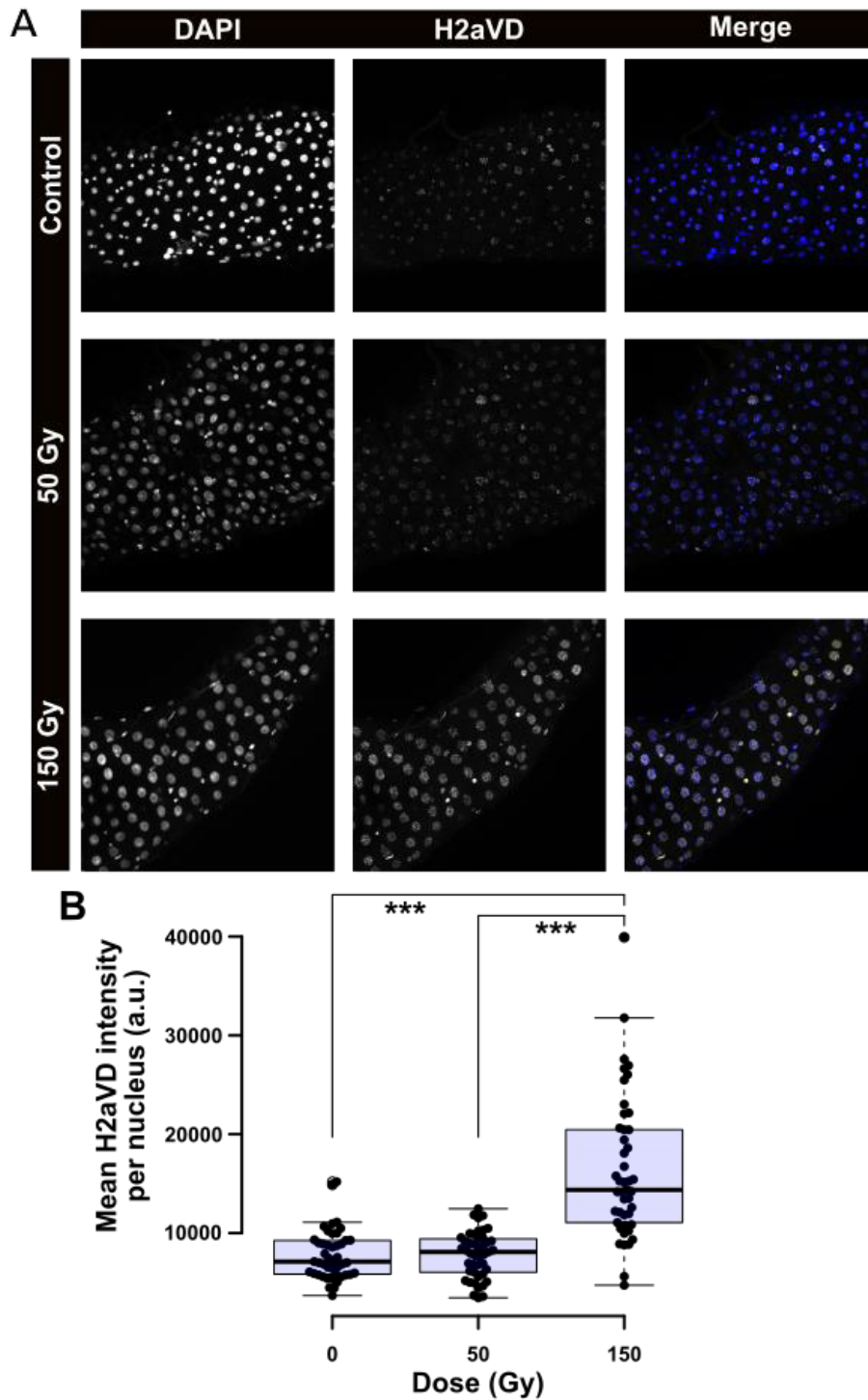
Figure 3.3: Dosage dependent changes in H2AvD levels within midguts of adult female w^{1118}. (**A**) representative maximum projections of confocal images, $n = 3 - 5$ midguts per dose and each midgut was imaged in three random locations. (**B**) nuclei were manually counted and H2AvD measured using ImageJ and ANOVA was performed followed by Tukey's multiple comparison testing. Boxes represent SD and whiskers minimum and maximum values range. *Drosophila* were exposed to radiation and kept at standard rearing condition for 7 days prior to dissection of midgut.

3.3.2   Reduced survival associated with radiation treatment

Since w^{1118} males and females responded differently to radiation treatment, the strain *Oregon R* was assayed to determine its radio-response and to verify if males are more sensitive to treatment (150 Gy), as observed in w^{1118} strain (**Section 3.3.1: Figure 3.2**). Young (<2 days *post* eclosion) *Oregon R* males were determined to be radio-sensitive, and females were radio-resistant supporting results obtained using w^{1118} strain (**Figure 3.4**). Irrespective of radiation treatment, females had a reduced lifespan compared to males. Treatment reduced survival for both sexes but led to a greater reduction in males (**Figure 3.4 A** & **B**).

A CoxPH model was generated with the explanatory variables: replicate, dose, sex and a potential interaction between dose and sex (**Figure 3.4 C**). Both replicate and dose were determined to be not significant (p = 0.96 and 0.51, respectively). Sex variable was a significant modulator of survival (p < 0.0001) with a HR of 0.2292 (0.1345–0.3905, 95% CI) indicating better survival for males (p = 6×10^{-8}). An interaction between sex and dose was identified as being significant with a HR of 1.0094 (1.0028-1.0162, 95% CI) indicating reduced survival for exposed males (p = 0.005), though the HR was close to 1. Testing for proportional hazards that are independent of time determined that sex and dose did not violate proportional hazards assumption (p = 0.0562, and p = 0.9343, respectively). Whereas replicate and interaction between sex and dose did violate proportional hazards assumption (p = 0.0252 & = 0.0103, respectively), similar to modelling performed on w^{1118} survival data in previous section.

Multiple WT strains were given a dose of 150 Gy and lifespan survival assayed to characterise their strain specific responses. It was determined that WT strains with distinct genetic backgrounds had varying reductions in survival associated with radiation treatment (**Figure 3.5**).

Oregon R

As described previously, *Oregon R* were radio-sensitive with exposure sufficient to reduce survival (**Figure 3.5 A** & **D**). A CoxPH model was generated with the explanatory variables of dose and replicate. Dose was determined to be a significant (p = 0.003) modulator of survival with a modest HR of 1.009 (1.0033-1.016, 95% CI) (**Figure 3.5 A'**). Proportional hazard assumption was met for both dose and replicate (p = 0.3438, and p = 0.439, respectively).

Samarkand

Samarkand were extremely radio-senstive with control average median survival of 76 days (69-76, CI 95%) and irradiated cohort of 49 days (49-49 days, 95% CI) (**Figure 3.5 B** & **D**). A CoxPH model was generated with the explanatory variables of dose and replicate. Dose was determined to be a significant ($p = 7 \times 10^{-7}$) modulator of survival with a HR of 1.02 (1.013-1.027, 95% CI) (**Figure 3.5 B'**). Proportional hazard assumption was met for both dose and replicate ($p = 0.5168$, and $p = 0.6492$, respectively).

Swedish C

Swedish C were radio-tolerant with exposure increasing survival, control cohort average median survival was 35 days (35-42 days, 95% CI) and irradiated cohort was 41 days (38-41 days, 95% CI) (**Figure 3.5 C** & **D**). A CoxPH model was generated with the explanatory variables of dose and replicate. Dose was determined to be a non-significant modulator of survival ($p = 0.076$) (**Figure 3.5 C'**). Proportional hazard assumption was met for both dose and replicate ($p = 0.6036$, and $p = 0.5366$, respectively).

Together these data demonstrate that the radiation response of *Drosophila* is not only sex but also genotype dependent, indicating that the radiation response in *Drosophila* is likely to be a polygenic trait as it is with humans. To definitively test whether it is a polygenic trait an experiment in which a radiosensitive and radioresistant strain would be crossed together and the radiation survival of progeny assayed. If the progeny displayed an intermediate survival then it would further indicate that the radiation response is polygenic.
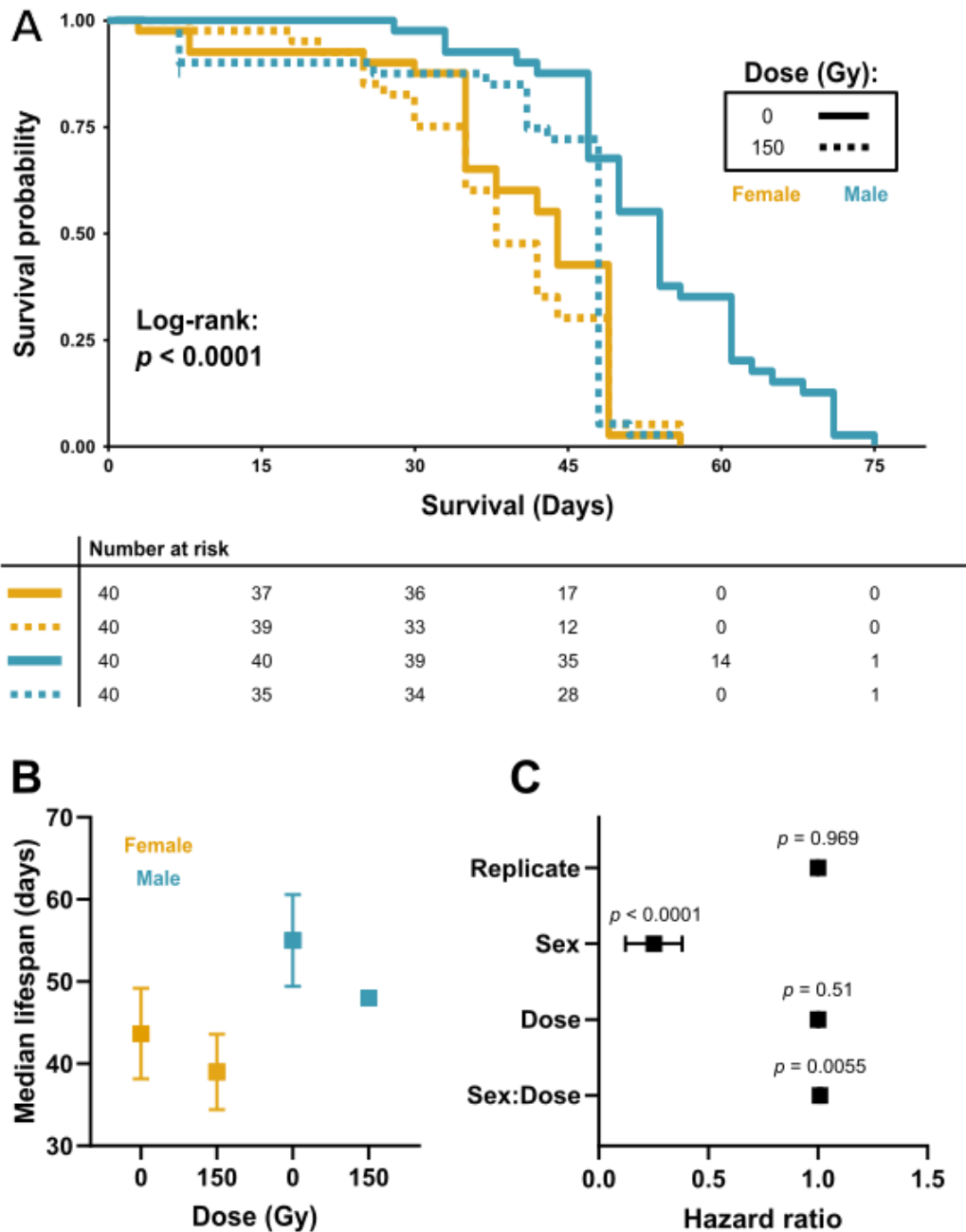
Figure 3.4: Sexual dimorphic response of *Oregon R* to radiation treatment. *Drosophila* were purped and mated for 48 hr prior to irradiation (150 Gy). **A** KM curves with risk table. **B** median lifespan from each technical replicate (vial) of each cohort with error bars representing 95% CI. **C** CoxPH model forest plot. *N* = 160 with 40 *Drosophila* in each arm.
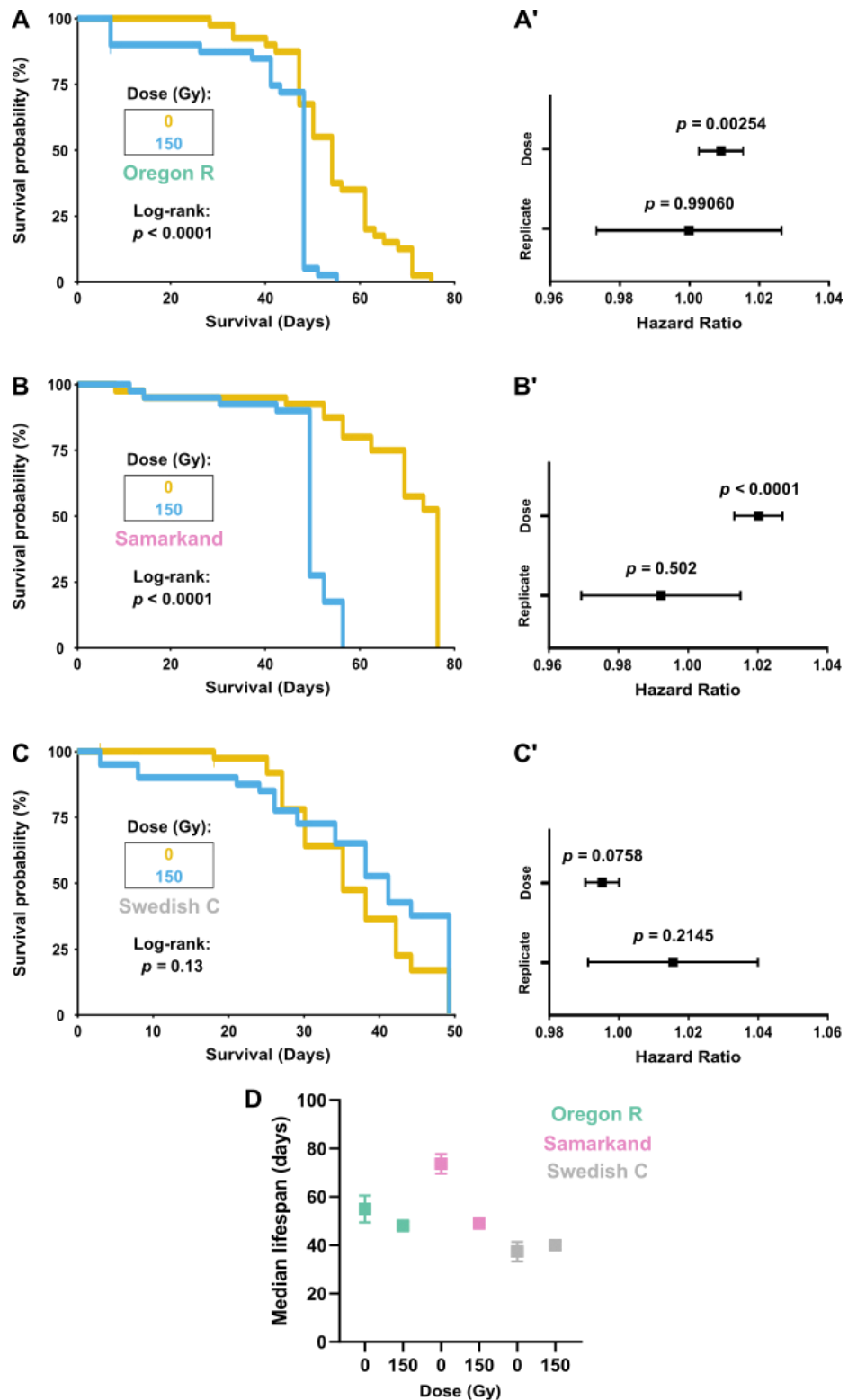
Figure 3.5: Distinct wildtype strains respond differently to radiation treatment. *Drosophila* males were purped and mated for 48 hr prior to irradiation (150 Gy). (**A**) *Oregon R* - KM curves with risk table. (**A'**) *Oregon R* CoxPH model (data derived from **Figure 3.4**). (**B**) *Samarkand* - KM curves with risk table. (**B'**) *Samarkand* – CoxPH model. (**C**) *Swedish C* – KM curves with risk table. (**C'**) *Swedish C* – CoxPH model. (**D**) median survival from each technical replicate (vial) of each cohort with error bars representing 95% CI.

3.3.3 Reduction of fertility associated with sub-lethal dosages of radiation

Reduction in survival *post* irradiation was observed in males of radio-sensitive strains, such as *Oregon R* and *Samarkand.* Hence, *Oregon R* was chosen for further analysis of other general measures of health in response to radiation treatment, such as fertility. There is strong evidence that radiation treatment drastically reduces fertility in humans (Lushbaugh & Casarett, 1976; Ash, 2014; Paithankar *et al.*, 2017). Two methods were used to quantifying fertility of *Drosophila* in both sexes: egg production and hatching rate. The working hypothesis was that fertility was reduced by radiation treatment and that both females and males were affected by treatment.

Female fertility

Female *Oregon R* had reduced fertility *post* radiation treatment (**Figure 3.6**). Overall egg production rate was significantly reduced in irradiated females when compared to the control cohort, 6 and 20 eggs produced per day, respectively (**Figure 3.6 A**). These means were determined to be significantly different (p = 0.0028, Welch two sample T-test) and data was shown to be normally distributed (p = 0.09916). Over the course of 6 days *post* irradiation, the control cohort had a peak in egg production three days *post* treatment which was 29 eggs, whereas the irradiated cohort had an earlier peak in egg production at two days *post* irradiation which was 18 eggs (**Figure 3.6 B**).

Overall hatching rate of eggs produced by irradiated females was reduced compared to control cohort, 8.7% and 84.4%, respectively. Hatching rate dataset was non-normally distributed percentage data (p < 0.0001), therefore a Kolmogorov-Smirnov test was performed which does not assume normal distribution. Hatching rate was determined to be significantly higher for control cohort (p = 0.0003) (**Figure 3.6 C**). Over the course of 6 days *post* irradiation, the control cohort had a peak in hatching rate of 77% at 3 days *post* treatment and the irradiated cohort had an earlier peak of 28% at one day *post* treatment (**Figure 3.6 D**).

Male fertility

Male *Oregon R* had reduced fertility *post* radiation treatment (**Figure 3.7**). Overall egg production rate was similar for females mated with irradiated males as compared to mating with non-irradiated males with 26 eggs produced per day by each cohort (**Figure 3.7 A**) (p = 0.7143, Welch two sample T-test). Over the course

of 8 days *post* irradiation, the control cohort had a peak in egg production at five days *post* treatment which was 46 eggs, whereas the irradiated cohort had a peak in egg production at 8 days which was 52 eggs per day (**Figure 3.7 B**).

Overall hatching rate of eggs produced by mating females with irradiated males was reduced compared to non-irradiated cohort, <1% and 56%, respectively (**Figure 3.7 C**). This dataset was not normally distributed ($p < 0.0001$, Shapiro-Wilks test), therefore a Kolmogorov-Smirnov test was performed which determined a significant difference in hatching rate between treatments ($p = 0.0017$) (**Figure 3.7 C**). Over the course of 8 days *post* irradiation, the control cohort had a peak in hatching rate of 84% at four days *post* treatment and the irradiated cohort had an earlier peak of 1.3% at one day *post* treatment (**Figure 3.7 D**).

These data clearly demonstrate that radiation treatment had a detrimental effect on the fertility of both male and female *Drosophila* which agrees with previous research done in *Drosophila* (Yushkova, 2019).
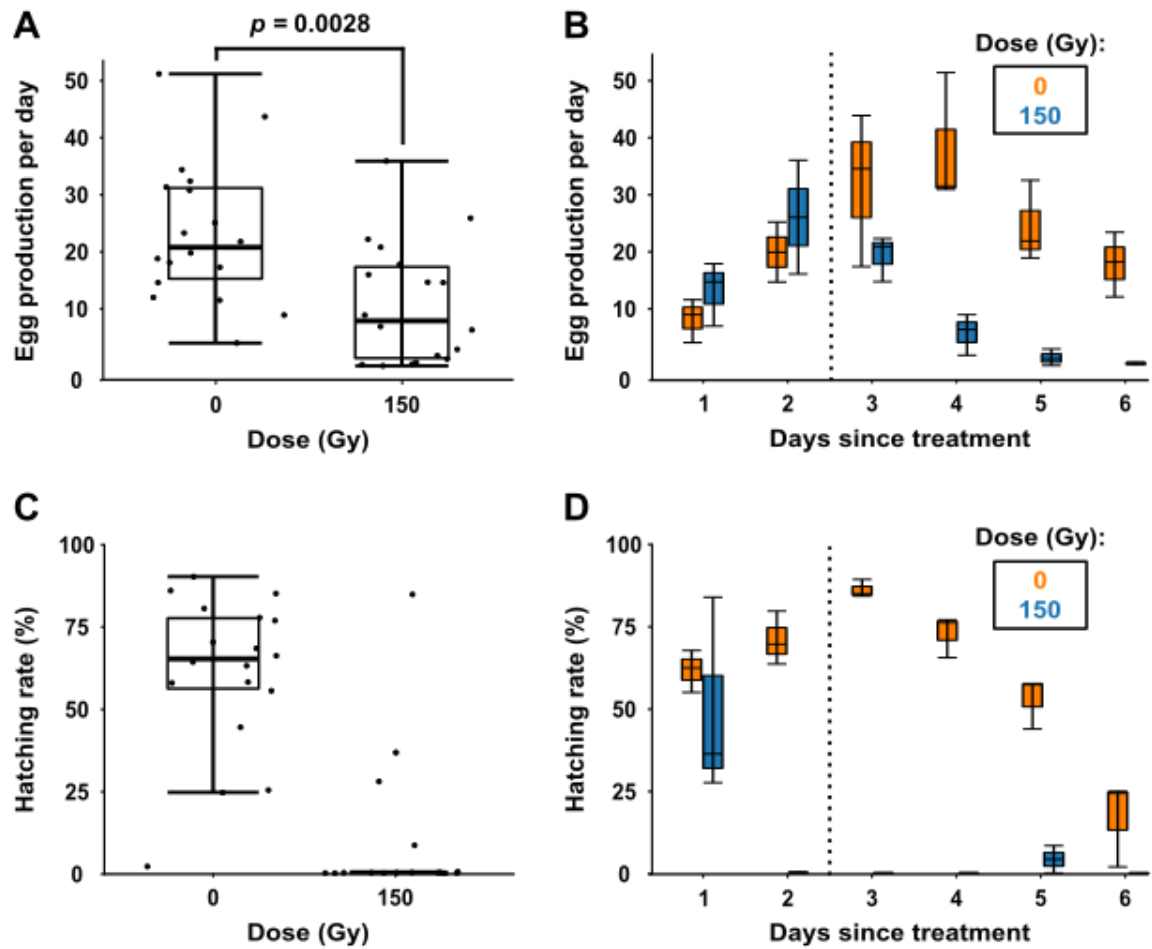
Figure 3.6: Adult females exposed to radiation showed reduced fertility. Virgin *Oregon R* females were irradiated (150 Gy) and allowed to mate with virgin males. (**A**) Average egg production normalised per female with T-test performed. (**B**) Average egg production per female per day, and males (non-irradiated) were removed 2 days *post* irradiation (⋯). (**C**) Average hatching rate (%) of eggs. (**D**) Average hatching rate of eggs per female per day, and males (non-irradiated) were removed 2 days *post* irradiation (⋯).
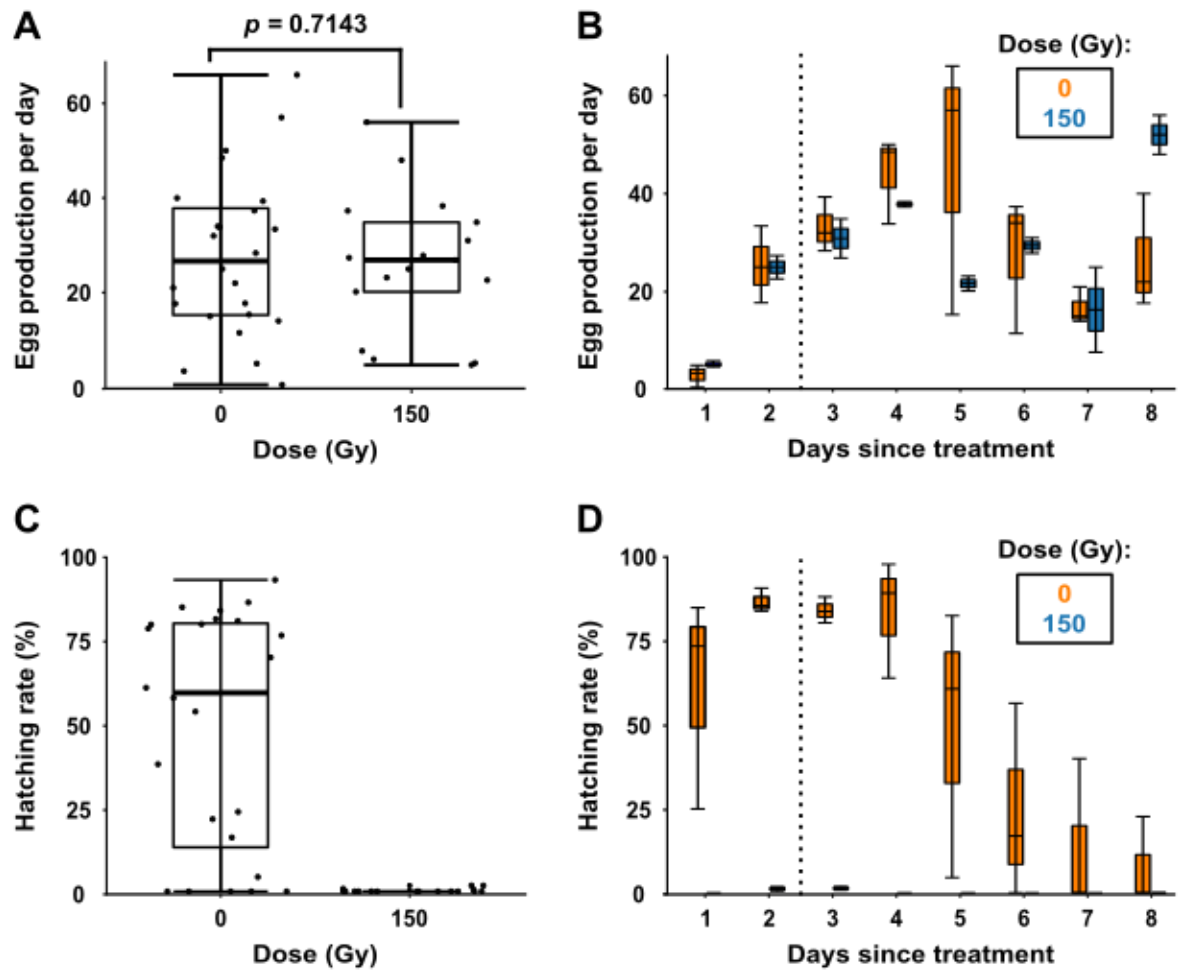
Figure 3.7: Adult males exposed to radiation showed reduced fertility. Virgin *Oregon R* males were irradiated (150 Gy) and allowed to mate with virgin females. (**A**) Average egg production normalised per female with t-test performed. (**B**) Average egg production per female per day, and males (irradiated and non-irradiated) were removed 2 days *post* irradiation (⋯). (**C**) Average hatching rate (%) of eggs. (**D**) Average hatching rate of eggs per female per day, and males (irradiated and non-irradiated) were removed 2 days *post* irradiation (⋯).

75

3.3.4 Long-term movement impairment due to radiation treatment

In addition to the negative impact on fertility, patients receiving RT to treat central nervous system malignancies can develop long-term symptoms of a neurological cognitive nature (Duffner *et al.*, 1985; Sudmeier *et al.*, 2015). In *Drosophila*, it has been shown that irradiation of larval developmental stages such as larval stages leads to long-term side effects such as movement deficiencies (Sudmeier *et al.*, 2015). However, it is unknown whether irradiation of young adults leads to long-term side effects. To determine if adult *Drosophila* develop long-term movement deficiencies *post* irradiation, RING assay was performed measuring multiple movement related metrics. Male w^{1118} were assayed, and two metrics were analysed from the dataset – distance travelled (**Figure 3.8**) and velocity (**Figure 3.9**).

At one day *post* irradiation (200 Gy), irradiated males at each second after stimulation travelled further than the non-irradiated males (**Figure 3.8 A**). The greatest difference was observed 10 seconds after stimulus however this difference in distance travelled was not significant between irradiated males (44.5 mm at 10 secs) and non-irradiated males (44 mm at 10 secs) (T-test, $p = 0.604$) (**Figure 3.8 B**). At 20 days *post* treatment, non-irradiated males consistently travelled further than the irradiated males (**Figure 3.8 C**). At 10 seconds after stimulus, there was significant difference between treatments, with irradiated males (46 mm at 10 secs) travelling the least distance than non-irradiated males (70 mm at 10 secs) ($p = 0.008$, Man-Whitney U test) (**Figure 3.8 D**).

Regarding changes in velocity one day *post* treatment, the velocity of irradiated males was slightly greater than non-irradiated males (**Figure 3.9 A**). The initial velocity (mm/sec at 2 seconds after stimulus) was compared between treatments, and the velocity for irradiated males (3.4 mm/sec) was not significantly faster than non-irradiated males (2.7 mm/sec) ($p = 0.15$, Man-Whitney U test) (**Figure 3.9 B**). At 20 days *post* treatment, the velocity of non-irradiated males was initially faster but eventually equalled that of non-irradiated males (**Figure 3.9 C**). The initial velocity was compared between treatments, and the velocity for irradiated males (2.8 mm/sec) was significantly slower than non-irradiated males (6.2 mm/sec) ($p < 0.0001$, Man-Whitney U test) (**Figure 3.9 D**).

The differences observed in movement capacity of *Drosophila post* irradiation suggest long-term changes to *Drosophila* health following radiation treatment, and

led me to further investigate long-term radiation effects on health, such as ability to withstand stress.
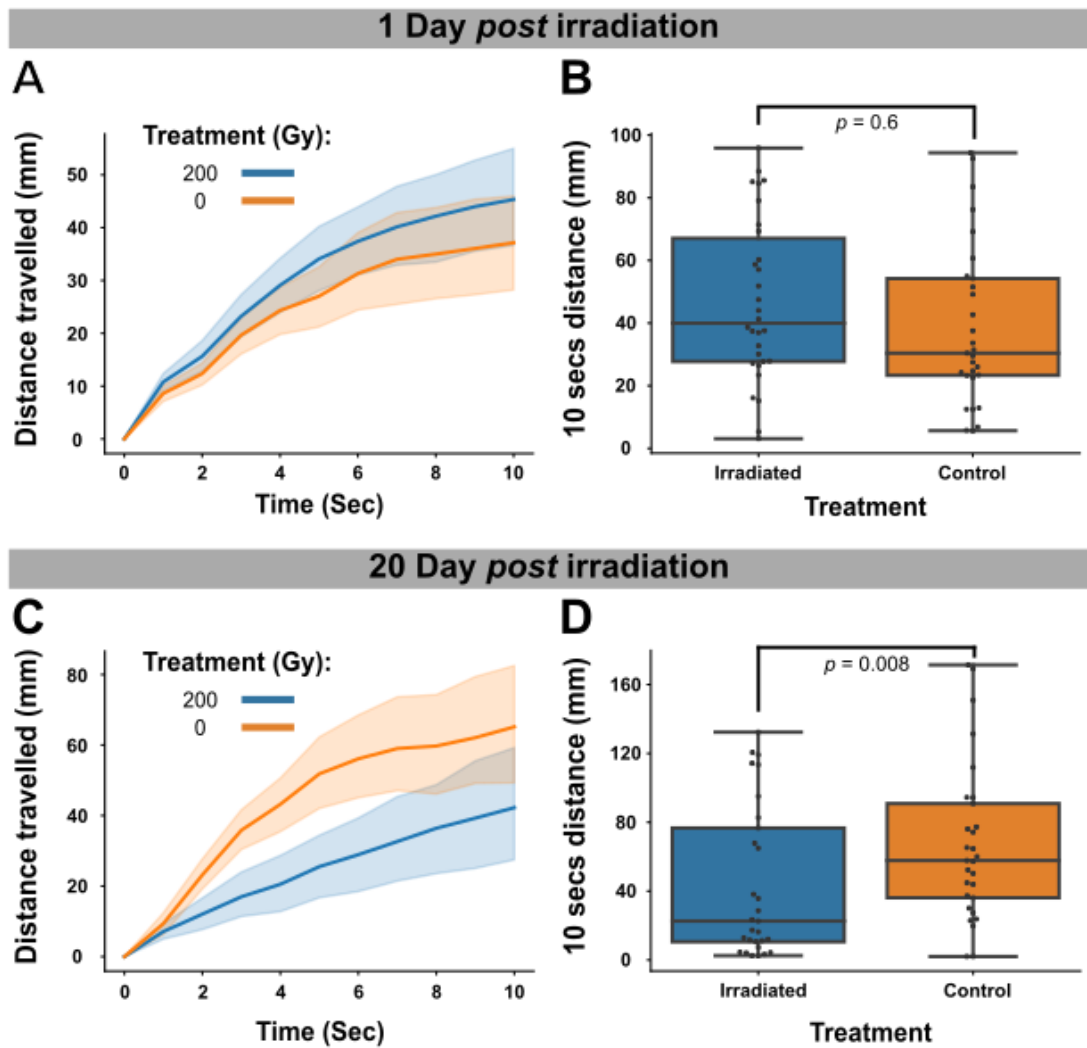
Figure 3.8: Radiation induces an age dependent decrease in negative geotaxis. 30 w^{1118} males were irradiated (200 Gy) and incubated for 1 and 20 days. (**A**) One day *post* irradiation, distance travelled over time with measurements taken in second increments. (**B**) One day *post* irradiation, distance travelled at 10 second cut-off point, whiskers represent data range and box 1st and 3rd data quartiles. (**C**) 20 day *post* irradiation, distance travelled over time with measurements taken in second increments. (**D**) 20 day *post* irradiation, distance travelled at 10 second cut-off point, whiskers represent data range and box 1st and 3rd data quartiles.
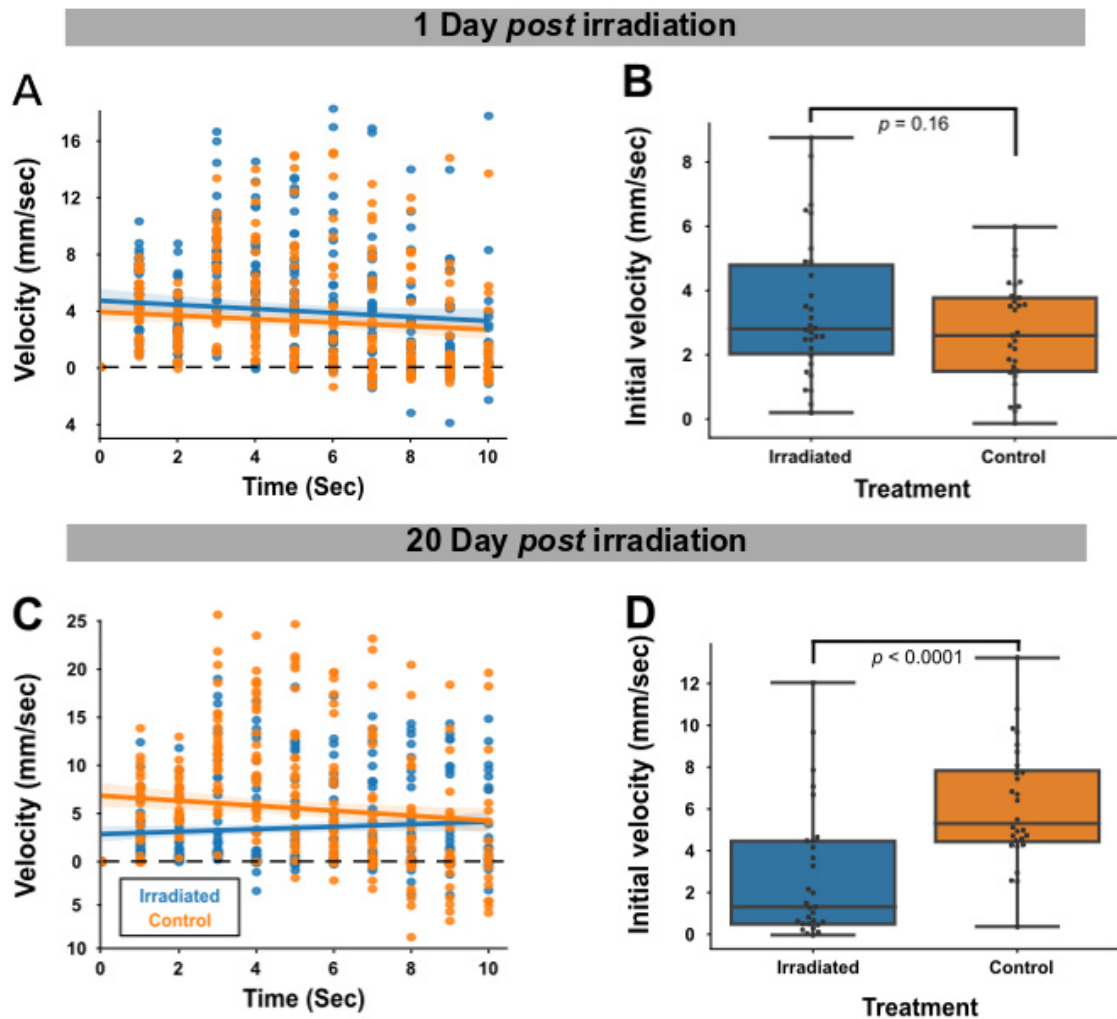
Figure 3.9: Radiation induces an age dependent decrease in velocity. 30 w^{1118} males were irradiated (200 Gy) and incubated for 1 and 20 days. (**A**) One day *post* irradiation, velocity over time with rolling average taken in three second increments. (**B**) One day *post* irradiation, initial velocity at 2 seconds, whiskers represent data range and box 1st and 3rd data quartiles. (**C**) 20 day *post* irradiation, velocity over time with rolling average taken in three second increments. (**D**) 20 day post irradiation, initial velocity at 2 seconds, whiskers represent data range and box 1st and 3rd data quartiles. (**A** & **B**) Dotted line indicates direction of travel – data above dotted line indicate *Drosophila* are travelling up and data below line indicates they are travelling down.

3.3.5 Radiation exposure has long-term effects on starvation response

In a diverse array of species, there has been evidence that within species there is a correlation between long-lived individuals and resistance to various environmental stressors (Martin, Austad & Johnson, 1996; Harshman, Hoffmann & Clark, 1999; Wang, Kazemi-Esfarjani & Benzer, 2004). Regarding *Drosophila*, it has been shown that mutants that are long-lived tend to be more resistant to environmental stress. An example being mutants of the G-protein-couple receptor *methuselah*, which are long-lived and also have enhanced resistance to environmental stresses such as heat, oxidative stress and starvation (Wang *et al.*, 2004; Paaby & Schmidt, 2008). Though the mechanism by which *methuselah* modulates survival is not fully elucidated its role in oxidative stress might be important. Aging cells accumulate ROS and develop sustained oxidative stress which eventually leads to irreparable damage - the oxidative stress theory of aging (Liguori et al., 2018). To determine if radiation alters the ability of *Drosophila* to withstand stress (starvation), two WT strains were assayed: the radio-resistant w^{1118} (**Figure 3.10 - 3.12**) and radio-sensitive *Oregon R* (**Figure 3.13**).

Male w^{1118} were starved one day after irradiation and it was determined, through inspection of survival curves that treatment did not influence starvation resistance at this timepoint (**Figure 3.10 A** & **B**). A CoxPH model was generated with the explanatory variables of radiation treatment and vial replicate (**Figure 3.10 C**). Interestingly, radiation treatment was determined to be a significant modulator of survival (p = 0.004) with a HR of 1.815 (1.204–2.735, 95% CI). Replicate was determined to be a weak but significant modulator of survival (p = 0.0005) with a HR of 1.012 (1.005–1.019, 95% CI). Proportional hazard assumption was met for both treatment (p = 0.829) and replicates (p = 0.079). There was considerable variation within the control cohort that likely contributed to radiation treatment being a significant modulator of starvation survival (**Figure 3.10 A** & **B**).

By contrast, treatment increased starvation resistance for w^{1118} males that were starved 10 days after treatment (**Figure 3.11 A** & **B**). A CoxPH model was generated with the explanatory variables of radiation treatment and vial replicate (**Figure 3.11 C**). Radiation treatment was determined to be a significant modulator of survival (p = 2.81x10^{-10}), with an estimated HR of 0.38 (0.2802–0.5122, 95% CI). Replicate was determined not to be a significant modulator of survival (p = 0.837). Proportional hazard assumption was met for both radiation treatment (p = 0.2596) and replicates (p = 0.1699).

When w^{1118} males were starved 20 day after irradiation, treatment increased starvation resistance further (**Figure 3.12 A** & **B**). A CoxPH model was generated with the explanatory variables of radiation treatment and vial replicate (**Figure 3.12 C**). Radiation treatment was determined to be a significant modulator of survival (p = 1.58×10^{-7}), with an estimated HR of 0.2887 (0.1815–0.4594, 95% CI). Replicate was determined not to be a significant modulator of survival (p = 0.742). Proportional hazard assumption was met for both radiation treatment (p = 0.0575) and replicates (p = 0.2256).

In regards to the radio-sensitive strain *Oregon R*, males were starved one day after irradiation only, and treatment did not influence starvation resistance (**Figure 3.13 A** & **B**). A CoxPH model was generated with the explanatory variables of radiation treatment and vial replicate (**Figure 3.13 C**). Radiation treatment was determined to be a significant but weak modulator of survival (p = 0.0128) with a HR of 1.0017 (1.0004–1.003, 95% CI). Replicate was determined to be a non-significant modulator of survival (p = 0.7151). Proportional hazard assumption was met for replicate (p = 0.2138), but not treatment (p = 0.0176).

It was expected that radiation treatment would reduce the capacity of *Drosophila* to withstand starvation stress, the results indicate that treatment does influence stress response and it is a chronic effect i.e. longer the time *post* irradiation the greater the effect of treatment on the stress response – a clear indication there is a long-term radiation response in *Drosophila*.
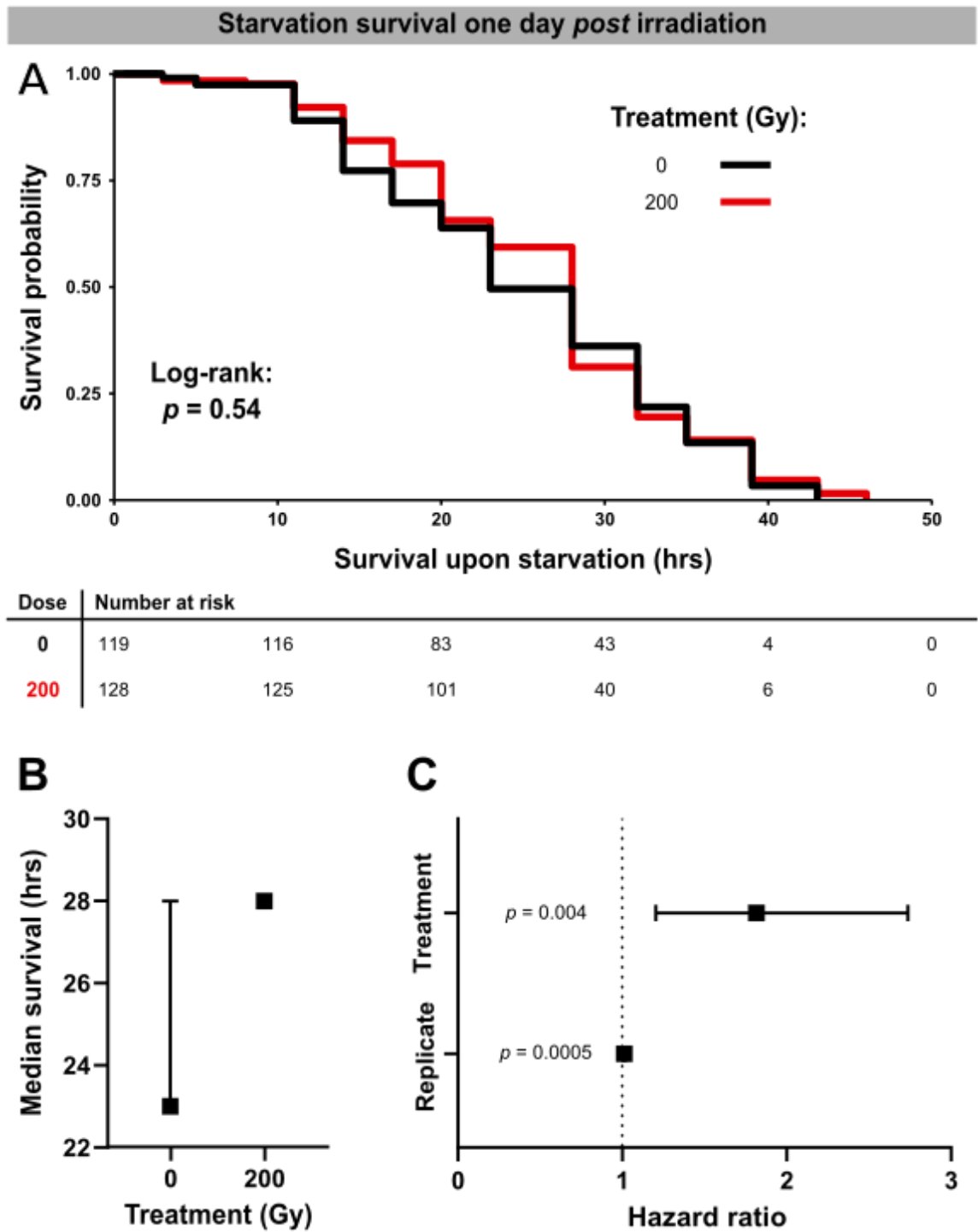
Figure 3.10: Survival upon starvation of male w^{1118} one day after irradiation. Male *Drosophila* were purped, reared under standard conditions and received a dose of 200 Gy. (**A**) KM curve risk table and *p* value derived from Log-rank testing, (**B**) median vial replicate survival for each cohort with 95% CI, (**C**) HRs derived from CoxPH model.
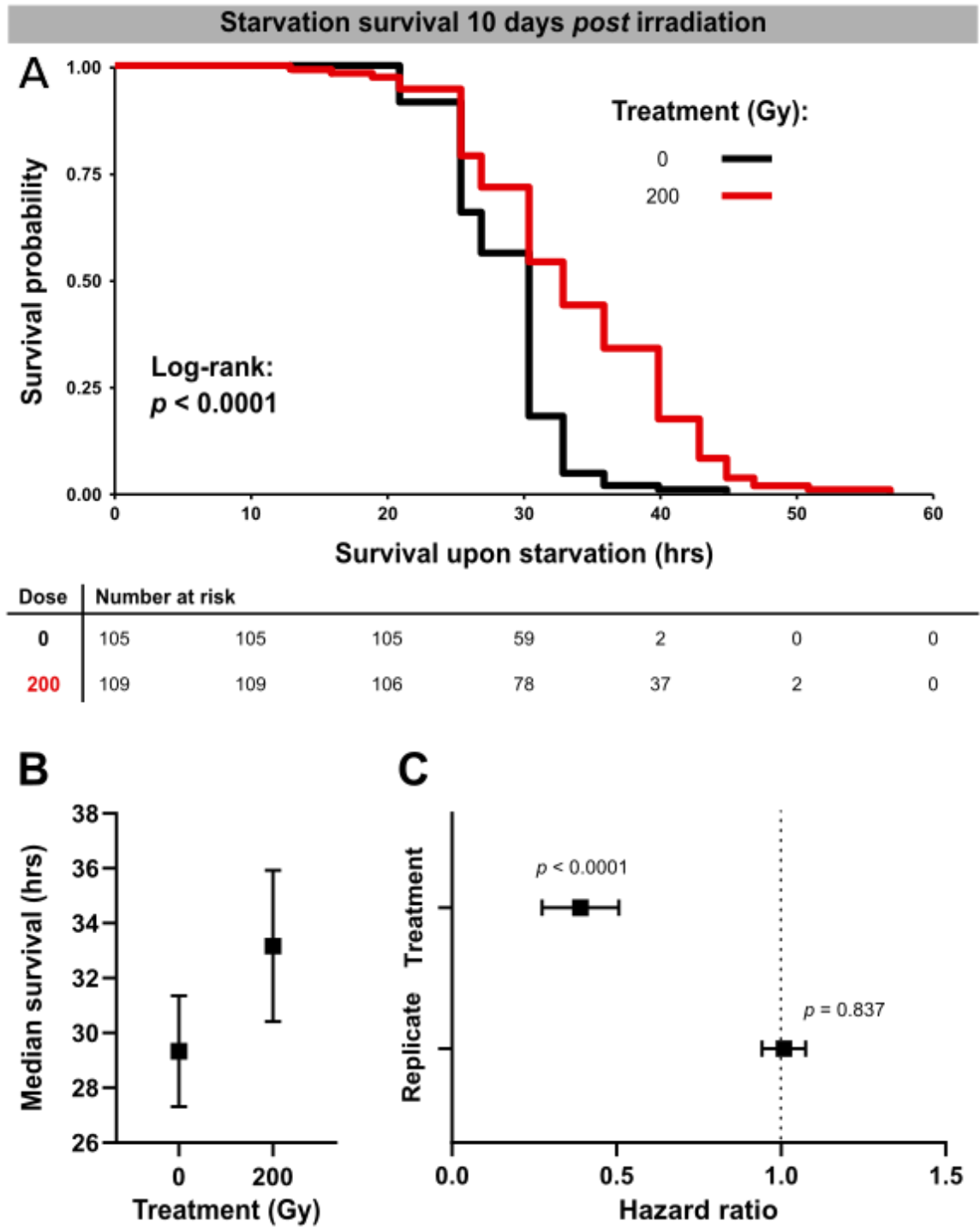
Figure 3.11: Survival upon starvation of male *w^{1118}* 10 day after irradiation. Male *Drosophila* were purped, reared under standard conditions and received a dose of 200 Gy. (**A**) KM curve risk table and *p* value derived from Log-rank testing, (**B**) median vial replicate survival for each cohort with 95% CI, (**C**) HRs derived from CoxPH model.
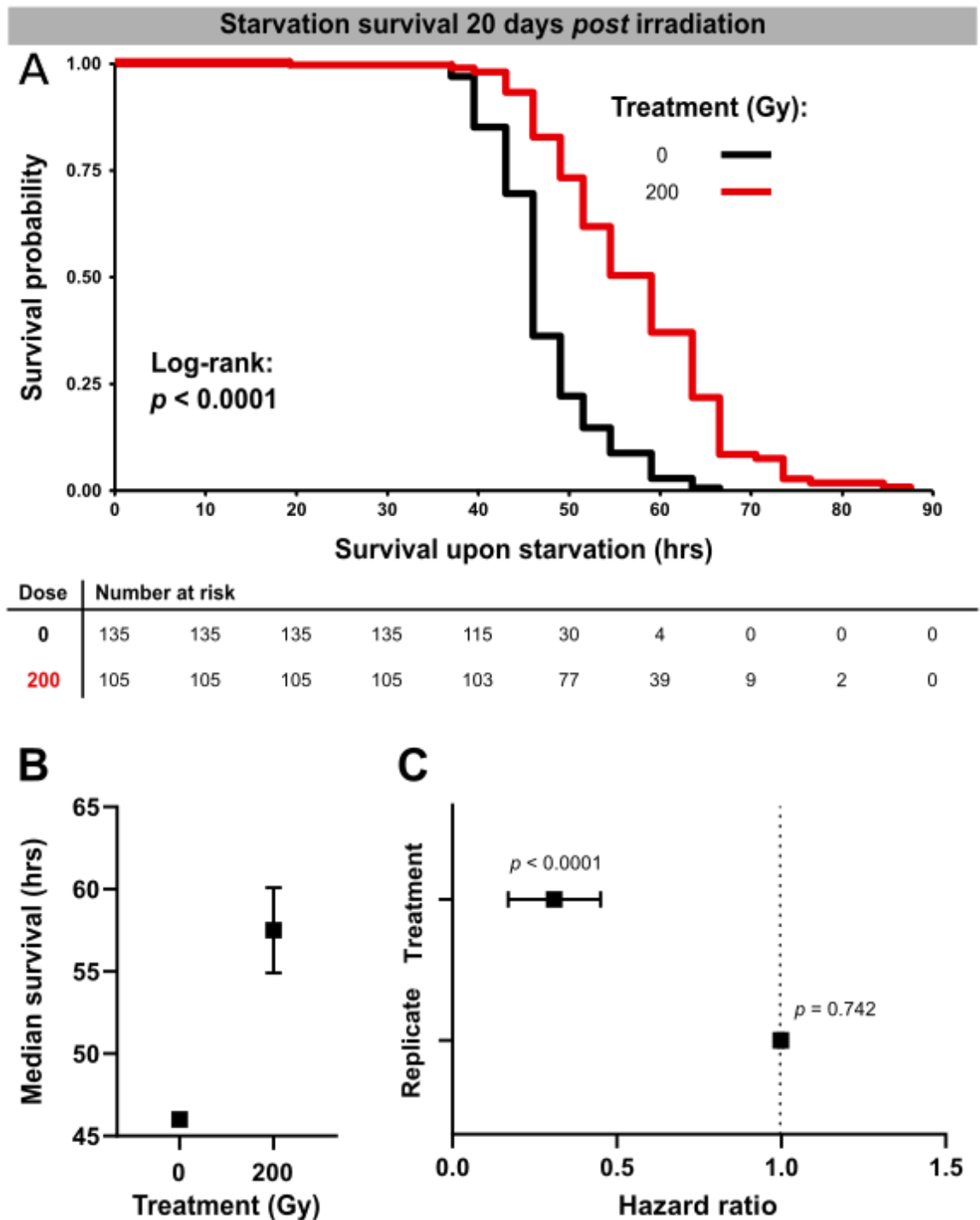
Figure 3.12: Survival upon starvation of male *w¹¹¹⁸* 20 day after irradiation. Male *Drosophila* were purped, reared under standard conditions and received a dose of 200 Gy. (**A**) KM curve risk table and *p* value derived from Log-rank testing, (**B**) median vial replicate survival for each cohort with 95% CI, (**C**) HRs derived from CoxPH model.
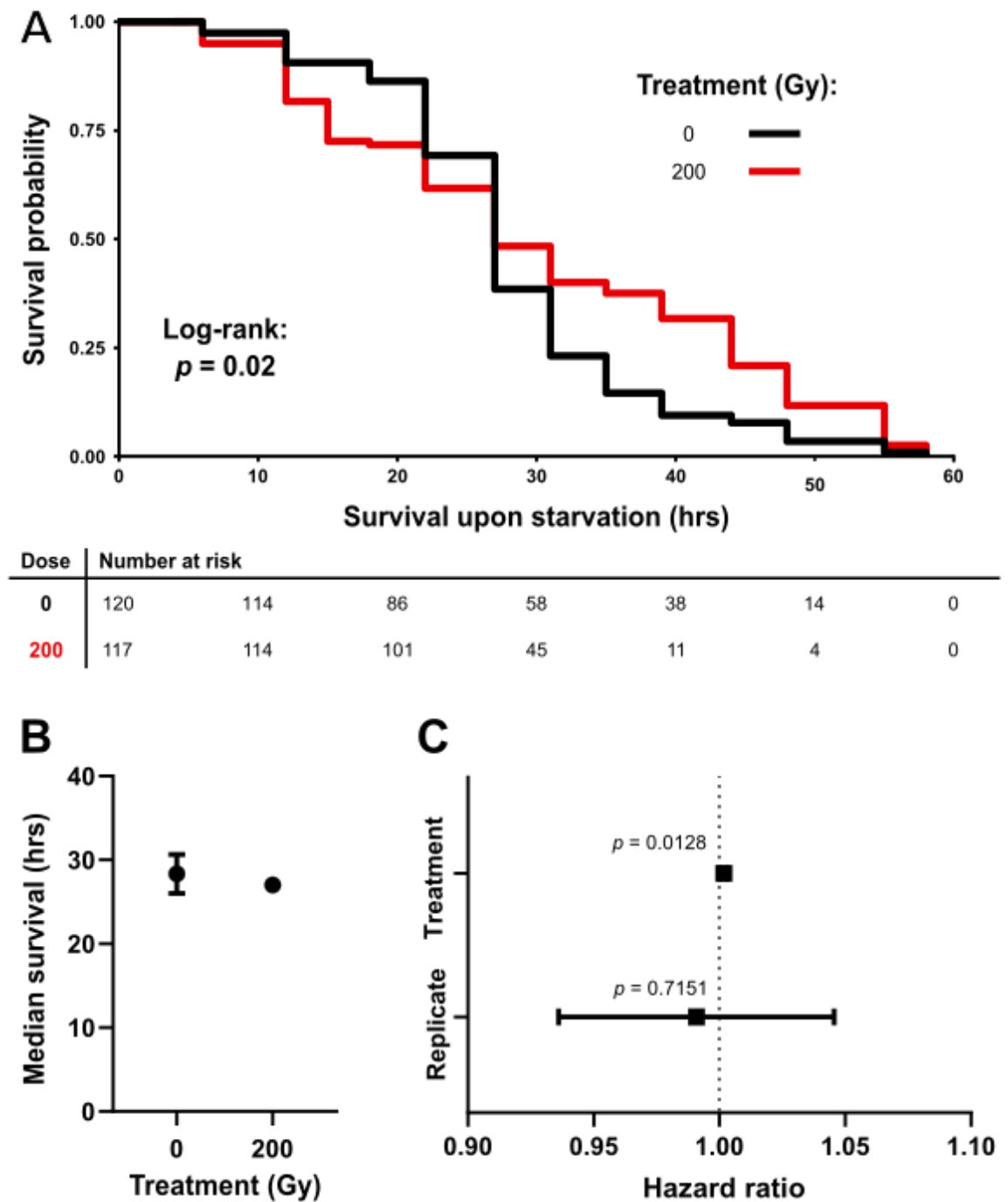
Figure 3.13: Survival upon starvation of male *Oregon R* one day after irradiation. Male *Drosophila* were purped, reared under standard conditions and received a dose of 200 Gy. (**A**) KM curve risk table and *p* value derived from Log-rank testing, (**B**) median vial replicate survival for each cohort with 95% CI, (**C**) HRs derived from CoxPH model.

3.3.6 Radiation exposure leads to long-term reduction in body weight

In mammals, changes in body weight have been associated with the immediate response to radiation (radiation sickness) (Ali, Shaikh, Abbas, Iftikhar, & Shaikh, 2017). In *Drosophila*, body weight has been shown to be modulated by multiple variables such as genotype and sex. Wet weight measurements of the DGRP have been published which show significant differences between strains (Jumbo-Lucioni et al., 2010). It has also been shown that the dry weight of females decreases as they age, which has been correlated to egg production (Nikhil, Ratna & Sharma, 2016). Two methods of measuring weight were used: – wet and dry weight, and both were assayed to help characterise *Drosophila* response to irradiation.

It was decided to first perform wet weight measurements of *Drosophila* as it would be a non-destructive assay and thus not requiring a large cohort and easier to perform. Wet weight measurements were taken for both sexes *post* irradiation (**Figure 3.14**). For females, the earliest significant difference between treatment cohorts occurred on day three with control weight of 1.19 mg/*Drosophila* and irradiated was 1.15 mg/*Drosophila* (**Figure 3.14 A**). Control weight remained higher than irradiated till day 20. For males, the differences between treatments appeared random as weight differences fluctuated between consecutive timepoints (**Figure 3.14 B**). Weight of irradiated males on day three was heavier at 0.75 mg/*Drosophila* than control males of 0.7 mg/*Drosophila*. However, at day 6, irradiated males were lighter at 0.61 mg/*Drosophila* than control males of 0.71 mg/*Drosophila*. Overall, the wet weight measurements have high variance within each arm as shown by the large whiskers of each box plot. It was decided to attempt to measure dry weight.

Optimisation of desiccation time was required for subsequent dry weight experimentation. Both sexes were killed via prolonged CO_2 exposure and left to desiccate with repeated measurements of weight taken (**Figure 3.15**). Weight loss of carcasses due to desiccation plateaued at 5.5 hr with less than a percentage change for longer incubations. Males at 72 hr had a weight reduction of 73% and females had a weight reduction of 69%. It was decided that subsequent experiments would include a 24 hr desiccation step as this was sufficient to ensure complete water loss of all carcasses.

Dry weight measurements were performed on both sexes *post* irradiation (**Figure 3.16**). For non-irradiated females, weight reduced with time, with initial weight one day prior treatment being 0.418 mg/*Drosophila* and weight at 20 days being 0.320 mg/*Drosophila* (**Figure 3.16 A**). For irradiated females, weight lowered considerably

one day after treatment to 0.253 mg/*Drosophila*, but between one day and 20 days showed a general increase in weight as time continued. At day 20, non-irradiated and irradiated female weights were similar (0.320 and 0.330 mg/*Drosophila*, respectively). For non-irradiated males, weight was stable and stayed the same with weight one day prior treatment being 0.206 mg/*Drosophila* and 20 days after treatment being 0.209 mg/*Drosophila* (**Figure 3.16 B**). For irradiated males, there is consistent loss of weight over time, with weight at 20 days after treatment being 0.150 mg/*Drosophila*, which was the lowest weight measured for any treatment arm at any timepoint.

Changes in *Drosophila* weights after irradiation, especially the significant decrease in weight of males suggested the importance of the midgut in the radiation response, prompting investigation into the role of the midgut in radiation.
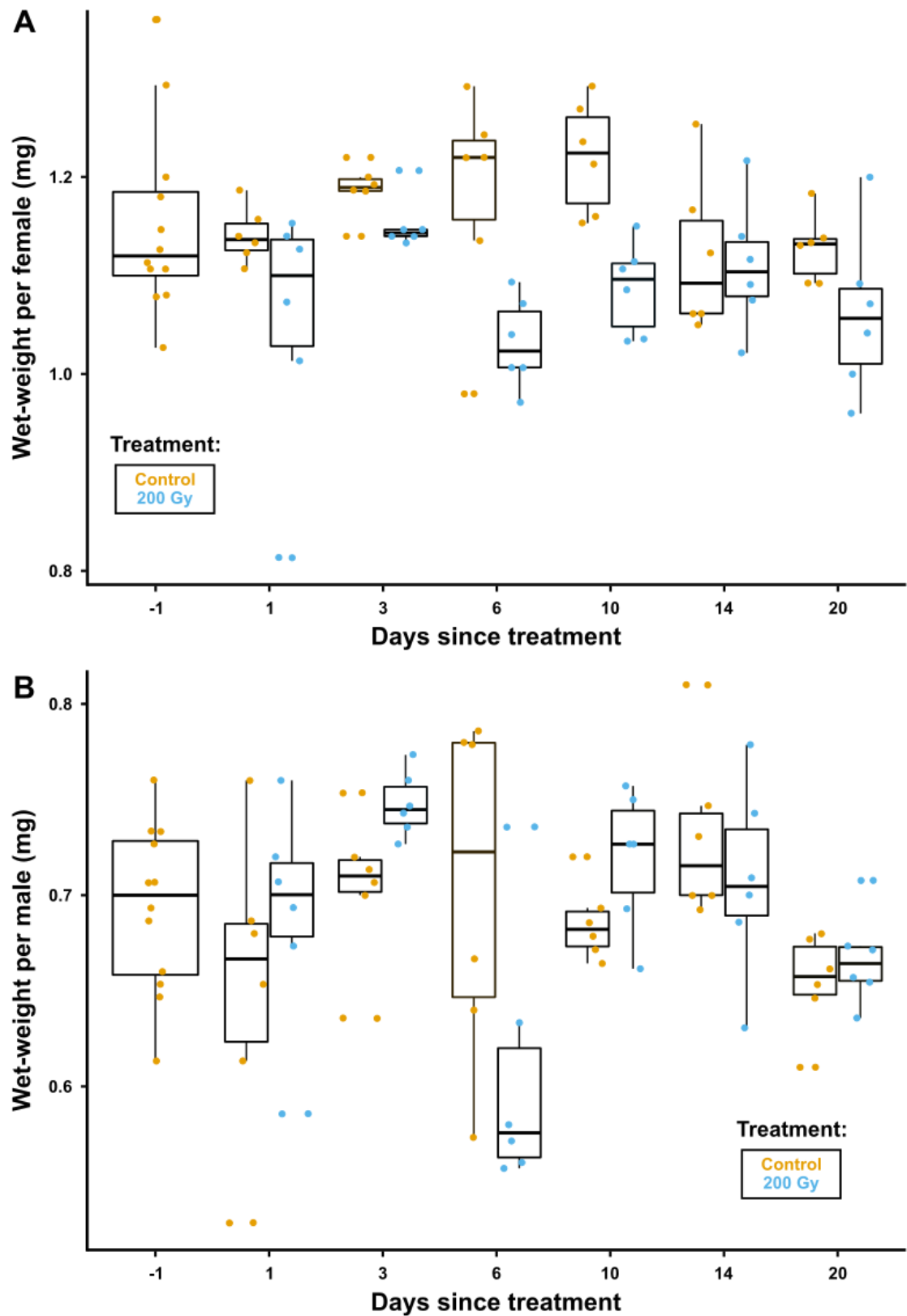
Figure 3.14: Wet weight of both sexes post irradiation. *w¹¹¹⁸* were allowed to mate for 48 hr followed by irradiation (200 Gy), replicates were six per arm with each replicate containing 15 *Drosophila* which were re-measured for subsequent timepoints. Boxes represent 1st and 3rd quartiles of data and whiskers the range. (**A**) Wet weight of females, (**B**) wet weight of males.
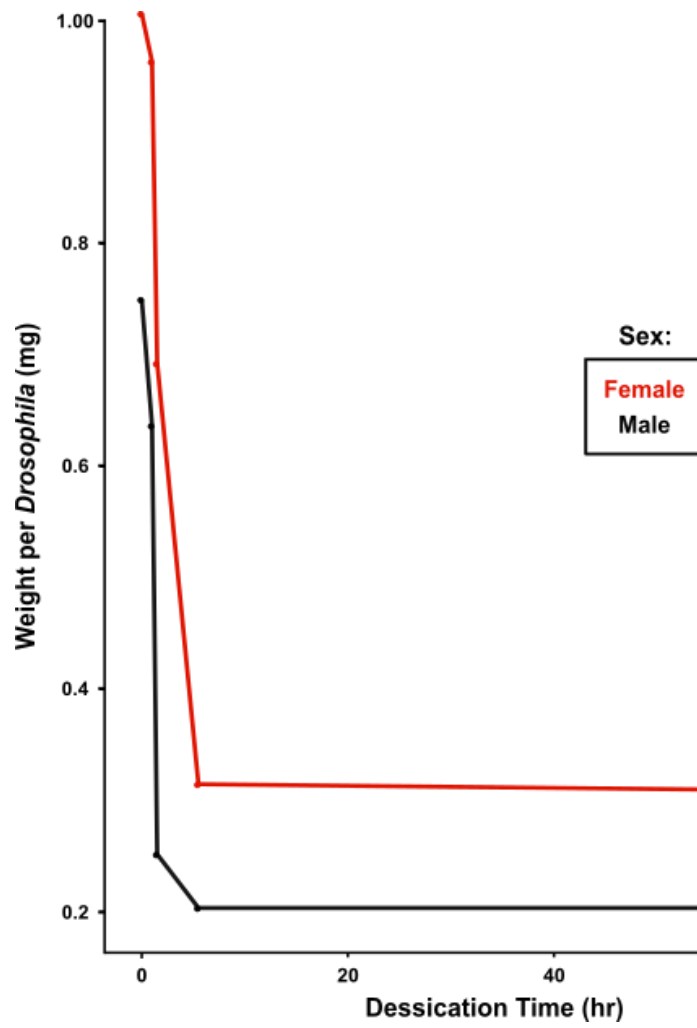
Figure 3.15: Determination of optimum desiccation time for measuring dry weight. *Drosophila* w^{1118} were allowed to mate for 48 hr and killed via prolonged CO_2 exposure. 30 *Drosophila* were pool-weighed per sex and per timepoint.
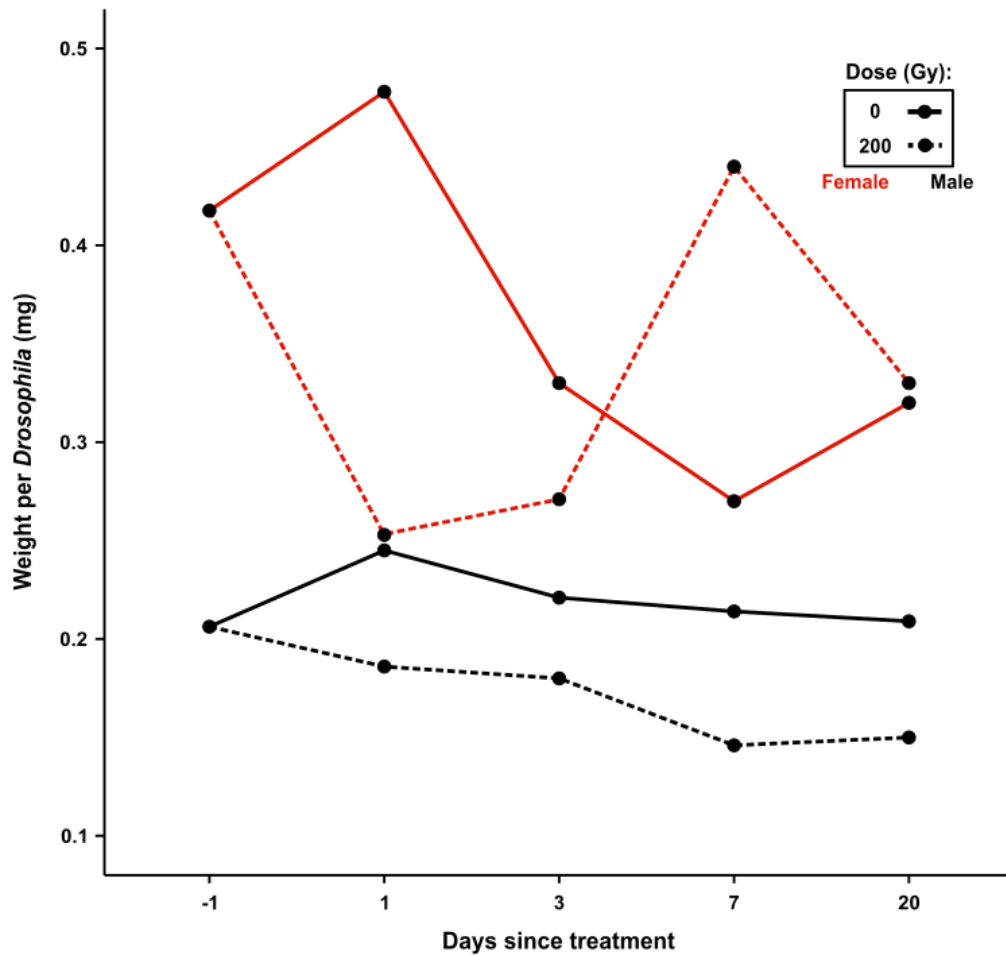
Figure 3.16: Dry weight of both sexes of *Drosophila post* irradiation. *Drosophila Oregon R* were allowed to mate for 48 hr and irradiated (200 Gy), each cohort consisted of 150 *Drosophila*, with each datapoint representing average pooled weight per cohort (30 individuals per datapoint).

3.3.7 Radiation treatment leads to reduction in frass output

A modified frass assay was validated to measure midgut health (**Section 2.4**). Briefly, this assay was used to measure frass output and frass pH composition. Frass pH composition was measured by adding the pH indicator BPB to *Drosophila* culture media. This allows for colour change indicating pH of frass with green being acidic (pH ≤ 4) and blue being less acidic (pH ≥ 5) (Cognigni *et al.*, 2011). This assay was used to characterise the frass output of various WT strains and then determine if radiation treatment led to perturbation in frass output and composition.

For all WT strains assayed there was variation between strains and changes associated with treatment status (**Figure 3.17 A**). It was determined that both genotype ($p < 0.0001$) and treatment ($p < 0.0001$) were significant modulators of frass output (two-way ANOVA). The interaction between genotype and treatment was significant ($p = 0.01$) and this was clearly seen for *DGRP-21* in which control had the highest recorded frass output (11 frass/*Drosophila*) but also the greatest reduction in frass when irradiation (6 frass/*Drosophila*, 45% reduction). Whereas, non-irradiated *Oregon R* had a relatively low frass output (5 frass/*Drosophila*) with a non-significant reduction when irradiated (4 frass/*Drosophila,* 20% reduction).

The composition of frass was genotype dependent but treatment independent (**Figure 3.17 B**). *w^1118^* control had the highest proportion of green frass (27%) and upon irradiation green frass decreased to 25% of total frass. However, error bar overlap between treatment arms indicates no significant difference. Meanwhile, *Oregon R* control had the lowest proportion of green frass (2%); this decreased to 1% after irradiation, but the difference was not significant.

Though the pH composition of frass was unaffected by radiation treatment, the total frass output of *Drosophila* was significantly reduced for the majority of strains assayed, possibly indicating reduced midgut functionality.
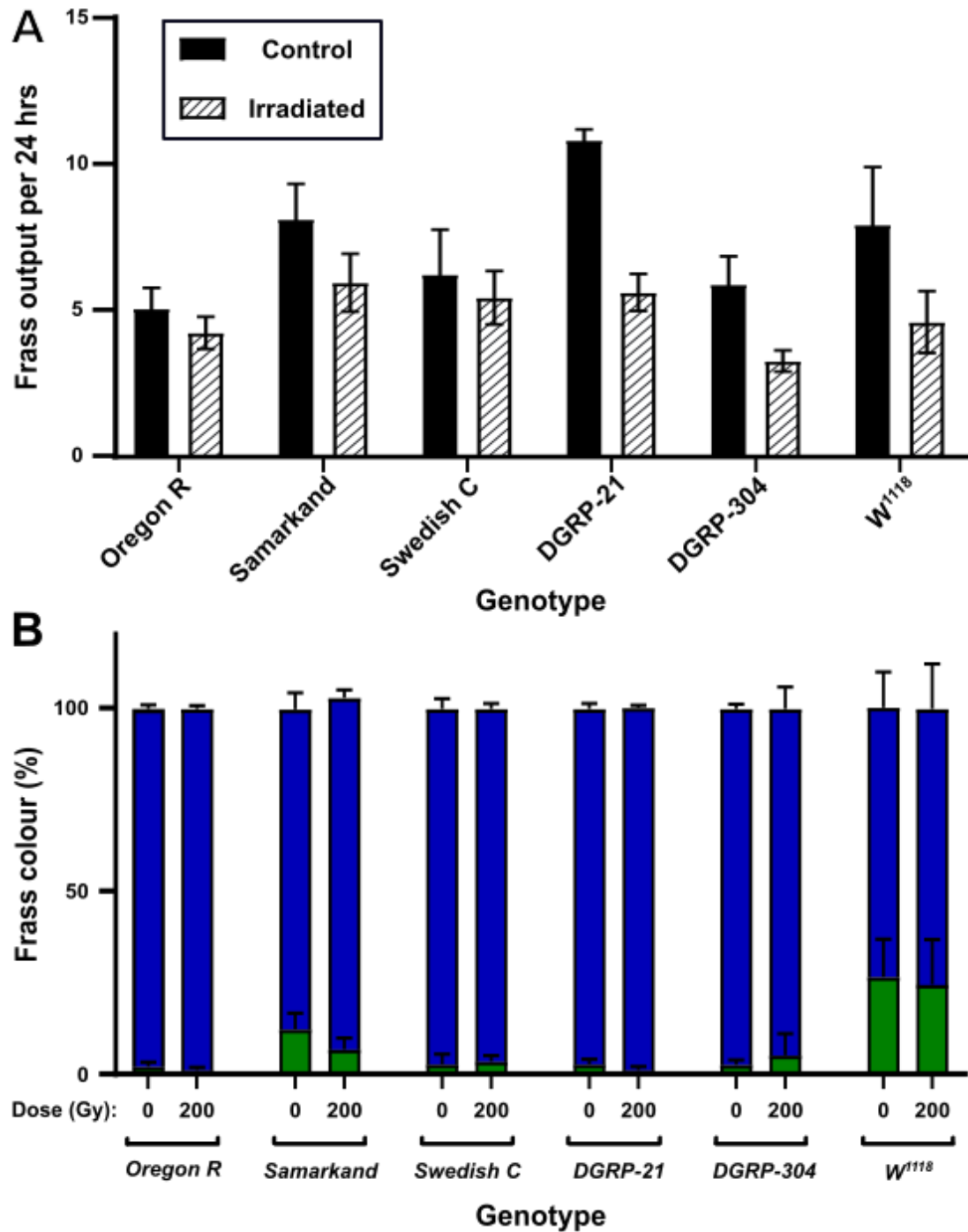
Figure 3.17: Radiation induced changes in frass output for various WT strains. Males from six strains were irradiated (150 Gy) and assayed with three technical replicates each consisting of 30 *Drosophila* per frass cage, and frass collected over 24 hr period. Represented data is normalised frass output per *Drosophila* per 24 hr period. (**A**) total frass output of various WT strains, (**B**) percentage of either green or blue frass for assayed strains. *Drosophila* were purped and reared at 25 ˚C and frass assayed 14 days *post* irradiation. Error bars represent standard error between samples.

3.4 Radiation induced tissue toxicity and oxidative stress

Long-term reduction in body weight (**Section 3.3.6**) and decrease in frass output (**Section 3.3.7**) *post* irradiation suggest that the midgut of *Drosophila* is affected by radiation treatment. This is in line with previously published data demonstrating that proliferative organs, such as the gonads are sensitive to radiation (Paithankar *et al.*, 2017). Since midgut is also a mitotic tissue, I decided to investigate if radiation treatment leads to long-term tissue toxicity in the midgut of *Drosophila*, and whether oxidative stress is a consequence of treatment. In humans it is currently unknown what is the aetiological cause of long-term side effects associated with radiation treatment (Bentzen, 2006). One possible idea is that of persistent and chronic oxidative stress, and *Drosophila* is well suited for this line of research. It has been shown that *Drosophila* are amenable to oxidative stress and multiple *Drosophila* tools are available (Niraula & Kim, 2019). Using *Drosophila* I wanted to ascertain the link between long-term oxidative stress and tissue toxicity following radiation treatment.

3.4.1 Radiation induced long-term DNA damage

The radio-resistant strain w^{1118} was exposed to radiation and H2AvD foci were quantified within the midgut at various timepoint *post* treatment to measure the amount of DNA DSB and overall DNA damage (**Section 1.5**).

At 7 days *post* irradiation, both dosages (50 and 150 Gy) appeared to increase the levels of H2AvD foci within midgut nuclei (**Figure 3.18 A**). ANOVA testing determined that treatment was a significant variable influencing H2AvD intensity ($p < 0.001$). There was no significant difference observed between control and 50 Gy treatment ($p = 0.849$), but 150 Gy treatment was significantly higher than control and 50 Gy (both $p = 2\times10^{-6}$) (**Figure 3.18 B**). In contrast, 14 days *post* irradiation, only 50 Gy treatment led to significantly increased levels of H2AvD foci as compared to control ($p = 1\times10^{-4}$) (**Figure 3.19**). However, 21 days *post* irradiation was similar to 7 days in which there was no significant differences between control and 50 Gy treated nuclei, but there was between 150 Gy and other treatments (both $p < 0.0001$) (**Figure 3.20**). Each timepoint was stained and imaged in a separate session and imaging settings such as laser intensity and digital gain were adjusted accordingly depending on the variability of antibody staining. Therefore, comparisons between timepoints is difficult and are limited to relative comparisons within time points i.e seven days since 50 Gy irradiation vs 7 days control.
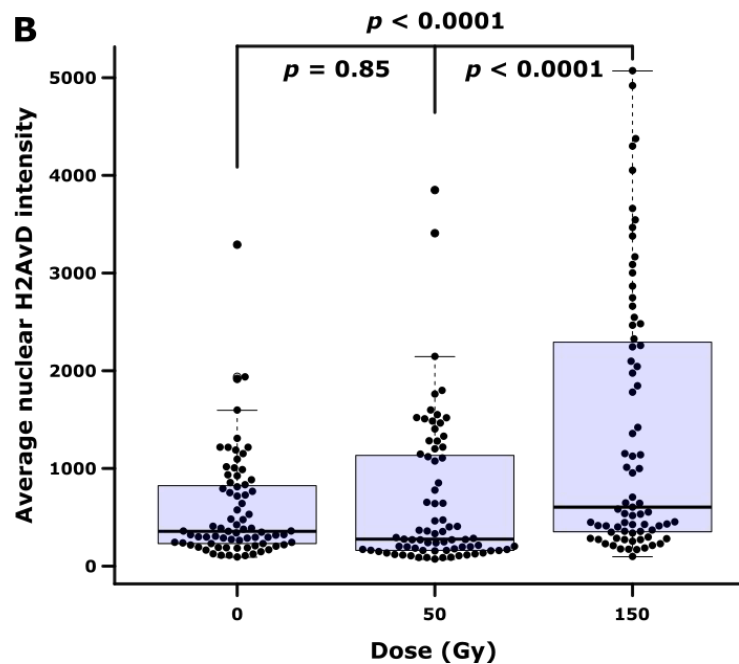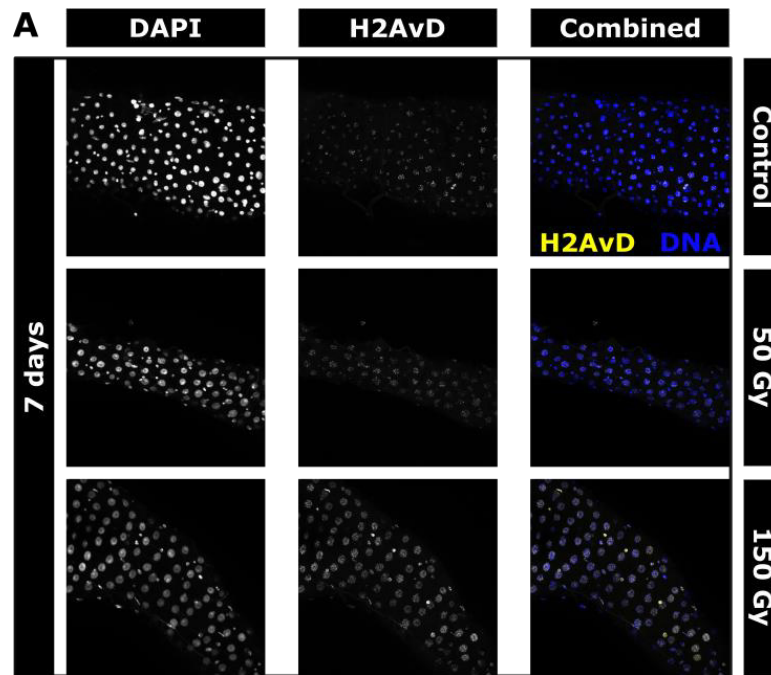
Figure 3.18: DNA damage within male _w^1118_ midguts 7 days _post_ irradiation. DNA damaged was quantified by visualising H2AvD foci, and male _Drosophila_ were exposed to various dosages of radiation (50, 100 and 150 Gy). (**A**) Images are representative maximum projections _n_ = 5 – 9 midguts per dose and each midgut was imaged in three random locations. (**B**) manually counted nuclei within Fiji, and R was used to perform ANOVA followed by Tukey's multiple comparison testing. 15 cells were measured from each stack, with a total of 75 cells per treatment. Boxes represent SD and whiskers min and max values range. _Drosophila_ were exposed to radiation and kept at standard rearing condition for 7 days prior to dissection of tissue.
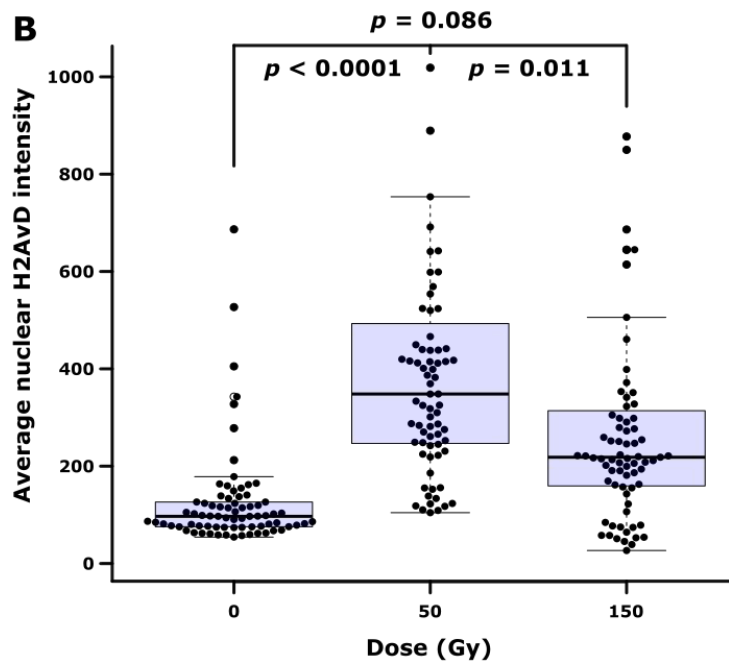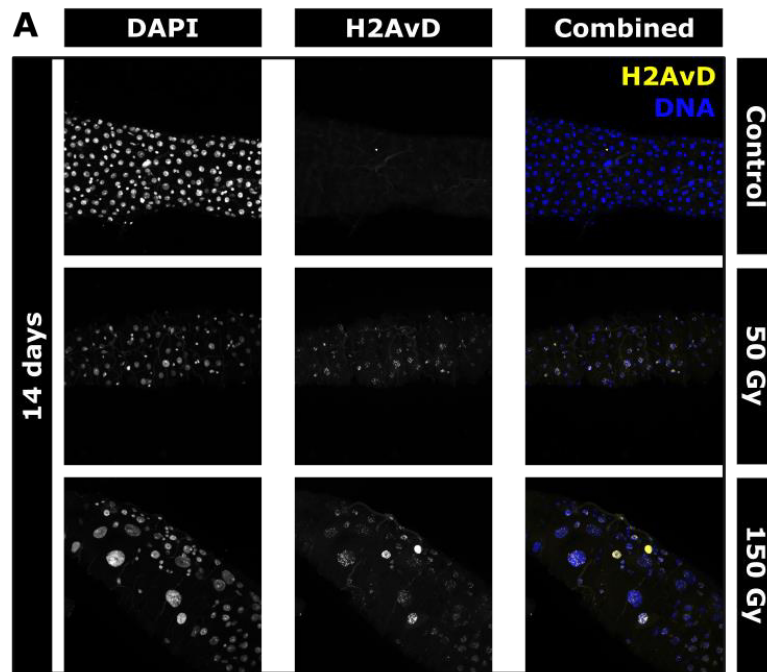
Figure 3.19: DNA damage within male *w^1118* midgut 14 days *post* irradiation. DNA damage was quantified by visualising H2AvD foci, and *Drosophila* were exposed to various doses of radiation (50, 100 and 150 Gy). (**A**) Images are representative maximum projections n = 5–9 midguts per dose and each midgut was imaged in three random locations. (**B**) 15 nuclei per were manually measured per stack, with a total of 75 cells per treatment. Boxes represent SD and whiskers min and max values range. *Drosophila* were exposed to radiation and kept at standard rearing condition for 14 days prior to dissection.
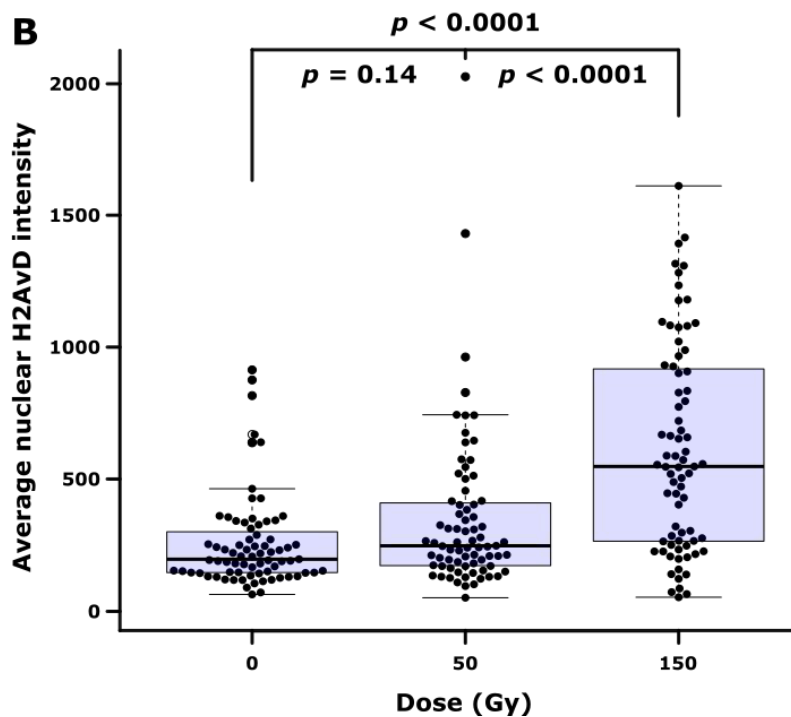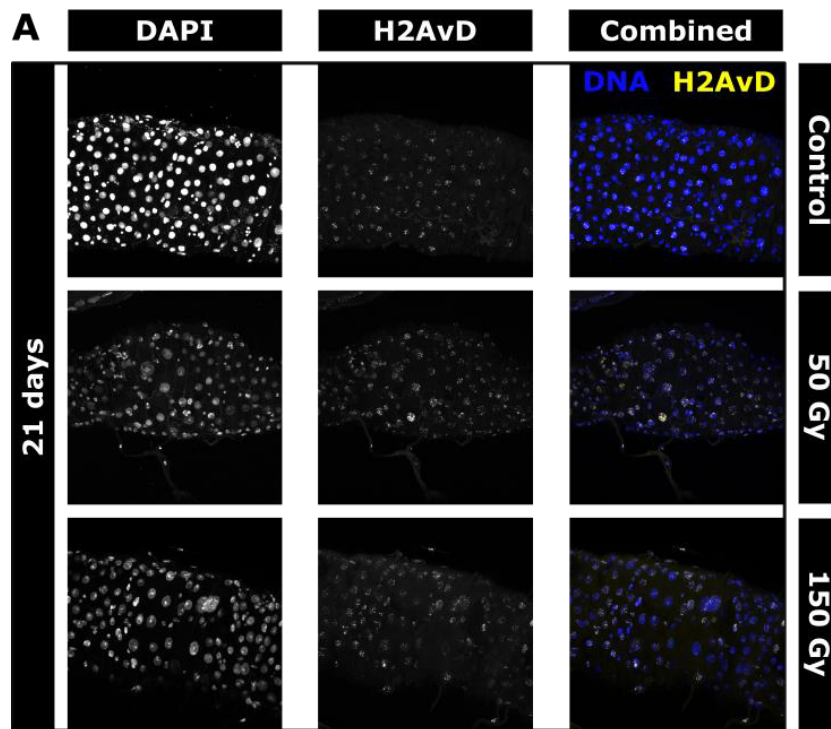
Figure 3.20: DNA damage within *w^1118* midgut 21 days post irradiation. DNA damaged was quantified by visualising H2AvD foci, and *Drosophila* were exposed to various dosages of radiation (50, 100 and 150 Gy). (**A**) Images are representative maximum projections n = 5 – 9 midguts per dose and each midgut was imaged in three random locations. (**B**) 15 nuclei per were manually measured per stack, with a total of 75 cells per treatment. Boxes represent SD and whiskers min and max values range. *Drosophila* were exposed to radiation and kept at standard rearing condition for 21 days prior to dissection.

3.4.2   Radiation treatment leads to midgut oxidative stress

A GFP reporter line (*GstD1::GFP*) has been extensively used by the *Drosophila* research community to study oxidative stress. *Glutathione S-transferase D1* (*GstD1*) is a transcriptional target of *cap-n-collar* (*cnc*) which is activated in oxidising conditions. Under normal physiological conditions, *cnc* is kept and repressed within the cytoplasm via binding to the *Keap1* complex. *Keap1* has several cysteine residues which in the presence of ROS become oxidised leading to conformational changes and freeing bound *cnc*, allowing the transcription of target genes such as *GstD1* (Deshmukh, Unni, Krishnappa, & Padmanabhan, 2017). The *GstD1::GFP* reporter line was used to test whether radiation treatment leads to oxidative stress, and whether certain tissues were more susceptible to radiation-induced oxidative stress, and finally whether oxidative stress persists long-term.

To determine which tissues and/or organ systems were under oxidative stress, paraffin sections of whole *Drosophila* were generated (**Figure 3.21**). The irradiated *Drosophila* had a number of tissues which had increased *GstD1* expression such as the fat body within the head, thorax and abdomen, the midgut within the abdomen, and the Malpighian tubules.

To determine if there was a difference in oxidative stress levels *post* treatment in males or females, *GstD1::GFP* expression within the midgut one day *post* irradiation was quantified (**Figure 3.22**). ANOVA testing determined that treatment was a significant modulator of GFP levels within the midgut ($p = 2 \times 10^{-16}$), sex was not a significant modulator ($p = 0.41$), whereas an interaction between sex and treatment was significant ($p = 2 \times 10^{-12}$). The interaction was evident when mean intensity values of each experimental arm were compared. Cells from irradiated males had significantly higher levels of cytoplasmic GFP at 8.31 a.u when compared to non-irradiated males at 4.54 a.u ($p = 2 \times 10^{-16}$, Tukey's test). Whereas for females there was no difference between treatments ($p = 0.077$). Therefore, short-term *post* treatment there was increased oxidative stress in males but not in females.

Focussing on the midgut, time series of oxidative stress showed increased GFP expression in irradiated midguts, and although GFP levels were higher in irradiated *Drosophila* compared to the control long-term, the greatest difference between treatment arms was one day *post* treatment (**Figure 3.23**).
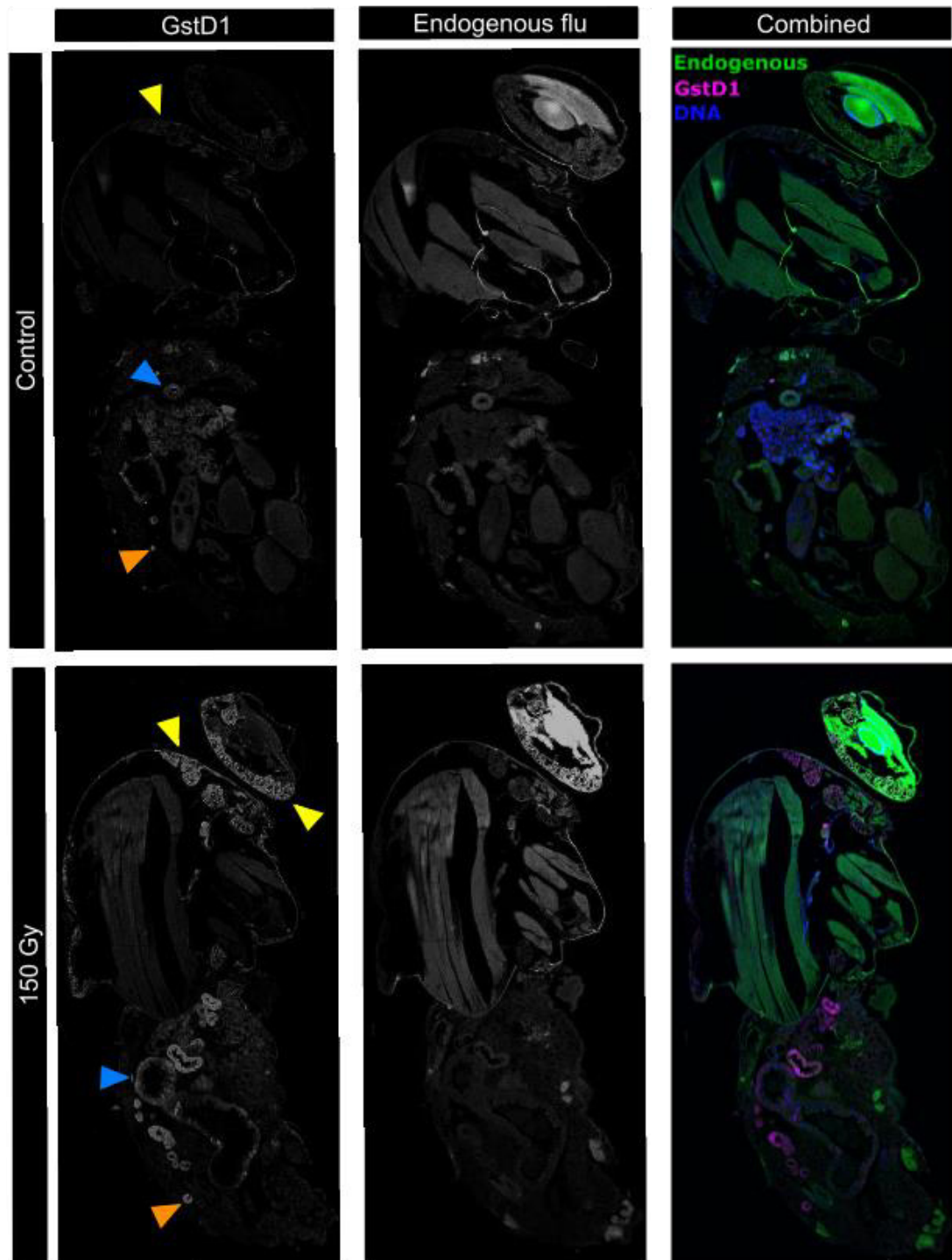
Figure 3.21 Radiation induces long-term upregulation of *GstD1* within specific tissues. Images of whole-body sections along the sagittal plane. Females were purped, irradiated 150 Gy and reared at 25°C for 10 days *post* treatment, followed by paraffin embedding and sectioning. Coloured triangles indicate tissues in each treatment: midgut (▲), Malpighian tubules (▲) and fat body (▲).
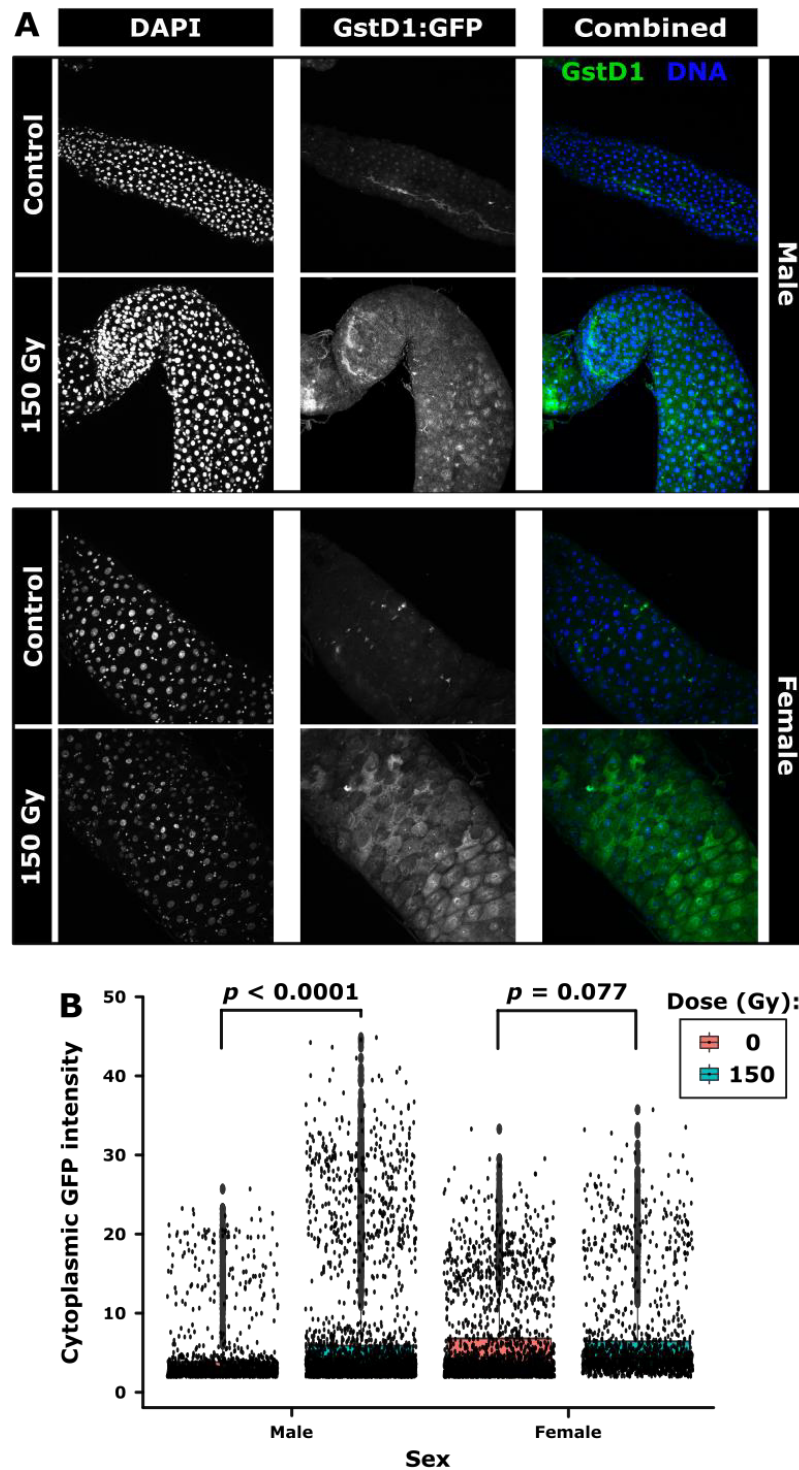
Figure 3.22: Radiation induces sexual dimorphic short-term (1 day *post* irradiation) changes in *GstD1* expression within the midgut of both sexes. (**A**) Images are representative maximum projections *n* = 5 – 9 midguts per dose and each midgut was imaged in three random locations. (**B**) Average cytoplasmic GstD1::GFP intensity was quantified using a custom designed Python image analysis script which relied on crowning segmentation (**Appendix 3**). *N* = 7,196 cells. Boxes represent SD and whiskers min and max values range. *Drosophila* were exposed to radiation (150 Gy) and kept at standard rearing condition for 1 day prior to dissection of tissue.
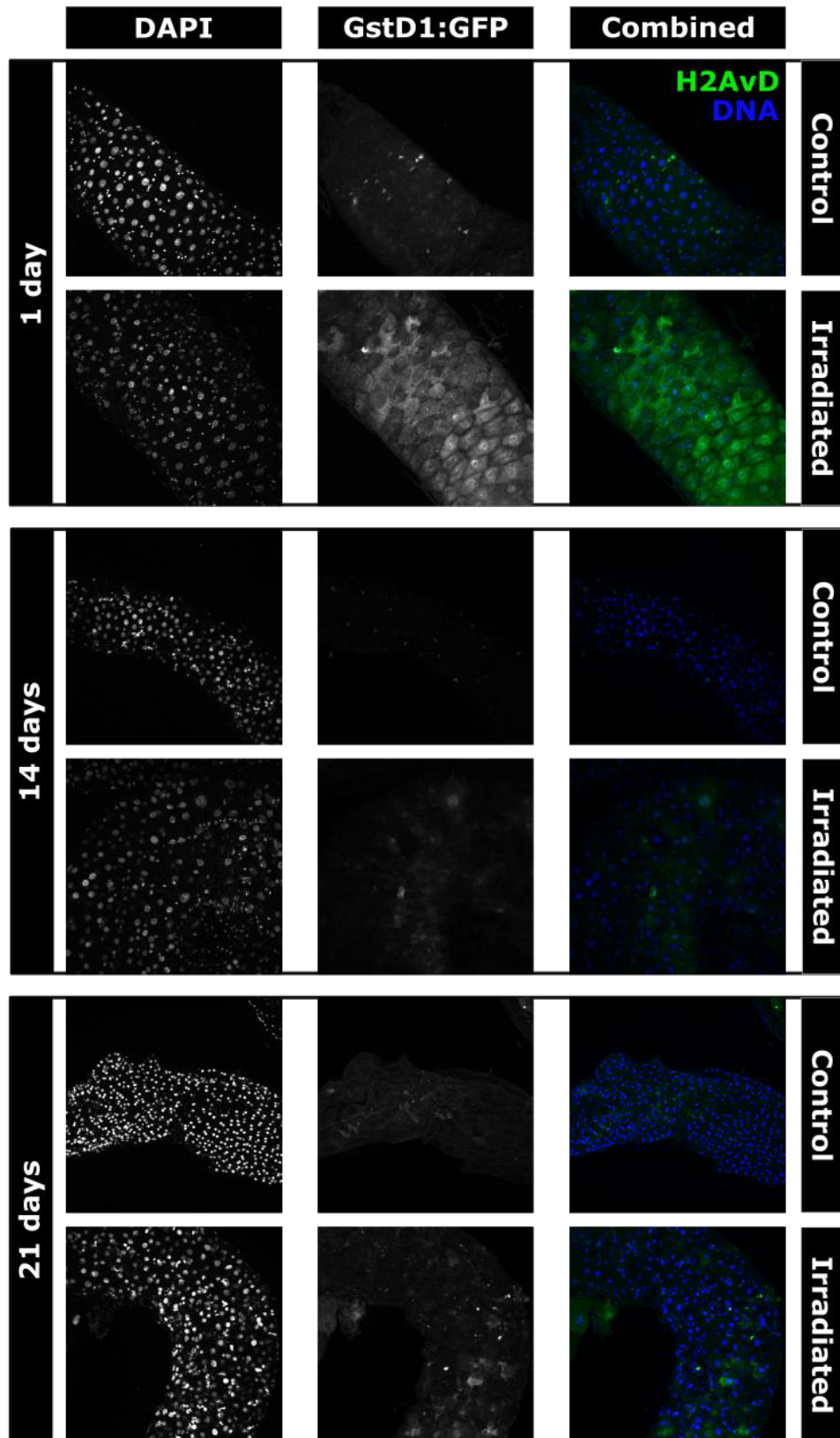
Figure 3.23: Radiation induces long-term upregulation of *GstD1* within the midgut of females. Images are representative maximum projections *n* = 5 − 9 midguts per dose and each midgut was imaged in three random locations. *Drosophila* were exposed to radiation (150 Gy) and kept at standard rearing condition for desired incubation prior to dissection of tissue.

3.4.3 Exploring the link between oxidative stress and DNA damage

I have shown that the midgut of *Drosophila* exhibits persistent DNA damage (**Section 3.4.1**) and oxidative stress (**Section 3.4.2**) as a direct consequence of irradiation. It was also observed that both *GstD1::GFP* signal and H2AvD levels showed varied intensities within irradiated midguts, with some cells demonstrating higher levels than others. I wanted to determine whether cells under high levels of radiation-induced oxidative stress showed higher levels of DNA damage. This potential correlation may shed some light on the underlying mechanism that drives the chronic DNA damage observed. To test whether there was a correlation between oxidative stress and DNA damage, the *GstD1::GFP* reporter was used to quantify whether cells that express high levels of GFP also had high levels of H2AvD staining. Two timepoints were chosen to study immediate and chronic effects *post* treatment.

One day *post* irradiation, upon visual inspection of confocal stacks H2AvD and GFP levels appeared to be higher in irradiated midguts (**Figure 3.24**). However, when data was analysed through use of custom image analysis script (**Appendix 3**), overall H2AvD and GFP levels were determined to be significantly lower in irradiated cells as compared to control (both $p < 0.0001$) (**Figure 3.24 B - C**). When comparing H2AvD levels against cytoplasmic GFP levels, irradiated tissue had a lower proportion of high-level H2AvD cells, whereas the control tissue had a lower proportion of high-level GFP expressing cells (**Figure 3.24 D**). ANOVA modelling (H2AvD nuclear levels ~ treatment * cytoplasmic *GstD1* levels) determined that there was a correlation between GFP levels and H2AvD, however, the correlation was negative: radiation treatment decreased GFP levels which led to increased H2AvD levels.

At 14 days *post* irradiation, there was no significant difference in H2AvD levels between irradiated and control nuclei ($p = 0.0614$) (**Figure 3.25 B**). Whereas there was a significant difference in cytoplasmic GFP levels between treatments ($p = 2 \times 10^{-16}$) (**Figure 3.25 C**). Similarly to one day *post* irradiation, irradiated midguts had a higher proportion of high-level H2AvD cells (**Figure 3.25 D**). ANOVA modelling (H2AvD nuclei levels ~ treatment * cytoplasmic *GstD1* levels) determined that both treatment and GFP levels significantly influenced H2AvD levels ($p = 0.00645$ and $p = 2 \times 10^{-16}$, respectively). Similarly to one day *post* irradiation, a significant but negative correlation was observed: radiation treatment decreased GFP levels which led to increased H2AvD levels.

Overall, at both time points *post* treatment, cells exhibiting radiation-induced DNA damage were not under higher levels of oxidative stress as was anticipated.
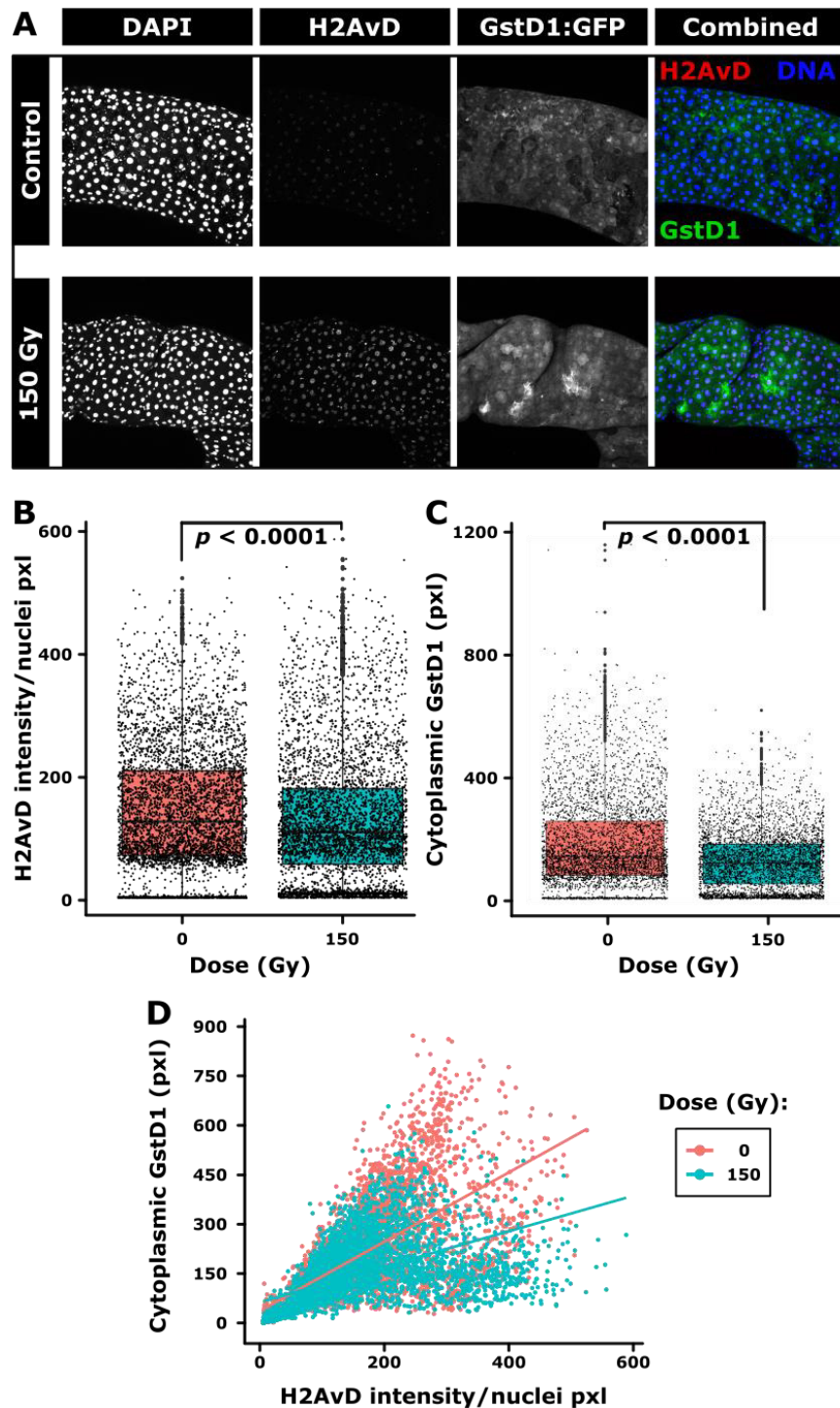
Figure 3.24: GstD1 and H2AvD levels within the midgut one day *post* irradiation. (**A**) Images are representative maximum projections *n* = 5 – 9 midguts per dose and each midgut was imaged in three random locations. (**B**) & (**C**) Nuclei size, H2AvD intensity, and cytoplasmic GstD1 GFP intensity was quantified using a custom designed Python image analysis script which relied on crowning segmentation (**Appendix 3**). (**D**) Cytoplasmic GstD1 data was trimmed to remove three datapoints which exceeded 900 intensity units. R was used to perform statistical analysis. Dataset consists of data for 9,025 cells. Boxes represent SD and whiskers min and max values range. *Drosophila* were exposed to radiation and kept at standard rearing condition for one day prior to dissection of tissue.
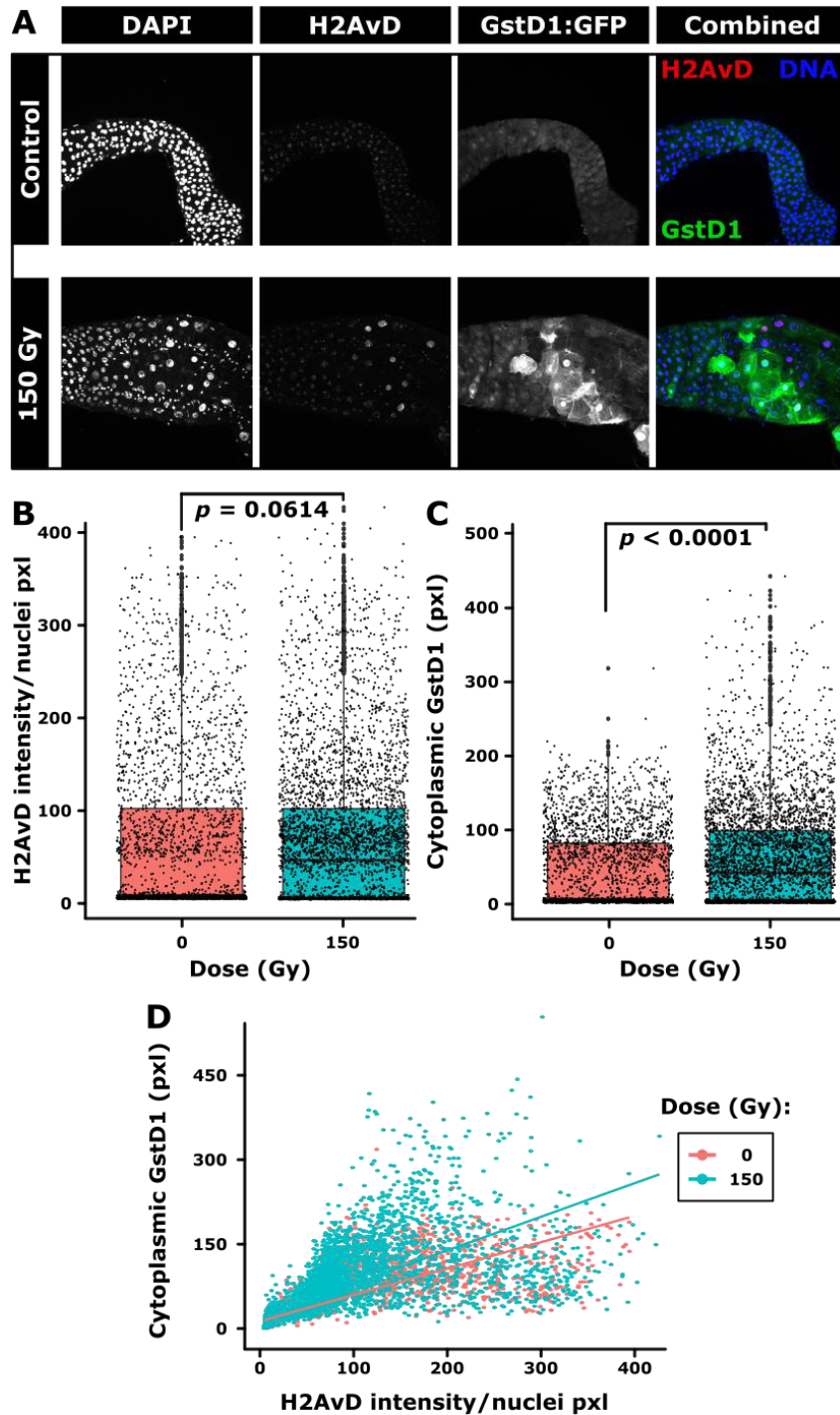
Figure 3.25: GstD1 and H2AvD levels within the midgut 14 days *post* irradiation. (**A**) Images are representative maximum projections *n* = 5 – 9 midguts per dose and each midgut was imaged in three random locations. (**B**) & (**C**) Nuclei size, H2AvD intensity, and cytoplasmic GstD1 GFP intensity was quantified using a custom designed Python image analysis script which relied on crowning segmentation (**Appendix 3**). (**D**) Cytoplasmic GstD1 data was trimmed to remove three datapoints which exceeded 900 intensity units. R was used to perform statistical analysis. Dataset consists of data for 7,474 cells. Boxes represent SD and whiskers min and max values range. *Drosophila* were exposed to radiation and kept at standard rearing condition for 14 days prior to dissection of tissue.

3.4.4 Exacerbating oxidative stress *post* irradiation

Since there was little correlation between radiation-induced oxidative stress and DNA damage, I wanted to investigate whether oxidative stress had any functional relevance to the health of *Drosophila post* irradiation. As starvation resistance has been successfully used as an assay in *Drosophila* that correlates with other measures of physiological health, I decided to perform starvation analysis to try and find an interaction between negative effects of radiation and oxidative stress. This approach offers the benefit of faster assaying, as compared to lifespan survival assaying. Previous work has shown that radiation treatment improves starvation survival (**Section 3.3.5**), I wanted to determine whether radiation treatment sensitises *Drosophila* to subsequent oxidative challenge via hydrogen peroxide (H_2O_2) feeding. This would help to elucidate whether oxidative stress plays a critical role in modulating survival *post* irradiation. It is expected that if oxidative stress plays a role, irradiated *Drosophila* exposed to H_2O_2 should demonstrate modulated survival compared to irradiated control *Drosophila*.

3.4.4.1 H_2O_2 dose optimisation

The optimal concentration of H_2O_2 to reduce survival of w^{1118} males under starvation was determined (**Figure 3.26**). From the concentrations assayed (0 – 30%), *Drosophila* showed a dosage dependent negative correlation between increasing concentration of H_2O_2 and reduction in survival (**Figure 3.26 A**), with control cohort demonstrating the longest median survival of 25 hr (21-29 hr, CI 95%) and the shortest median survival of 13 hr (13-16 hr, CI 95%) for cohort exposed to 30% H_2O_2 (**Figure 3.26 B**). A CoxPH model was generated with the explanatory variables of H_2O_2 dose and vial replicate (**Figure 3.26 C**). H_2O_2 dose was determined to be a significant modulator of survival ($p = 2.97 \times 10^{-12}$), with an estimated HR of 1.067 (1.048–1.087, 95% CI). Replicate was determined not to be a significant modulator of survival ($p = 0.065$). Both H_2O_2 dose and replicate passed the proportional hazards assumption ($p = 0.052$ & $p = 0.414$, respectively). It was decided that a H_2O_2 dose of 10% will be used for subsequent experiments.
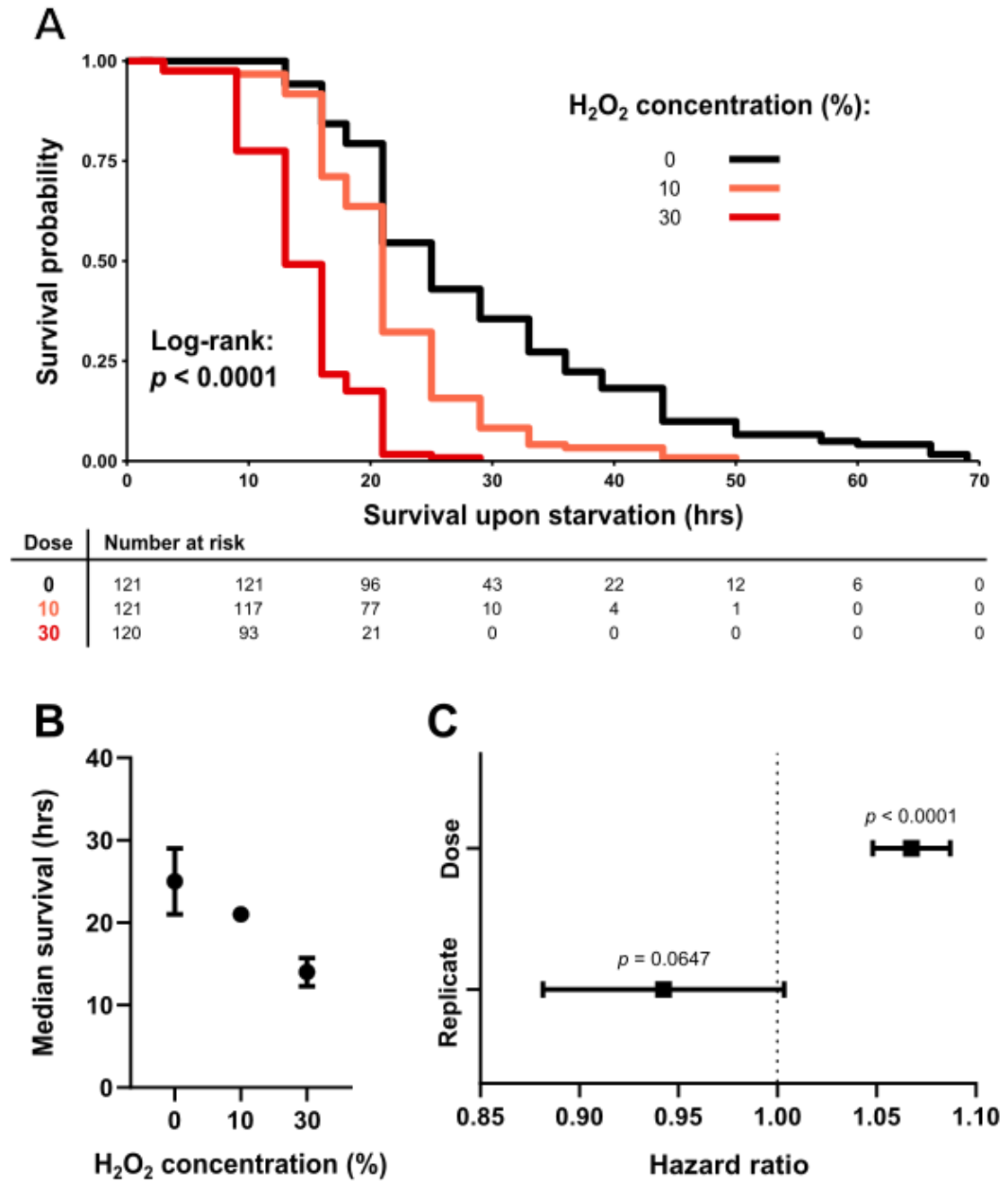
Figure 3.26: H₂O₂ reduces starvation resistance in *w¹¹¹⁸* males in a dose-dependent manner. Male adult *Drosophila* were purped as standard practice and allowed to mate for 48 hr, starvation and H_2O_2 feeding began simultaneously. (**A**) KM curve with *p* value derived from Log-rank testing, (**B**) median survival of vial replicates for each cohort with 95% CI, (**C**) HR derived from CoxPH model.

3.4.4.2 Interaction between radiation exposure and oxidative stress on starvation phenotype – w^{1118}

The starvation response of w^{1118} one day after irradiation was quantified to determine if there was an interaction between radiation treatment and oxidative stress. Radiation treatment appeared to be a non-significant modulator of survival in w^{1118}, whereas H_2O_2 exposure was a significant negative modulator of survival (**Figure 3.27 A** & **B**). A CoxPH model was generated with the explanatory variables of radiation treatment, H_2O_2 exposure, interaction between radiation and exposure, and vial replicate (**Figure 3.27 C**). H_2O_2 exposure was determined to be a significant modulator of survival ($p = 6.97 \times 10^{-12}$), with an estimated HR of 1.1062 (1.0748–1.139, 95% CI). Radiation treatment, an interaction, and replicate were not significant modulators of survival ($p = 0.159$, $p = 0.676$ and $p = 0.085$, respectively).

Similar to one day, starvation survival 10 days *post* irradiation, H_2O_2 exposure was a significant modulator of survival but not radiation treatment (**Figure 3.28 A** & **B**). A CoxPH model was generated with the explanatory variables of radiation treatment, H_2O_2 exposure, an interaction between radiation and exposure and vial replicate (**Figure 3.28 C**). Radiation treatment, H_2O_2 exposure and replicate were determined to be significant modulators of survival ($p = 0.027$, $p = 2 \times 10^{-16}$, and $p = 0.0047$, respectively), with estimated HRs of 1.0027 (1.0003–1.1.005, 95% CI), 1.2272 (1.1818–1.274, 95% CI), and 0.9999 (0.9996–1, 95% CI), respectively. An interaction between radiation treatment and H_2O_2 exposure was not significant modulator of survival ($p = 0.292$).

In contrast to one and 10 days *post* irradiation, on day 20 both irradiation and H_2O_2 exposure appeared to be significant modulators of survival in w^{1118} (**Figure 3.29 A** & **B**). A CoxPH model was generated with the explanatory variables of radiation treatment, H_2O_2 exposure, an interaction between radiation and exposure and vial replicate (**Figure 3.29 C**). Radiation treatment and H_2O_2 exposure were determined to be significant modulators of survival ($p = 6 \times 10^{-5}$, and $p = 2.25 \times 10^{-11}$, respectively), with estimated HRs of 0.9949 (0.9924–0.9974, 95% CI) and 1.1751 (1.1208–1.232, 95% CI), respectively. Vial replicate and an interaction between radiation treatment and H_2O_2 exposure were not significant modulators of survival ($p = 0.536$ and $p = 0.068$, respectively).
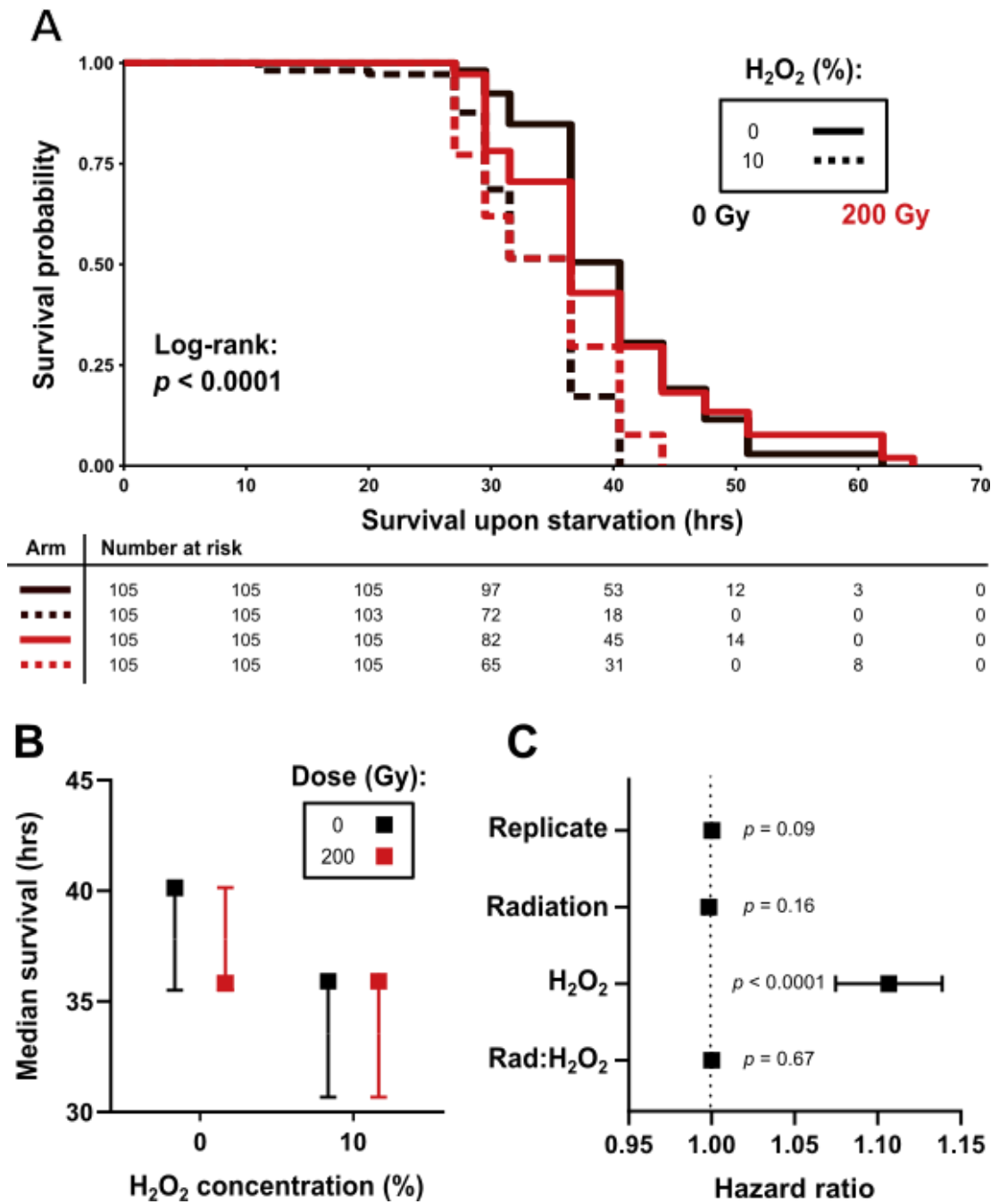
Figure 3.27: Starvation survival of male w^{1118} one day after irradiation (200 Gy) and exposure to H_2O_2. *Drosophila* were purped as standard practice and allowed to mate for 48 hr prior to irradiation, followed by 1 day incubation. (**A**) KM curve with risk table, (**B**) median survival of vial replicates for each cohort with 95% CI, (**C**) HR derived from CoxPH model.
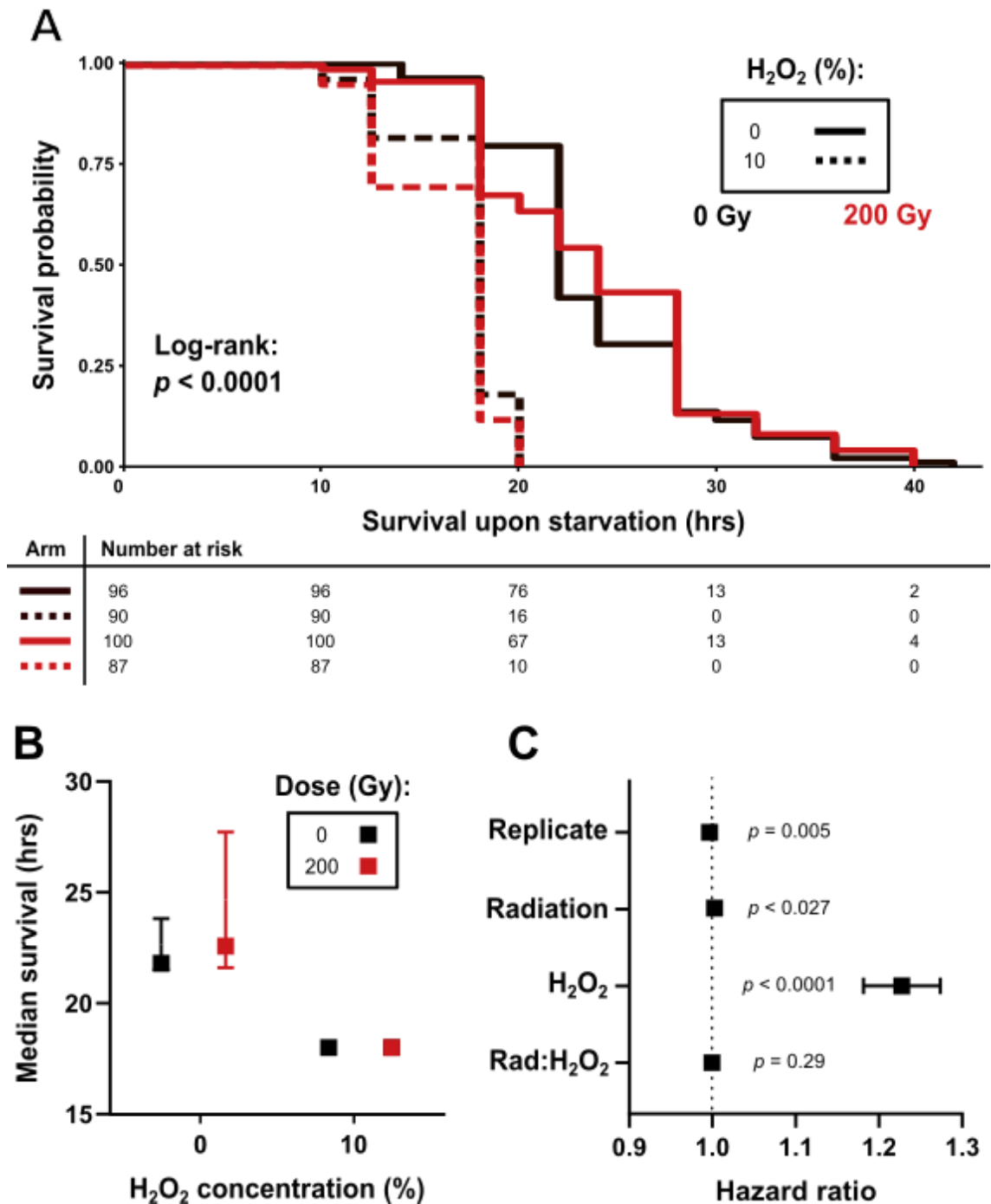
Figure 3.28: Starvation survival of male w^{1118} 10 day after irradiation (200 Gy) and exposure to H_2O_2. *Drosophila* were purped as standard practice and allowed to mate for 48 hr prior to irradiation, followed by 10 day incubation. (**A**) KM curve with risk table, (**B**) median survival of vial replicates for each cohort with 95% CI, (**C**) HR derived from CoxPH model.
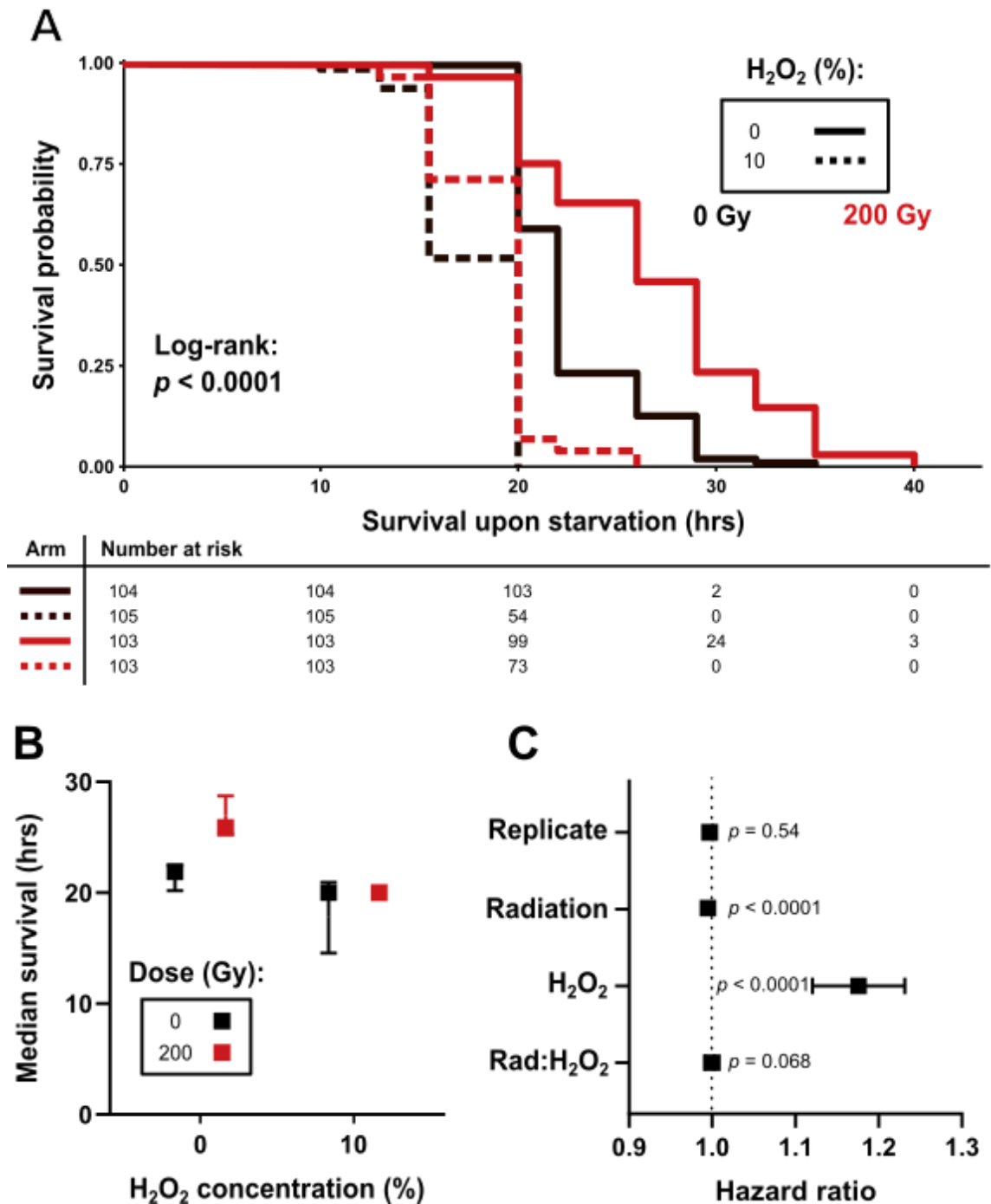
Figure 3.29: Starvation survival of male *w^1118* 20 day after irradiation (200 Gy) and exposure to H_2O_2. *Drosophila* were purped as standard practice and allowed to mate for 48 hr prior to irradiation, followed by 20 day incubation, after incubation *Drosophila* were starved for two hr and fed either H_2O_2 or H_2O. (**A**) KM curve with risk table, (**B**) median survival of vial replicates for each cohort with 95% CI, (**C**) HR derived from CoxPH model.

3.4.4.3 Interaction between radiation exposure and oxidative stress on starvation phenotype – *Oregon R*

Starvation survival on *Oregon R* strain was assayed 10 and 20 days *post* irradiation only (**Figure 3.30 - .31**). Similarly to w^{1118} at 10 days *post* treatment, radiation treatment was a non-significant modulator of survival, whereas H_2O_2 exposure was a significant modulator of survival (**Figure 3.30 A** & **B**). A CoxPH model was generated with the explanatory variables of irradiation, H_2O_2 exposure, an interaction between radiation and exposure and vial replicate (**Figure 3.30 C**). H_2O_2 exposure and vial replicate were determined to be significant modulators of survival ($p = 1.2x10^{-15}$ and $p = 0.0203$, respectively), with estimated HRs of 1.117 (1.0872–1.148, 95% CI) and 0.9999 (0.9999–1, 95% CI), respecitvely. Irradiation and an interaction were not significant modulators of survival ($p =0.145$ and $p = 0.265$, respectively).

In contrast to 10 days, 20 days *post* radiation treatment in *Oregon R* demonstrated a moderate increase in starvation survival following irradiation, and H_2O_2 exposure remained a significant modulator of reduced survival (**Figure 3.31 A** & **B**). A CoxPH model was generated with the explanatory variables of irradiation, H_2O_2 exposure, an interaction between radiation and exposure and vial replicate (**Figure 3.31 C**). Irradiation and H_2O_2 exposure were determined to be significant modulators of survival ($p = 0.022$, and $p = 2x10^{-16}$, respectively), with estimated HRs of 0.9981 (0.9965–0.9997, 95% CI) and 1.1841 (1.1413–1.2285, 95% CI), respectively. Vial replicate and an interaction between radiation treatment and H_2O_2 exposure were not significant modulators of survival ($p = 0.1581$ and $p = 0.1035$, respectively).

Collectively, these data suggest that long-term *post* irradiation *Drosophila* develop an enhanced survival to starvation. However in the presence of H_2O_2 the increase in survival associated with radiation treatment was not observed, as demonstrated by the similar median survival values between control and irradiated *Drosophila* exposed to H_2O_2.
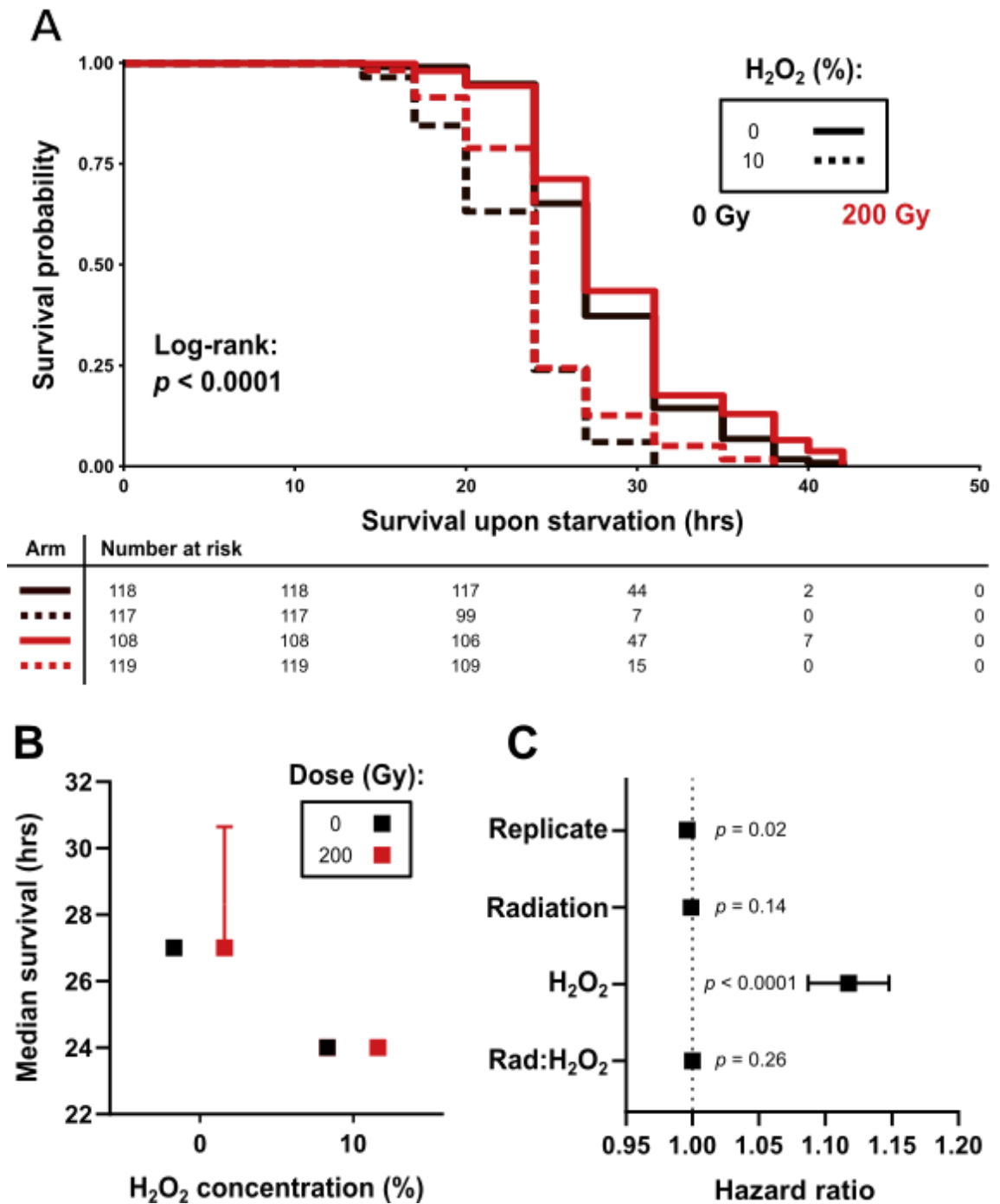
Figure 3.30: Starvation survival of male *Oregon R* 10 day after irradiation (200 Gy) and exposure to H$_2$O$_2$. *Drosophila* were purped as standard practice and allowed to mate for 48 hr prior to irradiation, followed by 10 day incubation. (**A**) KM curve with risk table, (**B**) median survival of vial replicates for each cohort with 95% CI, (**C**) HR derived from CoxPH model.
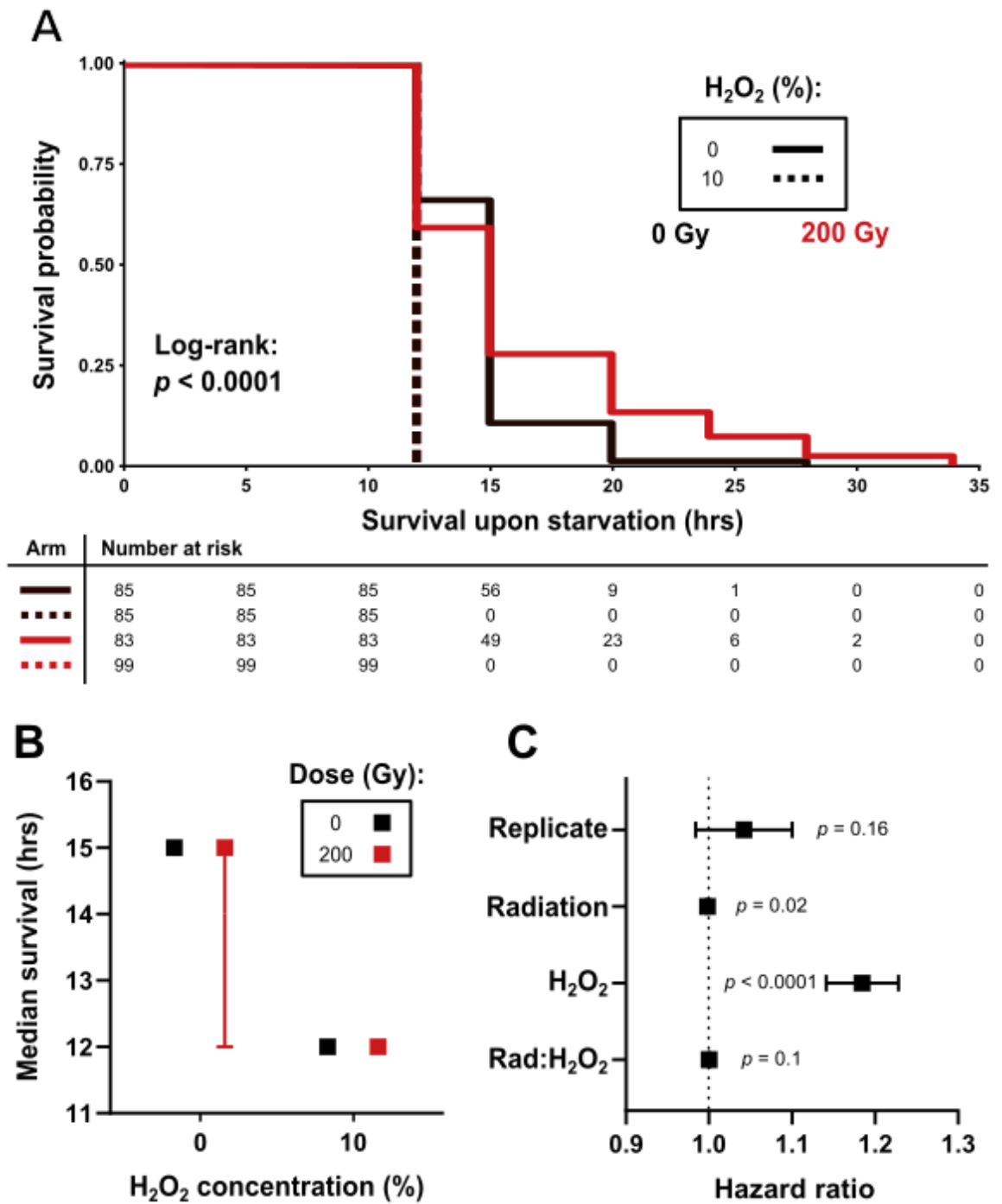
Figure 3.31: Starvation survival of male *Oregon R* 20 day after irradiation (200 Gy) and exposure to H₂O₂. *Drosophila* were purped as standard practice and allowed to mate for 48 hr prior to irradiation, followed by 20 day incubation. (**A**) KM curve with risk table, (**B**) median survival of vial replicates for each cohort with 95% CI, (**C**) HR derived from CoxPH model.

3.4.5 Recovery of normal oxidative status through NAC treatment

Inducing oxidative stress in *Drosophila* by feeding with H_2O_2 suggested that reduced survival observed in irradiated *Drosophila* may be independent of oxidative stress (**Section 3.4.4**). Hence, a different approach was employed to further characterise the role of oxidative stress in reduced survival associated with radiation treatment. N-acetyl cysteine (NAC) was used to protect the oxidative state of *Drosophila* before, during and after radiation treatment to see how it affected survival. NAC has been extensively used as a medication to treat a variety of issues in patients. It has been shown *in vitro* and specifically *in vivo* to act as an antioxidant (Ezeriņa *et al.*, 2018; Niraula & Kim, 2019). NAC was used to try and recover the oxidative state of *Drosophila post* irradiation via continuous feeding (*ad libitum* diet). A feeding dose of 1 mg/ml was used which has been shown to modulate *Drosophila* oxidative stress response withing having a negative impact on survival (Niraula & Kim, 2019).

Lifespan survival was assayed *post* irradiation (200 Gy) (**Figure 3.32**). Through visual inspection of KM curves, irradiation and NAC exposure resulted in reduced survival (**Figure 3.32 A**). This reduction in lifespan was confirmed through inspection of median survival times, the non-irradiated and non-exposed cohort had the longest survival time of 41 days (41 – 41 days, 95% CI), followed by non-irradiated and exposed cohort at 37 days (37 – 41 days, 95% CI), lastly irradiated cohorts that were NAC-exposed and non-exposed, demonstrated median survival values of 37 days (34 – 44 days, 95% CI) each (**Figure 3.32 B**). A CoxPH model was generated with the explanatory variables: NAC exposure, radiation treatment, an interaction between treatments, and vial replicate (**Figure 3.32 C**). NAC treatment was determined to be a significant modulator of survival ($p = 0.0021$), with exposure having an estimated HR of 1.067 (1.0193-1.091, 95% CI). Radiation treatment was also a significant modulator of survival ($p = 0.00026$), with an estimated HR of 1.0029 (1.0013-1.004, 95% CI). Replicate and an interaction (Rad:NAC) were determined not to be significant modulators of survival ($p = 0.2634$ and $p = 0.458$, respecitvely). Testing for proportional hazards that are independent of time using the Schoenfeld residual test determined that the variables of interaction (Rad:NAC) and replicate did not violate the proportional hazards assumption ($p = 0.307$ and $p = 0.169$, respectively). Variables of radiation and NAC treatment both violated the proportional hazards assumption ($p = 0.0069$ and $p = 0.0003$, respectively).

NAC treatment did not improve survival *post* irradiation, which supports my previous observations further showing that radiation-induced reduction in lifespan and health is independent of oxidative stress following radiation.
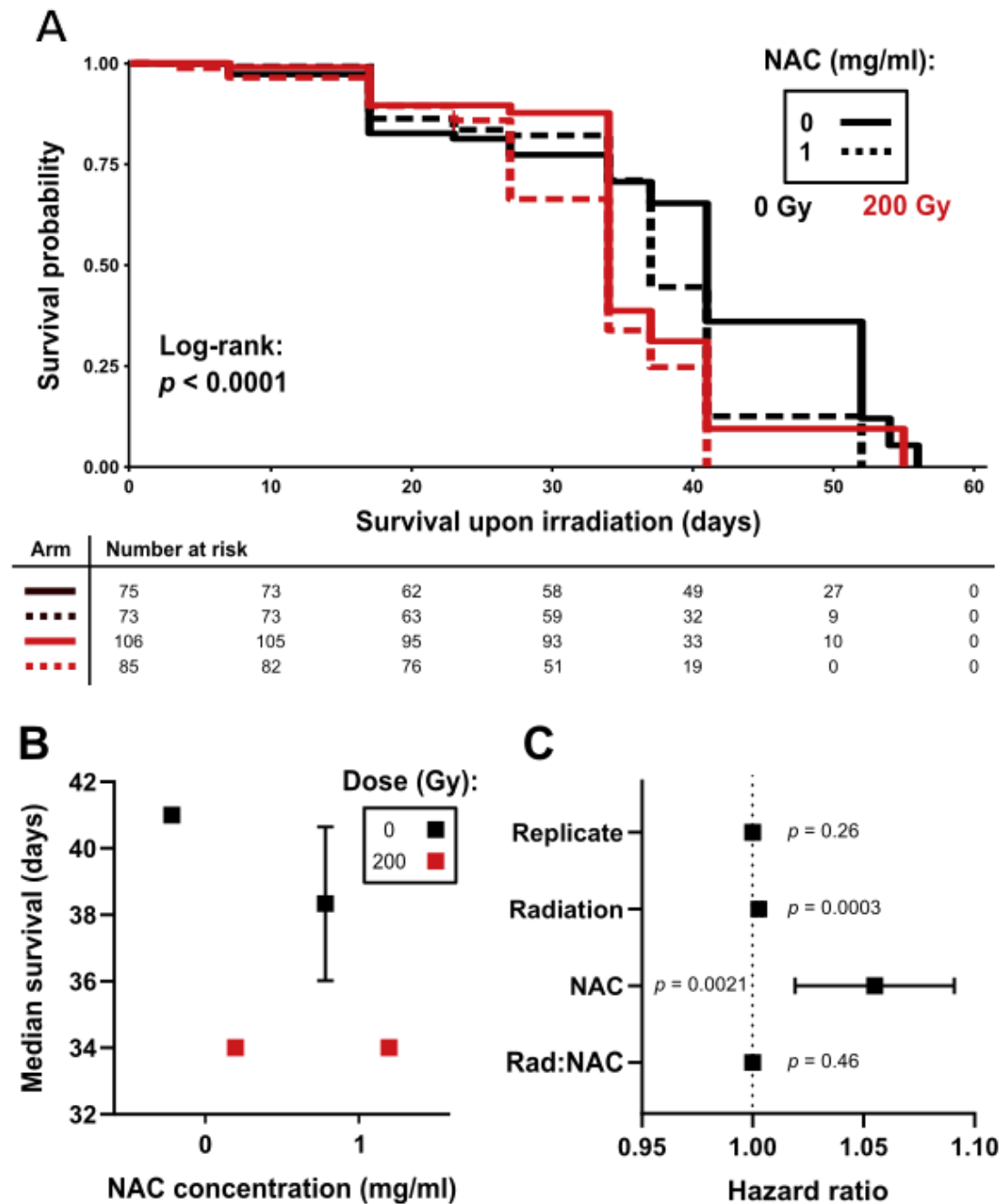
Figure 3.32: Survival of male *Oregon R* post irradiation (200 Gy) and with continuous feeding with N-acetyl cysteine. *Drosophila* were purped as standard practice and NAC fed *Drosophila* had an *ad libitum* diet from eclosion till death. (**A**) KM curve with risk table, (**B**) median survival of vial replicates for each cohort with 95% CI, (**C**) HR derived from CoxPH model.

3.5 Radiation-induced tissue remodelling

As oxidative stress does not appear to play a critical role in the health of *Drosophila*, other potential radiation-induced phenomena were explored. One of the more common long-term consequences of irradiation is fibrosis and tissue remodelling (Alsner, Andreassen & Overgaard, 2008; Straub *et al.*, 2015). Fibrosis is a repair mechanism in which fibrous connective tissue accumulates at the site of injury, this process can become pathological if left unchecked. Generally, severity depends on the tissue irradiated, but typically, a tissue that has undergone remodelling will have reduced functionality due to reduced volume and fibrotic constriction (strictures) (Capps, Fulcher, Szucs, & Turner, 1997), which may contribute to reduced survival following radiation treatment. The *Drosophila* orthologue of collagen is *Viking* (*Vkg*) and its accumulation has been shown to lead to activation of the Toll immunological pathways (Zang et al., 2015). This section will explore if midgut extracellular matrix (ECM) composition changes in response to radiation treatment and if tissue remodelling occurs upon irradiation.

3.5.1 No changes ECM of midgut *post* irradiation

Two weeks *post* irradiation, the thickness and intensity of Vkg surrounding the midgut was quantified (**Figure 3.33 A**). ANOVA testing determined that Vkg thickness around the midgut and signal intensity were non-significantly different between control (1.09 nm, 27.7 per ECM pixel) and irradiated (1.06 μm, 28.1 per ECM pixel) (p = 0.671 & p = 0.906, respectively) (**Figure 3.33 B** & **C**). Similarly, eight weeks *post* irradiation (**Figure 3.34 A**), Vkg layer thickness around the midgut and signal intensity were non-significantly different between control (1.21 μm, 33 per ECM pixel) and irradiated (1.30 μm, 29.8 per ECM pixel) (p = 0.274 & p = 0.269, respectively) (**Figure 3.34 B** & **C**).
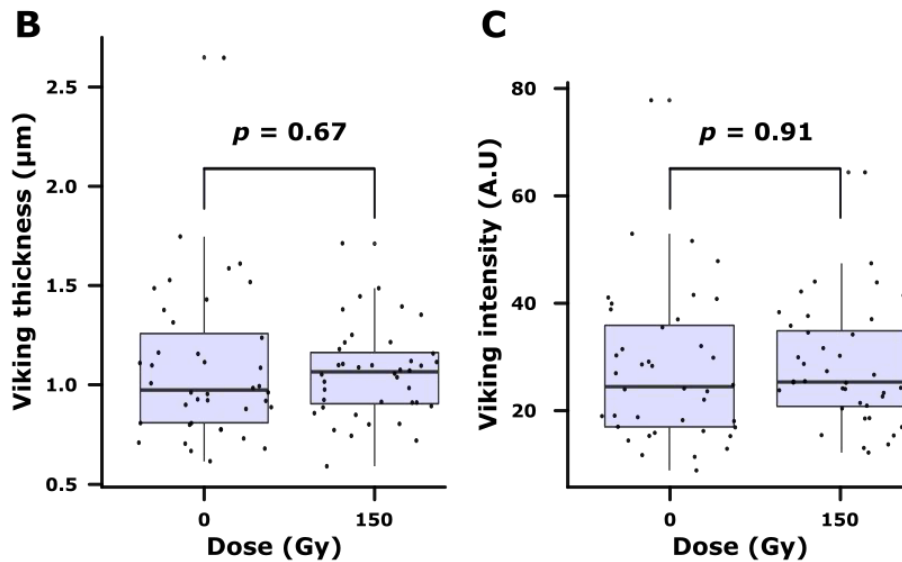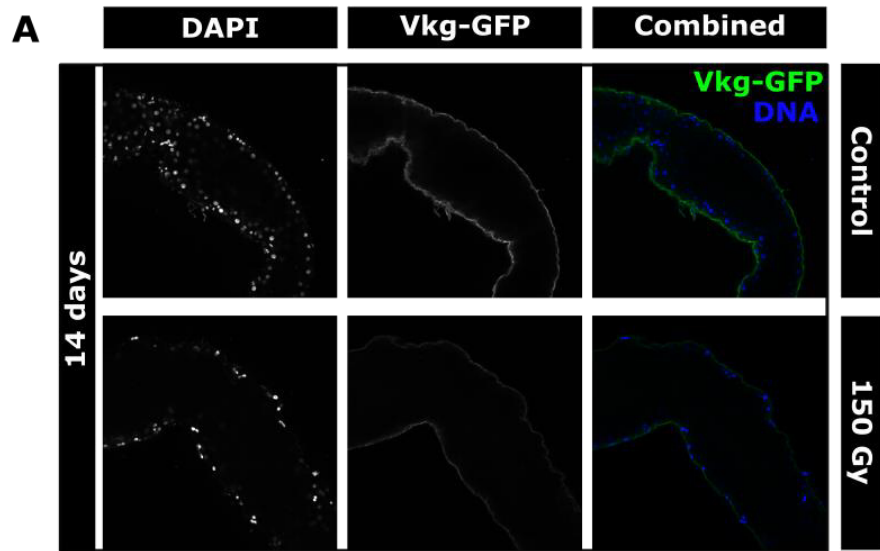
Figure 3.33: No change in Viking composition around the midgut 2 weeks *post* **irradiation.** (**A**) Images are selected slices of confocal stacks, *n* = 4 – 7 male midguts per dose and each midgut was imaged in three random locations. (**B**) Vkg thickness (μm) was manually quantified using ImageJ line measurement tool. (**C**) Average intensity of corresponding line measurements. Four midguts were selected from each treatment, and 10 thickness/intensity measurements were taken from randomly selected regions. ANOVA was performed to determine significance of both variables.
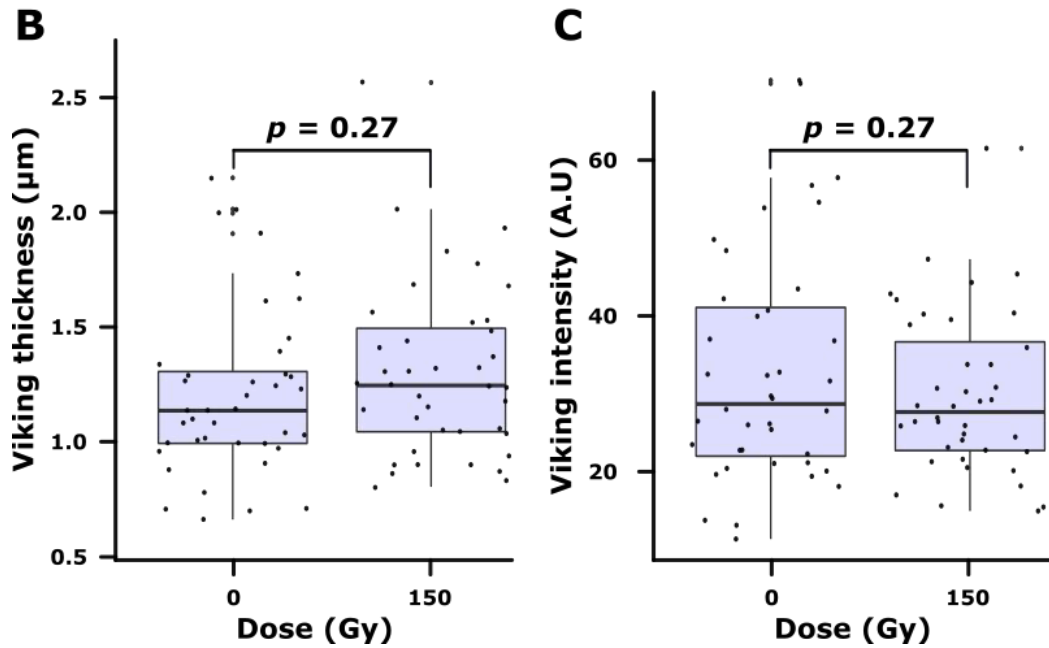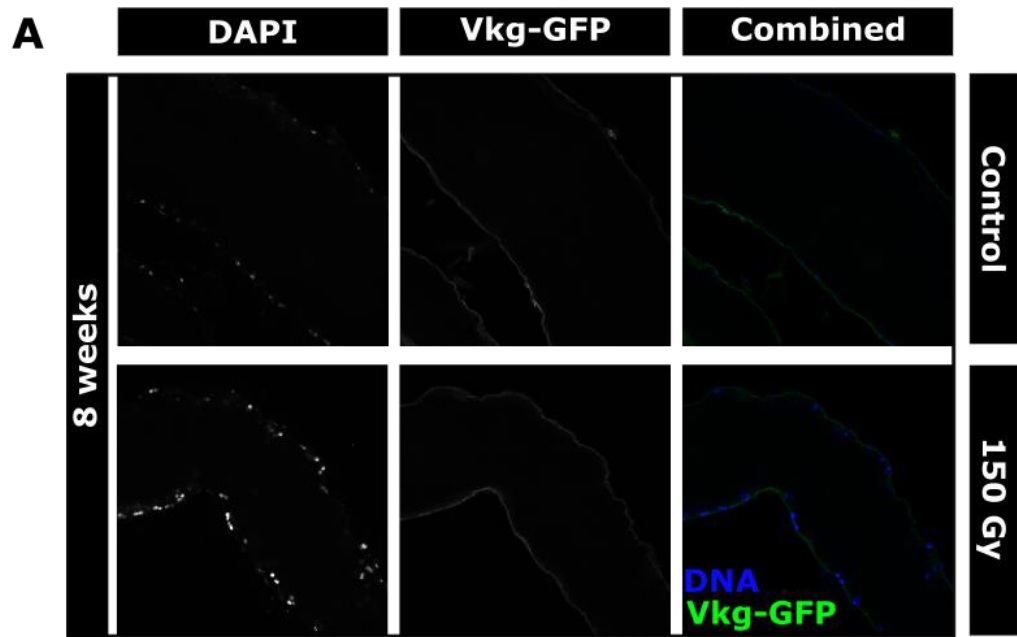
Figure 3.34: No change in Viking composition around the midgut 8 weeks *post* irradiation. (**A**) Images are selected slices of confocal stacks, *n* = 4 – 7 male midguts per dose and each midgut was imaged in three random locations. (**B**) Vkg thickness (μm) was manually quantified using ImageJ line measurement tool and LSMtoolbox plugin to access stack metadata. (**C**) Average intensity of corresponding line measurements. Four midguts were selected from each treatment, and 10 thickness/intensity measurements were taken from randomly selected regions. ANOVA was performed to determine significance of both variables.

3.5.2 Changes in nuclei distribution within the midgut *post* radiation treatment

To measure tissue remodelling, nuclei distribution within the midgut was analysed using a custom Python script that used 3D locations of each cell to determine the Euclidean distances of each nuclei in respect to other nuclei (**Appendix 4**). The radio-sensitive strain of *Oregon R* was used to measure long-term tissue remodelling, with a timeseries performed to quantify nuclei distribution within the midgut *post* treatment (**Figure 3.35**).

Tissue density (No. cells/10 nm^2) was quantified demonstrating that irradiated midguts show increased cell density 10 days *post* treatment, but not at any other timepoint (**Figure 3.36 A**). Irradiated nuclei had a density of 4.1 cells/10 nm^2 which was significantly higher than control nuclear density of 2.4 cells/10 nm^2 ($p = 0.004$). Two-way ANOVA determined that although dose was insignificant ($p = 0.12789$), time since treatment as well as the interaction between dose and were significant ($p = 0.0004$ and $p = 0.0011$, respectively). This suggests that radiation-induced remodelling of the midgut is a long-term process within *Drosophila* but quantification of more timepoints between 1 and 10 days *post* irradiation is required to verify this.
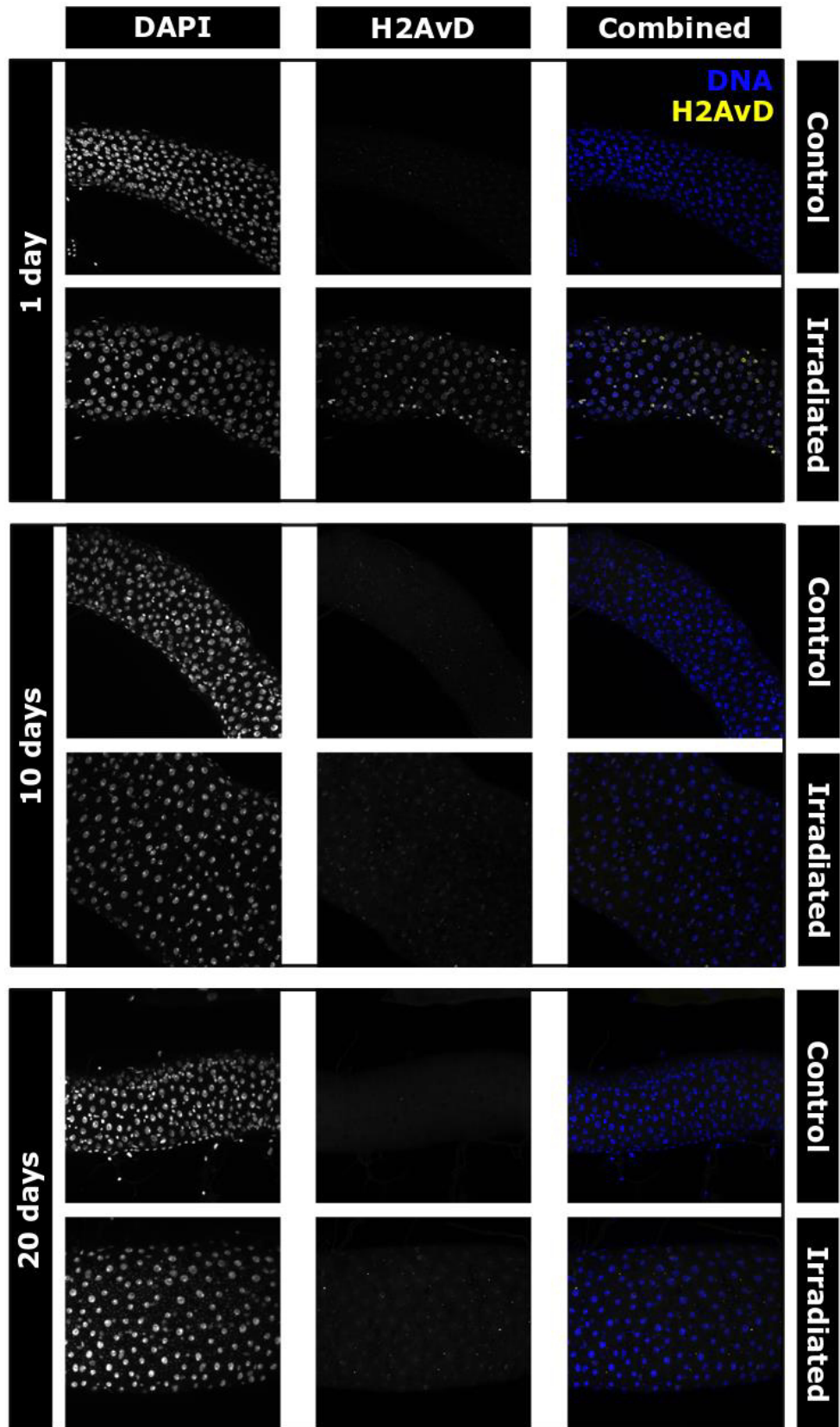
Figure 3.35: Nuclei density over time in the midgut of male *Oregon R.* *Drosophila* were purped and reared at 25°C and exposed to radiation (200 Gy). Images are representative maximum projections, $N = 12$.
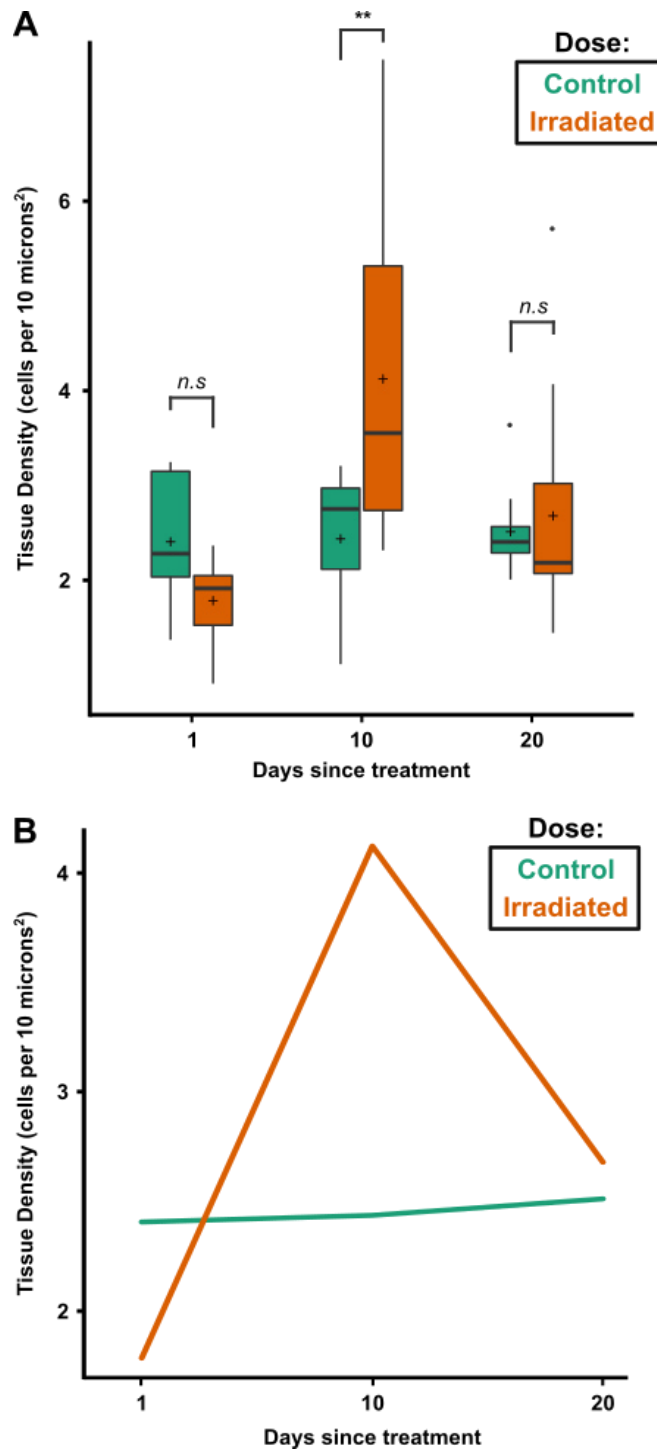
Figure 3.36: Radiation treatment leads to long-term changes in nuclear density. Adult male *Oregon R Drosophila* were purped and mated for 48 hr prior to 200 Gy exposure. Tissue density of nuclei was calculated for each stack, with each treatment having at least 12 stacks. (**A**) boxplots represent upper and lower quartiles of dataset, (**-**) median value, (**+**) mean value. (**B**) Calculated interaction plot. For each treatment at each timepoint, stacks were acquired from at least three biological replicates (midguts) and at least three technical replicates (positions within each midgut). Datasets for each timepoints comprised data from ~20,000 cells.

3.6 Mimicking human radiotherapy regimes

To evaluate my *Drosophila* model as a pre-clinical tool to study human long-term radiation toxicity, I compared the response of *Drosophila* to modulated radiation treatments to determine if different regimes lead to changes in survival, as is the case for patients. For patients, RT regimes are fractioned, which involves splitting the total dose into fractions that are given over the course of weeks to months (**Section 1.4**) (Fowler, 2001; Soares *et al.*, 2005). In contrast, I typically exposed *Drosophila* to a single radiation dose. Therefore, I quantified the response of *Drosophila* to different fractionated radiation regimes that mimicked the regimes that patients are typically exposed to during RT. Furthermore, I characterised the response of *Drosophila* to different dose rates since dose rate is a known modulator of curative outcome of cancer and survival (Hall & Brenner, 1991; Hall, 2014).

3.6.1   Fractionation

w^{1118} males were exposed to fractionated and non-fractionated radiation regimes (**Figure 3.37**). As the purpose of this experiment was to expose *Drosophila* to radiation similar to how humans receive RT, radiation treatment was given later in adult life at seven days *post* eclosion. The fractionated dose was split over the course of five consecutive days with 30 Gy given at the same time each day for a total dose of 150 Gy (**Figure 3.37 A**). When comparing the survival of *Drosophila* exposed to a single large dose to the fractionated cohorts, there appears to be a clear reduction in survival for non-fractionated cohort, and the fractionated cohort KM curve interlacing the control KM curve at least twice, indicating no significant difference in survival (**Figure 3.37 B** & **C**). A CoxPH model was generated from a subsetted dataset containing both the irradiated arms (fractionated and non-fractioned) with the explanatory variables: fractionation and replicate (**Figure 3.37 D**). Replicate was not a significant variable in modulating survival (p = 0.36). Fractionation was a significant variable ($p < 0.001$) in modulating survival and had an associated HR of 0.267 (0.198 – 0.364, 95% CI). Testing for proportional hazards that are independent of time determined that both replicate and fractionation did not violate the proportional hazards assumption (p = 0.68 and p = 0.91, respectively).

The levels of H2AvD staining within the midgut seven days after fractionation demonstrated that receiving either a single large dose of radiation or a fractionated dose results in increased H2AvD staining within the midgut of *Drosophila* that persisted seven days after regime completion (**Figure 3.38 A**). For all treatments

there appeared to be a positive correlation between increasing nuclei size and H2AvD staining, with nuclei from non-fractioned and fractionated samples having higher H2AvD staining (**Figure 3.38 B**). Due to the correlation between increasing nuclei size and H2AvD staining, it was decided to account for nuclei size when comparing H2AvD intensity between treatments, as it has been observed that radiation treatment induces morphological changes to nuclei within the midgut (**Section 3.3.5**). The average H2AvD intensity per nuclei pixel for control arm was 14.59 a.u, for fractionated it was 24.77 a.u, and for non-fractionated it was 29.22 a.u (**Figure 3.38 C**). ANOVA testing determined that treatment was a significant variable influencing H2AvD intensity per nuclei pixel ($p < 0.001$). Tukey's multiple comparison testing determined that all three treatment comparisons were highly significant ($p < 0.001$). These data suggest that receiving a single high dose of radiation is more detrimental to *Drosophila* compared to a fractionation approach, which appears to increase survival rates and result in lower levels of H2AvD staining within the midgut.
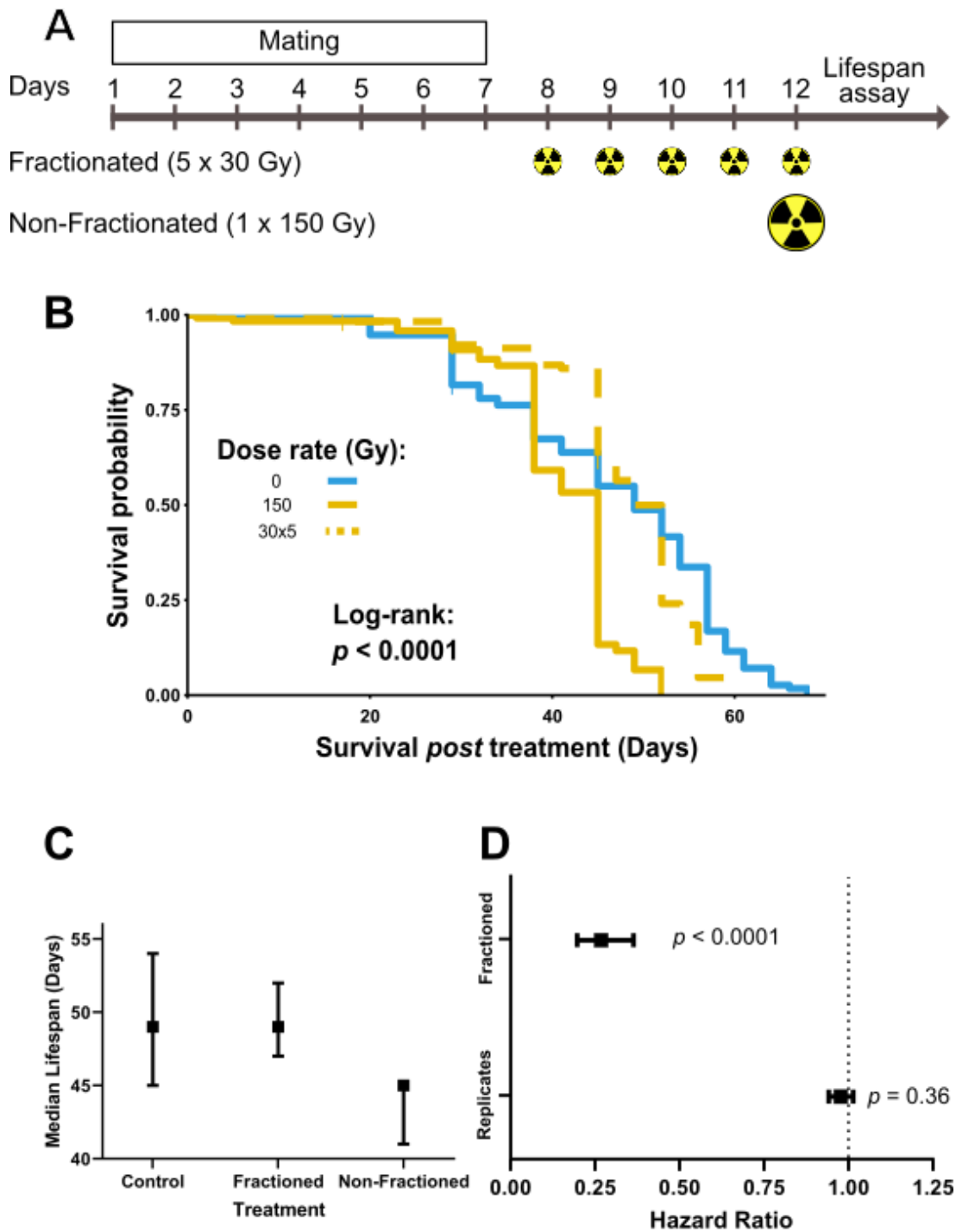
Figure 3.37: Fractionation of radiation treatment improves survival outcome in *w^{1118}* males. (**A**) Fractionation regime for each arm. (**B**) KM curves for each cohorts, vertical bars denote censoring. (**C**) represent 95% CI for median survival day of vial replicates, $N = 354$ with 114 - 120 *Drosophila* in each arm. (**D**) CoxPH model with derived HRs for fractionated and replicate variables. Whiskers represent 95% CI.
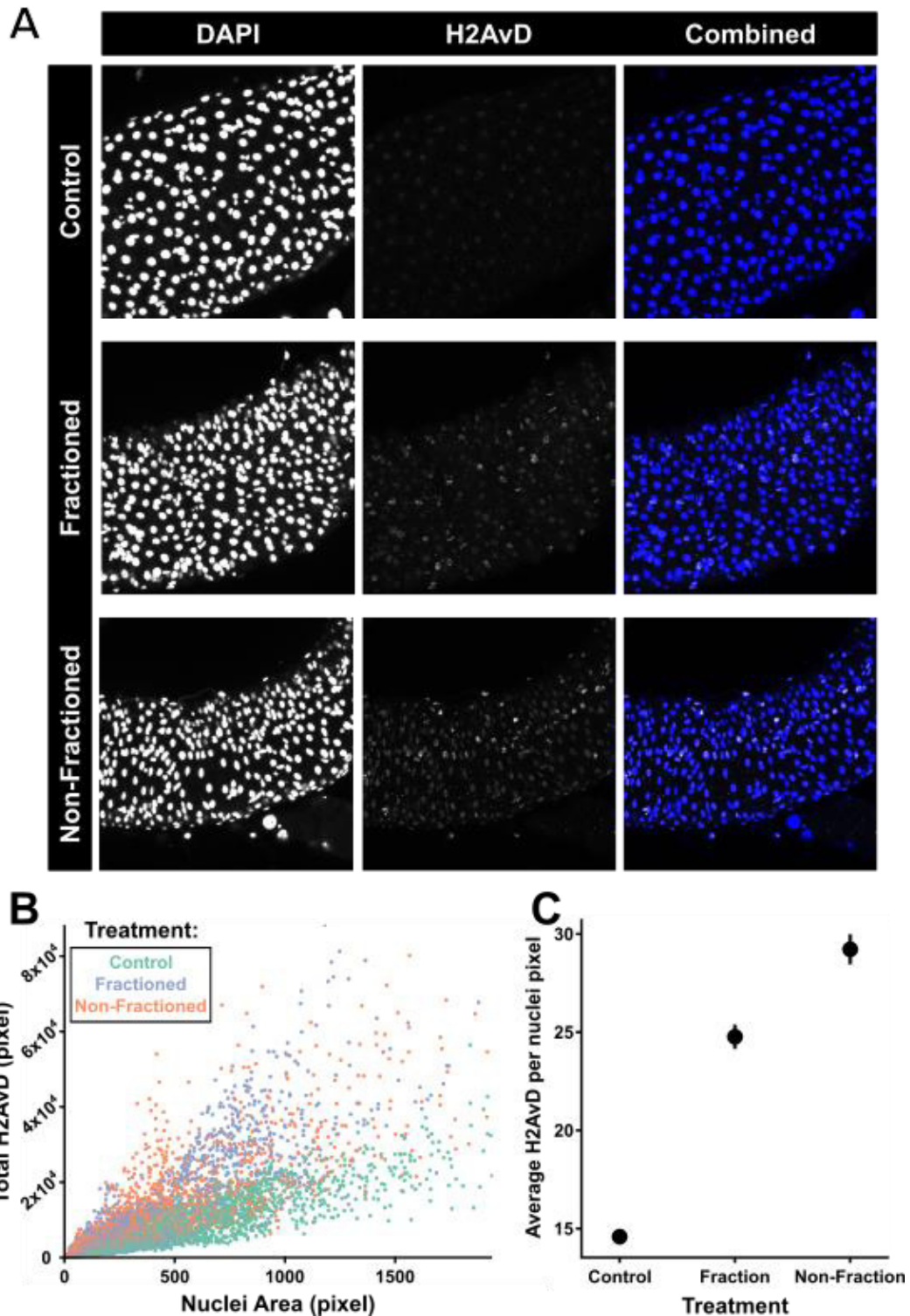
Figure 3.38: Fractionated radiation regime modulates systemic midgut DNA damage in *w^1118* males. (**A**) Representative maximum projections of midguts for each cohort from dose fractionation experiment. (**B**) Total H2AvD signal intensity per nuclei against nuclei pixel area, *N* = ~2,000 cells per treatment derived from 3 midguts with 3 stacks imaged for each midgut. (**C**) Average H2AvD intensity per nuclei pixel with 95% CI, ANOVA was performed followed by Tukey's multiple comparison test.

3.6.2 Hyper-Fractionation

To further validate the *Drosophila* radiation model and the results of the fractionation section, the ability of hyper-fractionation (HF) to modulate survival was studied. HF is the administration of radiation to patients in smaller and more frequent doses e.g. multiple small doses daily. This more intense treatment schedule has been shown to improve curative rate of some cancers via allowing for increased overall dose and better survival prognosis for patients (Stuschke & Thames, 1997). The aim of this section was to determine whether HF of treatment leads to better survival outcome for *Drosophila*.

Oregon R males were exposed to a HF regime which involved two radiation doses of 10 Gy daily over the course of 14 days for a total received dose of 200 Gy (**Figure 3.39 A**). As shown on the KM curves, the non-fractionated cohort had the greatest reduction in survival, followed by the HF cohort – though the HF cohort curve interlaces twice with the curve of control cohort (**Figure 3.39 B**). Median survival for control cohort was 42 days (40-48, 95% CI) which overlapped with median survival of HF cohort which was 40 days (38-42, 95% CI), but not with the non-fractionated cohort which had the lowest median survival of 38 days (33-38, 95% CI) (**Figure 3.39 C**). A CoxPH model was generated from subsetted dataset containing only the irradiated arms (HF and non-HF) with the explanatory variables: HF and replicate (**Figure 3.39 D**). Replicate was not a significant variable in modulating survival (p = 0.8). HF was a significant variable (p < 0.0001) in modulating survival and had an associated HR of 0.267 (0.198 – 0.364, 95% CI). Testing for proportional hazards that are independent of time determined that both replicate and HF did not violate the proportional hazards assumption (p = 0.68 and p = 0.91, respectively).

The levels of H2AvD staining within the midgut seven days after HF regime completion were quantified (**Figure 3.40**). Sum projections were analysed, and 15 nuclei were randomly selected from each projection. Interestingly, DAPI localisation within nuclei was diffused but only in tissue exposed to a single large dose of radiation (**Figure 3.40 A**). For that reason, this treatment had a modified analysis. H2AvD channel was used to select nuclei and a large bounding box was hand drawn to account for nuclei area. Upon visual inspection of projections, it was noted that the tissue undergoing HF had large nuclei sporadically positioned within the tissue (**Figure 3.40 A**). This led to looking at the distribution of nuclei area between treatments (**Figure 3.40 B**). Both irradiation treatments resulted in slightly larger

nuclei, with HF having largest nuclei (>40 pixels). H2AvD levels for both radiation treatments were significantly higher than control (**Figure 3.40 C**). Non-HF had the highest levels of H2AvD at 449 which was significantly higher than HF (373) ($p = 3.9\text{x}10^{-6}$), and control (174) ($p < 1\text{x}10^{-16}$).

Similarly to the fractionation experiment, HF demonstrated improved survival of *Drosophila* and reduced levels of DNA damage within the midgut.
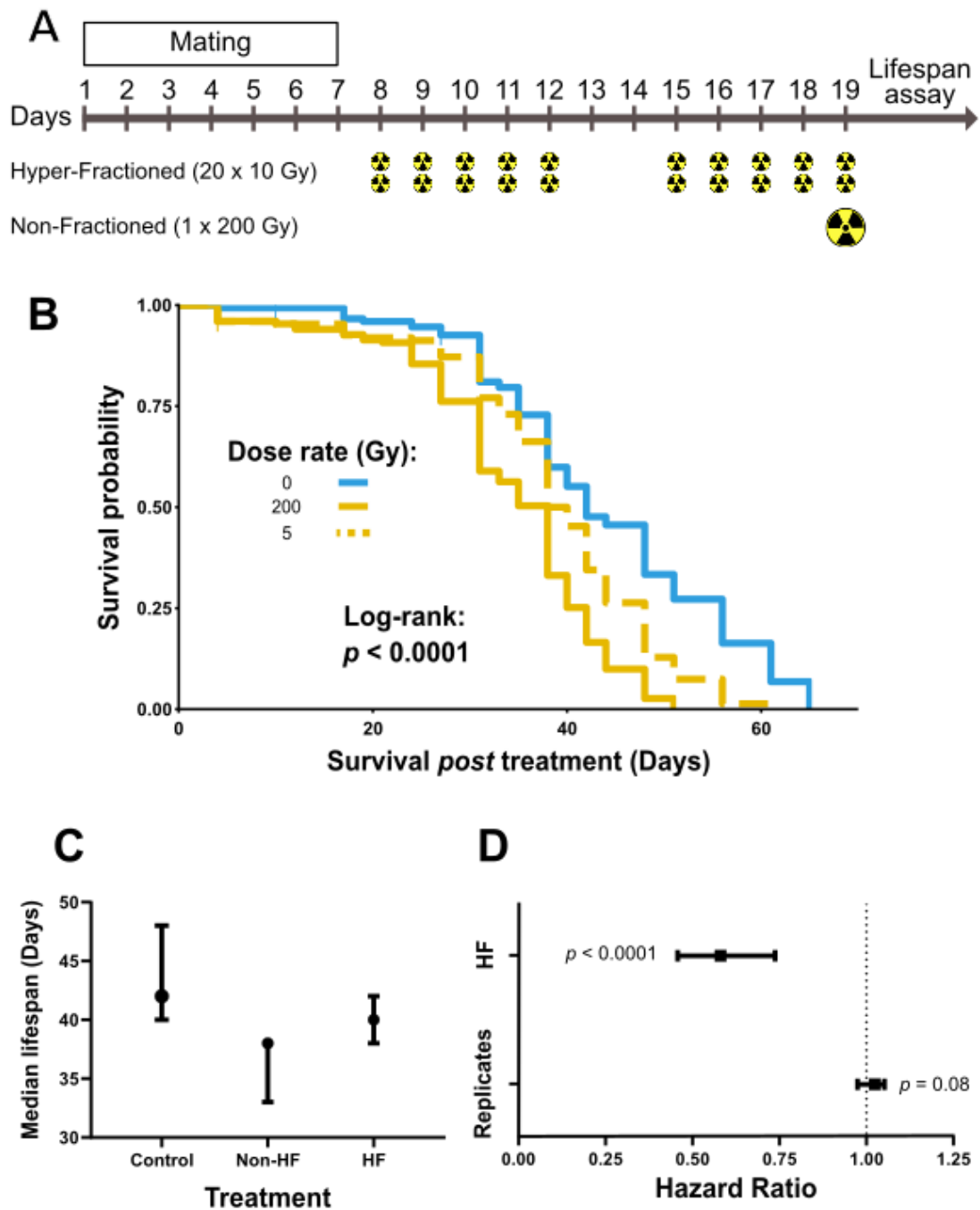
Figure 3.39: Hyper-fractionation regime improves survival outcome for *Oregon R* males. (**A**) Hyper-fractionation regime for each arm with total dose of 200 Gy. (**B**) KM curves for each cohorts, **I** (pipe) denotes censored *Drosophila*. (**C**) represent 95% Confidence intervals for median survival day, derived from Kaplan-Meir function. *N* = 354 with 114 - 120 *Drosophila* in each arm. (**D**) CoxPH model with derived HRs for fractionated and replicate variables (+ or − 95% CI).
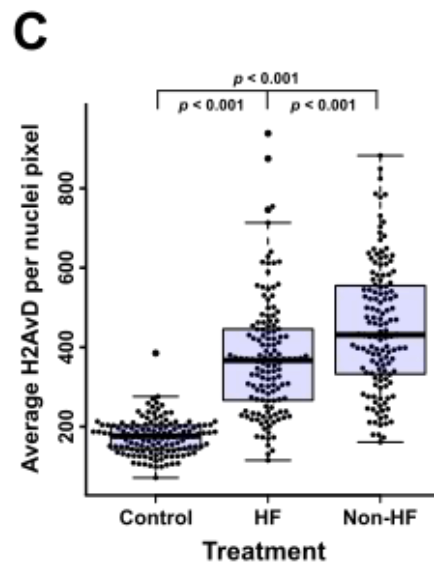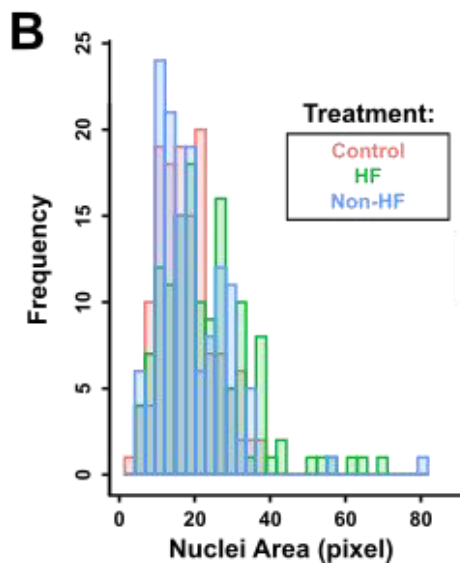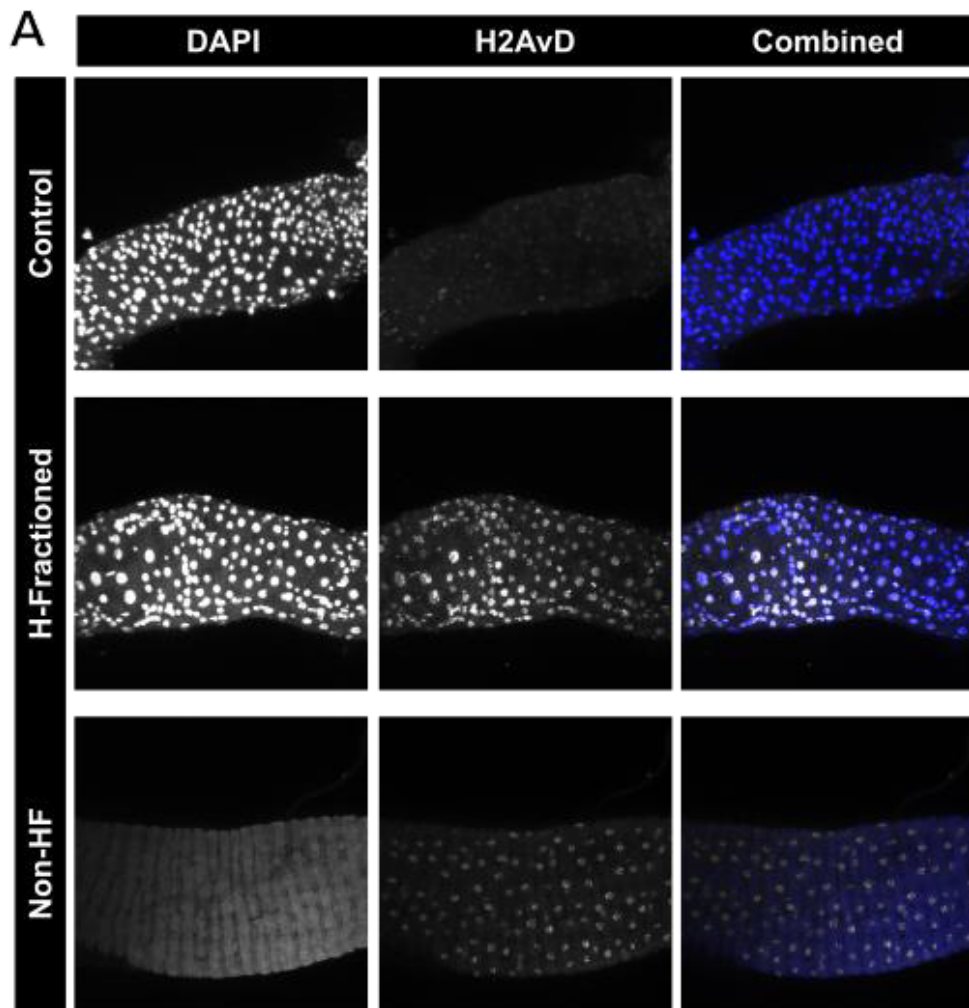
Figure 3.40: Hyper-fractionation regime modulates systemic midgut DNA damage of *Oregon R* males. (**A**) Representative maximum projections of midguts for each cohort. (**B**) Histogram of nuclei area (pixels), $N = 135$ cells per treatment derived from 3 midguts with 3 stacks imaged for each midgut. (**C**) Average H2AvD intensity per nuclei pixel per nucleus and boxplot showing quartiles of data, ANOVA was performed followed by Tukey's multiple comparison test.

3.6.3 Dose Rate

To further validate the model, I looked at the effect of dose rate. In humans, dose rates have been extensively studied and is a significant modulator of survival and treatment effectiveness (Hall & Brenner, 1991; Ślosarek *et al.*, 2014; Rühm *et al.*, 2018). However, it is unclear if dose rate has any effect on the survival of *Drosophila*.

Oregon R survival was measured after irradiation from two irradiators each with specific dose rates of 0.45 and 2 Gy/min (**Figure 3.41**). It can be seen that radiation treatment, irrespective of dose rate, reduces survival. Additionally, both radiation-treated KM curves interweaved multiple times, an indication that there was no significant difference between radiation treatments. Median survival time of low dose rate arm was 36 days (36-38, 95% CI) and high dose rate was 38 days (36-40, 95% CI): both of which were shorter than control median survival of 54 days (54-57, 95% CI) with no overlap of CIs (**Figure 3.41 B**). A CoxPH model was generated from the dataset with the explanatory variables: dose rate and replicate (**Figure 3.41 C**). However, testing for proportional hazards that are independent of time determined that replicate, and dose rate both violated the proportional hazards assumption ($p < 0.0001$ and $p < 0.0001$, respectively).

To see if the effect on survival correlated with long-term DNA damage in the midgut, I stained for H2AvD levels. Both dose rates led to increase in H2AvD levels in nuclei, as compared to non-irradiated midguts (**Figure 3.42 A**). H2AvD levels for both high and low dose rate treatments were not significantly different to each other (34.8 a.u and 32.1 a.u, respectively) ($p = 0.9$), but were significantly higher than control (7.1 a.u) (both $p = 0.001$) (**Figure 3.42 B**). Dataset was not normally distributed ($p = 0.01$, Shapiro-Wilks's test), therefore the non-parametric Kruskal-Wallis' test was used.
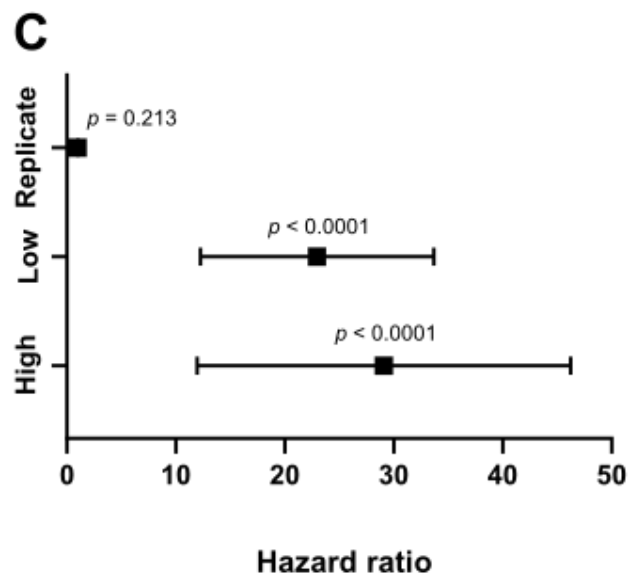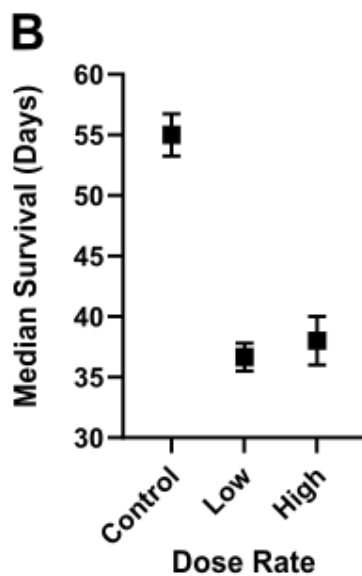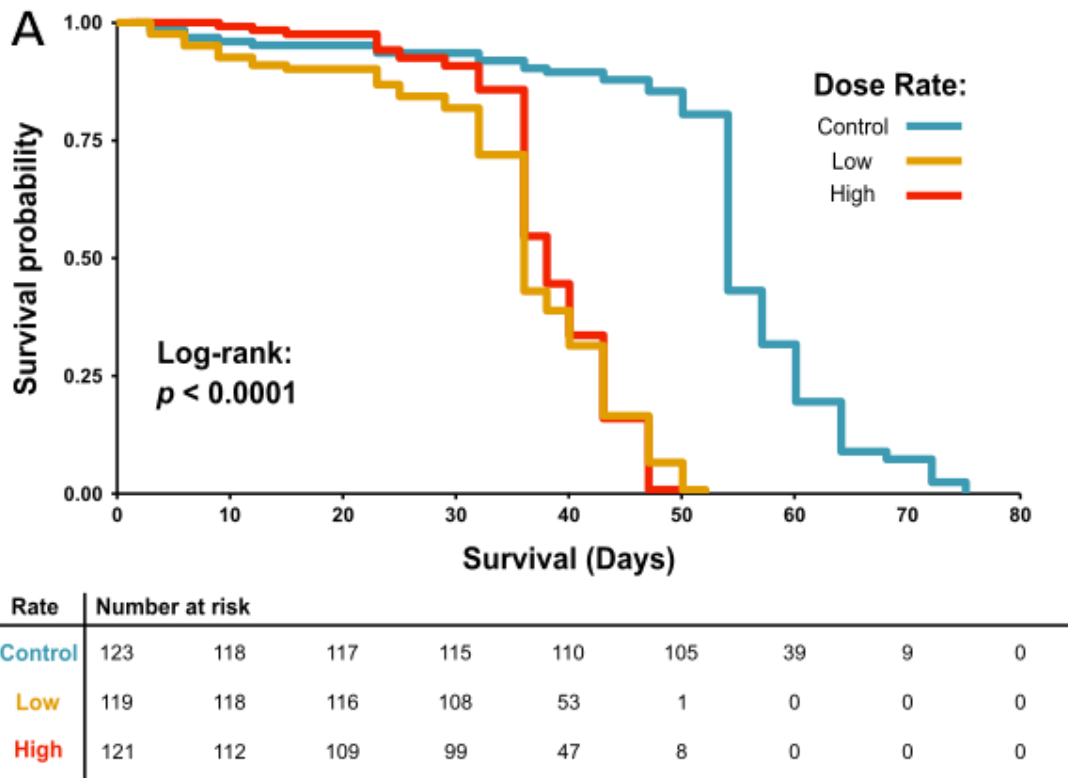
Figure 3.41: Dose rate does not modulate survival of *Oregon R* males. (**A**) KM curves for each cohorts, **l** denotes censored *Drosophila*, and risk table below. (**B**) Vial replicate median survival values for each cohort with 95% confidence intervals, *N* = 363 with 119 - 123 *Drosophila* in each arm. (**C**) CoxPH model with derived HRs for cohorts exposed to high and low dose rates (95% CI). Total dose was 200 Gy for both radiation treatment arms.
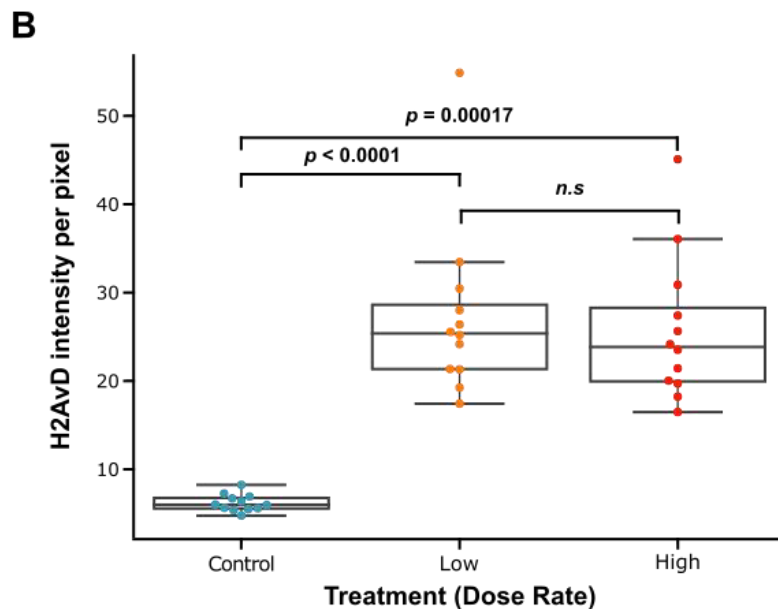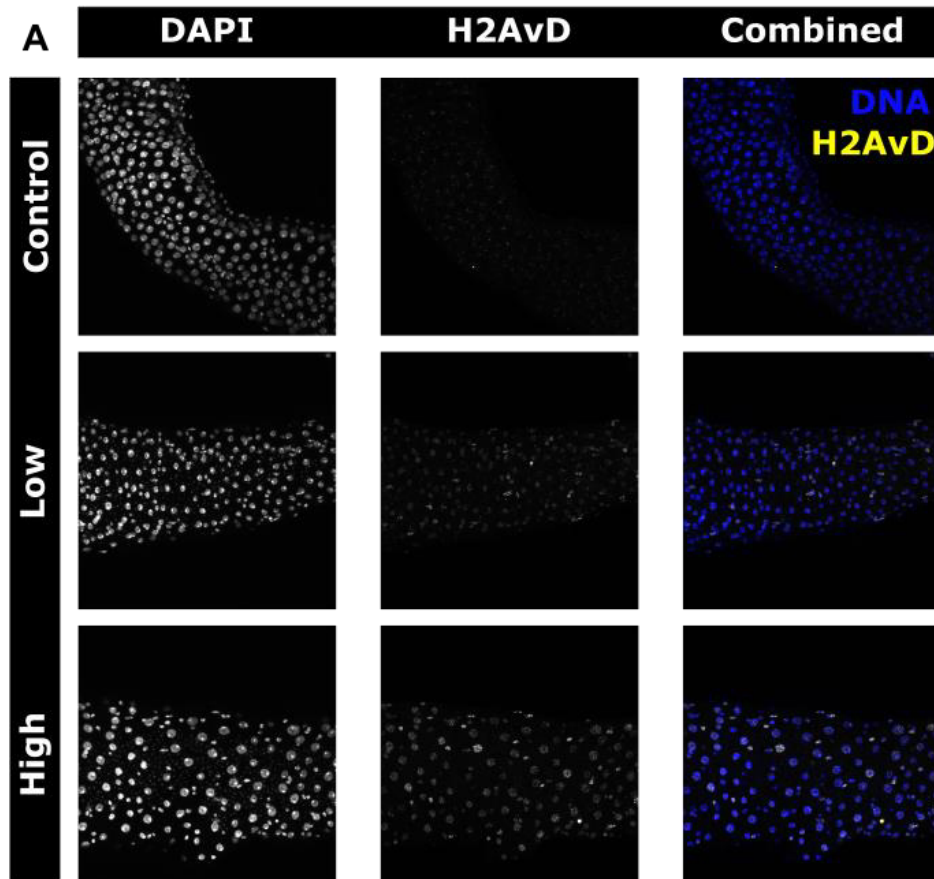
Figure 3.42: Dose rate does not immediately (one day) modulate DNA damage in the midgut. (**A**) Representative maximum projections of midguts for each cohort from dose rate experiment. (**B**) median values for each gut of average H2AVD intensity per nuclear pixel. *P* values derived from Dunn's nonparametric multiple comparisons test. *N* = 21,426 derived from four midguts and three positions imaged per midgut. A custom Python image analysis script was designed to quantify H2AvD intensity per nuclei pixel per sample from image stacks (**Appendix 5**).

3.7 Discussion

3.7.1 General reduction in health – multiple metrics

I wanted to identify a dose that significantly reduced survival *post* irradiation treatment but was titrated to allow *Drosophila* to survive long enough so we can study and develop a model for long-term tissue toxicity (**Section 3.3.1**). Furthermore, I wanted to confirm that the dose given led not only to a reduction in health (lifespan analysis) but also broad histological changes to study tissue specific responses. To check this, I performed H2AvD staining which indirectly measures the level of DSB within nuclei. I found that males demonstrated an expected reduction in lifespan corresponding to an increase in radiation dose (**Figure 3.3**) and that 150 – 200 Gy was the optimum radiation dose which I used for future experiments. For humans a whole-body irradiation of 100 Gy would be considered life-threatening, for example survivors of Hiroshima and Nagasaki were estimated to have lost ~1.3 years of life for every 1 Gy absorbed (Cologne & Preston, 2000). Whereas *Drosophila* can survive 150 Gy with only a modest reduction (13%) in lifespan – a clear indication that *Drosophila* are radio-resistant (**Figure 3.2**).

There are a number of prerequisites that would need to be met in order for a *Drosophila* long-term radiation response model to be a relevant pre-clinical tool (**Figure 3.1**) – one of which is that the radiation response is a polygenic trait as it is in humans. Multiple *Drosophila* strains with distinct lineages were lifespan assayed upon irradiation to determine if genotype was a significant modulator of survival (**Figure 3.5**). The North American strain *Oregon R* was determined to be radio-sensitive, whereas the European strain *Swedish C* was radio-resistant, two lines with distinct genetic backgrounds with significantly different sensitivities to radiation treatment. To corroborate the results presented, a number of published articles report *Oregon R* as being a radio-sensitive strain (Skorobagatko, Mazilov & Strashnyuk, 2020; Yushkova, 2019). Though genotype was determined to be a significant variable influencing radiation survival, the limited experiments performed here do not fully prove that the radiation response is a polygenic trait in *Drosophila*.

To further compare *Drosophila* radiation response to that of humans, several organ systems and health metrics were studied to see how radiation affects their function. Fertility and movement were negatively impacted by radiation treatment. In the radio-sensitive strain *Oregon R*, both irradiated males and females had reduced fertility *post* irradiation treatment (**Figures 3.6** & **3.7**), which agrees with previous studies exploring the effects of radiation on various aspects of fertility, and

specifically in *Oregon R* (Yushkova, 2019). Radiation treatment demonstrated to have a long-term negative effect on movement which is evident 20 days *post* treatment (**Figures 3.8** & **3.9**). It also indicates that either muscles involved in walking or the central nervous system have been under persistent damage or accrued unrepairable damage since the initial irradiation. This is an interesting observation, since it was hypothesised that radiation treatment would only have an effect on highly proliferative tissue e.g. midgut and gonads. However, either the muscle or central nervous system of *Drosophila* is under sustained damage as the result of treatment. The function of the midgut was also shown to be negatively impacted by radiation treatment, as demonstrated by reduced weight and amount of frass produced (**Sections 3.3.6** & **3.3.7**). Overall, a number of organ systems as well as general health of *Drosophila* were negatively impacted by radiation treatment. However, unexpectedly, radiation was shown to improve the response of *Drosophila* to starvation. The capacity of an organism to respond to stress can be a measure of its overall health (Martin *et al.*, 1996) and therefore my hypothesis was that upon irradiation *Drosophila* would become more susceptible to stress. However, when adult *Drosophila* were stressed by starvation, it was found that irradiation modulated *Drosophila* starvation response long-term with early timepoints showing no difference in starvation resistance between cohorts (**Figures 3.10** & **3.13**). Whereas starvation 20 days *post* irradiation led to an increase in starvation survival (**Figure 3.12**). Without further experimentation, it is unclear as to why radiation improves starvation survival odds, but there are number of possible explanations:

1. Increased storage of energy reserves such as fats, proteins, carbs.
2. Radiation reduces basal respiration rate – starvation has less of an effect as less nutrients required to maintain soma.
3. Older and irradiated *Drosophila* require less nutrients to survive because gonads have atrophied.

Currently it is unclear which of these possible explanations are the cause for enhanced survival long-term *post* irradiation. However, the possibility of increased storage supplies can be eliminated since my data showed that upon irradiation body weight of both male and female *Drosophila* was reduced and remained reduced for the duration of their lifespan (**Figure 3.16**). The initial weight loss is thought to be due to atrophy of gonads (multiple observation when dissecting other tissues), which also coincides with reduced fertility in females, specifically reduced egg deposition (**Figure 3.6**). The decrease in body weight eliminates the first possible

explanation as to why *Drosophila* have enhanced survival to starvation – increase in nutrient storage would increase overall body weight. However, to understand radiation-induced increased resistance to stress, further work needs to be performed which is beyond the scope of this PhD.

3.7.2   Radiation induced tissue toxicity and oxidative stress

It is unknown what is the biological cause of long-term radiation response in both humans and *Drosophila*. In humans, one possible explanation of the cause of long-term tissue toxicity is persistent oxidative stress (Alsner *et al.*, 2008; Wang *et al.*, 2010; Azzam *et al.*, 2012). However, due to the difficulties of studying oxidative stress in humans, it is unclear whether it is the cause or a consequence of long-term tissue toxicity. I used a GFP reporter line (*GstD1*::GFP) to study the involvement of oxidative stress in radiation response in *Drosophila*. Since *GstD1* is a direct target of the *Nrf2* pathway which is involved in detoxifying cells form xenobiotics, ROS and oxidised macromolecules, *GstD1* expression can be used as a direct measure of cellular oxidative stress (Ambrosone et al., 2006). Through whole-body sectioning it was clear that only some tissues develop/experience radiation-induced oxidative stress (**Figure 3.21**). This mimics well the established observation that, in patients receiving RT, the severity of their side effects is highly dependent on the location of the malignancies and therefore the site of irradiation. In general terms, the immediate side effects of radiation treatment can be localised to dysfunction of highly proliferative tissues e.g. skin, intestinal tract, and blood, whereas the long-term side effects are localised to non-/slowly proliferative tissues, such as lungs and brain. Within *Drosophila*, I have shown that tissues with proliferative capacity are particularly sensitive to radiation-induced oxidative stress, particularly the midgut (**Section 3.4.2**).

It was thought that oxidative stress is the aetiological cause of the late side effects of radiation treatment in patients receiving RT. Understanding the role of oxidative status in causing late tissue toxicity has been an area of active RT research. It appears that, at least in *Drosophila*, there is no correlation between the tissue damage and oxidative stress (**Sections 3.4.4** & **3.4.5**). Furthermore, induction of oxidative stress via H_2O_2 feeding did not result in reduced survival of irradiated *Drosophila*, indicating a lack of interaction between oxidative stress and lifespan *post* irradiation. This observation was further supported when NAC – a known antioxidant in both humans and *Drosophila* - was used but did not improve survival of irradiated *Drosophila* (**Figure 3.32**). In fact, survival analysis determined that

NAC treatment was slightly toxic to *Drosophila*, despite being reported as extending lifespan (Niraula & Kim, 2019). Perhaps other markers of oxidative stress should be considered for future work, such as genes involved in redox biology e.g. *Catalase*, *Superoxide Dismutase 1*, to provide broader biological context. Other markers of tissue toxicity such as levels of apoptosis, cell cycle perturbations, or autophagy should also be explored - all of which have been implicated in RT-induced tissue toxicity in humans (Bentzen, 2006).

3.7.3 Radiation induced tissue remodelling

In contrast to radiation-induced fibrosis reported in patients undergoing RT, *Drosophila* did not show an increase in midgut ECM composition as demonstrated by no change in the levels of the *Drosophila* orthologue of collagen – *Vkg* (**Section 3.3.5**). However, this does not mean that fibrosis does not occur in *Drosophila post* irradiation, other tissues and levels of other ECM (e.g. *perlecan*, *troll, lamanin A*) need to be studied before a definitive conclusion can be made. Nevertheless, tissue remodelling was shown to occur as dysplasia within the midgut, with nuclei arrangement in disarray.

3.7.4 Mimicking human radiotherapy regimes

With the *Drosophila* model demonstrating similar side effects to radiation treatment as those observed in humans, the model required to be validated using a more representative RT regime as experienced by patients. A fractionated radiation regime improved survival outcome in *Drosophila* (**Figure 3.37**). However, despite fractionated cohort having no significant change in lifespan, it did show systemic long-term midgut tissue toxicity. This could mean the midgut itself does not contribute to survival *post* irradiation treatment. It is thought that fractionation works by allowing peripheral healthy tissue time to repair damage induced by radiation whilst still inducing DNA damage in the higher proliferating tumour tissue (Fowler, 2001). Therefore, seeing a survival increase in *Drosophila* undergoing a fractionated regime is an indication that there is a tissue repair mechanism under way within *Drosophila*. Hyper-fractionation (HF) regime was also effective at improving survival outcome, however, it resulted in a partial recovery of lifespan (**Figure 3.39**), while fractionation of dose led to a complete recovery of lifespan (**Figure 3.37**). These experiments cannot be compared directly because the fractionation experiment was performed on a radio-resistant strain *w1118*, therefore derived Hazard ratios (HRs) are a function of both genotype and treatment regime, whereas HF experiment used a radio-sensitive strain *Oregon R*. Irrespective of genotype consideration, these

results show that *Drosophila* responds to radiation in a similar manner as humans and further validate the model as a preclinical model. Since HF is an area of active research and is still debated whether it is effective and worthwhile practice, *Drosophila* can be used to better explore this potential treatment regime (Frosina, 2021; Soares et al., 2012; Stuschke & Thames, 1997).

3.7.5 Chapter summary

The aim of this chapter was to develop a *Drosophila* model for long-term radiation-induced tissue toxicity, then once the model was developed it was used to try and determine if prolonged oxidative stress was the cause of long-term side effects of irradiation. Development of the model involved characterising the effects of radiation on *Drosophila* via assaying multiple phenotypes. Multiple lines were used during phenotyping, but two strains were extensively used: radio-resistant w^{1118} and radio-sensitive *Oregon R*. Interestingly, radio-resistant phenotype in terms of lifespan does not correlate with other metrics of health as seen with w^{1118} (**Figure 3.43**). *Drosophila* also showed specific tissue/organ sensitivity to radiation treatment, as it is observed in humans. This work focussed on the midgut which was found to be sensitive to treatment.

Using this newly developed model for radiation toxicity it was determined that although radiation induced persistent oxidative stress within *Drosophila*, it did not correlate with tissue damage. Lastly, work was performed to further develop the *Drosophila* model as a preclinical tool, which involved exploring how *Drosophila* respond to radiation regimes similar to those of RT patients. This work showed that *Drosophila* responds in a human-centric manner and hints, as of yet, unknown underlying repair mechanisms *post* irradiation – an area of potential future research.
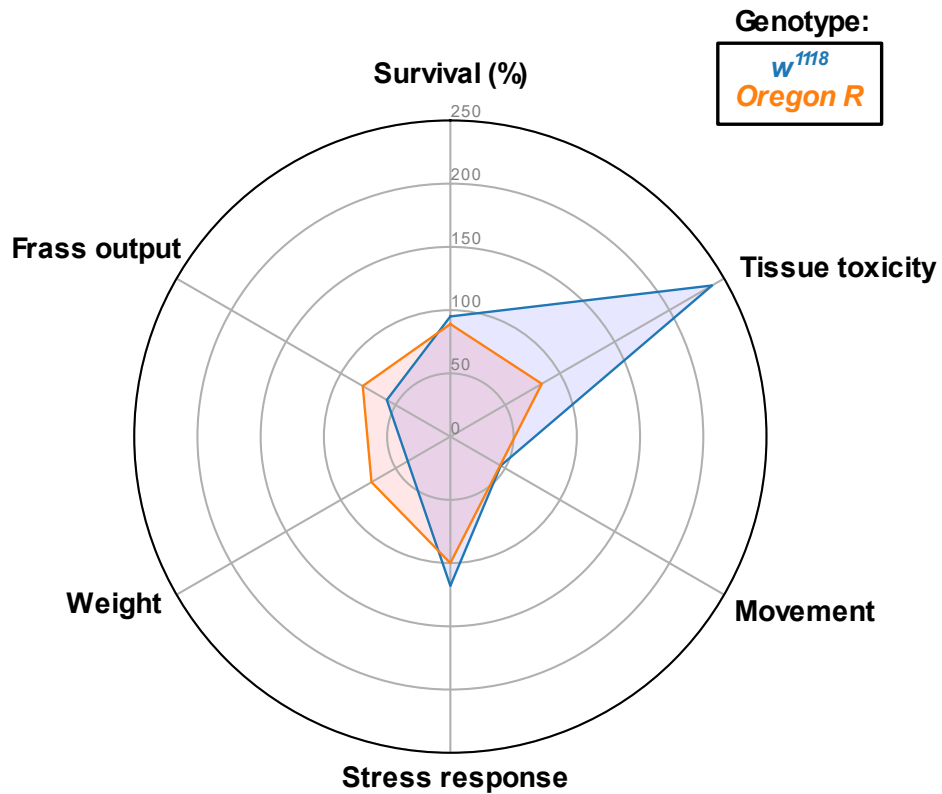
Figure 3.43: Multi-metric comparison of *Oregon R* and *w^1118* long-term radiation response. Radar plot metrics were measured in males and represent change (%) as compared to non-irradiated control. Survival is overall lifespan reduction, stress is change starvation survival 20 *post* treatment, fertility was hatching rate of eggs fertilised from sperm from irradiated males. Frass is comparison of output 14 days *post* treatment. Weight is dry body weight 20 days post treatment, and movement is initial velocity under RING assay 20 days *post* irradiation. Tissue toxicity is levels of H2AvD staining per nuclei pixel of midgut 20 days *post* irradiation. Data derived from experiments in which *Drosophila* were exposed to 200 Gy, except for w^1118 tissue toxicity, which was 21 days *post* irradiation at 150 Gy.

Chapter 4: Identification of loci associated with the radiation response

4.1 Introduction

In humans the radiation response is a highly polygenic trait with multiple genetic loci harbouring a small but significant risk associated with the more severe side effects (**Section 1.5**). Polygenicity has been assumed for decades by clinicians and radiologists, who observe such varied responses to treatment in individuals. Additionally, recent GWAS using radiation treated patients have identified a few loci involved in the radiation response. However, these studies suffer from a number of issues such as poorly defined clinical outcome, expensive trial design, and logistical issues associated with being potentially decade long studies. All these issues can be addressed and overcome by using *Drosophila* especially since I have shown that the radiation response of *Drosophila* has similar characteristics to that of the human response (**Chapter 3**). In this chapter, I present the multiple approaches that were used to identify genes associated with radiation response – GWAS, literature search, candidate approach, and tissue-specific transcriptional analysis. Both GWAS and transcriptional analysis are unbiased genome-wide approaches capable of identifying novel loci associated with radiation response trait.

4.1.1 Aims and Objectives

Aim 1 – Perform a GWAS using *Drosophila*

Objectives:

- Determine the feasibility of using the DGRP to perform a GWAS
- Quantify multiple phenotypic responses of the panel, both short-term and long-term

Aim 2 – Identify risk loci from *Drosophila* radiation research

Objectives:

- Perform systematic literature search to identify loci associated with the radiation response in *Drosophila*
- Identify which tissues are specifically affected by irradiation

Aim 3 – Candidate approach

Objectives:

- Backcross midgut-specific *Gal-4* driver lines into reference w^{1118} background
- Test multiple candidates that were identified through literature search

Aim 4 – Characterise radiation-induced transcriptome

Objectives:

- Identify which tissues are sensitive to radiation
- identify molecular pathways that are modulated through gene ontology analysis
- Generate gene lists for subsequent validation experiments

4.2 Materials and Methods

4.2.1 Drosophila strains

All stocks (**Table 4.1**) were maintained at 25°C with a 12 hr:12 hr light:dark photocycle and on *Drosophila* cornmeal medium, refer to **Section 2.2.2** for recipe.

Table 4.1: Wildtype *Drosophila* stocks used for Chapter 4.

Stock	Source (reference)
w^{1118}	Luis Teixeira (B# 5905)
Oregon R	BDSC # 25211
Samarkand	BDSC # 4270
Swedish C	BDSC # 4271
Urbana S	BDSC # 4272
DGRP # 91	BDSC # 28136
DGRP # 142	BDSC # 28144
DGRP # 790	BDSC # 28232
DGRP # 21	BDSC # 28122
DGRP # 310	BDSC # 28276
DGRP # 217	BDSC # 28154
DGRP # 808	BDSC # 28238
DGRP # 304	BDSC # 25177
DGRP # 57	BDSC # 29652
DGRP # 208	BDSC # 25174
DGRP # 513	BDSC # 29659
w;UAS-XRCC1-RNAi	BDSC # 61359
$w;Duox^{K}/Gla$	Derived from BDSC # 26167
$w;Duox^{Cy}/Gla$	Derived from BDSC # 880
w;UAS-Jafrac1	Heinrich Jasper (FBtp0082116)
w; UAS-Sod1, UAS-Cat;+	Fisun Hamaratoglu (Derived from BDSC # 24621 & 24754)
w;+,+/SM6b-TM6B	Derived from BDSC # 29002

4.2.2 Lifespan assay and analysis

Lifespan assay of *Drosophila* was performed as described in **Section 2.2.5**, and subsequent lifespan datasets were analysed as described in **Section 2.2.6**.

4.2.3 Determination of the relatedness of DGRP panel

Python package scipy [1.8.1] was used to perform principal component analysis (PCA) on DGRP sequence data that was downloaded from public server (http://dgrp2.gnets.ncsu.edu/data). The analysis clustered the lines based on how closely related they were to each other.

4.2.4 Dissection, immunohistofluoresence and imaging of *Drosophila*

Two weeks *post* irradiation, *Drosophila* midguts were dissected, stained, and imaged as described in **Section 3.2.7**. Primary staining was with anti-H2AvD (1:200, Rockland: pS137) and secondary staining was with anti-Rabbit-A594 raised in Goat (1:500, A21207). DNA was stained with Hoechst (1:10,000, Sigma-Aldrich: B2261) which was added alongside secondary antibodies.

4.2.5 Image analysis

For the analysis of H2AvD levels *post* irradiation in DGRP midguts, a Python script was written to automate the segmentation and quantification of H2AvD signal for each nucleus in each image stack. The image analysis pipeline was as follows: sum projections were generated by condensing Z axis. Hoechst (DAPI) channel was used to binarise image using an Otsu threshold and nuclei were closed via dilation and erosion. As projections can result in objects overlapping, a watershed was performed to separate overlapping nuclei. DAPI objects smaller than the arbitrary threshold of 10 pixels were presumed to be either debris or non-specific DAPI aggregates, and were removed from downstream analysis. For each segmented nucleus, nuclear area and total H2AvD intensity was recorded (**Appendix 5**). R was used for statistical analysis and multiple comparison T-test was performed comparing average H2AvD pixel intensity per nucleus.

4.2.6 RNA-seq analysis

Oregon R males were purped as previously described (**Section 2.2.5**) and were allowed to mate for two days prior to irradiation (200 Gy). *Drosophila* were maintained twice weekly via transfer to fresh media. 20 days *post* irradiation, tissues (brain, fat body, midgut, and flight muscle) were dissected directly into ice-cold PBS pre-treated with DEPC (1:1000) and autoclaved, with 10 *Drosophila* comprising each replicate. For brain-enriched samples *Drosophila* were decapitated and heads

stored on ice, midguts were dissected as previously described (**Section 3.2.7**), thorax was kept for flight muscle, and a sagittal cut was made along the abdominal carcass ensuring to remove testes and Malpighian tubules.

In triplicate, total RNA from 10 *Drosophila* (per replicate) was extracted from sorted tissues using the PureLink™ RNA column extraction kit (Thermo Fisher: 12183018A) by following manufacturer's instructions. The RNAase decontamination solution RNAase*Zap*™ (Thermo Fisher: AM9780) was used to periodically clean equipment and workspace during RNA extraction. RNA samples were stored overnight at -80°C till transport on dry-ice for sequencing (NovoGene Europe, Cambridge). cDNA libraries were constructed and sequenced through Illumina sequencing with at least 16.7 million pair-end reads at 150 bp length generated for each sample.

Sequence data processing followed the below pipeline for each replicate and UNIX scripts are cited for each step (**Appendix 7**):

1. **Quality control** using fastqc module to check quality of reads e.g. GC content for signs of PCR amplification bias and presence of overrepresented sequences, as well as trimming of adaptor sequences from reads (**Appendix 7: Read quality control**).
2. **Indexing** using STAR module to index *Drosophila* genome (r6.22) acquired from Flybase (**Appendix 7: Indexing genome**).
3. **Alignment** using STAR module both forward and reverse reads were mapped to the indexed genome (**Appendix 7: Read mapping**).
4. **Mark and remove duplicate reads** using PICARD module (**Appendix 7: Duplicate read marking**).
5. **Counting** using FeatureCount module to quantify number of mapped reads per indexed gene and thus determining gene differential expression (**Appendix 7: Read counting per gene**).

FeatureCount output was analysed in Rstudio using Sartools and deSEQ2 package (**Appendix 7: R script for differential expression analysis**).

4.3 Genome-wide association study

To identify loci involved in the radiation response, the original research plan involved performing GWAS on the DGRP using lifespan survival as a phenotypic readout of the radiation response of each strain. Due to the long nature of lifespan assays, potentially lasting months, and the size of the DGRP (~200 strains) I performed preliminary experiments on a subset of the DGRP panel (10 strains) to determine the appropriateness of using the panel for future work. Firstly, these preliminary experiments aimed to investigate the polygenicity of the radiation response in *Drosophila* by looking at radiation-induced changes in the lifespan of closely related strains. Secondly, I explored the possibility of using radiation-induced midgut toxicity as a faster, more affordable and quicker phenotype to measure rather than lifespan.

The DGRP has been used previously in a GWAS to identify genes involved in the response to catastrophic levels of radiation (~1300Gy; Vaisnav *et al.*, 2014), however the study was unsuccessful in identifying any significant loci associated with the trait. Nevertheless, I used its reported phenotypic data to select 10 radiation over-responder strains for preliminary analysis – five of the most sensitive and five resistant strains (**Table 4.2**). The lifespan survival of the radiation over-responder lines, as reported by Vaisnav *et al* (2014), was measured and clear differences in long-term survival after 200 Gy were observed. For example, RAL 513 was particularly sensitive to irradiation, whereas RAL 304 was resistant (**Figure 4.1 A** & **B**). However, there was no correlation observed between the radiation-induced survival of *Drosophila* determined by me and ability to fly *post* irradiation as determined in the Vaisnav study (**Figure 4.1 C**). In fact, radiation treatment led to an increase in survival for strains RAL 310, 21 and 710, which were classed as radio-sensitive in the Vaisnav study (**Figure 4.1 C**).

As survival analysis on ~5% of the panel took considerable time and effort to complete, prior to continuing to assay the rest of the DGRP, I investigated if another phenotype could be used as a proxy for lifespan analysis. **Chapter 3** demonstrated that radiation treatment results in DNA damage within the midgut that persists for weeks after irradiation, hence it was investigated if the levels of H2AvD lesions within midgut nuclei two weeks *post* treatment can be used to determine sensitivity of *Drosophila* lines to radiation treatment (**Figure 4.2**). A custom Python script was generated to segment nuclei and quantify H2AvD intensity values per nuclei (**Appendix 5**). Clear and significant differences in the number of H2AvD positive

nuclei and the intensity of lesions per nuclei were observed between strains. For example, RAL 808 had a larger proportion of high H2AvD intensity nuclei, whereas RAL 310 had a smaller proportion (**Figure 4.2 A** & **B**). As with the survival analysis, it was anticipated that strains would respond to treatment in a similar manner to that of the Vaisnav response, but no correlation was observed (**Figure 4.2 C**). However, all strains did exhibit increased levels of H2AvD staining as compared to their non-irradiated controls, with ratios ranging between 110 to 202%. This is in striking contrast to the survival dataset in which treatment had little or no significant effect on survival for some strains.

The panel has shown clear differences in response to radiation for both long-term survival and short-term midgut toxicity. To determine whether short-term toxicity could be used as a proxy phenotype for long-term survival, a correlation between both was sought (**Figure 4.3**). Linear regression determined a R^2 value of 0.2891 which indicates a weak positive correlation between negative survival outcome and increased midgut toxicity. However due to small N of 8 strains and a clustering of survival ratios near 100%, it is difficult to be confident in the robustness of the observed correlation – increasing the number of assayed strains would overcome this deficiency.

The relatedness of strains was analysed to try and determine whether it correlated with phenotypic responses (**Figure 4.4**). Hierarchical clustering grouped assayed strains into three distinct groups (**Figure 4.4 A**). Phenotypic response of strains to treatment did not correlate with their relatedness, with all three groups having random distributions for each phenotype (**Figure 4.4 B** & **C**).

Preliminary experiments successfully shown that the DGRP has a dynamic response to radiation treatment, as demonstrated by differences in survival *post* irradiation. However, radiation treatment also led to an increase in lifespan for some of the strains. A possible explanation for this is a hermetic effect i.e. the relatively low dose of radiation has stimulated the activation of reparative pathways improving lifespan and overall health (L. Koval, Proshkina, Shaposhnikov, & Moskalev, 2020). However, this would require further investigation. Quantification of lifespan of the whole DGRP would be a huge undertaking and since some strains responded unexpectedly, it was decided not to continue with the full GWAS as part of this PhD. Instead, other approaches to identify radiation risk loci were utilised such as a candidate-based approach (**Section 4.5**) and an RNA-seq analysis of the radiation induced transcriptome (**Section 4.6**).

Table 4.2: Selected members of the Drosophila genetic reference panel and their radiation response. * Radiation response as determined by Vaisnav, *et al.*, (2014).

| RAL # | Vaisnav response * | |
	Ability to fly (%)	Classification
91	98	Resistant
208	89	Resistant
142	82	Resistant
808	63	Resistant
57	56	Resistant
304	8	Resistant
513	0	Sensitive
790	0	Sensitive
21	0	Sensitive
310	0	Sensitive
217	0	Sensitive
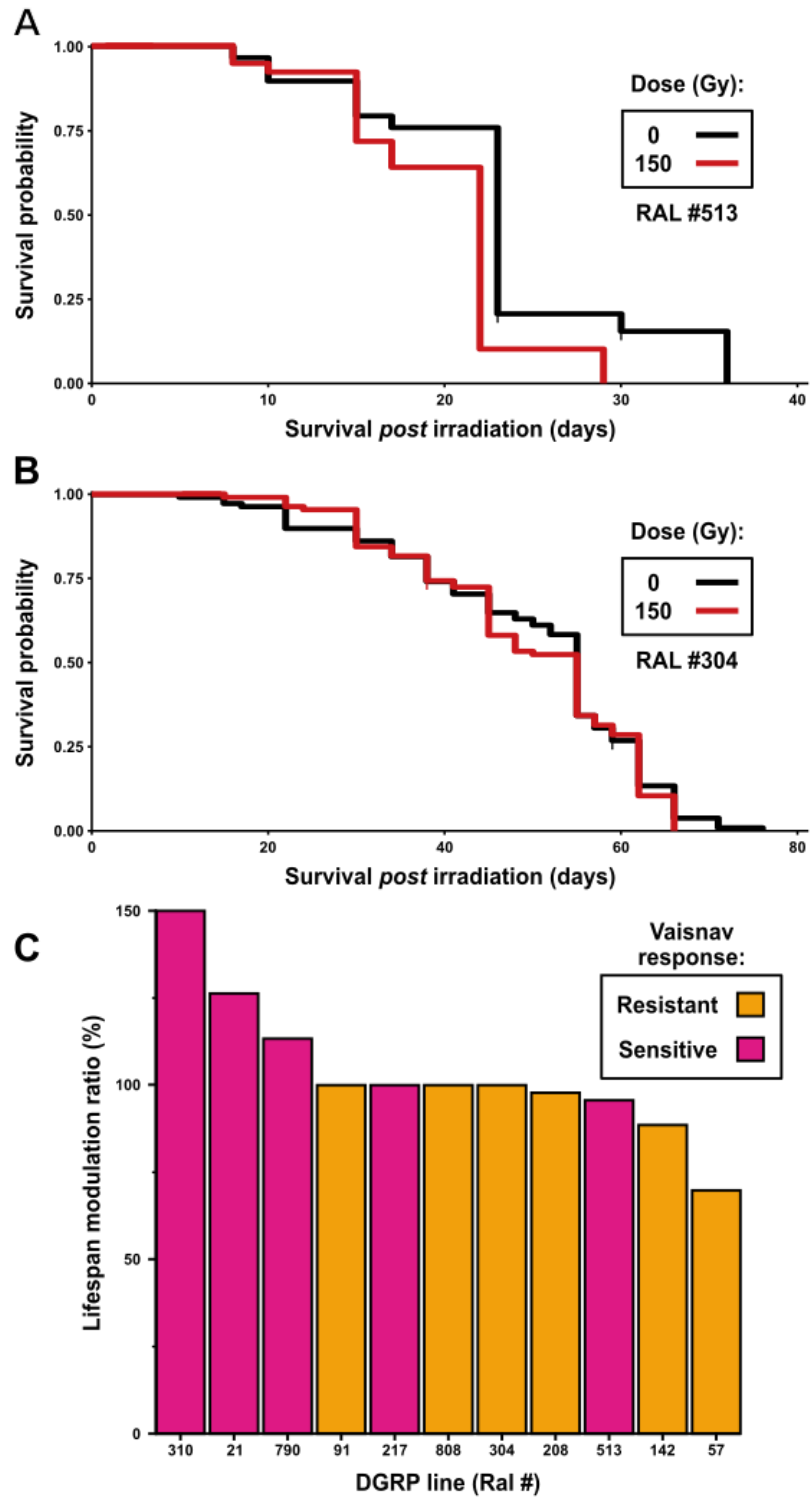
Figure 4.1: Selected members of DGRP showed varied survival *post* irradiation. For each strain *Drosophila* males were mated and purped as standard practice and allowed to mate for 48 hr followed by irradiation (150 Gy). (**A**) KM curve for RAL 513 which was determined to be mildly sensitive to treatment. (**B**) KM curve for RAL 304 which was determined to be resistant to treatment. (**C**) Comparison of the ratiometric change in lifespan for RAL lines *post* treatment. Colours represent previous reported radiation response of lines (**Table 4.2**).
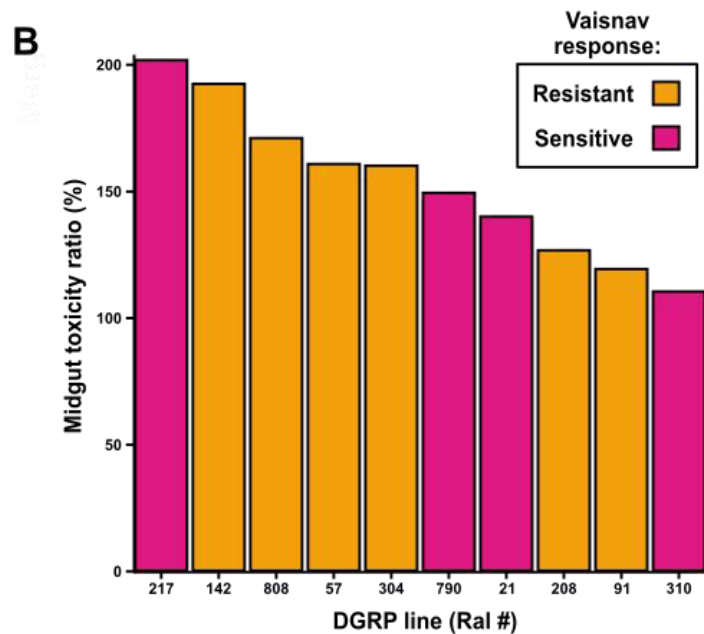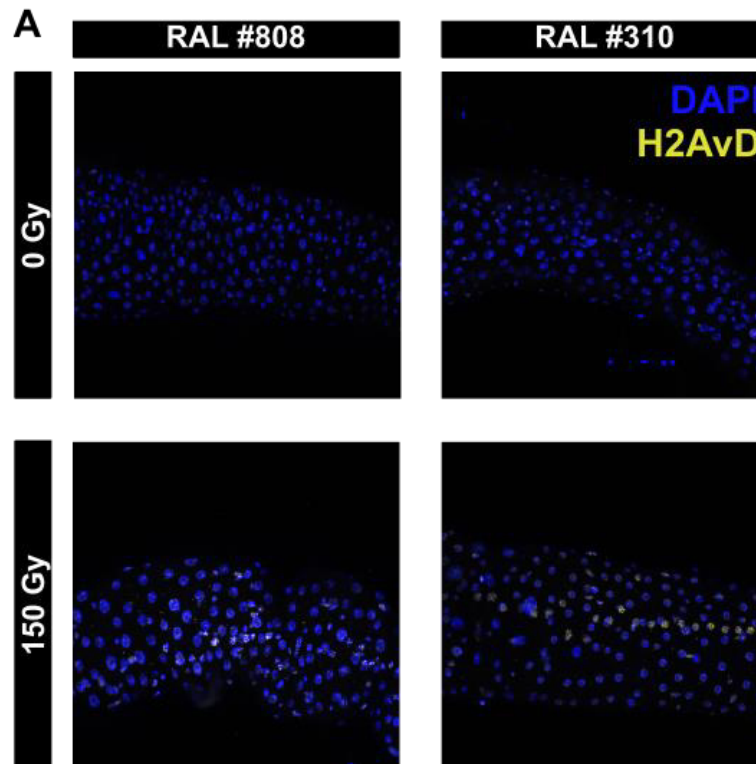
Figure 4.2: Selected members of DGRP showed varied levels of radiation-induced midgut toxicity. For each strain *Drosophila* males were mated and purped as standard practice and allowed to mate for 48 hr followed by irradiation (150 Gy). H2AvD staining in the midgut was performed two weeks after treatment completion. (**A**) Representative maximum projections for sensitive strain RAL #808. (**B**) Representative maximum projections for resistant strain RAL #310. (**C**) Comparison of ratiometric change in average H2AvD staining per nucleus for RAL lines. Colours represent previous reported radiation response of lines (**Table 4.2**).
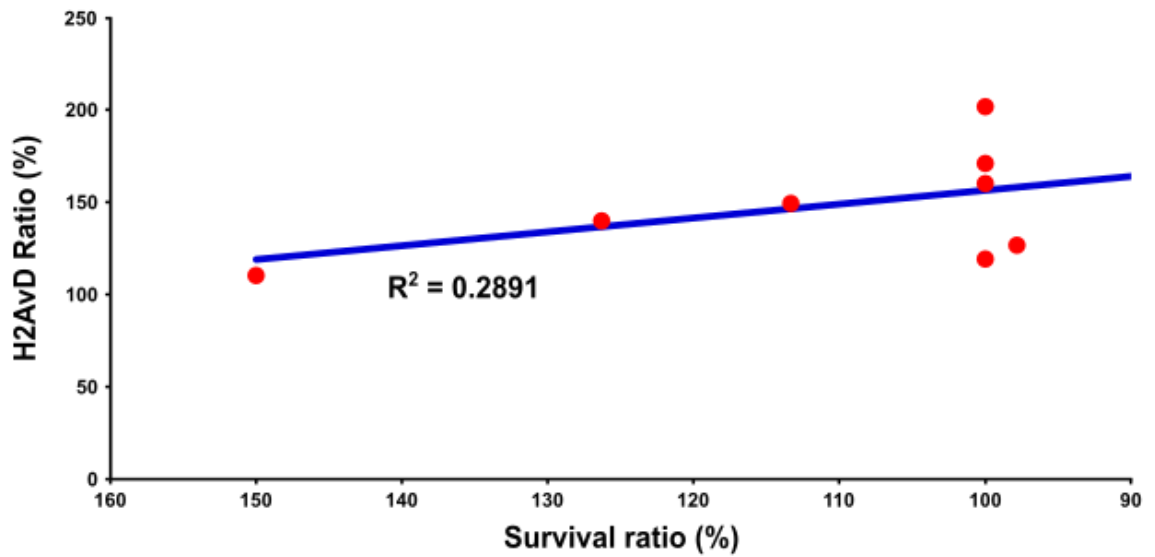
Figure 4.3: Short- and long-term responses to irradiation show little correlation. Survival ratio refers to ratiometric comparison of median survival values for strains. H2AvD ratio refers to ratiometric comparison of average H2AvD intensity per nucleus for each strain. Linear regression determined a R value of 0.2891 indicating a weak positive correlation between negative survival outcome and increased midgut toxicity.
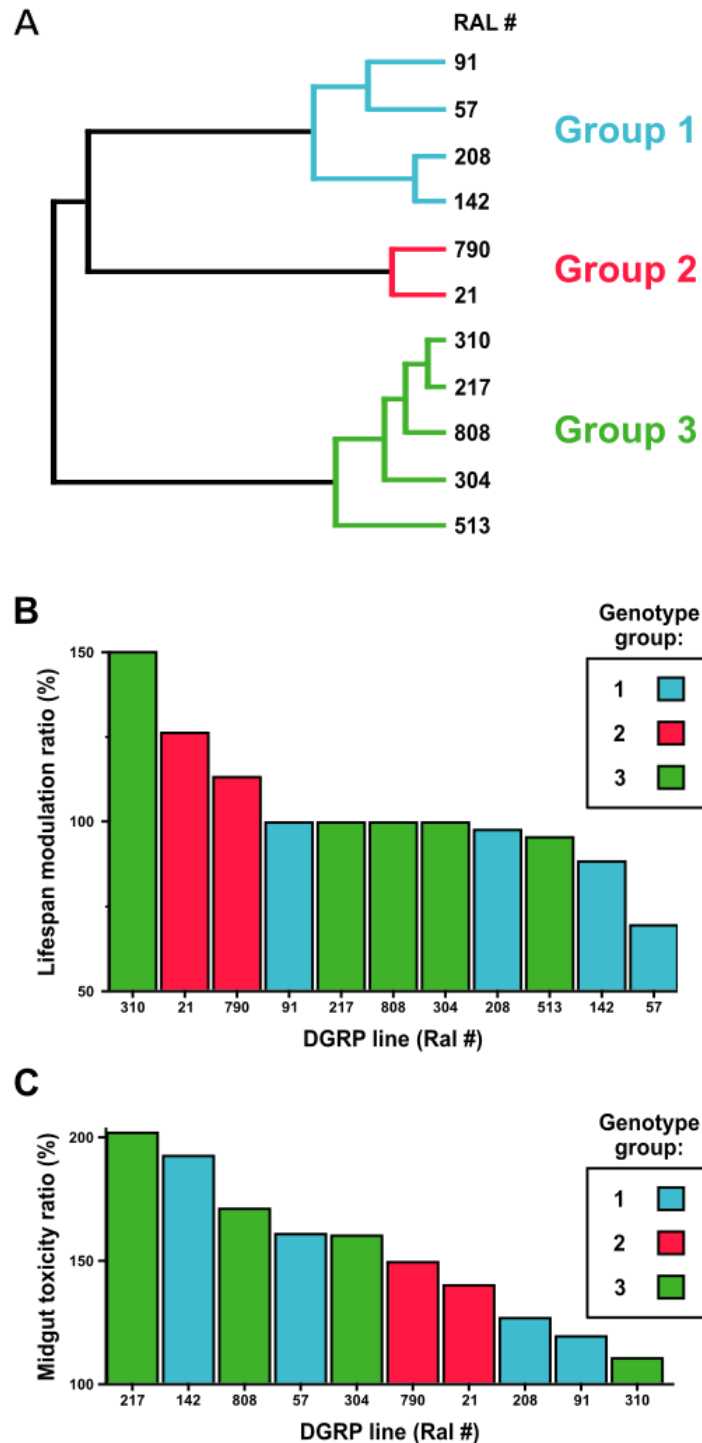
Figure 4.4: Closely related strains do not share similar phenotypic responses to irradiation. (**A**) Dendrogram of genotype-based hierarchical clustering of phenotyped RAL lines. Relatedness of strains was determined through PCA using the publicly available DGRP genotype dataset (http://dgrp2.gnets.ncsu.edu/data.html). (**B**) Comparison of the ratiometric change in lifespan for RAL lines *post* treatment (**Figure 4.1**). Colours represent genotypic groupings. (**C**) Comparison of ratiometric change in average H2AvD staining per nucleus for RAL lines (**Figure 4.2**). Colours represent genotypic groupings.

4.4 Literature search to identify risk loci

Before embarking on a candidate-based approach to identify radiation risk loci, a literature search was performed to compile a list of loci that have previously been identified to be involved in the radiation response of *Drosophila*. This was done to provide an overview of all up-to-date known loci associated with the radiation response and to better inform candidate-based studies. To identify potential risk loci specifically from *Drosophila* radiation research, I performed a systematic literature search through use of a custom Python script (**Appendix 6**), and the following search terms were used to search PubMed database:

> "(late **OR** long-term) **AND** (radiation **OR** radiotherapy **OR** irradiation **OR** ionization) **AND** (response **OR** toxicity **OR** effect **OR** reaction) **AND** (human **OR** mammalian) **NOT** (rat **OR** mouse)".

Both rat and mouse were excluded as Boolean search terms because without their exclusion 100s of articles were returned with little or no relevance, in particular multiple circadian rhythm studies involving rodents. The final query resulted in 83 compiled articles, which were screened/filtered manually using the title and abstract text, and 58 were discarded as irrelevant. The remaining articles were fully read and 25 presented functional data of risk loci. Lastly, five articles were *post-hoc* added as they were known to have identified risk loci, but did not come up in the initial search (**Figure 4.5**). In total, this literature search successfully identified 51 loci associated with radiation sensitivity in *Drosophila* (**Table 4.3**).

Risk loci involved in DNA repair

As majority of the compiled risk loci were identified through candidate and hypothesis driven studies a large proportion (14 out of 51) of the genes are associated with DNA repair. Some of these risk loci have been identified in multiple studies, with *meiotic 9* (*mei-9*), involved in DNA repair, being the most extensively studied risk loci (**Table 4.3**). Also, most of the loci have been functionally validated such as *Growth arrest and DNA damage-inducible 45* (*Gadd45*) which is a DNA repair gene that has been shown through mutant analysis to be essential for larvae survival upon irradiation. Indeed, the literature search demonstrated that the vast majority of loci identified are involved in processes such as DNA repair and regulation of oxidative stress responses, suggesting the importance of these processes in the radiation response.

Risk loci involved in oxidative stress

As mentioned previously (**Chapter 3: Section 3.4**), radiation reacts with water (radiolysis) producing ROS which can interact with macromolecules and induce oxidative damage and stress (Azzam et al., 2012). Radiation-induced oxidative damage has been extensively studied in humans, and ROS imbalances have been shown to persist long-term (Robbins & Zhao, 2004). From looking at the *Drosophila* research, it is clear that radiation induces oxidative stress, at least short-term. Genes involved in oxidative metabolism have been shown to have an immediate increase in expression *post* irradiation such as *GstT4* (Kuzin et al., 2014). It is unclear whether these genes are simply expressed transiently short-term or have a more sustained long-term expression.

It is also not clear whether expressional changes to oxidative stress genes has a direct effect on the health and survival of irradiated *Drosophila* with recent work showing that changes in levels of antioxidant enzymes (*SOD*, *GSTs*) *post* irradiation were 'inadequate' to explain radiation tolerance (Paithankar, Raghu, & Patil, 2018).

Risk loci involved in immunity

In mammals, irradiation can lead to the localised accumulation and persistent activation of immune cells leading to chronic inflammation (Kaur & Asea, 2012). To that end, the levels of antimicrobial peptides *Drs* and *DroA* were quantified to study the levels of systemic inflammation in *Drosophila post* irradiation (Sharma *et al.*, 2020). The fat body of irradiated *Drosophila* had sustained elevated levels of both peptides up to 35 days *post* treatment. *Drs* and *DroA* encode antifungal peptides and during infection are expressed and released by both the fat body and haemocytes to kill pathogens (Simon et al., 2008; Yang et al., 2006).

Another study quantified the expression of various antimicrobial peptides within the adult brain either five or fifteen days *post* irradiation (Lisa J. Sudmeier, Samudrala, Howard, & Ganetzky, 2015). All antimicrobial peptides had significantly increased expression both short-term (five days) and long-term (fifteen days) *post* irradiation both within the head and whole-body. Proteins tested included *AttC* and *Dipt* which encode antibacterial peptides specific against Gram-negative bacteria (Lemaitre, Reichhart, & Hoffmann, 1997; Rabel et al., 2004). Though these peptides do not directly facilitate inflammation, their increase in expression does indicate an activated immune response which if left unresolved can be pathogenic. Additionally, It is not clear whether these peptides are expressed in direct response to irradiation

or possibly due to secondary opportunistic infections that have resulted from a weakened immune system.

Risk loci typical expression pattern

Using freely available FlyAtlas transcriptional dataset, tissue specific expression patterns of identified risk loci were evaluated and no particular tissue was found to be enriched (**Table 4.4**) (Krause, Overend, Dow, & Leader, 2022). All loci were expressed in multiple tissues, except for *AttC*, which is only expressed in the circulatory system.

There was little consistency in the models and methods of irradiation amongst discussed studies, with a range of dosages used as well as different types of radiation treatment (**Figure 4.6 A**). This lack of standardisation is problematic, as I have shown in my thesis that decline in survival and tissue damage from radiation treatment is dosage-dependent (**Chapter 3**). Additionally, a re-analysis of the Shrestha transcriptional dataset determined that dose was indeed a significant variable that influenced the *post* irradiation transcriptome of *Drosophila* (**Figure 4.6 B**) (Shrestha et al., 2017). Therefore, the genes significantly identified may not be functionally relevant to the organism at the same dosage.

The information gathered in the literature search has provided a valuable overview of known risk loci associated with the radiation response in *Drosophila* and was used as the basis for my candidate screen. Although most loci identified in the search have already been validated, I was able to narrow my search of potential candidates to genes involved in DNA repair and oxidative stress responses.
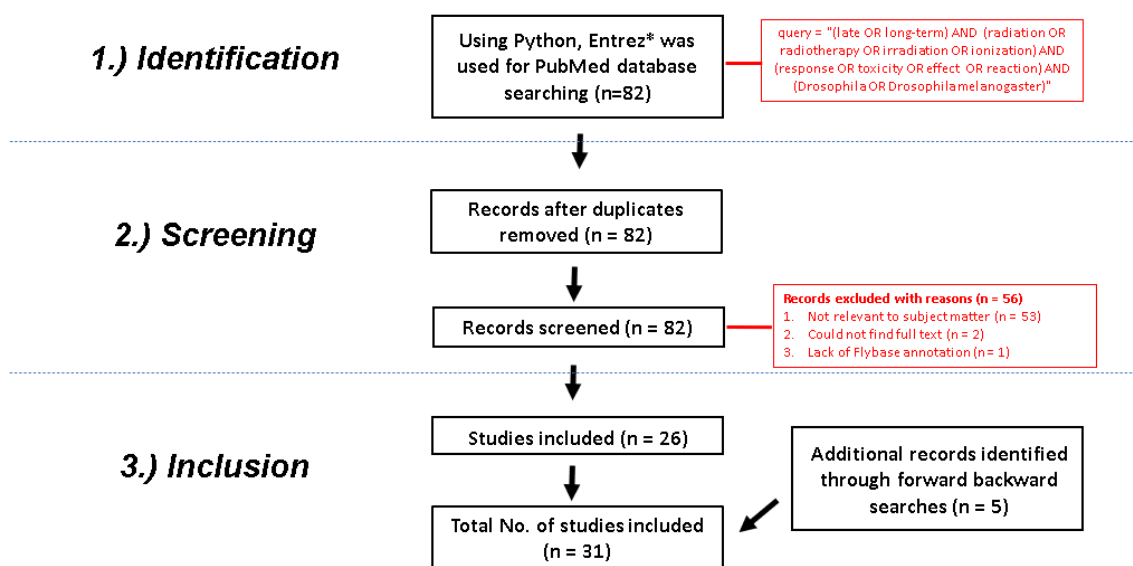
Figure 4.5: Literature search of PubMed database for genes involved in *Drosophila* radiation response. Illustrated is the stepwise process of identifying and screening articles to identify risk loci. Forward citation searches refer to finding all relevant articles that cite back to a particular article. Whereas backward citation searches refer to searching through all cited references within a particular article for relevant articles.

Table 4.3: Identified loci associated with the radiation response of *Drosophila*.

Gene (Symbol)	FlyBase ID	Sources
DNA ligase 4 (*DNAlig4*)	FBgn0030506	(Gorski et al., 2003)
rad54 (*okr*)	FBgn0002989	(Gorski et al., 2003; L. Koval et al., 2020)
Drosomycin (*Drs*)	FBgn0283461	(Moskalev et al., 2015; Sharma et al., 2020; Lisa J. Sudmeier, Samudrala, et al., 2015)
Drosomycin-like 1 (*DroA*)	FBgn0052274	(Sharma et al., 2020; Lisa J. Sudmeier, Samudrala, et al., 2015)
Diptericin A (*Dipt*)	FBgn0004240	(Lisa J. Sudmeier, Samudrala, et al., 2015)
Attacin-C (*AttC*)	FBgn0041579	(Lisa J. Sudmeier, Samudrala, et al., 2015)
Cecropin C (*CecC*)	FBgn0000279	(Lisa J. Sudmeier, Samudrala, et al., 2015)
Metchnikowin (*Mtk*)	FBgn0014865	(Moskalev et al., 2015; Lisa J. Sudmeier, Samudrala, et al., 2015)
Glutathione S transferase D1 (*GstD1*)	FBgn0001149	(Moskalev et al., 2015)
Superoxide dismutase 1 (*Sod1*)	FBgn0003462	(Proshkina, Lashmanova, & Dobrovolskaya, 2016)
Growth arrest and DNA damage-inducible 45 (*Gadd45*)	FBgn0033153	(L. Koval et al., 2020; Moskalev et al., 2015; Proshkina et al., 2016)
Xeroderma pigmentosum, complementation group C (*Xpc*)	FBgn0004698	(L. Koval et al., 2020; Proshkina et al., 2016)
spindle B (*spn-B*)	FBgn0003480	(L. Koval et al., 2020; Proshkina et al., 2016)
Heat-shock-protein-70 (*Hsp70*)	FBgn0286924	(Moskalev et al., 2015; Proshkina et al., 2016)
Cytochrome P450 6g1 (*Cyp6g1*)	FBgn0025454	(Kuzin et al., 2014)
Glutathione S transferase T4 (*GstT4*)	FBgn0030484	(Kuzin et al., 2014)
spineless (*ss*)	FBgn0003513	(Kuzin et al., 2014)
meiotic 9 (*mei-9*)	FBgn0002707	(Fukunaga & Kondo, 1985; Kennison & Ripoll, 1981; L. Koval et al., 2020)
meiotic 41 (*mei-41*)	FBgn0004367	(Fritz-Niggli and Schaeppi-Buechi, 1991)
mutagen-sensitive 302 (*mus302*)	FBgn0287696	(Fritz-Niggli and Schaeppi-Buechi, 1991)
NK7.1 (*NK7.1*)	FBgn0024321	(Vaisnav et al., 2014)
Lackluster (*lackluster*)	FBgn0086299	(Vaisnav et al., 2014)
pannier (*pnr*)	FBgn0003117	(Vaisnav et al., 2014)
lincRNA.1043 (*CG14621*)	FBgn0031183	(Vaisnav et al., 2014)
Discoidin domain receptor (*Ddr*)	FBgn0053531	(Vaisnav et al., 2014)
CG42324	FBgn0259224	(Sharma et al., 2020)
musashi (*msi*)	FBgn0011666	(Sharma et al., 2020)
CG1824	FBgn0030403	(Sharma et al., 2020)
reaper (*rpr*)	FBgn0011706	(Sharma et al., 2020)
head involution defective (*hid*)	FBgn0003997	(Sharma et al., 2020)
Connector of kinase to AP-1 (*Cka*)	FBgn0044323	(Sharma et al., 2020)
Death caspase-1 (*Dcp-1*)	FBgn0010501	(Lisa J. Sudmeier, Samudrala, et al., 2015)
Hus1-like (*hus1-like*)	FBgn0026417	(L. Koval et al., 2020)
loki (*lok* or *mnk*)	FBgn0019686	(L. Koval et al., 2020)
Proliferating cell nuclear antigen (*PCNA* or *Mus209*)	FBgn0005655	(L. Koval et al., 2020)
Recombination repair protein 1 (*Rrp1*)	FBgn0004584	(L. Koval et al., 2020)
BRCA2 (*Brca2*)	FBgn0050169	(L. Koval et al., 2020)
Ku80 (*Ku80*)	FBgn0041627	(L. Koval et al., 2020)
WRN exonuclease (*WRNexo*)	FBgn0038608	(L. Koval et al., 2020)
Bloom syndrome helicase	FBgn0002906	(L. Koval et al., 2020)
E2F transcription factor 1 (*e2f1*)	FBgn0011766	(D. Li et al., 2021)
p53 (*p53*)	FBgn0039044	(D. Li et al., 2021)
grapes (*grp*)	FBgn0261278	(Jaklevic et al., 2006)

Table 4.4: Expression pattern of identified radiation risk loci. Data acquired from FlyAtlas 2 (Krause et al., 2022). Data represents adult males with fragments per kilobase of exon per million mapped (FPKM) values shown. Colouring of heatmap compares level of expression of individual genes between tissues. Malpighian tubules (MT) and salivary glands (SG).

Gene symbol	Tissue-specific expression Pattern (FPKM)												
	Whole body	Head	Eye	Brain	Crop	Midgut	Hindgut	MT	Fat body	SG	Heart	Testis	Carcass
DNAlig4	2.3	2.3	3.1	3.2	2.2	3.8	2.3	3.3	1.5	2.6	2.3	6.8	2.3
okr	1.2	1.4	2.3	1.7	1.5	1.5	1	2.1	1.3	2.1	1.9	3	1.5
Drs	437	357	33	5.4	102	4.3	6	174	46	5989	60	17	117
DroA	0	0		0	0	0	0	0	0	0.5	0	1	1
Dipt	104	350	26	0.7	1.7	2.9	4.8	1.8	3.1	4.8	19	3.2	18
AttC	82	245	40	1.2	1.4	0	1	0.6	12	6.2	35	16	16
CecC	3.4	27	1.5	0.2	1.3	0	0	0.4	0.7	69	2.5	1.1	2.1
Mtk	1140	4500	122	9.3	22	0.4	2.6	8	36	42	27	11	74
Sod1	352	271	400	131	489	343	289	383	822	210	1487	105	681
Gadd45	3.9	4.3	2.7	6	2.2	12	36	15	3.4	8.3	4.1	2.5	4.1
Xpc	8.1	13	14	29	7.4	8.8	6	9.7	4.2	5.7	7.9	15	7.9
spn-B	0.9	0.8	0.6	1	1.2	0.6	0.4	0.6	0.1	0.8		1.9	0.6
Hsp70	0	0	0.1	0	0.1	0	0	0	0	0	0	0	0
Cyp6g1	128	97	141	1.9	10	471	7.3	997	244	29	201	3.1	211
GstT4	137	31	44	1.5	339	792	248	23	246	93	210	13	99
ss	0.7	1.8	0.7	0.1	0.1	0	0	0	0	0.1	0.1	0.5	0.1
mei-9	1	1.2	1.5	2.4	1	1.2	0.9	1.2	0.6	1.1	1.2	1.6	0.9
mei-41	0.7	0.7	1	1.1	0.8	0.9	0.5	0.8	0.7	0.8	1.2	1.6	0.7
mus302	2	5.5	4.8	7.1	1.3	1.6	1.2	1	1.6	1.2	1.5	4.2	1.8
rad201	N/A												
NK7.1	3.4	6	7	9.1	0.9	4.1	2.4	4.8	1.8	1.9	4.8	5.7	3.1
lackluster	N/A												
pnr	0.7	0.7	0.4	0.1	0.4	0.4	0.1	0.2	0.4	1	2.3	0.2	1.1
CG14621	7.1	5.5	6.1	6	5.2	8.5	3.8	4.4	6.4	15	8	15	4.9
Ddr	1	4	1.6	10	0.1	0.2	0	0.1	0.1	0.3	0.1	0.2	0.4
CG42324	5.1	7.2	3.2	5.7	0.5	0.2	0.2	31	13	1.6	9.5	2.1	5.6
msi	7	26	35	19	5	0.8	0.2	0.1	0.5	1.3	1.4	8.7	2.4
CG1824	7.2	4.8	11	6.7	9.4	17	12	9.5	7.6	11	15	5.5	11
rpr	0.4	1	0.1	1.9	0.2	0.3	0.2	0.1	0.1	0.3	0.1	2.7	0.4
hid	2.2	2.7	2.2	1	5.6	2.1	2.7	0.8	1.1	1.1	1.1	2.6	2.3
Cka	14	16	15	17	13	15	11	11	14	10	13	29	10
GstD1	227	222	128	66	345	425	235	354	74	203	314	272	191
Dcp-1	1.8	1.8	2.1	4.2	0.5	16	2.1	1	0.9	1.3	1.5	2	0.9
hus1-like	3.7	4.6	4.5	3.6	5.3	5	5	4	5.5	6.5	4.9	2.1	3.1
lok (mnk)	1.6	1.1	2	0.8	4.3	3.1	4	2.9	1.1	3.9	1.8	3.1	2.3
PCNA (Mus209)	1.6	0.8	1.1	0.6	1.5	1.2	1.3	0.6	0.9	1.3	1.1	11	1.1
Rrp1	1.9	1.6	0.7	3.9	4.5	0.9	2.7	0.8	1	1.7	2.6	6.8	1.4
Brca2	1.8	2.3	3.1	4.5	3.5	3.6	2.2	1.7	2.4	3	3.5	2.7	3.8
Ku80	2.4	2	1.5	2.2	1.9	3.7	1.7	3.5	1.1	1.5	1.9	9.2	1.5
WRNexo	0.3	0.1	0.3	0.1	0.3	0.3	0.3	0.1	0	0.3	0.1	3.1	0.3
Blm (Mus309)	1.3	1	1.1	2	0.8	0.7	0.6	0.6	0.5	0.9	0.9	10	0.8
e2f1	6.4	8.5	10	9.3	10	12	9.9	12	10	9.9	9	4.1	7.9
p53	2	2.6	2.8	2.9	4.4	5.5	3.9	5.5	1.4	4.5	2.9	3.6	3.1
grp	5.2	9.2	5.7	25	7.8	7.7	5.1	6	2.2	8	4	19	4.3
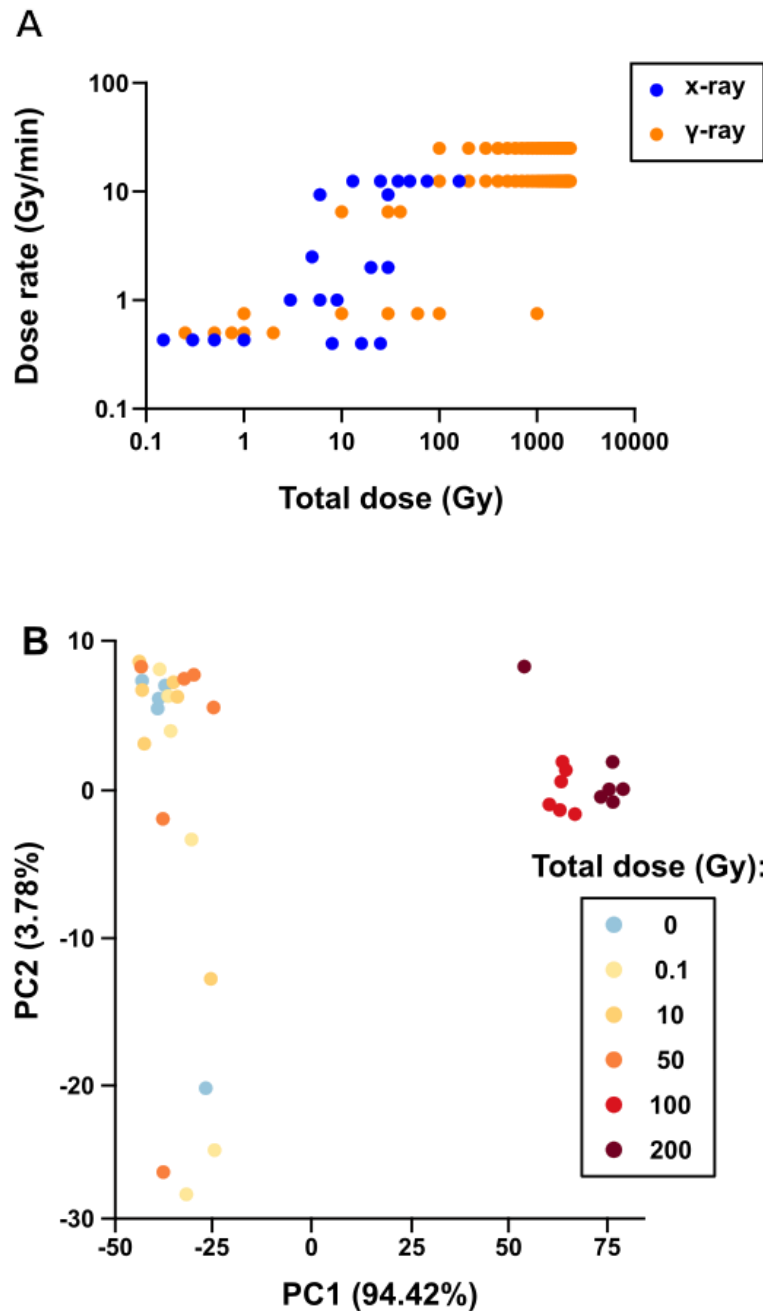
Figure 4.6: Non-standardisation in *Drosophila* radiation research. For studies which identified risk loci, technical details were collated. (**A**) shows dose rate against total dose used to irradiate *Drosophila*, and the type of radiation used. (**B**) PCA analysis of *Drosophila* transcriptome 20 days *post* irradiation treatment at various dosages (0.1, 10, 50, 100 and 200 Gy). Data originally generated by Shrestha but reanalysed to perform PCA (Shrestha et al., 2017).

4.5 Candidate approach

For the candidate gene approach, five candidates were selected based on their function and involvement in DNA repair and oxidative stress, as suggested by the literature search (**Section 4.4**). Selected loci were *Dual oxidase*, *X-ray repair cross complementation 1*, *Jafrac1*, *Superoxide dismutase* and *Catalase* for reasons to be discussed later on in this section. Candidates were functionally tested to determine if their genetic manipulation specifically within the midgut led to modulated radiation survival. This functional testing was performed by either knockdown, overexpression, or mutant analysis, depending on availability of tools.

4.5.1 Backcross of driver lines

The radiation response is a highly polygenic trait (**Section 4.3**), and it was anticipated that this would pose a technical issue when performing future functional work. Working with genetic tools with distinct genetic backgrounds would introduce confounding variance in phenotypic responses. Therefore, two *Gal*4 lines were chosen: *Myosin1A-Gal4* (expressed by all midgut cell types) and *escargot-Gal4* (highly expressed by intestinal stem cells) which allowed for midgut cell-type specific expression, and they were backcrossed into w^{1118} background, allowing w^{1118} to act as a genotypic control line for future experiments. This was achieved by tracking the w^+ rescue of the *Myosin1A-Gal4* P-element insertion for 16 generations of crossing with w^{1118} (**Figure 4.7**). Each generation consisted of ~50 individuals, each with a unique 2nd chromosome *Myosin1A*/w^{1118} recombination chromosome. The resultant stock was balanced by the fused *SM6-TMB6b* balancer which ensured that the backcrossed chromosome and WT 3rd chromosome segregated together. This was followed by the making a homozygous stock for driver and WT 3rd chromosome. This backcrossing approach was also performed on *Duox* mutants (*Duox^{Cy}* and *Duox^{K}*) and the dominant curly wing phenotype was used as the marker.

To confirm that *Gal4* elements were not disrupted from backcrossing, they were crossed with *UAS-GFP* lines to check for the expected expression pattern within the midgut (**Figure 4.8**). Based on morphology of GFP signal, it appears that only intestinal stem cells (ISCs) are expressing GFP with the *escargot-Gal4* driver (**Figure 4.8 A**). This is the expected expression pattern for *escargot*, as shown in the Flygut-seq database (**Figure 4.8 B**) (Dutta, Xiang & Edgar, 2013). *Myosin1A-Gal4* driver led to low but ubiquitous GFP expression which was expected from Flygut-seq (**Figure 4.8 A** & **B**).
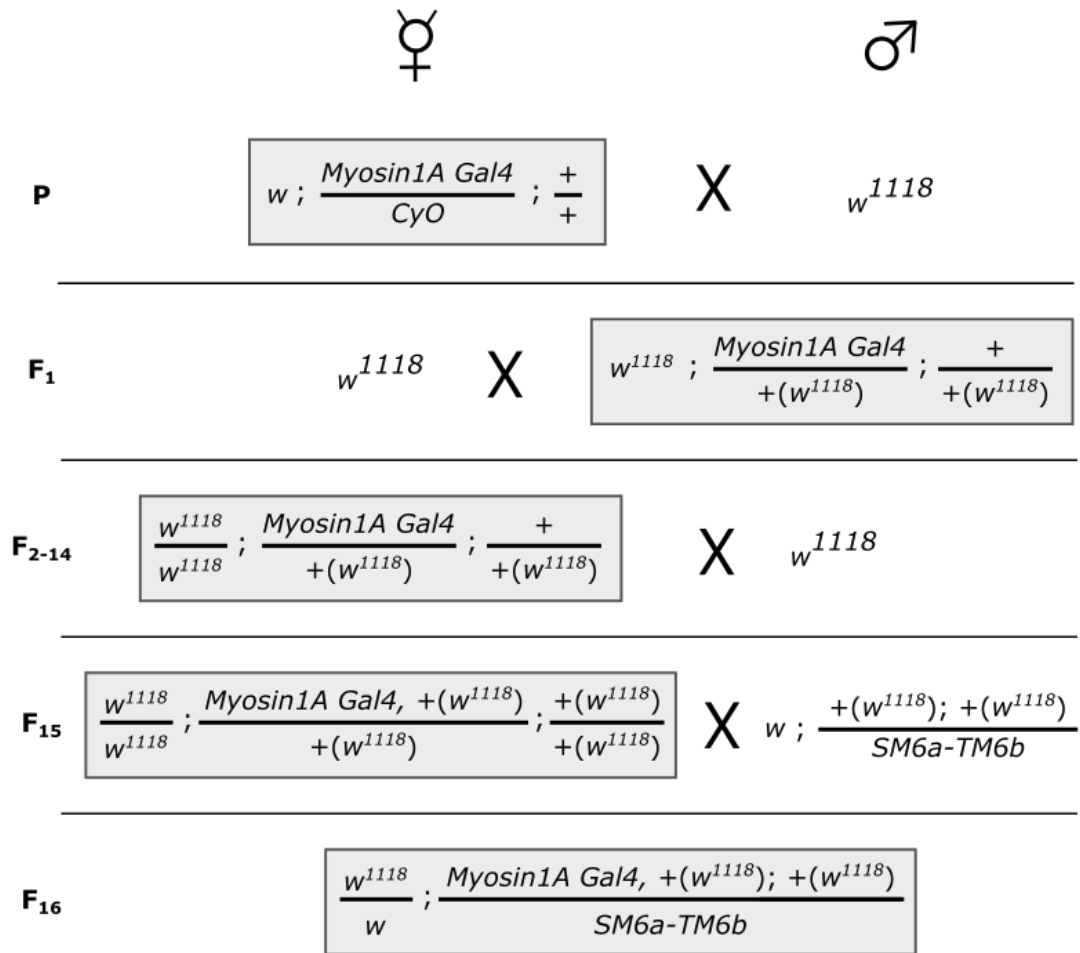
Figure 4.7: Backcrossing of driver lines into w^{1118} WT genetic background. Mating scheme was performed for both *Myosin1A-Gal4* and *Escargot-Gal4* lines.
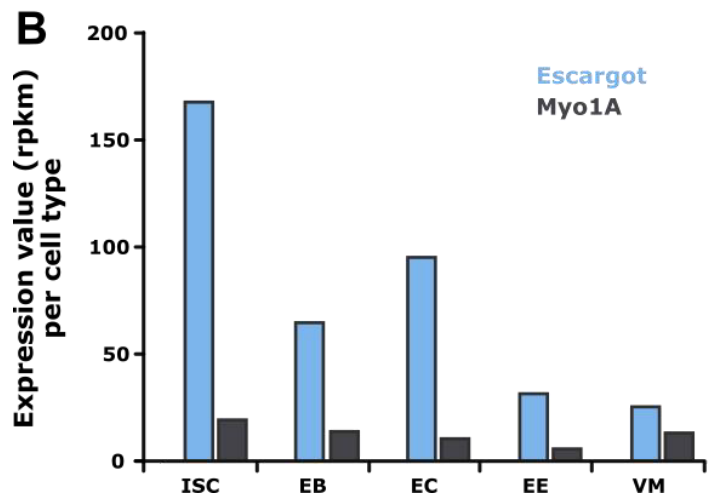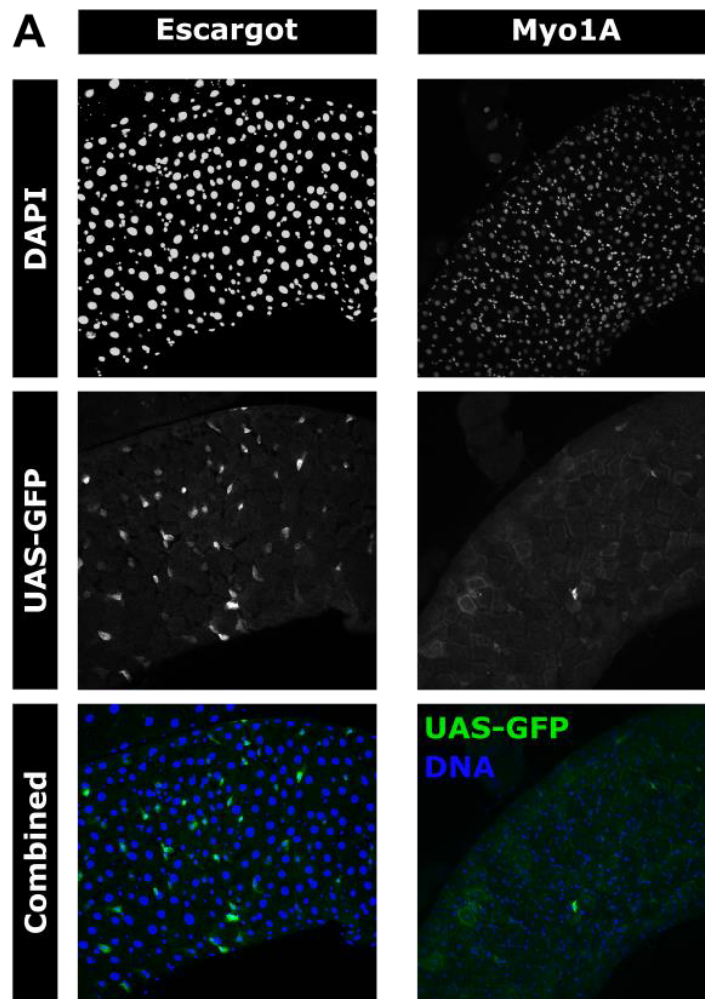
Figure 4.8: Expression patterns of backcrossed *Gal-4* lines within the midgut. (**A**) Backcrossed *escargot* and *myo1A Gal4* elements' expression patterns within the midgut. (**B**) Reads per kilobase per million (RPKM) value for each marker within each cell type of the midgut: intestinal stem cell (ISC), entereoblast (EB), entereocyte (EC), entereoendocrine (EE) and visceral muscle (VM). Data derived from the Flygut-seq RNA-seq profiling project (http://flygutseq.buchonlab.com/).

4.5.2 *Dual oxidase*

Previous work within Joaquin de Navascues' lab indicated that *CyO* balanced stocks were more susceptible to radiation treatment. Mutations in *Dual oxidase* (*Duox*) are the cause of the curly wing phenotype of *CyO. Duox* is involved in innate immunity and has high expression within the midgut. Upon pathogen stimulation *Duox* produces H_2O_2 within the lumen of the midgut in an attempt to regulate microbial colonization of the midgut (Kim & Lee, 2014). To study the role of *Duox* in the radiation response, two mutants were collected for survival analysis: *Duox^{Cy}* and *Duox^{K}* (**Table 4.1**). As the genetic backgrounds of these stocks were unknown, they were backcrossed into *w^{1118}* line which allowed the use of *w^{1118}* line as a reference control genotype. Backcrossing was performed similarly to the previous driver line backcrossing (**Section 4.5.1**). Briefly, mutant alleles were crossed to *w^{1118}* and mutant progeny were collected. This was repeated for each allele for ~13 generations, followed by balancing with the *In(2LR), Glazed* inversion due to the recessive lethality of *Duox^{K}* and *Duox^{Cy}*. For lifespan survival assaying, *Duox^{mutant}/Gla* stock was crossed with *w^{1118}*, and males selected that were *Duox^{mutant}/+*, with *w^{1118}* stock assayed as the genotypic control. Note that *Duox* work was performed *prior* to dose optimisation and these experiments involved exposing *Drosophila* to 50 Gy, as this had been previously shown in the lab to be sufficient to significantly reduce survival (unpublished).

Lifespan survival was performed on *Duox^{Cy}* mutant *post* irradiation (50 Gy) (**Figure 4.9**). Through visual inspection of KM curves, female irradiated *Duox^{Cy}* showed shortest survival of 48 days (44 – 50 days, 95% CI) as compared to any other cohort (**Figure 4.9 A**). However, it was not significantly different to *Duox^{Cy}* non-irradiated survival of 49 days (46 – 52 days, 95% CI) (p = 0.05907) (**Figure 4.9 B**). A CoxPH model was generated with the explanatory variables: radiation treatment, genotype, an interaction between treatment and genotype, and vial replicate (**Figure 4.9 C**). Genotype was a significant modulator of survival (p = 0.0418) with an estimated HR of 0.6512 (0.4309 – 0.9842, 95% CI). Radiation treatment, an interaction (treatment:genotype), and vial replicate were all determined not to be significant modulators of survival (p = 0.0616, p = 0.6514 and p = 0.8642, respectively). Testing for proportional hazards that are independent of time using the Schoenfeld residual test determined that the variables of radiation treatment, an interaction (treatment:genotype), and vial replicate did not violate the proportional hazards assumption (p = 0.518, p = 0.172, and p = 0.170, respectively). The variable of genotype did violate the proportional hazards assumption (p = 0.032).

Lifespan survival of $Duox^K$ mutant was assayed *post* irradiation (50 Gy) (**Figure 4.10**). Visual inspection and statistical analysis of KM curves showed no significant difference between genotypes and no significant interaction (Dose~Genotype) (**Figure 4.10 A** - **C**). Testing for proportional hazards that are independent of time using the Schoenfeld residual test determined that no variable violated the proportional hazards assumption ($p > 0.13$).
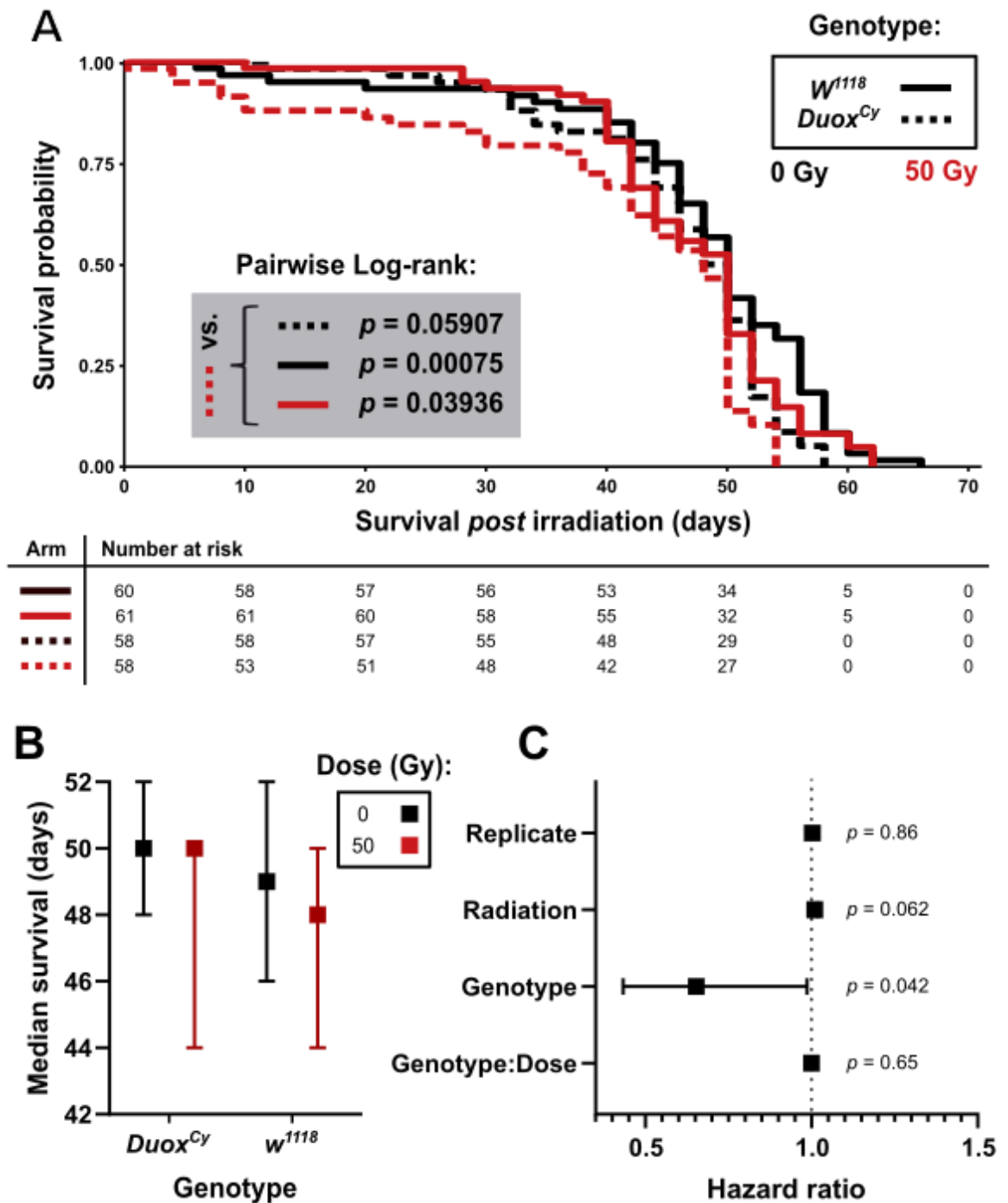
Figure 4.9: _Duox^Cy_ mutant does not exhibit reduced survival _post_ radiation treatment. _Drosophila_ females were purpled as standard practice and allowed to mate for 48 hr prior to irradiation (50 Gy). (**A**) KM curve with risk table, (**B**) median survival of vial replicates for each cohort with 95% CI, (**C**) HR derived from CoxPH model.
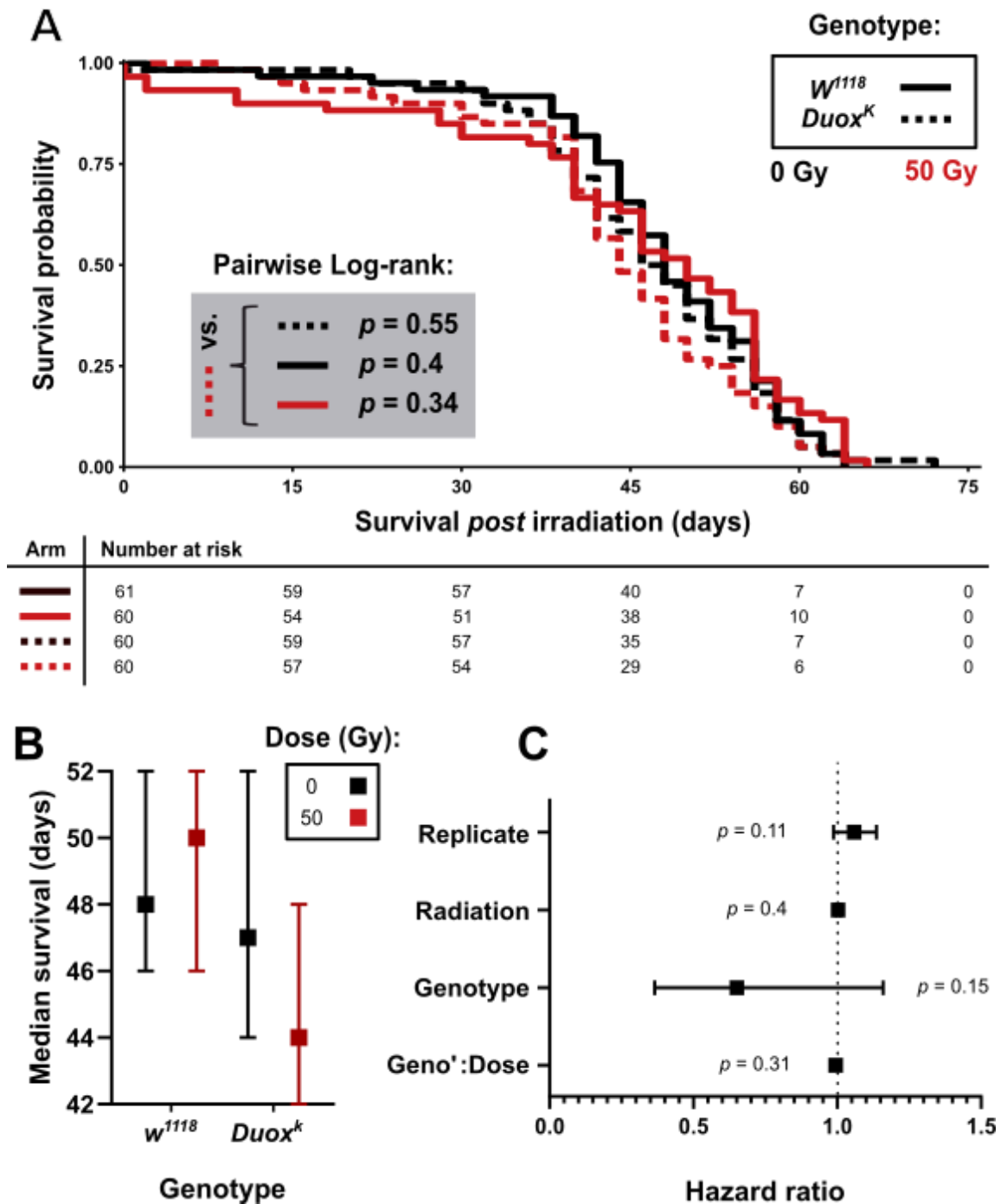
Figure 4.10: *Duox^K* **mutant does not exhibit reduced survival** *post* **radiation treatment.** *Drosophila* females were purpled as standard practice and allowed to mate for 48 hr prior to irradiation (50 Gy). (**A**) KM curve with risk table, (**B**) median survival of vial replicates for each cohort with 95% CI, (**C**) HR derived from CoxPH model.

4.5.3 *X-ray repair cross complementation 1*

X-ray repair cross complementation 1 (*XRCC1*) is a highly conserved gene between humans and *Drosophila*, which is involved in the repair of various types of DNA damage such as single and DSBs. XRCC1 participates mainly in the base excision repair pathway where it interacts with other proteins such as DNA ligase III and helps to facilitate the removal of base pair lesions within the genome. Mammalian cell lines that are mutant for XRCC1 have increased sensitivity to wide range of genotoxic agents including ionising radiation (Caldecott, 2003). Further, in patients who have undergone RT to treat prostate cancer certain polymorphisms in *XRCC1* locus have been associated with poorer prognosis and survival (Gao, Price, Dahut, Reed, & Figg, 2010). *XRCC1* has yet to be identified to be involved in the radiation response of *Drosophila*. To test if *XRCC1* is involved in the radiation response, a *UAS-XRCC1-RNAi* line (BDSC # 61359, VALIUM20 vector) that expresses dsRNA against *XRCC1* was used to knockdown expression within the midgut using both the *myosin* and *escargot* gal4 driver lines. Crosses and resulting experimental progeny were reared at 25°C for the duration of their survival/lifespan.

Lifespan survival was assayed *post* irradiation (150 Gy) when *XRCC1* was knockdown within the midgut using the *myosin-gal4* driver (**Figure 4.11**). Visual inspection of KM curves showed that treatment reduced survival in both genotypes (**Figure 4.11 A** & **B**). A CoxPH model was generated with the explanatory variables: radiation treatment, genotype, and an interaction between treatment and genotype (**Figure 4.11 C**). Treatment was determined to be a significant modulator of survival ($p = 6.48 \times 10^{-6}$) with exposure having an estimated HR of 1.0041 (1.0023-1.006, 95% CI). Genotype was also a significant modulator of survival ($p = 0.0003$) with an estimated HR of 0.5923 (0.4458-0.787, 95% CI). An interaction between treatment and genotype was identified ($p = 0.001$) however the estimated HR of 1.0043 (1.0018-1.007) indicated a small effect size. Testing for proportional hazards that are independent of time using the Schoenfeld residual test determined that the variable of treatment did not violate the proportional hazards assumption ($p = 0.42$). However, both genotype and the interaction did violate the proportional hazards assumption ($p < 0.0001$ and $p = 0.0002$, respectively).

Lifespan survival was assayed *post* irradiation (150 Gy) when *XRCC1* was knocked-down specifically in midgut ISCs using *escargot-gal4* driver (**Figure 4.12**). Visual inspection of KM curves showed that treatment reduced survival in w^{1118} control genotype (**Figure 4.12 A** & **B**). A CoxPH model was generated with the explanatory

variables: radiation treatment, genotype, and an interaction between treatment and genotype (**Figure 4.12 C**). Treatment was determined to be a significant modulator of survival (p = 1.21x10^{-10}) with exposure having an estimated HR of 1.0063 (1.004-1.008, 95% CI). Genotype was a non-significant modulator of survival (p = 0.939). An interaction between treatment and genotype was identified (p = 2.9x10^{-5}) however the estimated HR of 0.995 (0.992-0.997) indicates small effect size. Testing for proportional hazards that are independent of time using the Schoenfeld residual test determined that the interaction between treatment and genotype did not violate the assumption (p = 0.35). However, treatment and genotype violated the assumption (p = 0.0004 and p = 0.0004, respectively).

These results suggest that depletion of *XRCC1* specifically within ISCs acts to desensitise *Drosophila* to radiation treatment. Whereas depletion of *XRCC1* within the entire midgut had no effect on radiation survival. Further repeats with increased replicates are required in order to robustly confirm these observations, in addition checking the efficiency of *XRCC1* knockdown.
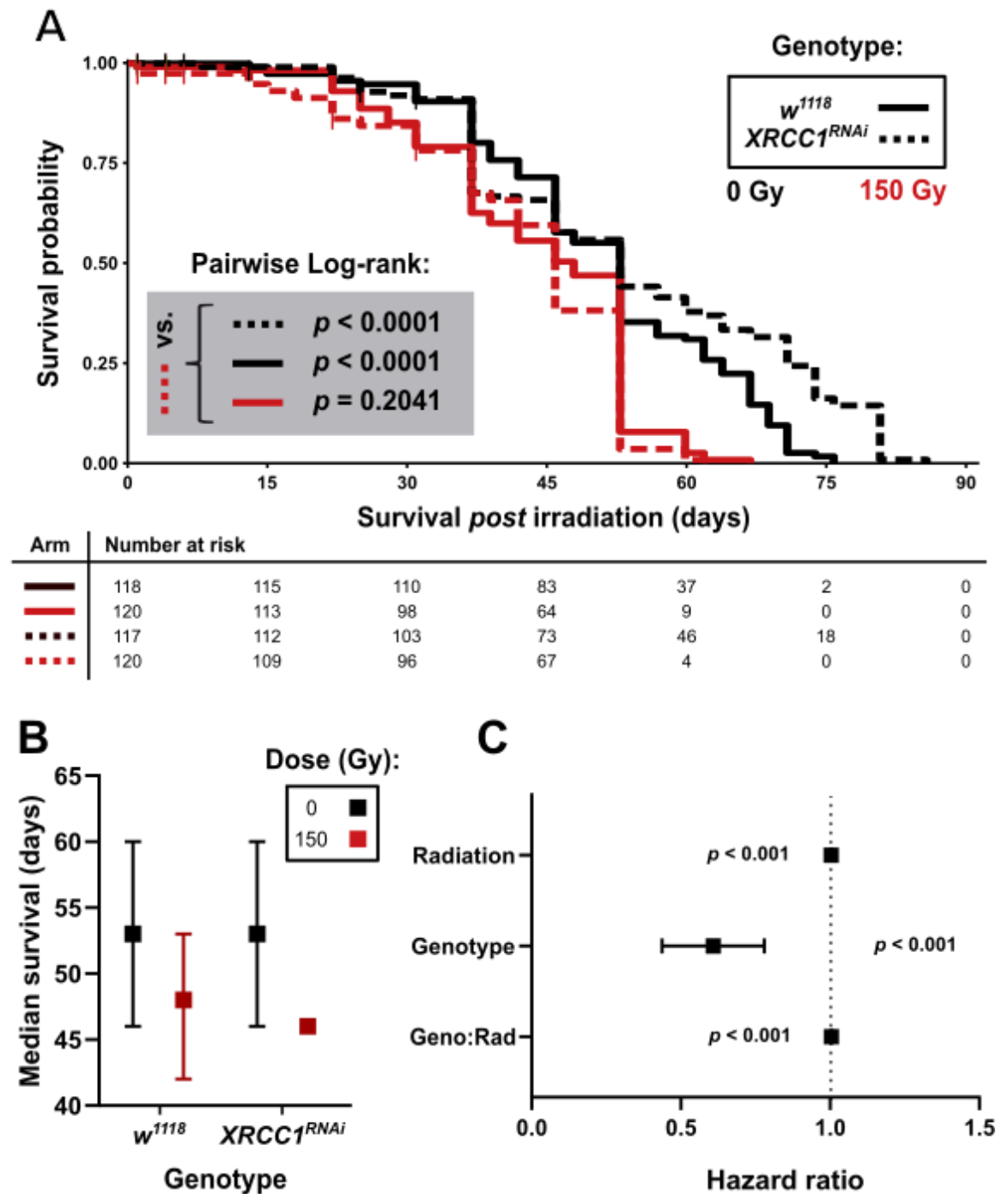
Figure 4.11: *XRCC1* knockdown in midgut does not further reduce radiation survival. *Drosophila* were crossed and desired offspring selected (*w*; *myosin-gal4/ UAS-XRCC1-RNAi*) and mated for 48 hr followed by irradiation (150 Gy). (**A**) Male KM curve with risk table, (**B**) median survival of vial replicates for each cohort with 95% CI, (**C**) HR derived from CoxPH model.
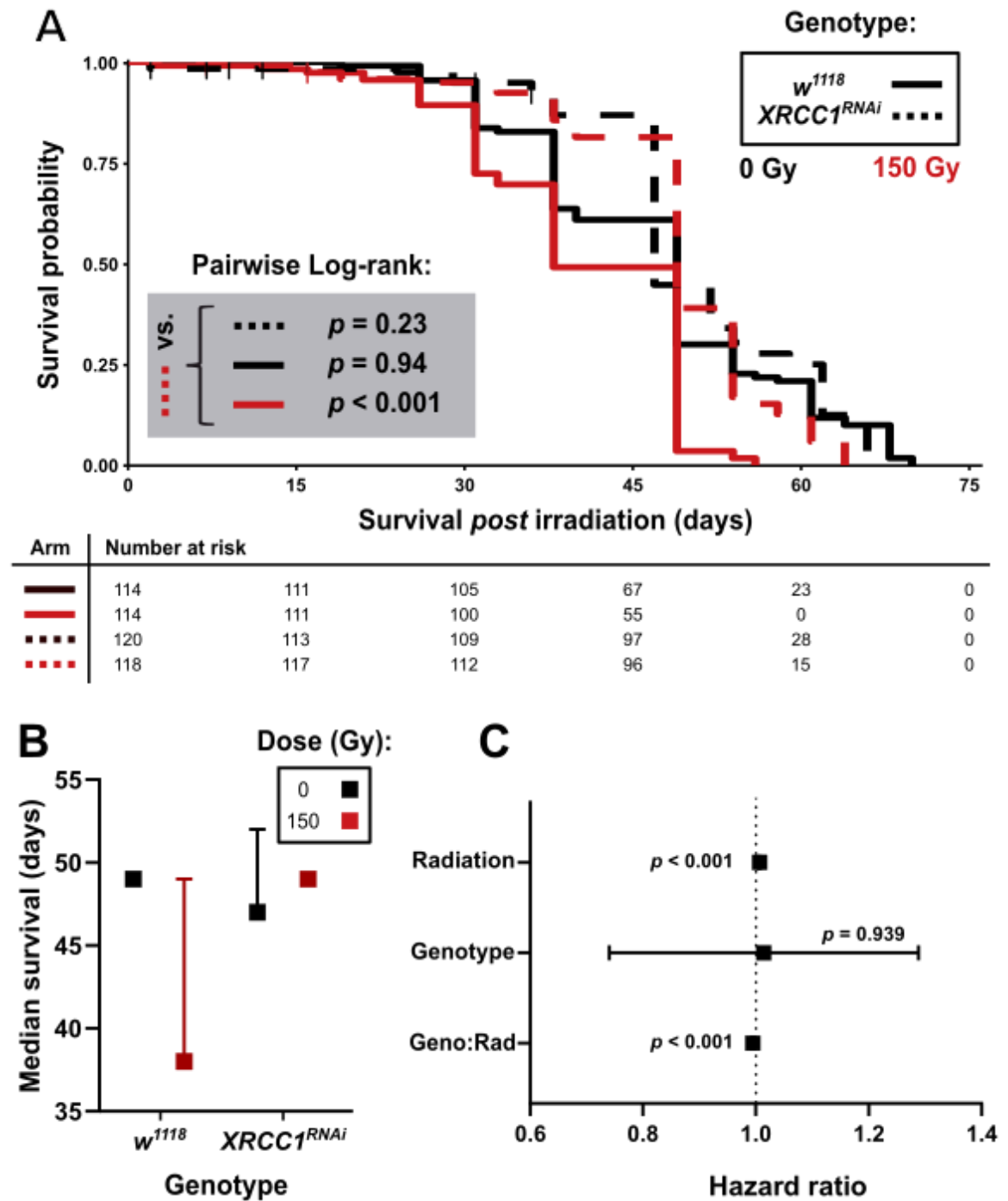
Figure 4.12: *XRCC1* knockdown in midgut ISCs does not influence radiation survival. *Drosophila* were crossed and desired offspring selected (*w*; *Escargot-gal4/ UAS-XRCC1-RNAi*) and mated for 48 hr followed by irradiation (150 Gy). (**A**) Male KM curve with risk table, (**B**) median survival of vial replicates for each cohort with 95% CI, (**C**) HR derived from CoxPH model.

4.5.4 *Jafrac1*

Jafrac1 (*Jafrac*) is a member of the antioxidant peroxiredoxin family, it has thiol-specific peroxidase activity and catalyses the reduction of H_2O_2 into H_2O (DeGennaro et al., 2011). Therefore, it plays an important and conserved role in maintaining a healthy cellular redox state in both humans and *Drosophila*. Though *Jafrac* was not identified as a gene involved in the *Drosophila* radiation response it has the potential to be a risk gene due to its role in sequestering ROS species. Further, it has been shown to be involved in maintaining midgut health by reducing the levels of dysplasia in the aging *Drosophila* midgut (Biteau et al., 2010). To test whether *Jafrac* is involved in the radiation response, it was overexpressed within the midgut followed by lifespan survival analysis.

Lifespan survival was assayed *post* irradiation (150 Gy) when *Jafrac* was overexpressed specifically in midgut enterocytes using *myosin-gal4* driver (**Figure 4.13**). Visual inspection of KM curves showed that treatment reduced survival, and that overexpression of *Jafrac* did not modulate lifespan (**Figure 4.13 A** & **B**). A CoxPH model was generated with the explanatory variables: radiation treatment, genotype, and an interaction between treatment and genotype (**Figure 4.13 C**). Treatment was determined to be a significant modulator of survival ($p = 9.6 \times 10^{-16}$) with exposure having an estimated HR of 1.011 (1.008-1.014, 95% CI). Both genotype and an interaction were determined to be non-significant modulators of survival ($p = 0.5$ and $p = 0.07$, respectively). Testing for proportional hazards that are independent of time using the Schoenfeld residual test determined that neither treatment, genotype or an interaction violated the assumption ($p = 0.1$, $p = 0.05$ and $p = 0.07$, respectively).

I concluded that overexpression of *Jafrac* within the midgut enterocytes did not influence lifespan or radiation survival.
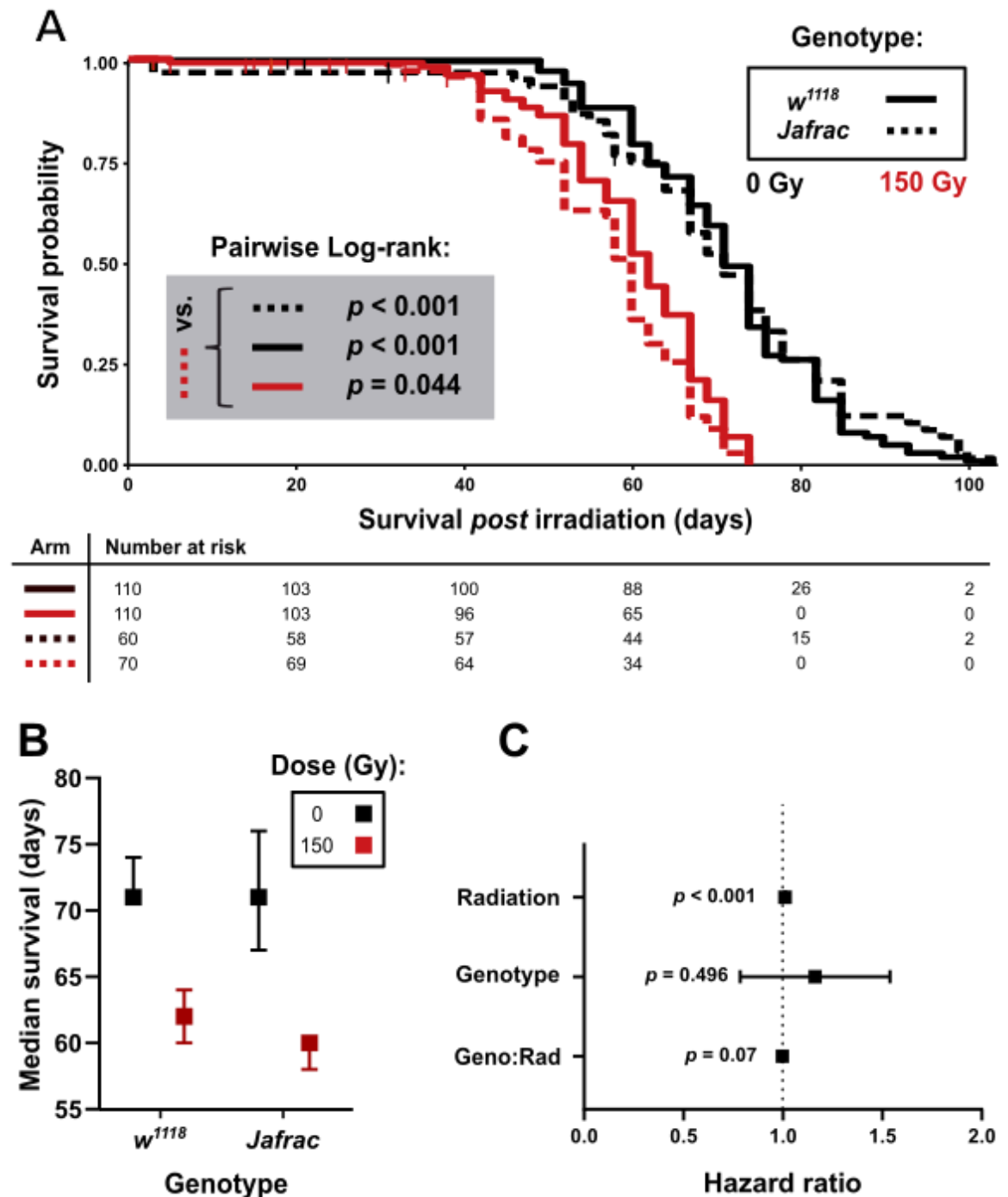
Figure 4.13: Overexpression of *Jafrac* in enterocytes does not improve survival *post* irradiation. *Drosophila* males were mated and purpled as standard practice, desired genotypes selected and allowed to mate for 48 hr followed by irradiation (150 Gy). (**A**) KM curve with risk table, (**B**) median survival of vial replicates for each cohort with 95% CI, (**C**) HR derived from CoxPH model.

4.5.5 *Superoxide dismutase 1 & Catalase*

Superoxide dismutase 1 (*SOD*) catalyses in the cytoplasm the dismutation and reduction of ROS such as superoxide (O_2^-) into oxygen (O_2) and H_2O_2, whereas *Catalase* (*Cat*) catalyses the decomposition of H_2O_2 into H_2O and O_2 (Landis & Tower, 2005). These enzymes are crucial in maintaining redox homeostasis and act as the first line of defence against ROS perturbations (Radyuk *et al.*, 2004). Orthologues are found in majority of living species, and they are expressed almost ubiquitously in all adult *Drosophila* tissues (Radyuk *et al.*, 2004). Due to their critical function, high conservation between *Drosophila* and humans and involvement in redox biology, *SOD* and *Cat* are enticing candidates to study their involvement in the radiation response. Additionally, *SOD* was identified as a risk candidate from the literature search (**Table 4.3**). Further, *Drosophila* toxicological studies have shown that Quercetin and epicatechin treatment can induce increased *SOD1* expression which was linked to the radioprotective effect of the pharmaceuticals (Proshkina, Lashmanova & Dobrovolskaya, 2016). Here, I overexpressed *SOD* and *Cat* within the midgut, to ascertain whether it modulated radiation survival.

Survival was assayed *post* irradiation (200 Gy) when *SOD* and *Cat* were overexpressed specifically in midgut enterocytes using *myosin-gal4* driver (**Figure 4.14**). Visual inspection of KM curves showed that treatment reduced survival only in w^{1118} genotype (**Figure 4.14 A** & **B**). A CoxPH model was generated with the explanatory variables: radiation treatment, genotype, and an interaction between treatment and genotype (**Figure 4.14 C**). However, modelling determined that no variable significantly influenced survival ($p > 0.11$).

Survival was assayed *post* irradiation (200 Gy) when *SOD* and *Cat* were overexpressed specifically in midgut ISCs using *escargot-gal4* driver (**Figure 4.15**). Visual inspection of KM curves showed that treatment reduced survival in both genotypes (**Figure 4.15 A** & **B**). A CoxPH model was generated with the explanatory variables: radiation treatment, genotype, and an interaction between treatment and genotype (**Figure 4.15 C**). Both treatment and genotype were significant modulators of survival ($p = 0.001$ and $p = 0.042$, respectively) with estimated HRs of 1.57 (1.192-2.069, 95% CI) and 1.329 (1.01-1.748, 95% CI), respectively. There was no significant interaction between treatment and genotype ($p = 0.371$). Testing for proportional hazards that are independent of time using the Schoenfeld residual test determined that all variables violated the assumption ($p < 0.05$).

Therefore, overexpression of *SOD* and *Cat* in either the midgut enterocytes or ISCs did not improve survival *post* irradiation treatment. However, the effect size of irradiation was small making it difficult to interpret results.
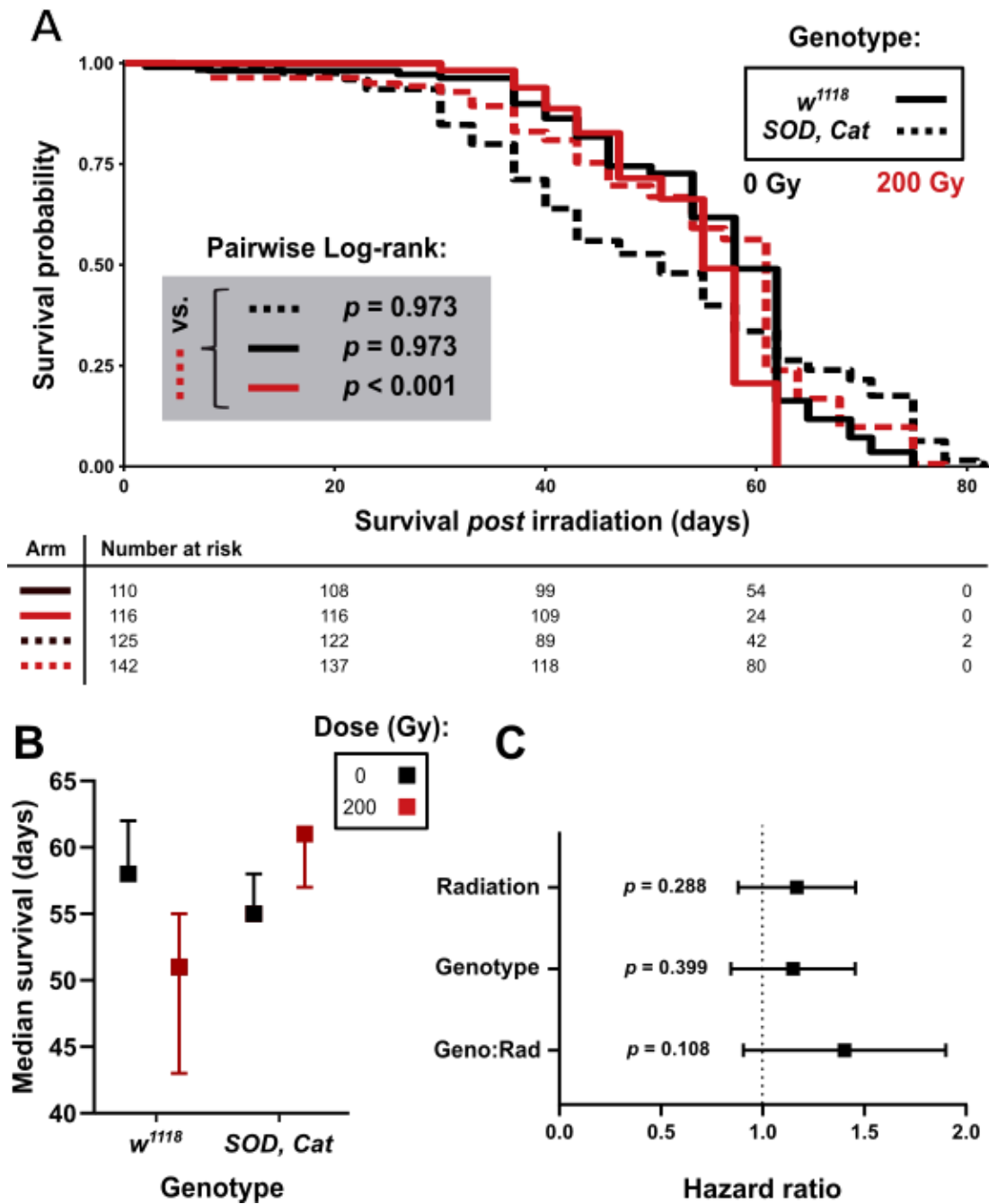
Figure 4.14: Overexpression of *SOD* and *Cat* in enterocytes does not improve survival *post* irradiation. *Drosophila* males were mated and purpled as standard practice, desired genotypes selected and allowed to mate for 48 hr followed by irradiation (200 Gy). (**A**) KM curve with risk table, (**B**) median survival of vial replicates for each cohort with 95% CI, (**C**) HR derived from CoxPH model.
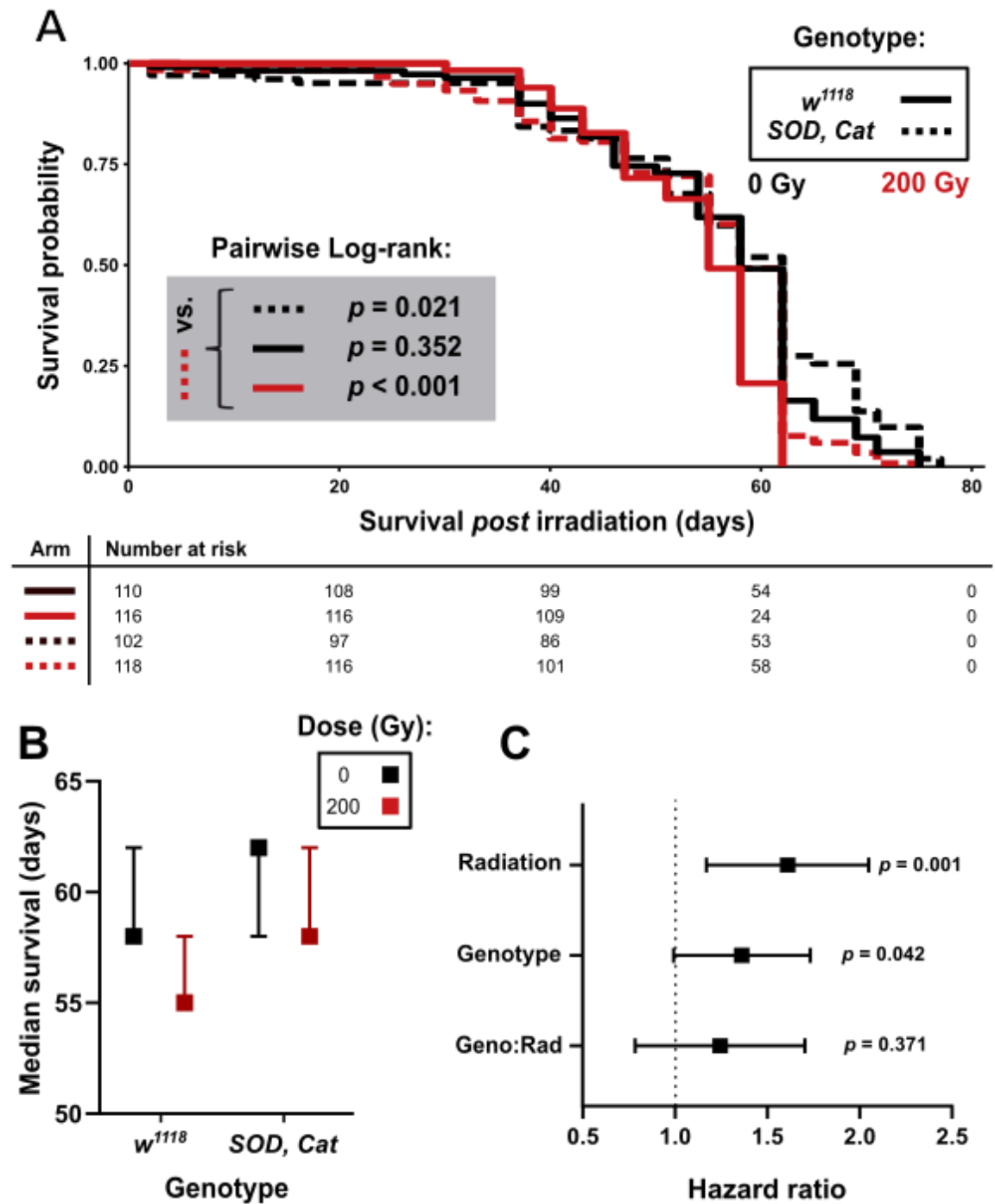
Figure 4.15: Overexpression of *SOD* and *Cat* in ISCs does not improve survival *post* irradiation. *Drosophila* males were mated and purpled as standard practice, desired genotypes selected and allowed to mate for 48 hr followed by irradiation (200 Gy). (**A**) KM curve with risk table, (**B**) median survival of vial replicates for each cohort with 95% CI, (**C**) HR derived from CoxPH model.

4.6 Transcriptome analysis

The quantification of the transcriptome was performed due to the lack of positive hits when testing candidate genes (**Section 4.5**). It was difficult to ascertain whether the negative results obtained were because midgut health was not crucial for radiation survival, or that the manipulated gene under study was not involved in modulating the radiation response. Therefore, I decided to quantify the transcriptome of multiple male adult tissues long-term (20 days) *post* irradiation, by performing RNA-seq. Control tissues were derived from sibling males that were reared and aged in replicate vials alongside irradiated males. I expected this experiment would help to answer whether the midgut was particularly sensitive to irradiation, and would also generate gene lists for future functional testing.

Oregon R males were purped, irradiated (200 Gy) and aged as previously described (**Section 2.2.5**). The radiation-induced transcriptome was quantified for the midgut, abdominal tissue enriched in fat body, thorax tissue enriched in flight muscle, and heads enriched in neural tissue (**Figure 4.16**). The head had the highest number of upregulated genes at 934, followed by the abdominal tissue (645 genes), thorax tissue (302 genes) and midgut (101 genes) (**Figure 4.16 A**). For all tissues, the majority of genes were downregulated, the abdominal tissue had the highest number of downregulated genes at 2649, and the midgut had the least at 578 genes (**Figure 4.16 B**). It was later observed that for all tissues the majority of downregulated genes were testes specific. Reviewing the number of reads per samples determined that there was testes-specific contamination in all three control samples. The likely explanation for this is due to the time of sample collection since treatment – the testes in irradiated *Drosophila* had already atrophied and disintegrated, whereas in non-irradiated *Drosophila* the testes would not have atrophied as much. Therefore, the control-specific testes contamination is the result of naturally aged testes undergoing atrophy and dispersing tissue material including mRNA amongst the other tissues and organs. To that end, for each tissue differentially expressed genes (DEGs) were filtered based on the following:

1.) Whether the gene has already been characterised as testes-specific – this was done using flybase batch downloader and checking expression data (Krause et al., 2022).
2.) DEGs which had no or little expression (< 10 reads per sample) within all three irradiated replicates were also classified as contamination.

As anticipated applying this manual filtering did not alter the upregulated DEG lists but did significantly reduce the downregulated DEG lists (**Figure 4.17**). The head tissue had the least amount of testes contamination with 43 DEGs (4% reduction) identified as testes-specific genes as compared to the abdominal tissue which had 2211 DEGs (84% removed). Considering the spatial relationship of the head and abdomen to the testes, these reductions show that the contamination was more concentrated within the abdominal tissue as this is where the testes reside, and the further away the tissue from the testes, the less contamination.

Tissues were individually analysed, and comparative analysis of tissue transcriptomes was performed. Also, the expression pattern of candidates identified through literature search was checked (**Section 4.4**) as well as previously functionally tested candidates (**Section 4.5**).
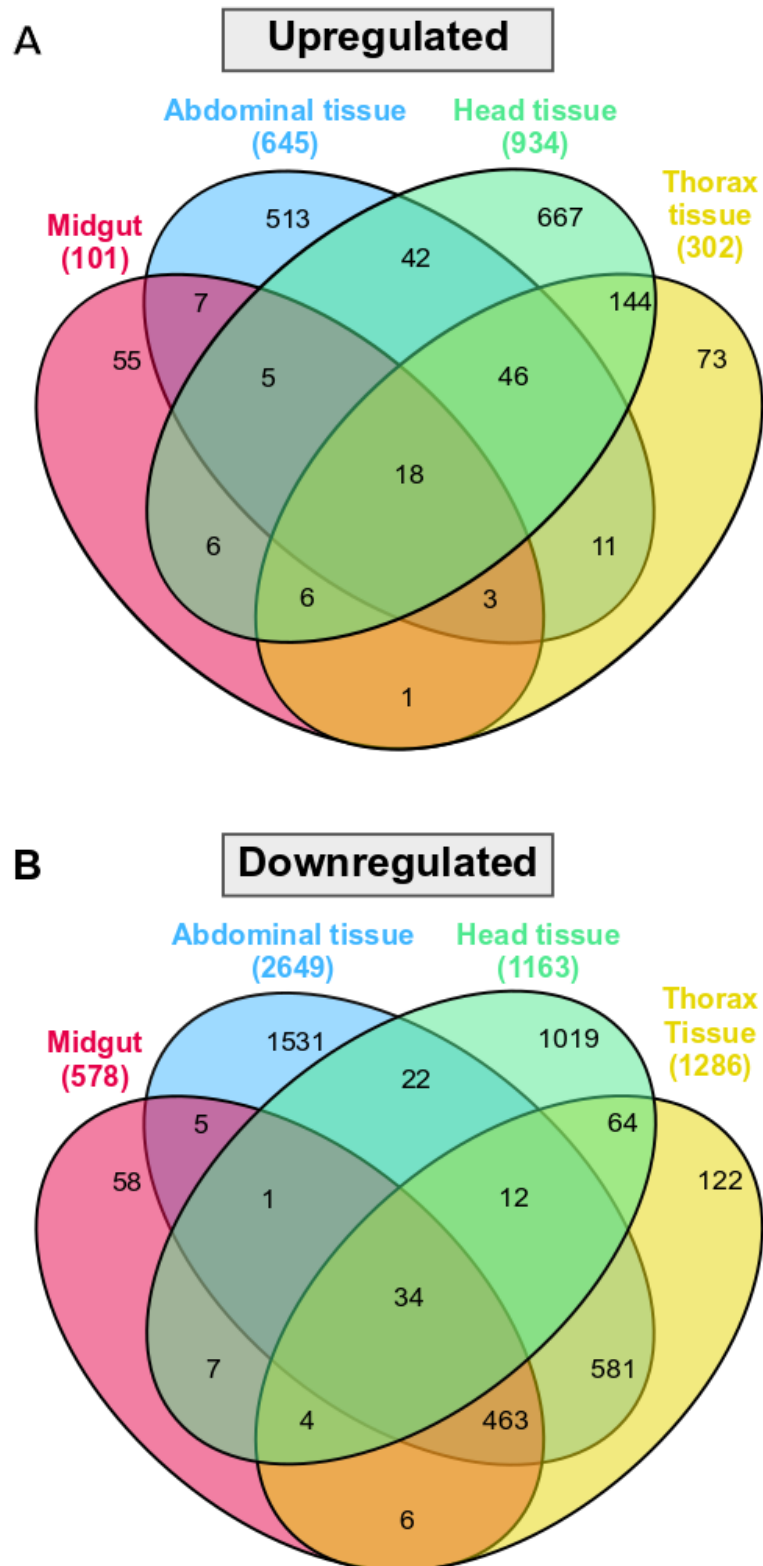
Figure 4.16: Summary of differentially expressed genes in various tissues *post* irradiation. (**A**) genes upregulated *post* irradiation in each tissue (No. of genes). (**B**) genes downregulated *post* irradiation in each tissue (No. of genes). Numbers within Venn diagrams refer to number of differentially expressed (DE) genes shared between tissues.
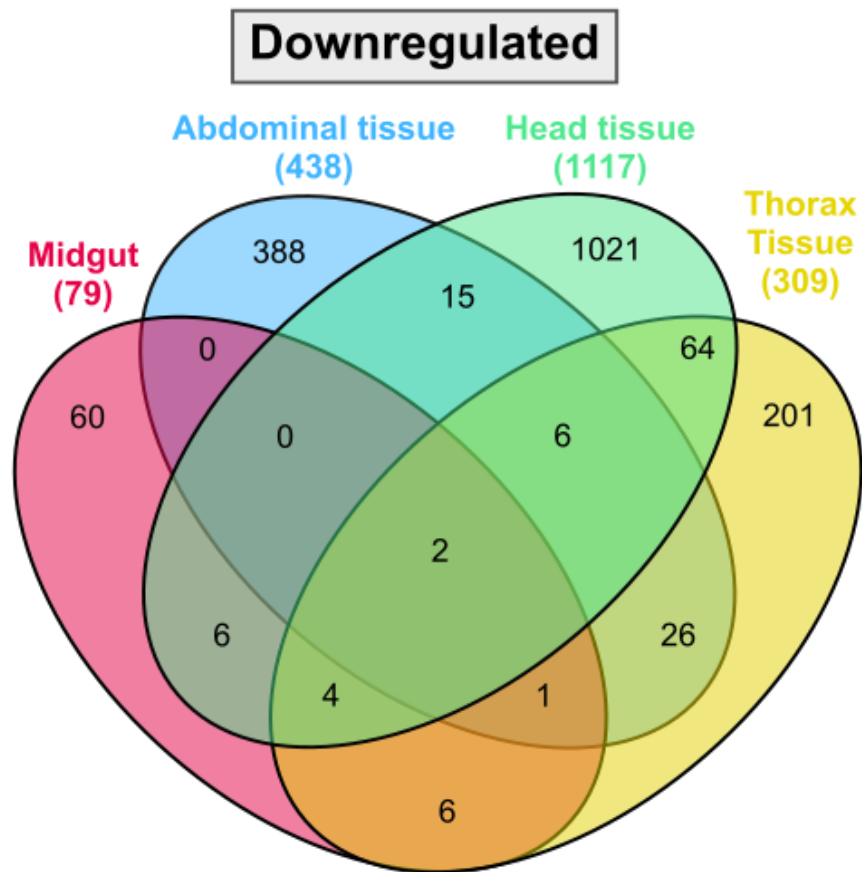
Figure 4.17: Summary of differentially expressed genes *post* irradiation after testes-specific genes filtered. (**A**) genes upregulated *post* irradiation in each tissue (No. of genes). (**B**) genes downregulated *post* irradiation in each tissue (No. of genes). Numbers within Venn diagrams refer to number of differentially expressed (DE) genes shared between tissues.

4.6.1 Radiation-induced transcriptome of various tissues

Radiation-induced transcriptional profile of the midgut

The long-term transcriptome of the midgut *post* irradiation was successfully quantified with a total of 180 DEGs (up- and downregulated combined) (**Table 4.5 & 4.6**). Twelve of the most upregulated DEGs have yet to be fully characterised with CG3339 having the greatest fold change (log$_2$ fold change = 3.252) (**Table 4.5**). The upregulated DEGs appear not to have a specific function for example the product of *sNPF* acts through ERK-insulin pathway and is involved in organism growth, carbohydrate metabolism and locomotion (Kyu-Sun et al., 2009). Whereas, *BomBc1* expression is induced via Toll signalling and has a role in bacterial and fungal infections (Clemmons, Lindsay, & Wasserman, 2015). Regarding the most downregulated genes, ten have yet to be fully characterised (**Table 4.6**). The characterised downregulated genes show a similar pattern as the upregulated list in which they are involved in a wide variety of processes. Of particular interest is *esg* which was significantly downregulated in the midgut (log$_2$ fold change = -1.449). *esg* is a transcription factor expressed by ISCs and is required to maintain pluripotency (Dutta et al., 2015). The high level of *esg* expression within ISCs was why it was used as a driver (Gal4 system) to express genes of interest during candidate validation studies (**Section 4.5**). Its unexpected downregulation *post* irradiation might explain the lack of positive data from the candidate studies. *esg* expression levels *post* irradiation would need be validated because it is also expressed in male testes and therefore might represent further testes contamination (Krause et al., 2022).

GO analysis was performed on the 180 DEGs (**Table 4.7**) and a number of biological processes involved in metabolism were modulated such as: carbohydrate binding (GO:0030246), mannosidase activity (GO:0015923) and alpha-mannosidase activity (GO:0004559) were identified.

Radiation-induced transcriptional profile of the head

The head transcriptome *post* irradiation was successfully quantified with a total of 2,096 DEGs (**Table 4.8 & 4.9**). Ten of the most upregulated DEGs have yet to be fully characterised (**Table 4.8**). From the upregulated DEGs, two genes *Mur89F* and *Muc26B* were significantly upregulated (log$_2$ fold change = 6.531 & 5.137, respectively). Both genes are components of the ECM and as previously discussed, uncontrolled accumulation and deposition of ECM components (fibrosis) is a

common long-term symptom of irradiation in humans (**Chapter 3: Section 3.5**). Eleven of the downregulated DEGs have yet to be fully charactered (**Table 4.9**). Of the downregulated DEGs that have been characterised four do not produce proteins (*lncRNA*:*CR44768*, *asRNA*:*CR46354*, *asRNA*:*CR45520* & *mir-2a-2*), and the others appear to be a random assortment of genes based on their functions. For example *mag* is a lipase that degrades dietary triglycerides for fatty acid absorption (Sieber & Thummel, 2012), and *Mabi* acts to induce both caspase-dependent and - independent apoptosis within the head during development (Tanaka, Takahashi, Fuse, & Takano-Shimizu-Kouno, 2014).

A number of biological processes involved in response to stimulus were modulated such as response to stimulus (GO:0050896), response to external stimulus (GO:0009605), and cellular response to stimulus (GO:0051716) (**Table 4.10**).

Radiation-induced transcriptional profile of the thorax

Thorax tissue transcriptome *post* irradiation was successfully quantified with a total of 611 DEGs (**Table 4.11 & 4.12**). Ten of the upregulated DEGs have yet to be fully characterised (**Table 4.11**). From the upregulated DEGs, three odorant receptors were upregulated *Or22a* ($\log_2$ fold change = 4.547), *Or19b* ($\log_2$ fold change = 3.746), and *Obp83b* ($\log_2$ fold change = 3.357). It is assumed that these genes were upregulated within the neurones contained within the thorax however the reason for their upregulation remains unclear. Thirteen of the downregulated DEGs have yet to be fully characterised (**Table 4.12**).

Many processes involved in DNA repair were modulated: damaged DNA binding (GO:0003684), double-strand break repair (GO:0006302), cellular response to DNA damage stimulus (GO:0006974), and DNA repair (GO:0006281) (**Table 4.13**). These results are particularly encouraging because radiation is genotoxic, and therefore the repair of DNA would be expected and necessary for survival *post* treatment.

Radiation-induced transcriptional profile of the abdomen

Abdominal tissue transcriptome *post* irradiation was successfully quantified with a total of 740 DEGs (**Table 4.14 & 4.15**). Seven of the most significantly DEGs have yet to be fully validated with *CG11350* having the highest level of upregulation ($\log_2$ fold change = 6.106) (**Table 4.14**). *CecC* the second highest upregulated DEG ($\log_2$ fold change = 6.106) has been previously shown to be upregulated within the brain

in irradiated *Drosophila* long-term (35 days) *post* X-ray irradiation (**Section 4.4**) (Lisa J. Sudmeier, Samudrala, et al., 2015). *CecC* encodes an antibacterial peptides specific against Gram-negative bacteria, and its upregulation might indicate secondary opportunistic infection due to irradiation.

A wide variety biological processes were found to be enriched within the abdominal DEGs (**Table 4.16**). Processes included humoral immune response to fungal and bacterial pathogens (WP:WP3660) – further indication of secondary infection.

Table 4.5: Top 20 upregulated genes within the midgut long-term *post* irradiation. Shown genes represent most upregulated genes in irradiated samples from the 101 upregulated in midgut.

Flybase ID	Gene name (Symbol)	Fold Change (log$_2$)	Adjusted *p* value
FBgn0039510	*CG3339*	3.252	0.00209906
FBgn0034291	*CG5770*	2.798	0.00001455
FBgn0032840	*short neuropeptide F precursor (sNPF)*	2.554	0.00031564
FBgn0085256	*CG34227*	2.544	0.00126910
FBgn0034328	*Bomanin Bicipital 1 (BomBc1)*	2.189	0.00000402
FBgn0033602	*Cuticular protein 47Ee (Cpr47Ee)*	2.16	0.01016400
FBgn0062565	*Odorant receptor 19b (Or19b)*	2.129	0.01633974
FBgn0031918	*CG6055*	2.08	0.00075905
FBgn0035607	*CG4835*	1.876	0.00024822
FBgn0003483	*spindle E (spn-E)*	1.827	0.04310913
FBgn0039411	*dysfusion (dysf)*	1.816	0.00000000
FBgn0262357	*CG43055*	1.811	0.00406021
FBgn0034317	*CG14499*	1.748	0.00000000
FBgn0263412	*long non-coding RNA:CR43458 (lncRNA:CR43458)*	1.733	0.00444026
FBgn0034318	*CG14500*	1.651	0.00000753
FBgn0031910	*CG15818*	1.521	0.00000000
FBgn0040972	*CG16978*	1.52	0.00000830
FBgn0035176	*materazzi (mat)*	1.458	0.00113960
FBgn0051446	*CG31446*	1.449	0.00255941
FBgn0261989	*CG42807*	1.448	0.00000171

Table 4.6: Top 20 downregulated genes within the midgut long-term *post* irradiation. Due to control-specific testes contamination genes were manually curated and known testes specific genes were removed. From the 578 downregulated genes, 79 remained and top 20 most downregulated were selected for table.

Flybase ID	Gene name (Symbol)	Fold Change (log$_2$)	Adjusted *p* value
FBgn0002939	*neither inactivation nor afterpotential D (ninaD)*	-1.79	0.00000001
FBgn0051091	*CG31091*	-2.366	0.00000001
FBgn0053965	*CG33965*	-2.229	0.00000000
FBgn0037616	*CG8136*	-1.406	0.02631826
FBgn0038598	*CG7131*	-2.474	0.01516180
FBgn0034052	*CG8299*	-1.375	0.01699307
FBgn0021776	*miranda (mira)*	-1.143	0.00000001
FBgn0051538	*CG31538*	-0.989	0.01951407
FBgn0000615	*exuperantia (exu)*	-3.117	0.01706567
FBgn0032068	*Lysosomal alpha-mannosidase V (LManV)*	-2.047	0.00002202
FBgn0002732	*Enhancer of split malpha, Bearded family member*	-1.72	0.00015655
FBgn0001981	*escargot (esg)*	-1.449	0.00005709
FBgn0051636	*CG31636*	-1.518	0.00506274
FBgn0053337	*CG33337*	-1.325	0.00206809
FBgn0032069	*Lysosomal alpha-mannosidase VI (LManVI)*	-1.236	0.00354429
FBgn0032066	*Lysosomal alpha-mannosidase III (LManIII)*	-2.028	0.00052956
FBgn0085345	*CG34316*	-1.863	0.01765574
FBgn0039774	*Ceramidase (CDase)*	-1.046	0.00000001
FBgn0002609	*Enhancer of split m3, helix-loop-helix (E(spl)m3-HLH)*	-1.158	0.01960998
FBgn0028945	*CG7631*	-2.119	0.00000002

Table 4.7: Gene ontology analysis on differentially expressed genes within the midgut *post* irradiation. G:Profiler was used and 180 genes were included in the GO analysis. ID column refers to ontology pathway reference number and which database it was derived: GO: molecular function, biological process and cellular compartment, Kyoto encyclopaedia of genes and genomes (KEGG), WikiPathways (WP), and TRANSFAC (TF).

ID	Description	Adjusted *p* value	No. of genes
GO:0016798	hydrolase activity of glycosyl bonds	6.53429E-05	11
GO:0004559	alpha-mannosidase activity	0.000161776	5
GO:0015923	mannosidase activity	0.000240254	5
GO:0030246	carbohydrate binding	0.000400705	11
GO:0016787	hydrolase activity	0.004500538	44
GO:0004497	monooxygenase activity	0.034294561	8
GO:0004553	hydrolase activity of O-glycosyl compounds	0.045631193	7
GO:0006013	mannose metabolic process	4.46921E-05	5
GO:0046466	membrane lipid catabolic process	0.015120555	4
GO:0030149	sphingolipid catabolic process	0.015120555	4
GO:0005576	extracellular region	2.12354E-05	36
GO:0043564	Ku70:Ku80 complex	0.034672599	2
KEGG:00511	Other glycan degradation	6.49697E-06	6
KEGG:04711	Circadian rhythm - fly	0.016732758	3
KEGG:04142	Lysosome	0.026418573	7
HP:0007232	Spinocerebellar tract disease in lower limbs	1.10832E-05	5
HP:0005791	Cortical thickening of long bone diaphyses	1.10832E-05	5
HP:0430022	Abnormality of the sphenoid sinus	3.82702E-05	5
HP:0025406	Asthenia	0.000100684	5
HP:0011334	Facial shape deformation	0.000133574	6
HP:0005619	Thoracolumbar kyphosis	0.000210826	6
HP:0010665	Bilateral coxa valga	0.000223498	5
HP:0004570	Increased vertebral height	0.000440996	5
HP:0002503	Spinocerebellar tract degeneration	0.000440996	5
HP:0031123	Recurrent gastroenteritis	0.000797643	5
HP:0100712	Abnormal lumbar spine morphology	0.001334555	6
HP:0003133	Abnormality of the spinocerebellar tracts	0.001349039	5
HP:0003302	Spondylolisthesis	0.001349039	5
HP:0008821	Hypoplastic inferior ilia	0.001349039	5
HP:0000935	Thickened cortex of long bones	0.002162776	5
HP:0100039	Thickened cortex of bones	0.002162776	5
HP:0004684	Talipes valgus	0.002162776	5
HP:0010885	Avascular necrosis	0.004686121	11
HP:0010471	Oligosacchariduria	0.007048878	5
HP:0000900	Thickened ribs	0.009851988	5
HP:0001334	Communicating hydrocephalus	0.014976212	7
HP:0002942	Thoracic kyphosis	0.014976212	7
HP:0000938	Osteopenia	0.019109974	16
HP:0002797	Osteolysis	0.024075655	8
HP:0000546	Retinal degeneration	0.029898645	16
HP:0001876	Pancytopenia	0.037591733	9
HP:0012157	Subcortical cerebral atrophy	0.039190611	5
HP:0012145	Abnormality of multiple cell lineages in the bone marrow	0.040776996	10
HP:0007722	Retinal pigment epithelial atrophy	0.040896533	8

Table 4.8: Top 20 upregulated genes within the head long-term *post* irradiation. Shown genes represent highest upregulated genes in irradiated samples from the 934 upregulated in head tissue.

Flybase ID	Gene name (Symbol)	Fold Change (log$_2$)	Adjusted *p* value
FBgn0065048	*snoRNA:U3:54Aa (snoRNA:U3:54Aa)*	7.003	0.00000402
FBgn0037428	*Osiris 18 (Osi18)*	6.951	0.00000412
FBgn0038492	*Mucin related 89F (Mur89F)*	6.531	0.00006073
FBgn0004649	*yolkless (yl)*	6.389	0.00008905
FBgn0028856	*CG18063*	6.274	0.00002882
FBgn0040602	*CG14545*	5.831	0.00000000
FBgn0086027	*snoRNA:Or-CD1*	5.616	0.00052098
FBgn0065047	*snoRNA:U3:54Ab (snoRNA:U3:54Ab)*	5.466	0.00000000
FBgn0261799	*doublesex cognate 73A (dsx-c73A)*	5.431	0.00488750
FBgn0262891	*CG43246*	5.377	0.00544642
FBgn0029968	*Ionotropic receptor 7g (Ir7g)*	5.344	0.00821429
FBgn0262008	*CG42826*	5.337	0.00699747
FBgn0035750	*CG14826*	5.284	0.00973626
FBgn0266854	*CR45315*	5.276	0.00180685
FBgn0040950	*Mucin 26B (Muc26B)*	5.137	0.00133236
FBgn0036362	*CG10725*	5.072	0.01449231
FBgn0036951	*CG7017*	5.033	0.00466989
FBgn0052079	*CG32079*	5.011	0.01996463
FBgn0267216	*long non-coding RNA:CR45656 (lncRNA:CR45656)*	4.946	0.02694343
FBgn0263040	*CG43335*	4.915	0.02528587

Table 4.9: Top 20 downregulated genes within the head long-term *post* irradiation. Due to control-specific testes contamination genes were manually curated and known testes specific genes were removed. From the 1162 downregulated genes, 1117 remained and top 20 most downregulated were selected for table.

Flybase ID	Gene name (Symbol)	Fold Change ($\log_2$)	Adjusted *p* value
FBgn0036996	*magro (mag)*	-2.587	0.04485215
FBgn0051823	*CG31823*	-2.135	0.04892607
FBgn0035300	*CG1139*	-2.055	0.04246922
FBgn0032493	*Mabiki (Mabi)*	-1.506	0.01239665
FBgn0265993	*long non-coding RNA:CR44768 (lncRNA:CR44768)*	-1.541	0.01368661
FBgn0034505	*CG16739*	-1.659	0.00165816
FBgn0053234	*CG33234*	-1.549	0.00948555
FBgn0034506	*CG13870*	-1.456	0.01847001
FBgn0053233	*CG33233*	-1.249	0.02982739
FBgn0083951	*CG34115*	-1.104	0.02984817
FBgn0085485	*CG34456*	-1.46	0.00128481
FBgn0286034	*antisense RNA:CR46354 (asRNA:CR46354)*	-1.116	0.04231094
FBgn0053348	*Chemosensory protein B 42a (CheB42a)*	-1.489	0.00354375
FBgn0267076	*antisense RNA:CR45520 (asRNA:CR45520)*	-1.037	0.03366433
FBgn0036607	*CG13059*	-1.408	0.00818269
FBgn0051528	*CG31528*	-0.995	0.03647306
FBgn0265629	*CG44437*	-0.987	0.03186362
FBgn0262460	*mir-2a-2 stem loop (mir-2a-2)*	-0.949	0.01261653
FBgn0026397	*Odorant receptor 22b (Or22b)*	-1.074	0.01013352
FBgn0053349	*pickpocket 25 (ppk25)*	-1.333	0.00030372

Table 4.10: Gene ontology analysis on differentially expressed genes in the head *post* irradiation. G:Profiler was used and 2,096 genes were included in the GO analysis. ID column refers to ontology pathway reference number and which database it was derived: GO: molecular function, biological process and cellular compartment, Kyoto encyclopaedia of genes and genomes (KEGG), WikiPathways (WP), TRANSFAC (TF), and human phenotype ontology (HP).

ID	Description	Adjusted *p* value	No. of genes
GO:0005488	binding	3.73372E-15	1165
GO:0097367	carbohydrate derivative binding	3.5829E-13	280
GO:0032553	ribonucleotide binding	5.27697E-12	241
GO:0005515	protein binding	1.07336E-11	667
GO:0043168	anion binding	1.14361E-11	273
GO:0017076	purine nucleotide binding	1.17095E-11	239
GO:0032555	purine ribonucleotide binding	1.62639E-11	237
GO:0035639	purine ribonucleoside triphosphate binding	2.92676E-11	232
GO:1901265	nucleoside phosphate binding	5.1885E-11	265
GO:0000166	nucleotide binding	5.1885E-11	265
GO:0065008	regulation of biological quality	1.92596E-31	369
GO:0050896	response to stimulus	7.03452E-29	672
GO:0009605	response to external stimulus	8.42705E-20	271
GO:0065007	biological regulation	2.51501E-17	896
GO:0032501	multicellular organismal process	5.77962E-17	725
GO:0023052	signaling	3.67972E-16	431
GO:0051716	cellular response to stimulus	3.7825E-16	475
GO:0007154	cell communication	3.8454E-16	438
GO:0009987	cellular process	8.91437E-14	1421
GO:0032879	regulation of localization	3.13515E-13	156
GO:0005886	plasma membrane	5.23526E-28	408
GO:0071944	cell periphery	3.52286E-27	477
GO:0031226	intrinsic component of plasma membrane	1.36232E-17	161
GO:0005887	integral component of plasma membrane	7.20238E-16	154
GO:0034702	ion channel complex	1.31555E-13	47
GO:1902495	transmembrane transporter complex	1.00139E-12	50
GO:0030054	cell junction	1.44565E-12	160
GO:0042995	cell projection	1.72087E-12	195
GO:0120025	plasma membrane bounded cell projection	1.77787E-12	193
KEGG:04070	Phosphatidylinositol signaling system	0.029575439	20
TF:M02376	Factor: Ubx; motif: NTTAATTA	0.000444479	932
TF:M03144	Factor: H2.0; motif: TTWATDA	0.000476564	932
TF:M02358	Factor: repo; motif: TTAATTA	0.000476564	932
TF:M02285	Factor: Awh; motif: YTAATTA	0.000476564	932
TF:M02309	Factor: HGTX; motif: TTAATTA	0.000476564	932
TF:M02375	Factor: zen2; motif: NTAATKA	0.000476564	932
TF:M02338	Factor: en; motif: YTAATTR	0.000476564	932
TF:M03153	Factor: PHDP; motif: YTAATTN	0.000476564	932
TF:M02312	Factor: Lim1; motif: TTAATTA	0.000476564	932
TF:M02344	Factor: hbn; motif: TTAATTR	0.000476564	932
HP:0008002	Abnormality of macular pigmentation	0.018407351	19

Table 4.11: Top 20 upregulated genes within the thorax tissue *post* irradiation.
Shown genes represent highest upregulated genes in irradiated thorax samples, from a total of 302 genes upregulated.

Flybase ID	Gene name (Symbol)	Fold Change (log$_2$)	Adjusted *p* value
FBgn0030544	*(CG13403)*	5.924	0.01468888
FBgn0038350	*Aldehyde oxidase 4 (AOX4)*	5.437	0.00009783
FBgn0267217	*long non-coding RNA:CR45657 (lncRNA:CR45657)*	5.316	0.02842842
FBgn0026398	*Odorant receptor 22a (Or22a)*	4.547	0.00816652
FBgn0267216	*long non-coding RNA:CR45656 (lncRNA:CR45656)*	4.373	0.02205148
FBgn0040602	*(CG14545)*	4.194	0.00000001
FBgn0032551	*(CG18636)*	3.966	0.04176493
FBgn0037078	*(CG12971)*	3.927	0.00852462
FBgn0038676	*(CG6026)*	3.86	0.01099610
FBgn0062565	*Odorant receptor 19b (Or19b)*	3.746	0.00159394
FBgn0261989	*(CG42807)*	3.498	0.00016951
FBgn0052625	*(CG32625)*	3.484	0.00000001
FBgn0038873	*(CG5892)*	3.426	0.03291233
FBgn0010403	*Odorant-binding protein 83b (Obp83b)*	3.357	0.02100895
FBgn0286204	*ichor (ich)*	3.356	0.00695920
FBgn0028999	*nervous fingers 1 (nerfin-1)*	3.32	0.02363805
FBgn0065047	*snoRNA:U3:54Ab (snoRNA:U3:54Ab)*	3.289	0.00000145
FBgn0035512	*Cuticular protein 64Ac (Cpr64Ac)*	3.234	0.00125418
FBgn0052107	*(CG32107)*	3.068	0.00250461
FBgn0054043	*(CG34043)*	3.015	0.01499877

Table 4.12: Top 20 downregulated genes within the thorax long-term *post* irradiation. Due to control-specific testes contamination genes were manually curated and known testes specific genes were removed. From the 1286 downregulated genes, 309 remained and top 20 most downregulated were selected for table.

Flybase ID	Gene name (Symbol)	Fold Change ($\log_2$)	Adjusted *p* value
FBgn0270925	*(CG4836)*	-7.463	0.00000002
FBgn0031751	*(CG9016)*	-5.719	0.00000001
FBgn0061197	*salto (salto)*	-5.629	0.00000006
FBgn0003889	*beta-Tubulin at 85D (betaTub85D)*	-5.574	0.00000004
FBgn0034144	*(CG5089)*	-5.287	0.00004098
FBgn0052436	*(CG32436)*	-5.172	0.00000003
FBgn0265508	*antisense RNA:CR44370 (asRNA:CR44370)*	-4.818	0.00000002
FBgn0032061	*(CG9314)*	-4.768	0.00000003
FBgn0035988	*(CG3982)*	-4.664	0.00000009
FBgn0032049	*beta-site APP-cleaving enzyme (Bace)*	-4.518	0.00625607
FBgn0267727	*Pendulin (Pen)*	-4.386	0.00000001
FBgn0051538	*(CG31538)*	-4.337	0.00000009
FBgn0038248	*(CG7886)*	-4.319	0.00000002
FBgn0040859	*long non-coding RNA:CR32658 (lncRNA:CR32658)*	-4.315	0.00000002
FBgn0036687	*(CG6652)*	-4.276	0.00000139
FBgn0032144	*(CG17633)*	-4.071	0.01518516
FBgn0039398	*(CG14540)*	-4.015	0.00000002
FBgn0037616	*(CG8136)*	-3.953	0.00000003
FBgn0031574	*Tubulin tyrosine ligase-like 4B (TTLL4B)*	-3.923	0.00000005
FBgn0038598	*(CG7131)*	-3.817	0.00000001

Table 4.13: Gene ontology analysis on differentially expressed genes in thorax tissue *post* irradiation. G:Profiler was used and 1,586 genes were included in the GO analysis. ID column refers to ontology pathway reference number and which database it was derived: GO: molecular function, biological process and cellular compartment, Kyoto encyclopaedia of genes and genomes (KEGG), WikiPathways (WP), TRANSFAC (TF), and human phenotype ontology (HP).

ID	Description	Adjusted *p* value	No. of genes
GO:0003824	catalytic activity	0.000032312	229
GO:0017171	serine hydrolase activity	0.000260436	36
GO:0016491	oxidoreductase activity	0.004259765	52
GO:0008236	serine-type peptidase activity	0.005925463	29
GO:0042162	telomeric DNA binding	0.008076482	5
GO:0003684	damaged DNA binding	0.008560685	7
GO:0004252	serine-type endopeptidase activity	0.011474026	27
GO:0016787	hydrolase activity	0.040835619	108
GO:0006302	double-strand break repair	0.000036682	19
GO:0006974	cellular response to DNA damage stimulus	0.000492877	30
GO:0006303	double-strand break repair via nonhomologous end joining	0.000898883	6
GO:0006281	DNA repair	0.000993704	26
GO:0071897	DNA biosynthetic process	0.009371481	11
GO:0006572	tyrosine catabolic process	0.043778849	4
GO:0006259	DNA metabolic process	0.049664195	34
GO:0005576	extracellular region	0.000001261	90
GO:0035861	site of double-strand break	0.000048141	7
GO:0090734	site of DNA damage	0.000048141	7
GO:0005615	extracellular space	0.000084679	58
GO:0030870	Mre11 complex	0.014412231	3
GO:0005662	DNA replication factor A complex	0.014412231	3
KEGG:03450	Non-homologous end-joining	0.000032118	5
KEGG:03440	Homologous recombination	0.012817991	6
KEGG:03430	Mismatch repair	0.049974497	5
WP:WP565	DNA replication	0.021588287	6

Table 4.14: Top 20 upregulated genes within abdominal tissue *post* irradiation. Shown genes represent highest upregulated genes in irradiated thorax samples, from a total of 302 genes upregulated.

Flybase ID	Gene name (Symbol)	Fold Change (log$_2$)	Adjusted *p* value
FBgn0035552	*(CG11350)*	6.106	0.00501194
FBgn0000279	*Cecropin C (CecC)*	5.524	0.00857764
FBgn0035256	*(CG13930)*	5.433	0.00250548
FBgn0038676	*(CG6026)*	4.826	0.00781132
FBgn0029807	*(CG3108)*	4.624	0.03435984
FBgn0039839	*pickpocket 24 (ppk24)*	4.56	0.01313909
FBgn0003411	*sisterless A (sisA)*	4.409	0.02690666
FBgn0019809	*gcm2 (gcm2)*	4.359	0.02458376
FBgn0265731	*long non-coding RNA:CR44538 (lncRNA:CR44538)*	3.981	0.02943109
FBgn0035281	*Cuticular protein 62Bc (Cpr62Bc)*	3.966	0.00453705
FBgn0062565	*Odorant receptor 19b (Or19b)*	3.831	0.00349521
FBgn0004045	*Yolk protein 1 (Yp1)*	3.584	0.00000005
FBgn0038350	*Aldehyde oxidase 4 (AOX4)*	3.331	0.00005390
FBgn0031542	*(CG15414)*	3.19	0.00520255
FBgn0005391	*Yolk protein 2 (Yp2)*	3.156	0.00015270
FBgn0036044	*Z band alternatively spliced PDZ-motif protein 67 (Zasp67)*	2.974	0.04485995
FBgn0037563	*(CG11672)*	2.956	0.00108770
FBgn0011283	*Odorant-binding protein 28a (Obp28a)*	2.884	0.00310317
FBgn0264820	*(CR44028)*	2.878	0.04811358
FBgn0039795	*Serpin 100A (Spn100A)*	2.797	0.01385051

Table 4.15: Top 20 downregulated genes within abdominal tissue long-term ***post*** **irradiation.** Due to control-specific testes contamination genes were manually curated and known testes specific genes were removed. From the 2649 downregulated genes, 438 remained and top 20 most downregulated were selected for table.

Flybase ID	Gene name (Symbol)	Fold Change (log$_2$)	Adjusted p value
FBgn0034144	*(CG5089)*	-5.998	0.00574172
FBgn0038373	*(CG4546)*	-5.479	0.00000001
FBgn0037616	*(CG8136)*	-4.908	0.00000001
FBgn0051538	*(CG31538)*	-4.577	0.00000000
FBgn0038952	*(CG7069)*	-4.21	0.00000013
FBgn0263048	*Glycerol-3-phosphate dehydrogenase 3 (Gpdh3)*	-3.792	0.00000166
FBgn0025111	*Adenine nucleotide translocase 2 (Ant2)*	-3.704	0.00000001
FBgn0031690	*(CG7742)*	-3.661	0.00025510
FBgn0264307	*orb2 (orb2)*	-3.636	0.00000057
FBgn0033268	*Odorant-binding protein 44a (Obp44a)*	-3.498	0.00001057
FBgn0046225	*(CG17230)*	-3.348	0.00000525
FBgn0032481	*(CG16972)*	-3.242	0.00002367
FBgn0053189	*(CG33189)*	-3.226	0.00004521
FBgn0001226	*Heat shock protein 27 (Hsp27)*	-3.223	0.00000002
FBgn0035047	*Painting of fourth (Pof)*	-3.212	0.00000467
FBgn0039501	*Tubulin tyrosine ligase-like 6B (TTLL6B)*	-3.073	0.00000963
FBgn0053293	*(CG33293)*	-2.996	0.00003141
FBgn0036763	*Tryptophanyl-tRNA synthetase, mitochondrial (TrpRS-m)*	-2.982	0.00000113
FBgn0052686	*(CG32686)*	-2.967	0.00019743
FBgn0032117	*alpha1,3-fucosyltransferase B (FucTB)*	-2.919	0.00002238

Table 4.16: Gene ontology analysis on differentially expressed genes in abdominal tissue *post* irradiation. G:Profiler was used and 3,293 genes were included in the GO analysis. ID column refers to ontology pathway reference number and which database it was derived: GO: molecular function, biological process and cellular compartment, Kyoto ecyclopaedia of genes and genomes (KEGG), TRANSFAC (TF), and human phenotype ontology (HP).

ID	Description	Adjusted *p* value	No. of genes
GO:0005488	binding	0.0000000	669
GO:0005515	protein binding	0.0000001	385
GO:0043167	ion binding	0.0000798	290
GO:0036094	small molecule binding	0.0009251	149
GO:0030554	adenyl nucleotide binding	0.0010220	104
GO:0043168	anion binding	0.0012422	139
GO:0097159	organic cyclic compound binding	0.0013827	312
GO:0005524	ATP binding	0.0014373	101
GO:0017076	purine nucleotide binding	0.0019311	120
GO:0048518	positive regulation of biological process	0.0000000	238
GO:0009987	cellular process	0.0000000	801
GO:0048522	positive regulation of cellular process	0.0000000	219
GO:0065007	biological regulation	0.0000001	490
GO:0007010	cytoskeleton organization	0.0000001	105
GO:0016043	cellular component organization	0.0000002	337
GO:0050789	regulation of biological process	0.0000004	446
GO:0032502	developmental process	0.0000005	326
GO:0071840	cellular component organization or biogenesis	0.0000021	348
GO:0048856	anatomical structure development	0.0000034	306
GO:0110165	cellular anatomical entity	0.0000000	912
GO:0005622	intracellular anatomical structure	0.0000000	673
GO:0043226	organelle	0.0000007	585
GO:0043229	intracellular organelle	0.0000066	572
GO:0043227	membrane-bounded organelle	0.0000425	532
GO:0099081	supramolecular polymer	0.0000843	48
GO:0005737	cytoplasm	0.0001340	476
GO:0099512	supramolecular fiber	0.0003719	46
GO:0005856	cytoskeleton	0.0011009	84
GO:0043231	intracellular membrane-bounded organelle	0.0021965	503
KEGG:04711	Circadian rhythm - fly	0.0181225	6
WP:WP3660	Humoral immune response to fungal and bacterial pathogen	0.0168222	9
HP:0007067	Distal peripheral sensory neuropathy	0.0011221	8
HP:0001427	Mitochondrial inheritance	0.0158062	8
HP:0000763	Sensory neuropathy	0.0421108	18

4.6.2 Transcriptional signature of radiation treatment

DEGs in multiple *Drosophila* tissues *post* irradiation were compared to identify shared genes (**Table 4.17**). Nineteen genes were identified and were thought to represent a transcriptional signature of radiation treatment. Only two genes were downregulated in all tissues: *Cyp305a1* and *CG31538*. *Cyp305a1* has been shown to be involved in metabolism, chemical detoxification, and acts as a rate-limiting enzyme in the production of Ecdysone – a steroidal hormone which induces ecdysis (Niwa et al., 2011). There were seventeen upregulated genes and five have yet to be characterised. *PGRP-SB1* is one of the upregulated genes and encodes a peptidoglycan recognition protein that has enzymatic activity against the cell walls of Gram-negative bacteria (Zaidman-Rémy et al., 2011). *PGRP-SB1* upregulation in all tissues is a strong indication of a systemic immune response as either a direct or indirect response to irradiation.

Though this transcriptional signature of irradiation is a small list of genes, a number of molecular and biological processes were enriched (**Table 4.18**). Four out of the six terms identified were involved in the manipulation of DNA such as: telomeric DNA binding (GO:0042162), DNA geometric change (GO:0032392), DNA duplex unwinding (GO:0032508), and DNA conformation change (GO:0071103).

Table 4.17: Transcriptional signature of irradiation. Transcriptional signature – genes either downregulated or upregulated in all tissues. There were 2 significantly downregulated and 17 upregulated genes.

Downregulated		Upregulated	
Flybase ID	**Gene name (Symbol)**	**Flybase ID**	**Gene name (Symbol)**
FBgn0036910	*Cytochrome P450 305a1 (Cyp305a1)*	FBgn0005640	*Ecdysone-induced protein 63E (Eip63E)*
FBgn0051538	*(CG31538)*	FBgn0010173	*Replication Protein A 70 (RpA-70)*
		FBgn0011703	*Ribonucleoside diphosphate reductase large subunit (RnrL)*
		FBgn0011774	*Inverted repeat-binding protein (Irbp)*
		FBgn0031643	*(CG3008)*
		FBgn0032393	*Nfs1 cysteine desulfurase (Nfs1)*
		FBgn0033205	*(CG2064)*
		FBgn0034756	*Cytochrome P450 6d2 (Cyp6d2)*
		FBgn0035165	*(CG13887)*
		FBgn0036290	*(CG10638)*
		FBgn0036881	*Cuticular protein 76Bd (Cpr76Bd)*
		FBgn0038344	*obelus (obe)*
		FBgn0039411	*dysfusion (dysf)*
		FBgn0040972	*(CG16978)*
		FBgn0043578	*Peptidoglycan recognition protein SB1 (PGRP-SB1)*
		FBgn0062565	*Odorant receptor 19b (Or19b)*
		FBgn0267991	*long non-coding RNA:CR46258 (lncRNA:CR46258)*

Table 4.18: Gene ontology analysis on transcriptional signature of irradiation.
G:Profiler was used and 3,293 genes were included in the GO analysis. ID column refers to ontology pathway reference number and which database it was derived: GO: molecular function, biological process and cellular compartment, Kyoto ecyclopaedia of genes and genomes (KEGG) and WikiPathways (WP).

ID	Description	Adjusted *p* value
GO:0042162	telomeric DNA binding	0.01271727
GO:0008106	alcohol dehydrogenase (NADP+) activity	0.042968224
GO:0004033	aldo-keto reductase (NADP) activity	0.047985659
GO:0032392	DNA geometric change	0.028342082
GO:0032508	DNA duplex unwinding	0.028342082
GO:0071103	DNA conformation change	0.041179487

4.6.3 Transcriptional pattern of risk genes identified through literature search

A literature search presented in **Section 4.4** shows a list of genes that have previously been identified to be involved in the radiation response of *Drosophila*. Of the genes identified, none were DE in all tissues that were transcriptionally analysed (**Table 4.19**). 23 out of the 44 genes were not significantly DE in any of the tissues. Only *Ku80* was significantly DE within the midgut ($\log_2$ fold change = 0.827), and was found to have increased expression in the head ($\log_2$ fold change =1.732) and thorax tissue ($\log_2$ fold change = 1.721). *Ku80* is involved in non-homologous end joining pathway of DNA repair, and *Drosophila* studies have shown it is involved in the radiation response. Additionally, *Gadd45* which is involved in DNA damage sensing, and previous mutant analysis identifying it to be involved in *Drosophila* radiation response, has been shown to be significantly DE in three tissues: head ($\log_2$ fold change = 1.735), thorax tissue ($\log_2$ fold change = 1.32), and abdominal tissue ($\log_2$ fold change = 0.839) (L. Koval et al., 2020). This potentially highlights that risk loci may only harbour risk in a tissue-context dependent manner.

Table 4.19: Radiation-induced expression response of genes identified through literature search. Fold change (FC) is $\log_2$. Significant data is coloured, with positive fold change coloured green and negative in red.

Gene	Midgut FC ($\log_2$)	Midgut p value	Brain FC ($\log_2$)	Brain p value	Muscle FC ($\log_2$)	Muscle p value	Fat body FC ($\log_2$)	Fat body p value
DNAlig4	0.299	0.531	0.898	5.9E-07	0.841	0.01469	-0.097	0.84265
okr	0.193	0.96074	0.346	0.34819	0.155	0.85724	0.235	0.62896
Drs	-0.557	0.92004	2.104	1.4E-21	0.962	0.14991	-0.625	0.37724
DroA	0	-	0.782	-	1.168	0.77463	1.493	-
Dipt	-1.232	0.76752	3.986	9.9E-12	1.52	0.01995	0.632	0.84924
AttC	-1.198	0.87373	2.299	0.03477	1.553	0.0046	0.543	0.73193
CecC	0.664	0.96835	2.682	0.00067	1.558	0.29002	5.524	0.00858
Mtk	0.244	0.97951	2.479	0.00017	1.287	0.04445	1.557	0.20138
Sod1	-0.074	0.93663	-0.111	0.32312	-0.283	0.37569	0.295	0.25075
Gadd45	0.354	0.06752	1.735	4.3E-34	1.32	2E-07	0.839	0.00032
Xpc	0.435	0.08558	0.194	0.26035	0.284	0.19825	0.086	0.79673
spn-B	0.307	0.95047	0.366	0.59028	0.167	0.92841	-0.071	0.94142
Hsp70								
Cyp6g1	0.045	0.98003	-0.607	0.00319	-0.695	0.00194	0.177	0.50913
GstT4	-0.079	0.97622	-0.072	0.85807	-0.555	0.12763	0.043	0.95065
ss	0.922	0.80243	-0.229	0.6195	-0.189	0.86463	0.611	0.40469
mei-9	0.034	0.99201	0.261	0.41371	0.19	0.79023	0.378	0.43349
mei-41	0.097	0.97951	0.116	0.7716	-0.052	0.97202	-0.067	0.90638
mus302								
rad201								
NK7.1	-0.068	0.96876	0.03	0.90519	0.184	0.75378	-0.046	0.91739
lackluster								
pnr	-0.173	-	0.464	0.52881	0.337	0.78131	0.623	0.49627
CG14621	-0.019	0.99275	0.239	0.2047	0.529	0.02787	0.466661081	0.70323
Ddr	1.13	0.66957	-0.461	0.01235	-0.119	0.90373	1.42	0.00829
CG42324	0.172	0.92004	-0.339	0.01566	-0.091	0.91375	0.395	0.03594
msi	-0.074	0.98405	0.225	0.17843	0.247	0.6901	-0.085	0.88995
CG1824	-0.148	0.88043	0.041	0.84606	-0.132	0.87269	-0.096	0.59877
rpr	0.283	0.97951	0.288	0.68688	0.461	0.66848	-0.429	0.72137
hid	0.147	0.9615	0.47	0.05632	0.488	0.20198	0.295	0.32599
Cka	0.233	0.50049	-0.192	0.14135	0.074	0.91968	0.058	0.84545
GstD1	-0.013	0.99267	0.484	2.1E-07	0.187	0.49335	0.23	0.20286
Dcp-1	-0.027	0.99645	-0.057	0.90166	-0.443	0.56284	-0.136	0.89103
hus1-like	0.011	0.99723	0.965	0.04199	0.518	0.50417	0.011	0.98823
lok (mnk)	0.004	0.99872	-0.053	0.91114	-0.03	0.97224	-0.22	0.49111
PCNA (Mus209)	0.614	0.68362	2.969	6.1E-25	1.499	0.00035	-1.94	9.8E-06
Rrp1	0.701	0.05225	0.232	0.43762	0.538	0.50417	-0.371	0.52504
Brca2	0.131	0.94238	0.161	0.54113	0.039	0.95456	0.094	0.81236
Ku80	0.827	7.1E-06	1.732	1.1E-43	1.721	6.6E-14	0.507	0.18593
WRNexo	0.67	0.92006	1.719	0.13783	0.55	0.8394	-2.436	0.02489
Blm (Mus309)	-0.101	0.97951	0.038	0.93684	0.13	0.8828	-1.53	0.05539
e2f1	-0.005	0.99645	-0.045	0.79195	0.322	0.53901	0.003	0.9939
p53	0.1	0.93928	0.19	0.45478	0.312	0.57961	-0.274	0.33284
grp	0.138	0.90177	-0.093	0.69051	-0.004	0.99682	-0.35	0.34757

4.6.4 Transcriptional pattern of functionally tested genes

The transcription pattern of five selected loci from **Section 4.5** was checked. Two genes were DE, and only in the head (**Table 4.20**). *XRCC1* and *Jafrac1* were significantly upregulated at 0.585 and 0.374 FC (log$_2$), respectively.

Table 4.20: Radiation-induced expression pattern of candidates that were previously functionally tested.

Tissue	Gene	Fold Change (log$_2$)	Adjusted *p* value
Midgut	Duox	0.275	0.946681883
	XRCC1	0.097	0.954989246
	Jafrac1	0.058	0.979512539
	SOD1	-0.074	0.936625882
	Catalase	0.089	0.96631008
Brain	Duox	-0.27	0.469158
	XRCC1	0.585	0.000284
	Jafrac1	0.374	0.001006
	SOD1	-0.111	0.323122
	Catalase	0.002	0.990659
Muscle	Duox	0.102	0.8598
	XRCC1	0.401	0.053162159
	Jafrac1	0.276	0.219996591
	SOD1	-0.283	0.375687184
	Catalase	-0.19	0.62935
Fat body	Duox	0.792	0.114094
	XRCC1	-0.276	0.243644
	Jafrac1	0.169	0.258257
	SOD1	0.295	0.250753
	Catalase	0.254	0.361682

4.7 Discussion

4.7.1 Genome-wide association study

Using *Drosophila* to perform a GWAS offers the advantage of readily available genetic tools such as highly inbred and isogenic strains and an already sequenced panel of WT strains which reflects the natural variation within a population (DGRP) (MacKay *et al.*, 2012; Vaisnav *et al.*, 2014). For a GWAS to be successful a trait must be quantifiable in order to significantly associate phenotype with genotype. To that end, preliminary experiments were performed on a small subset of the DGRP quantifying short-term midgut toxicity and long-term lifespan survival (**Section 4.3**). Preliminary experiments were successful, and strains demonstrated dynamic phenotypic responses (**Figure 4.1** & **4.2**). However, little correlation between short- and long-term phenotypes was observed (**Figure 4.3**). As lifespan survival analysis is a relatively long experiment, it was hoped that short-term survival could be used as a proxy phenotype to measure overall health.

Differences in short- and long-term phenotypic responses within strains may be an indication that *Drosophila* exhibit distinct temporal responses to irradiation, similar to humans (Allan & Travis, 2005; Bentzen, 2006). In humans, two distinct phases of the radiation response have been observed, immediate (radiation sickness) and long-term, with distinct genetic architecture underpinning the responses.

It was decided that, due to time constraints, the remaining ~190 strains of the DGRP would not be phenotyped. Instead, other methods to identify genes involved in the radiation response were explored, including literature search, candidate approach and transcriptome (RNA-seq) analysis.

4.7.2 Literature search for risk loci

Literature search successfully identified 51 loci that are involved in the radiation response of *Drosophila*. Many of these loci (*DNAlig4*, *okr*, *Gadd45*, *Xpc*, *mei-9*, *mei-41*, *mus302*, *mus209*, *BRCA2*, *Blm*, *p53*) were identified through candidate-based and hypothesis-driven approaches, and therefore, the majority are involved in various DNA repair pathways (**Table 4.3**). However, a number of genes involved in both immunity and oxidative stress have also been identified – suggesting a more complicated and sustained response to irradiation within *Drosophila*. Reviewing of the radiation research highlighted a number of inconsistencies within the field. Inconsistencies include:

Dose – total dose and dose rate vary considerably between studies (**Figure 4.6**). Published transcriptional datasets have shown that total dose is a significant factor that influences the transcriptome of *Drosophila* (Shrestha et al., 2017).

Model – genes were identified using either larvae or adults of various ages. In general, tissues with a higher proliferative rate tend to be more sensitive to irradiation. For humans, radiation-sensitive tissues include: bone marrow, intestinal tract and skin (reviewed in Bentzen, 2006). Whereas, in *Drosophila* the larvae stages where the highly proliferative imaginal tissues are actively and profusely dividing are extremely sensitive to radiation (Paithankar *et al*., 2017). Due to the variation in sensitivity to radiation that is dependent on life-stage, it is reasonable to assume that risk loci such as *mei-9* and *Gadd45* that are involved in DNA repair may play a more crucial role in modulating radiation response in larvae than in adult life-stages.

Temporal-specificity – there was little standardisation in the age of *Drosophila* that were assayed for functional experiments in literature. My characterisation work of the radiation response has shown that radiation-induced midgut toxicity increases long-term (**Chapter 3**). It has also been shown that the radiation-induced transcriptome of *Drosophila* dynamically alters over time and alterations persist long-term (Shrestha et al., 2017). Also, age at which adults are irradiated is a significant prognostic factor, the older the adult at the time of irradiation, the more sensitive they are to treatment (Parashar, Frankel, Lurie, & Rogina, 2008).

These issues make it difficult to interpret results across studies and future work should aim to screen and validate these genes in a systematic and standardised manner, and specifically within adult *Drosophila*.

4.7.3 Functional validation of candidate genes

Prior to performing functional validation of candidate genes using the *Gal4/UAS* expression system, it was decided to 'homogenise' the genetic background of driver lines to that of a WT genetic background (*w^1118^*). Though it is not clear how much of the driver chromosomes have been substituted, through recombination, to that of the *w^1118^* background, it was assumed that 16 generations of backcrossing were sufficient to homogenise the majority of the driver chromosome. Genotyping of the recombined drivers and comparing against the genotypes of the parental stocks

(both driver line and w^{1118}) would yield a definitive answer to the level of homogenisation, however that approach was decided to be unnecessary and expensive. Instead, when examining the phenotypic responses of non-irradiated cohorts, in majority of experiments genotype did not appear to be a significant modulator of survival (**Section 4.5**).

From the five gene studied, none were successfully identified to modulate the radiation response of *Drosophila*. *Duox* was assayed prior to dose optimisation work and subsequent experiments have shown that a total dose of 50 Gy is not sufficient to significantly reduce survival (**Section 3.3.1**). *Duox* has been shown to be involved in redox homeostasis, and radiation-induced oxidative stress has been implicated to be the underlying cause of long-term side effects in humans. The hypothesis was that *Duox* mutants would be radio-sensitive due to impaired redox homeostasis but because radiation dose was not sufficient to induce significant lifespan changes, it is unclear whether lack in change of survival is a false negative result. This experiment could be repeated but with a higher total dose (> 150 Gy) to successfully validate *Duox*.

XRCC1 was tested by using a RNAi line to knockdown expression, however the efficiency of knockdown was not validated. Only when *XRCC1* was knocked-down in enterocytes was genotype a significant variable: *XRCC1* knockdown slightly increased lifespan in non-irradiated cohort. Considering the importance of DNA repair, it was anticipated that impair of a crucial DNA repair pathway would reduce as opposed to increase survival (Caldecott, 2003). This result may indicate that the efficiency of *XRCC1* knockdown was low, and that qPCR testing of transcript levels would be the next course of action. Also, good practice when knockdown genes is to use multiple RNAi lines.

4.7.4   Radiation-induced transcriptome

The transcriptome long-term *post* radiation treatment was successfully quantified for thorax tissue, head, midgut and abdominal tissue (**Section 4.6**). For all tissues more genes were downregulated than upregulated after treatment (**Figure 4.16**). It was later observed that all control samples were contaminated with disintegrated testes and thus a large proportion of downregulated DEGs were testes-specific genes. Manual filtering based on transcript numbers in each sample successfully removed teste-specific genes from gene lists (**Figure 4.17**).

19 genes that shared expression patterns in all tissues were thought to be a transcriptional signature of radiation treatment (**Table 4.17**). 6 out of the 19 genes have not been fully characterised making them potentially interesting hits for characterisation and further functional analysis. GO analysis identified a small number of biological processes that were enriched which were involved with DNA unwinding and conformational changes (**Table 4.18**).

It is encouraging that a number of immune genes (*CecC, AttC, Mtk, Drs* and *DroA*) that were previously identified in the literature to be involved in the *Drosophila* radiation response were DE in the transcriptomics dataset (**Table 4.19**). In addition, the transcriptional signature of irradiation gene list included *PGRP-SB1* which encodes a peptide with antimicrobial activity (Zaidman-Rémy et al., 2011). Typically in humans radiation induces a degree of inflammation which is partially due to the localised accumulation of immune cells and their over stimulation (Kaur & Asea, 2012). Though *Drosophila* cannot generate a canonical inflammatory response (swelling at site of insult) due to their open circulatory systems, the transcriptional datasets generated here further support the growing *Drosophila* literature of sustained immune activity *post* irradiation – and thus *Drosophila* may be well suited to study the immune aspect of human radiobiology.

4.7.5   General conclusions

This chapter aimed to identify genes associated with the radiation response of *Drosophila*. This was attempted in a number of ways including an aborted GWAS using the DGRP, a literature search to compile a list of previously functionally identified genes, a number of candidate genes were functionally tested to ascertain their role in modulating survival, and lastly an RNA-seq experiment was performed to identify genes.

The candidate work was unsuccessful in identifying genes involved in the radiation response. Quantification of tissue specific transcriptome long-term successfully generated a number of significantly DE genes. An intersect of genes that are co-differentially expressed in all irradiated tissues showed a potential transcriptional signature of irradiation. Future work should focus on this potential signature of irradiation, through validation and functional studies.

Chapter 5: Discussion

5.1 Introduction

This thesis demonstrates a number of novel findings. A long-term *Drosophila* model of radiation-induced tissue toxicity was developed. This model was used to identify genes involved in the radiation response in *Drosophila* via various approaches such as literature search and tissue specific transcriptomic analysis. Gene lists were compiled showing tissue specific responses to treatment. Finally, five candidate genes were functionally assessed in the context of the midgut, exploring their role in modulating overall treatment survival.

5.2 Long-term model for radiation damage

Newly developed model definitively showed that adult *Drosophila* exhibit genotype dependent resistance to irradiation as measured by various health metrics: lifespan, fertility and body weight reductions, despite historically being described as radioresistant (**Section 3.3**). It was also shown that *Drosophila* have a chronic response to treatment but no correlation between tissue damage and oxidative stress was observed. This is despite the fact that tissues such as the midgut exhibit sustained oxidative stress (**Section 3.4**). Additionally, subjecting *Drosophila* to radiation regimes similar to RT regimes experienced by patients showed a conserved response to treatment in which fractionation of total dose led to improved survival (**Section 3.6**). Despite successes, this *Drosophila* model has a number of issues which will be discussed.

Radiation-derived reactive oxygen species

The first issue with the model was that oxidative stress was not extensively studied. Imbalances in ROS production or quenching can lead to oxidative stress and RT has been shown to induce the generation of excess ROS in humans, however ROS levels *post* irradiation were not quantified during this PhD (Azzam *et al.*, 2012; Wei *et al.*, 2019). There are multiple ROS species such as superoxide radicals (O_2^-), H_2O_2 and hydroxyl radicals (OH) and when perturbed each has unique detrimental biological consequences. Multiple reagents and *Drosophila* tools are available to quantify their levels, however due to time constraints and the difficultly of measuring molecular species with nanosecond half-lifes, the levels of ROS *post* irradiation were not studied (Albrecht *et al.*, 2011; Wang *et al.*, 2013; Li, Young & Sun, 2018).

Oxidative stress as the aetiological cause of chronic radiation toxicity

Within the midgut, oxidative stress did not correlate with DNA DSB which was a proxy measure of DNA damage and tissue toxicity. Firstly, like the quantification of oxidative stress, testing for DNA damage was limited. Ionizing radiation directly induces various structural changes to DNA, primarily DSBs, but also the less frequent single strand breaks (SSB), or indirectly through oxidisation of DNA mediated by radiation-induced ROS (Borrego-Soto, Ortiz-López & Rojas-Martínez, 2015). The characterisation of the various types of DNA damage *post* irradiation may help in better understanding the consequences of persistent radiation-induced oxidative stress within the midgut. For example, the levels of oxidised base modification 8-oxoguanine (8-oxo-G) may have a significant correlation with oxidative stress and specific antibodies are commercially available, and have been successfully used in *Drosophila* (Gonzalez-Hunt, Wadhwa & Sanders, 2018; Weavers, Wood & Martin, 2019).

Midgut is radiosensitive but may not modulates radiation survival

It has been shown that radiation induces oxidative stress within the midgut, and that the levels of oxidative stress are higher than in other adult tissues (**Section 3.4.2**). Measuring midgut functionality through quantification of frass showed reduced output *post* treatment (**Section 3.3.7**). Further, there appears to be tissue remodelling long-term, with less nuclei and greater distance between them *post* treatment (**Section 3.5.2**). Characterisation of the radiation transcriptome of various tissues further confirmed that the midgut was responding long-term (**Section 4.6**). However, as discussed, the majority of DE genes were downregulated: an indication of a general decline of transcription possibly due to loss of genome integrity. Also, the testing of several candidate genes which involved midgut-specific genetic manipulations did not yield improved survival outcome *post* treatment (**Section 4.5**). Therefore, there is little evidence that the midgut is an important tissue in modulating radiation survival. Though it is clearly sensitive to treatment, that sensitivity has yet to be linked to overall health in the context of irradiation. The next section will describe future experimental approaches that can help to further explore the role, if any, of the midgut in modulating the radiation response (**Figure 5.1**).

5.3 Identifying genes involved in the radiation response

A number of approaches were employed to identify candidate risk loci, with relative success rates attached to each approach. The literature search was successful in

identifying over 50 genetic loci that were already functionally linked to the radiation response (**Section 4.4**). Additionally, the radiation-induced transcriptome was quantified for multiple tissues, with 100s of promising hits identified (**Section 4.6**). Nevertheless, each approach at identifying genes involved in the radiation response presented in this thesis encountered a number of issues.

5.3.1 Issues

GWAS – lack of correlation between phenotypes

Using the DGRP to perform a GWAS on the radiation response has been attempted twice previously (**Section 1.6.2**). The first study did not identify any significant SNPs and this has been attributed to poorly defined phenotype endpoint which was the ability to fly 24 hr *post* irradiation (Vaisnav et al., 2014). The second attempt identified five loci but again this small number of significant hits, none of which were involved in DNA repair, is an indication that the study was not very successful (Sharma et al., 2020). A number of DNA repair genes have already been functionally validated to be involved in the radiation response, and therefore were expected to be identified in either GWAS (**Section 4.4**).

It was decided that a GWAS using the DGRP had the potential to elucidate the genetic architecture of the radiation response, but the experimental design needed to be modified. To that end, a lower dose of 150 Gy was used as this has been shown to have a significant effect on survival (**Section 3.3.1**), and a more appropriate phenotype was assayed which was of overall lifespan survival: the ultimate measure of overall health. Lastly, Vaisnav *et al.*, (2014) concluded that the lack of any positive hits was due to the small size of the panel at the time (154 members), and it was calculated that >700 DGRP lines would be required to identify SNPs involved in the radiation response (Vaisnav et al., 2014). I was planning to assay 205 sequenced strains and use a more sensitive assay of the DGRP to overcome the underpower issue of the first study.

Preliminary experiments on a small subset of the DGRP determined little correlation between the level of DSB within the midgut and overall survival *post* treatment (**Section 4.3**). Therefore, work was discontinued as it was estimated it would take too long, be too expensive and preliminary work was not encouraging. Though work was discontinued, the approach of measuring survival overcame the issues of the previous studies such as inappropriate assay. However, lifespan survival analysis can be longwinded and this is probably why the original GWAS studies never attempted it (Vaisnav et al., 2014).

Literature search – lack of standardisation between studies

Literature search though successful in identifying a number of genes, pointed at risk loci that had been identified from hypothesis driven research, and therefore largely contained genes involved in DNA repair. However, there was little consistency in the models and methods of irradiation. For example, both dose and radiation type varied greatly between studies (**Section 4.4**). This is important considering the re-analysis of published transcriptional datasets, which determined that dose was a significant variable that influenced the *post* irradiation transcriptome of *Drosophila* (Shrestha et al., 2017). Therefore, the genes significantly identified may not be functionally relevant to the organism at the same dosage. In order for the future use of *Drosophila* as a model for radiation toxicity there must be standardisation, such as a proposed dose range of 100 – 200 Gy and relatively similar dose rates such as ~0.5 Gy/min.

Candidate approach – no genes were positively identified

A number of genes were functionally assayed to determine their involvement in the radiation response (**Section 4.5**). This approach was unsuccessful as no gene was found to modulate health *post* irradiation when genetically manipulated within the midgut. Reviewing of this approach has led to the realisation that there were two distinct issues:

1. It has been shown that the midgut is sensitive to irradiation (**Section 3.3.7**); however, it is unknown whether this sensitivity directly correlates to reduction in overall health.
2. It has also been shown that tissues have unique transcriptomes *post* treatment. These unique transcriptomes are an indication of tissue specific response to treatment. Negative results from functional testing of candidates may simply indicate that those particular loci are not involved in the midgut response to irradiation.

5.3.2   Future approach to validate candidate genes

A number of genes have been identified to be potentially involved in the radiation response and they now need to be validated whilst addressing the issues mentioned above. Issues included that the functional tests assumed that the midgut was essential for *post* irradiation survival; this assumption makes a definitive interpretation of negative results difficult. I propose expansion of functional testing beyond just genetic manipulation of the midgut, but to include other tissues, such as

those that have had their radiation-induced transcriptomes characterised. The transcriptomic datasets show that all tissues characterised had dynamic and largely unique radiation-induced transcriptomic signatures.

Genes should be validated in the context of tissue specific risk, and this approach can be built upon previous candidate work (**Section 4.5**). Firstly, tissue-specific driver lines can be acquired and backcrossed into a reference background, similar to *Myosin1A-Gal4* and *Esg-Gal4* backcrossing (**Section 4.5.1**). Driver lines could include: *tubulin-Gal4* as a ubiquitous driver, *FatBody-Gal4* for fat body, *Mef2-Gal4* for muscle, *Myosin1A-Gal4* for midgut, and lastly *elav-Gal4* as a pan-neuronal driver (Shchedrina et al., 2009; Xu et al., 2019). Multi-armed lifespan survival experiments can be performed in which a gene of interest is manipulated within the whole fly and in each individual tissue, allowing for identification of potential risk associated with treatment and tissue-specific manipulation. It may not be the case that tissue specific genetic manipulation will lead to a discernible change in lifespan *post* treatment; therefore it is proposed to perform tissue specific assays to measure tissue functioning (**Figure 5.1**). Midgut specific assays have already been optimised such as the frass quantification assay (**Section 2.2.4**), and movement assaying which could be used to measure muscle and head functionality (**Section 3.3.4**). Functionality of the fat body is not so easily assayed due to its diverse array of functions, however, considering that the radiation induced transcriptome of multiple tissues indicated the modulation of biological processes involved in metabolism, it is proposed to measure a phenotype linked to metabolism such as fat utilisation (**Section 4.6.1**). The fat body cells contain the largest store of triglycerides within *Drosophila* and these fatty acids can be mobilised and diffused into the haemolymph under stress such as in infection or under starvation (Arrese & Soulages, 2004). Oil Red O is a dye that binds directly to lipids and could be used to stain the fat body and haemolymph to determine the ratiometric difference of fat levels between the tissues *post* irradiation (Baumbach, Xu, Hehlert, & Kühnlein, 2014).

The above approach of validating RNA-seq hits can also be used to further functionally validate the genes identified from the literature search (**Section 4.4**). Those genes need further functional validation to address issues previously discussed, such as inconsistent experimental conditions and model (larvae vs. adults). Additionally, it is unknown whether those genes convey tissue-specific risk and employing the above discussed functional testing would screen genes for their tissue-specific risk.
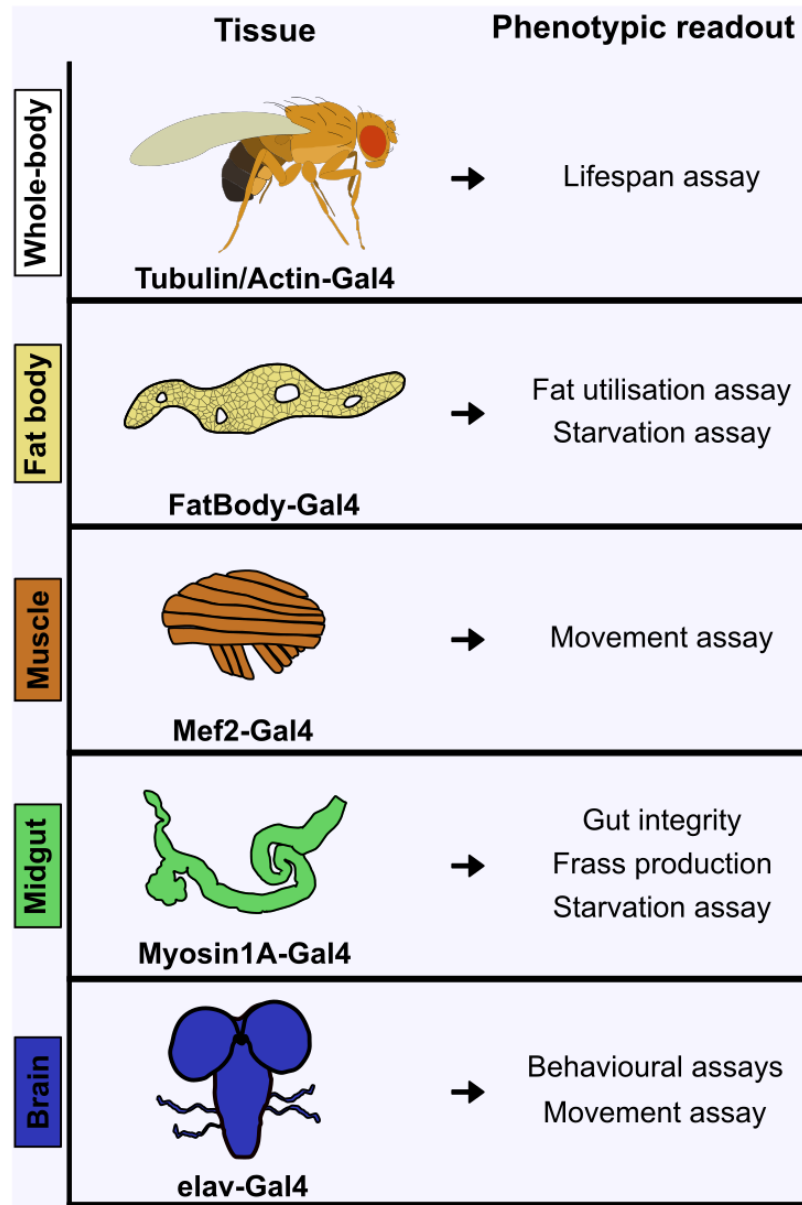
Figure 5.1: Potential strategy for validating potential risk loci. The role of candidate genes could be explored through the use of tissue specific Gal4 lines that have been backcrossed into a reference genetic background.

5.4   Overall conclusions

Here I present a model for radiation-induced long-term tissue toxicity; the model has shown that *Drosophila* respond to radiation in a similar manner to humans. *Drosophila* have a dynamic and temporal response to irradiation where we see entire tissues undergoing sustained damage and remodelling, and reduced functionality. Despite surviving weeks after initial insult, we see long-term effects of treatment that persist and, in some instances, exacerbate with time. With the modifications to the experimental design discussed in this chapter, genes identified in this thesis can be validated and further potential genetic interactions can be studied to elucidate the mechanisms underlying the radiation response within *Drosophila*. This work has highlighted that genetic loci may convey tissue-specific risk to irradiation, and this has direct bearing on human studies. Radiogenomicists want to develop an all-encompassing SNP-based genomic test for radiation sensitivity, perhaps the reason why they have yet to develop this test is because tissue specificity has yet to be fully accounted for during studies.

References

Ahmad, S., Schwarz, M., Flick, R. J., Rees, C. A., Harawa, M., Simon, K., Robson, J. A., Kazembe, P. N. (2016). The survival package Introduction. *Tropical Medicine & International Health*, *21*(4), 170–485. Retrieved from https://www.ncbi.nlm.nih.gov/pmc/articles/PMC/1881304/

Albrecht., S. C., Barata, A. G., Großhans, J., Teleman, A. A., & Dick, T. P. (2011). In vivo mapping of hydrogen peroxide and oxidized glutathione reveals chemical and regional specificity of redox homeostasis. *Cell Metabolism*, *14*(6), 819–829. https://doi.org/10.1016/j.cmet.2011.10.010

Ali, S., Shaikh, F., Abbas, K., Iftikhar, A., & Shaikh, B. (2017). Silymarin ameliorates radiation sickness and weight loss: An experimental study on rodents. *Journal of the Liaquat University of Medical and Health Sciences*, *16*(4), 222–227. https://doi.org/10.22442/jlumhs.171640538

Alsner, J., Andreassen, C. N., & Overgaard, J. (2008). Genetic Markers for Prediction of Normal Tissue Toxicity After Radiotherapy. *Seminars in Radiation Oncology*, *18*(2), 126–135. https://doi.org/10.1016/j.semradonc.2007.10.004

Ambrosone, C. B., Tian, C., Ahn, J., Kropp, S., Helmbold, I., von Fournier, D., … Chang-Claude, J. (2006). Genetic predictors of acute toxicities related to radiation therapy following lumpectomy for breast cancer: A case-series study. *Breast Cancer Research*, *8*(4), 1–7. https://doi.org/10.1186/bcr1526

Andreassen, C. N. (2005). Can risk of radiotherapy-induced normal tissue complications be predicted from genetic profiles? *Acta Oncologica*, *44*(8), 801–815. https://doi.org/10.1080/02841860500374513

Apidianakis, Y., & Rahme, L. G. (2011). Drosophila melanogaster as a model for human intestinal infection and pathology. *DMM Disease Models and Mechanisms*, *4*(1), 21–30. https://doi.org/10.1242/dmm.003970

Arnold, M., Rutherford, M., Lam, F., Bray, F., Ervik, M., & Soerjomataram, I. (2019). CBP SURVMARK-2 online tool: International Cancer Survival Benchmarking. Lyon, France: International Agency for Research on Cancer. Retrieved September 21, 2021, from http://gco.iarc.fr/survival/survmark

Arrese, E. L. &, & Soulages, J. L. (2004). INSECT FAT BODY: ENERGY, METABOLISM, AND REGULATION. *Environmental Stress and Cellular Response in Arthropods*, (87), 19–58. https://doi.org/10.1201/9781420023336.ch3

Ash, P. (2014). The influence of radiation on fertility in man. *The British Institute of*

Radiology, *53*(628).

Azzam, E. I., Jay-Gerin, J. P., & Pain, D. (2012). Ionizing radiation-induced metabolic oxidative stress and prolonged cell injury. *Cancer Letters*, *327*(1–2), 48–60. https://doi.org/10.1016/j.canlet.2011.12.012

BANGHAM, J. (2019). Living collections: care and curation at Drosophila stock centres. *BJHS Themes*, *4*(September 2019), 123–147. https://doi.org/10.1017/bjt.2019.14

Barnett, G. C., West, C. M. L., Dunning, A. M., Elliott, R. M., Coles, C. E., Pharoah, P. D. P., & Burnet, N. G. (2009). Normal tissue reactions to radiotherapy: Towards tailoring treatment dose by genotype. *Nature Reviews Cancer*, *9*(2), 134–142. https://doi.org/10.1038/nrc2587

Baumbach, J., Xu, Y., Hehlert, P., & Kühnlein, R. P. (2014). Gαq, Gγ1 and Plc21C control drosophila body fat storage. *Journal of Genetics and Genomics*, *41*(5), 283–292. https://doi.org/10.1016/j.jgg.2014.03.005

Bence, M., Jankovics, F., Lukácsovich, T., & Erdélyi, M. (2017). Combining the auxin-inducible degradation system with CRISPR/Cas9-based genome editing for the conditional depletion of endogenous Drosophila melanogaster proteins. *FEBS Journal*, *284*(7), 1056–1069. https://doi.org/10.1111/febs.14042

Bentzen, S. M. (2006a). Preventing or reducing late side effects of radiation therapy : radiobiology meets molecular pathology, *6*(September), 702–713. https://doi.org/10.1038/nrc1950

Bentzen, S. M. (2006b). Preventing or reducing late side effects of radiation therapy: Radiobiology meets molecular pathology. *Nature Reviews Cancer*, *6*(9), 702–713. https://doi.org/10.1038/nrc1950

Bergom, C., West, C. M., Higginson, D. S., Abazeed, M. E., Arun, B., Bentzen, S. M., … Woodward, W. A. (2019). The Implications of Genetic Testing on Radiation Therapy Decisions: A Guide for Radiation Oncologists. *International Journal of Radiation Oncology Biology Physics*, *105*(4), 698–712. https://doi.org/10.1016/j.ijrobp.2019.07.026

Biteau, B., Karpac, J., Supoyo, S., DeGennaro, M., Lehmann, R., & Jasper, H. (2010). Lifespan extension by preserving proliferative homeostasis in Drosophila. *PLoS Genetics*, *6*(10), 1–15. https://doi.org/10.1371/journal.pgen.1001159

Borrego-Soto, G., Ortiz-López, R., & Rojas-Martínez, A. (2015). Ionizing radiation-induced DNA injury and damage detection in patients with breast cancer. *Genetics and Molecular Biology*, *38*(4), 420–432.

https://doi.org/10.1590/S1415-475738420150019

Bradburn, M. J., Clark, T. G., Love, S. B., & Altman, D. G. (2003). Survival Analysis Part III: Multivariate data analysis - Choosing a model and assessing its adequacy and fit. *British Journal of Cancer*, *89*(4), 605–611. https://doi.org/10.1038/sj.bjc.6601120

Buchanan, M. (2017). Colonizing mars. *Nature Physics*, *13*(11), 1035. https://doi.org/10.1038/nphys4311

Bushberg, J. T. (2020). Radiation Exposure and Contamination. Retrieved September 23, 2021, from https://www.msdmanuals.com/en-gb/professional/injuries-poisoning/radiation-exposure-and-contamination/radiation-exposure-and-contamination

Caldecott, K. W. (2003). XRCC1 and DNA strand break repair. *DNA Repair*, *2*(9), 955–969. https://doi.org/10.1016/S1568-7864(03)00118-6

Capps, G. W., Fulcher, A. S., Szucs, R. A., & Turner, M. A. (1997). Imaging Features of Radiation-induced Changes in the Abdomen. *Radiographics*, *17*(6), 1455–1473. https://doi.org/10.1148/radiographics.17.6.9397458

Catapult, B. A. and the M. D. (2018). State of the Discovery Nation 2018 and the role of the Medicines Discovery Catapult, (January), 1–36.

Chancellor, J. C., Blue, R. S., Cengel, K. A., Auñón-Chancellor, S. M., Rubins, K. H., Katzgraber, H. G., & Kennedy, A. R. (2018). Limitations in predicting the space radiation health risk for exploration astronauts. *Npj Microgravity*, *4*(1), 1–11. https://doi.org/10.1038/s41526-018-0043-2

Clark, R. I., Salazar, A., Yamada, R., Fitz-Gibbon, S., Morselli, M., Alcaraz, J., … Walker, D. W. (2015). Distinct Shifts in Microbiota Composition during Drosophila Aging Impair Intestinal Function and Drive Mortality. *Cell Reports*, *12*(10), 1656–1667. https://doi.org/10.1016/j.celrep.2015.08.004

Clark, T. G., Bradburn, M. J., Love, S. B., & Altman, D. G. (2003). Survival Analysis Part I: Basic concepts and first analyses. *British Journal of Cancer*, *89*(2), 232–238. https://doi.org/10.1038/sj.bjc.6601118

Clemmons, A. W., Lindsay, S. A., & Wasserman, S. A. (2015). An Effector Peptide Family Required for Drosophila Toll-Mediated Immunity. *PLoS Pathogens*, *11*(4), 1–17. https://doi.org/10.1371/journal.ppat.1004876

Cognigni, P., Bailey, A. P., & Miguel-Aliaga, I. (2011). Enteric neurons and systemic signals couple nutritional and reproductive status with intestinal homeostasis.

Cell Metabolism, *13*(1), 92–104. https://doi.org/10.1016/j.cmet.2010.12.010

Colinet, H., & Renault, D. (2012). Metabolic effects of CO2 anaesthesia in Drosophila melanogaster. *Biology Letters*, *8*(6), 1050–1054. https://doi.org/10.1098/rsbl.2012.0601

Cologne, J. B., & Preston, D. L. (2000). Longevity of atomic-bomb survivors, *356*, 303–307.

DeGennaro, M., Hurd, T. R., Siekhaus, D. E., Biteau, B., Jasper, H., & Lehmann, R. (2011). Peroxiredoxin Stabilization of DE-Cadherin Promotes Primordial Germ Cell Adhesion. *Developmental Cell*, *20*(2), 233–243. https://doi.org/10.1016/j.devcel.2010.12.007

Delaney, G., Jacob, S., Featherstone, C., & Barton, M. (2005). The role of radiotherapy in cancer treatment: Estimating optimal utilization from a review of evidence-based clinical guidelines. *Cancer*, *104*(6), 1129–1137. https://doi.org/10.1002/cncr.21324

Deshmukh, P., Unni, S., Krishnappa, G., & Padmanabhan, B. (2017). The Keap1–Nrf2 pathway: promising therapeutic target to counteract ROS-mediated damage in cancers and neurodegenerative diseases. *Biophysical Reviews*, *9*(1), 41–56. https://doi.org/10.1007/s12551-016-0244-4

Donya, M., Radford, M., ElGuindy, A., Firmin, D., & Yacoub, M. H. (2014). Radiation in medicine: Origins, risks and aspirations. *Global Cardiology Science and Practice*, *2014*(4), 57. https://doi.org/10.5339/gcsp.2014.57

Dutta, D., Dobson, A. J., Houtz, P. L., Gläßer, C., Revah, J., Korzelius, J., … Buchon, N. (2015). Regional Cell-Specific Transcriptome Mapping Reveals Regulatory Complexity in the Adult Drosophila Midgut. *Cell Reports*, *12*(2), 346–358. https://doi.org/10.1016/j.celrep.2015.06.009

Dutta, D., Xiang, J., & Edgar, B. A. (2013). RNA expression profiling from UNIT 2F.2 FACS-Isolated cells of the drosophila intestine. *Current Protocols in Stem Cell Biology*, *1*(SUPPL.27), 1–12. https://doi.org/10.1002/9780470151808.sc02f02s27

Ezeriņa, D., Takano, Y., Hanaoka, K., Urano, Y., & Dick, T. P. (2018). N-Acetyl Cysteine Functions as a Fast-Acting Antioxidant by Triggering Intracellular H 2 S and Sulfane Sulfur Production. *Cell Chemical Biology*, *25*(4), 447-459.e4. https://doi.org/10.1016/j.chembiol.2018.01.011

Ferlay, J., Colombet, M., Soerjomataram, I., Dyba, T., Randi, G., Bettio, M., … Bray, F. (2018). Cancer incidence and mortality patterns in Europe: Estimates for 40 countries and 25 major cancers in 2018. *European Journal of Cancer*, *103*,

356–387. https://doi.org/10.1016/j.ejca.2018.07.005

Ferlay, J., Steliarova-Foucher, E., Lortet-Tieulent, J., Rosso, S., Coebergh, J. W. W., Comber, H., … Bray, F. (2013). Cancer incidence and mortality patterns in Europe: Estimates for 40 countries in 2012. *European Journal of Cancer*, *49*(6), 1374–1403. https://doi.org/10.1016/j.ejca.2012.12.027

Ferlay, J., Ervik, M., Lam, F., Colombet, M., Mery, L., Piñeros, M., ... & Bray, F. (2018). Global cancer observatory: cancer today. Lyon, France: international agency for research on cancer, 3(20), 2019.

Flatt, T. (2011). Survival costs of reproduction in Drosophila. *Experimental Gerontology*, *46*(5), 369–375. https://doi.org/10.1016/j.exger.2010.10.008

Fowler, J. F. (2001). Biological factors influencing optimum fractionation in radiation therapy. *Acta Oncologica*, *40*(6), 712–717. https://doi.org/10.1080/02841860152619124

Fritz-niggli, H. &, & Schaeppi-Buechi, C. (1991). Adaptive Response to Dominant Lethality of Mature (Class A) and Immature (Class B) Oocytes of D. Melanogaster to Low Doses of Ionizing Radiation: Effects in Repair-proficient (yw) and Repair-deficient Strains (Mei 41D5 and Mus 302D1). *International Journal of Radiation Biology*.

Frosina, G. (2021). Improving control of high-grade glioma by ultra-hyper-fractionated radiotherapy. Journal of Neuroscience Research.

Fukunaga, A., & Kondo, S. (1985). Evidence for cell-replacement repair of X-ray-induced teratogenic damage in male genital imaginal discs of Drosophila melanogaster. *Mutation Research - Fundamental and Molecular Mechanisms of Mutagenesis*, *151*(2), 243–250. https://doi.org/10.1016/0027-5107(85)90076-4

Galenza, A., Hutchinson, J., Campbell, S. D., Hazes, B., & Foley, E. (2016). Glucose modulates Drosophila longevity and immunity independent of the microbiota. *Biology Open*, *5*(2), 165–173. https://doi.org/10.1242/bio.015016

Gao, R., Price, D. K., Dahut, W. L., Reed, E., & Figg, W. D. (2010). Genetic polymorphisms in XRCC1 associated with radiation therapy in prostate cancer. *Cancer Biology and Therapy*, *10*(1), 13–18. https://doi.org/10.4161/cbt.10.1.12172

Gonzalez-Hunt, C. P., Wadhwa, M., & Sanders, L. H. (2018). DNA damage by oxidative stress: Measurement strategies for two genomes. *Current Opinion in Toxicology*, *7*, 87–94. https://doi.org/10.1016/j.cotox.2017.11.001

Gorski, M. M., Eeken, J. C. J., Jong, A. W. M. De, Klink, I., Loos, M., Ron, J., … Pastink, A. (2003). The Drosophila melanogaster DNA Ligase IV Gene Plays a Crucial Role in the Repair of Radiation-Induced DNA Double-Strand Breaks and Acts Synergistically With Rad54, *1941*(December), 1929–1941.

Hall, E. J. (2014). Radiation Dose-Rate: A Factor of Importance in Radiobiology and Radiotherapy. *The British Institute of Radiology*, *45*(530).

Hall, E. J., & Brenner, D. J. (1991). The dose-rate effect revisited: Radiobiological considerations of importance in radiotherapy. *International Journal of Radiation Oncology, Biology, Physics*, *21*(6), 1403–1414. https://doi.org/10.1016/0360-3016(91)90314-T

Harshman, L. G., Hoffmann, A. A., & Clark, A. G. (1999). Selection for starvation resistance in Drosophila melanogaster: Physiological correlates, enzyme activities and multiple stress responses. *Journal of Evolutionary Biology*, *12*(2), 370–379. https://doi.org/10.1046/j.1420-9101.1999.00024.x

Hellweg, C. E., & Baumstark-Khan, C. (2007). Getting ready for the manned mission to Mars: The astronauts' risk from space radiation. *Naturwissenschaften*, *94*(7), 517–526. https://doi.org/10.1007/s00114-006-0204-0

Ho, A. Y., Atencio, D. P., Peters, S., Stock, R. G., Formenti, S. C., Cesaretti, J. A., … Rosenstein, B. S. (2006). Genetic Predictors of Adverse Radiotherapy Effects: The Gene-PARE project. *International Journal of Radiation Oncology Biology Physics*, *65*(3), 646–655. https://doi.org/10.1016/j.ijrobp.2006.03.006

Jaklevic, B., Uyetake, L., Lemstra, W., Chang, J., Leary, W., Edwards, A., … Tin, T. S. (2006). Contribution of growth and cell cycle checkpoints to radiation survival in drosophila. *Genetics*, *174*(4), 1963–1972. https://doi.org/10.1534/genetics.106.064477

Johansen, J., Bentzen, S. M., Overgaard, J., & Overgaard, M. (1994). Evidence for a positive correlation between in vitro radiosensitivity of normal human skin fibroblasts and the occurrence of subcutaneous fibrosis after radiotherapy. *International Journal of Radiation Biology*, *66*(4), 407–412. https://doi.org/10.1080/09553009414551361

Jumbo-Lucioni, P., Ayroles, J. F., Chambers, M. M., Jordan, K. W., Leips, J., Mackay, T. F. C., & De Luca, M. (2010). Systems genetics analysis of body weight and energy metabolism traits in Drosophila melanogaster. *BMC Genomics*, *11*(1). https://doi.org/10.1186/1471-2164-11-297

Kassambara, A., Kosinski, M. & Biecek, P. (2017). Package "survminer." *R Package*.

Katzenberger, R. J., Loewen, C. A., Wassarman, D. R., Petersen, A. J., Ganetzky, B., & Wassarman, D. A. (2013). A Drosophila model of closed head traumatic brain injury. *Proceedings of the National Academy of Sciences of the United States of America*, *110*(44). https://doi.org/10.1073/pnas.1316895110

Kaur, P., & Asea, A. (2012). Radiation-induced effects and the immune system in cancer. *Frontiers in Oncology*, *2*, 1–10. https://doi.org/10.3389/fonc.2012.00191

Kennison, J. A., & Ripoll, P. (1981). SPONTANEOUS MITOTIC RECOMBINATION AND EVIDENCE FOR AN X-RAY-INDUCIBLE SYSTEM FOR THE REPAIR OF DNA DAMAGE IN DROSOPHILA MELANOGASTER repair systems for DNA damage in eukaryotes . Drosophila melanogaster presents an excellent system for the genetic and bio. *Genetics*, 91–103.

Kerns, S. L., Kundu, S., Oh, J. H., Singhal, S. K., Janelsins, M., Travis, L. B., … Rosenstein, B. S. (2015). The Prediction of Radiotherapy Toxicity Using Single Nucleotide Polymorphism-Based Models: A Step Toward Prevention. *Seminars in Radiation Oncology*. https://doi.org/10.1016/j.semradonc.2015.05.006

Kim, S.-H., & Lee, W.-J. (2014). Role of DUOX in gut inflammation: lessons from Drosophila model of gut-microbiota interactions. *Frontiers in Cellular and Infection Microbiology*, *3*, 1–12. https://doi.org/10.3389/fcimb.2013.00116

Koval, L., Proshkina, E., Shaposhnikov, M., & Moskalev, A. (2020). The role of DNA repair genes in radiation-induced adaptive response in Drosophila melanogaster is differential and conditional. *Biogerontology*, *21*(1), 45–56. https://doi.org/10.1007/s10522-019-09842-1

Koval, T. M., Myser, W. C., Hart, R. W &, & Hink, W. F. (1978). Comparison of survival and unscheduled DNA synthesis between an insect and a mammalian cell line following X-ray treatments.

Krause, S. A., Overend, G., Dow, J. A. T., & Leader, D. P. (2022). FlyAtlas 2 in 2022: Enhancements to the Drosophila melanogaster expression atlas. *Nucleic Acids Research*, *50*(D1), D1010–D1015. https://doi.org/10.1093/nar/gkab971

Kuzin, B. A., Nikitina, E. A., Cherezov, R. O., Vorontsova, J. E., Slezinger, M. S., Zatsepina, O. G., … Savvateeva-popova, E. V. (2014). Combination of Hypomorphic Mutations of the Drosophila Homologues of Aryl Hydrocarbon Receptor and Nucleosome Assembly Protein Family Genes Disrupts Morphogenesis , Memory and Detoxification, *9*(4). https://doi.org/10.1371/journal.pone.0094975

Kyu-Sun, L., Seung-Hyun, H., Ae-Kyeong, K., Sung-Kyu, J., O-Yu, K., & Yu, K. (2009). Processed short neuropeptide F peptides regulate growth throughthe ERK-insulin pathway in Drosophila melanogaster. *FEBS Letters*, *583*, 2573–

2577.

Lacombe, D., Tejpar, S., Salgado, R., Cardoso, F., Golfinopoulos, V., Aust, D., … Stupp, R. (2014). European perspective for effective cancer drug development. *Nature Reviews Clinical Oncology*, *11*(8), 492–498. https://doi.org/10.1038/nrclinonc.2014.98

Landis, G. N., & Tower, J. (2005). Superoxide dismutase evolution and life span regulation. *Mechanisms of Ageing and Development*, *126*(3), 365–379. https://doi.org/10.1016/j.mad.2004.08.012

Lemaitre, B., Reichhart, J. M., & Hoffmann, J. A. (1997). Drosophila host defense: Differential induction of antimicrobial peptide genes after infection by various classes of microorganisms. *Proceedings of the National Academy of Sciences of the United States of America*, *94*(26), 14614–14619. https://doi.org/10.1073/pnas.94.26.14614

Li, D., Ge, Y., Zhao, Z., Zhu, R., Wang, X., & Bi, X. (2021). Distinct and Coordinated Regulation of Small Non-coding RNAs by E2f1 and p53 During Drosophila Development and in Response to DNA Damage. *Frontiers in Cell and Developmental Biology*, *9*, 1–16. https://doi.org/10.3389/fcell.2021.695311

Li, W., Young, J. F., & Sun, J. (2018). NADPH oxidase-generated reactive oxygen species in mature follicles are essential for Drosophila ovulation. *Proceedings of the National Academy of Sciences of the United States of America*, *115*(30), 776–7770. https://doi.org/10.1073/pnas.1800115115

Liguori, I., Russo, G., Curcio, F., Bulli, G., Aran, L., Della-Morte, D., … Abete, P. (2018). Oxidative stress, aging, and diseases. *Clinical Interventions in Aging*, *13*, 757–772. https://doi.org/10.2147/CIA.S158513

Linford, N. J., Bilgir, C., Ro, J., & Pletcher, S. D. (2013). Measurement of lifespan in Drosophila melanogaster. *Journal of Visualized Experiments*, (71), 1–9. https://doi.org/10.3791/50068

Lushbaugh, C. C., & Casarett, G. W. (1976). The effects of gonadal irradiation in clinical radiation therapy: A review. *Cancer*, *37*(2 S), 1111–1120. https://doi.org/10.1002/1097-0142

MacKay, T. F. C., Richards, S., Stone, E. A., Barbadilla, A., Ayroles, J. F., Zhu, D., … Gibbs, R. A. (2012). The Drosophila melanogaster Genetic Reference Panel. *Nature*, *482*(7384), 173–178. https://doi.org/10.1038/nature10811

Mair, W., Goymer, P., Pletcher, S. D., & Partridge, L. (2003). Demography of dietary restriction and death in Drosophila. *Science*, *301*(5640), 1731–1733. https://doi.org/10.1126/science.1086016

Martin, G. M., Austad, S. N., & Johnson, T. E. (1996). oxidative damage and environmental stresses, *13*, 25–34.

Mettler, F. A., & Voelz, G. L. (2002). Major Radiation Exposure — What to Expect and How to Respond. *New England Journal of Medicine*, *346*(20), 1554–1561. https://doi.org/10.1056/nejmra000365

Moskalev, A., Zhikrivetskaya, S., Krasnov, G., Shaposhnikov, M., Proshkina, E., Borisoglebsky, D., … Kudryavtseva, A. (2015). A comparison of the transcriptome of Drosophila melanogaster in response to entomopathogenic fungus, ionizing radiation, starvation and cold shock. *BMC Genomics*, *16*(13), 1–18. https://doi.org/10.1186/1471-2164-16-S13-S8

Mosse, I. B., & Lyakh, I. P. (1994). Influence of melanin on mutation load in Drosophila populations after long-term irradiation. *Radiation Research*, *139*(3), 357–359. https://doi.org/10.2307/3578834

Muller, H. J. (1930). The frquency of translocations produced by X-rays in Drosophila. *Genetics, 15*, 284–310.

Musk, E. (2017). Making Humans a Multi-Planetary Species. *New Space*, *5*(2), 46–61. https://doi.org/10.1089/space.2017.29009.emu

NASA. (2020). NASA's Lunar Exploration Program Overview. *Nasa*, (September), 74. Retrieved from https://www.nasa.gov/sites/default/files/atoms/files/artemis_plan-20200921.pdf

National Cancer Institute. (2019). Types of Cancer Treatment. Retrieved September 22, 2021, from https://www.cancer.gov/about-cancer/treatment/types

Nichols, C. D., Becnel, J., & Pandey, U. B. (2012). Methods to Assay Drosophila Behavior. *Journal of Visualized Experiments*, (61). https://doi.org/10.3791/3795

Nicolas, G. (1989). Immediate And Latent Effects Of Carbon Dioxide On Insects. *Annual Review of Entomology*, *34*(1), 97–116. https://doi.org/10.1146/annurev.ento.34.1.97

Nikhil, K. L., Ratna, K., & Sharma, V. K. (2016). Life-history traits of Drosophila melanogaster populations exhibiting early and late eclosion chronotypes. *BMC Evolutionary Biology*, *16*(1), 1–14. https://doi.org/10.1186/s12862-016-0622-3

Niraula, P., & Kim, M. S. (2019). N-Acetylcysteine extends lifespan of Drosophila via modulating ROS scavenger gene expression. *Biogerontology*, *20*(4), 533–543. https://doi.org/10.1007/s10522-019-09815-4

Niwa, R., Sakudoh, T., Matsuya, T., Namiki, T., Kasai, S., Tomita, T., & Kataoka, H. (2011). Expressions of the cytochrome P450 monooxygenase gene Cyp4g1 and its homolog in the prothoracic glands of the fruit fly Drosophila melanogaster (Diptera: Drosophilidae) and the silkworm Bombyx mori (Lepidoptera: Bombycidae). *Applied Entomology and Zoology*, *46*(4), 533–543. https://doi.org/10.1007/s13355-011-0074-6

Oppitz, U., Baier, K., Wulf, J., Schakowski, R., & Flentje, M. (2001). The in vitro colony assay: A predictor of clinical outcome. *International Journal of Radiation Biology*, *77*(1), 105–110. https://doi.org/10.1080/095530001453168

Paaby, A. B., & Schmidt, P. S. (2008). Functional significance of allelic variation at methuselah, an aging gene in Drosophila. *PLoS ONE*, *3*(4). https://doi.org/10.1371/journal.pone.0001987

Paithankar, J. G., Deeksha, K., & Patil, R. K. (2017). Gamma radiation tolerance in different life stages of the fruit fly Drosophila melanogaster, *3002*. https://doi.org/10.1080/09553002.2016.1266056

Paithankar, J. G., Ghodke, T. S., & Patil, R. K. (2020). Insight into the evolutionary profile of radio-resistance among insects having intrinsically evolved defence against radiation toxicity. *International Journal of Radiation Biology*, *0*(0), 1–21. https://doi.org/10.1080/09553002.2020.1859153

Paithankar, J. G., Raghu, S. V., & Patil, R. K. (2018). Levels and fluxes in enzymatic antioxidants following gamma irradiation are inadequate to confer radiation resistance in Drosophila melanogaster. *Molecular Biology Reports*, *45*(5), 1175–1186. https://doi.org/10.1007/s11033-018-4270-0

Parashar, V., Frankel, S., Lurie, A. G., & Rogina, B. (2008). The effects of age on radiation resistance and oxidative stress in adult Drosophila melanogaster. *Radiation Research*, *169*(6), 707–711. https://doi.org/10.1667/RR1225.1

Patricia K. Duffner, Michael E.Cohen, P. R. M. T. & S. B. L. (2013). The Long-term effects of cranial irradiation on the central nervous system. *Journal of Chemical Information and Modeling*, *53*(9), 1689–1699.

Proshkina, E., Lashmanova, E., & Dobrovolskaya, E. (2016). Geroprotective and Radioprotective Activity of Quercetin , (-) -Epicatechin , and Ibuprofen in Drosophila melanogaster, *7*, 1–16. https://doi.org/10.3389/fphar.2016.00505

Pusey, A. W. M. (1900). ROENTGEN-RAYS IN THE TREATMENT OF SKIN DISEASES AND FOR THE REMOVAL OF HAIR. *Centennial Paper*, (18), 302–315.

Rabel, D., Charlet, M., Ehret-Sabatier, L., Cavicchioli, L., Cudic, M., Otvos, L., &

Bulet, P. (2004). Primary Structure and in Vitro Antibacterial Properties of the Drosophila melanogaster Attacin C Pro-domain. *Journal of Biological Chemistry*, *279*(15), 14853–14859. https://doi.org/10.1074/jbc.M313608200

Radyuk, S. N., Klichko, V. I., & Orr, W. C. (2004). Profiling Cu,Zn-superoxide dismutase expression in Drosophila melanogaster - A critical regulatory role for intron/exon sequence within the coding domain. *Gene*, *328*(1–2), 37–48. https://doi.org/10.1016/j.gene.2003.12.016

Redon, C., Pilch, D., Rogakou, E., Sedelnikova, O., Newrock, K., & Bonner, W. (2002). Histone H2A variants H2AX and H2AZ. *Current Opinion in Genetics & Development*, *12*, 162–169. https://doi.org/10.1016/j.febslet.2004.12.092

Robbins, M. E. C., & Zhao, W. (2004). Chronic oxidative stress and radiation-induced late normal tissue injury: A review. *International Journal of Radiation Biology*, *80*(4), 251–259. https://doi.org/10.1080/09553000410001692726

Rühm, W., Azizova, T., Bouffler, S., Cullings, H. M., Grosche, B., Little, M. P., … Woloschak, G. E. (2018). Typical doses and dose rates in studies pertinent to radiation risk inference at low doses and low dose rates. *Journal of Radiation Research*, *59*(February), ii1–ii10. https://doi.org/10.1093/jrr/rrx093

Russell, N. S., Grummels, A., Hart, A. A. M., Smolders, I. J. H., Borger, J., Bartelink, H., & Begg, A. C. (1998). Low predictive value of intrinsic fibroblast radiosensitivity for fibrosis development following radiotherapy for breast cancer. *International Journal of Radiation Biology*, *73*(6), 661–670. https://doi.org/10.1080/095530098141915

Shang, W. S., Tang, B. B., Shi, Q. Q., Tian, A. M., Zhou, X. Y., Yao, Z. H., … Wang, M. (2020). Unusual Location of the Geotail Magnetopause Near Lunar Orbit: A Case Study. *Journal of Geophysical Research: Space Physics*, *125*(4). https://doi.org/10.1029/2019JA027401

Sharma, A., Akagi, K., Pattavina, B., Wilson, K. A., Nelson, C., Watson, M., … Kapahi, P. (2020). Musashi expression in intestinal stem cells attenuates radiation-induced decline in intestinal permeability and survival in Drosophila. *Scientific Reports*, *10*(1), 1–16. https://doi.org/10.1038/s41598-020-75867-z

Shchedrina, V. A., Vorbrüggen, G., Lee, B. C., Kim, H. Y., Kabil, H., Harshman, L. G., & Gladyshev, V. N. (2009). Overexpression of methionine-R-sulfoxide reductases has no influence on fruit fly aging. *Mechanisms of Ageing and Development*, *130*(7), 429–443. https://doi.org/10.1016/j.mad.2009.04.003

Shrestha, S., Vanasse, A., Cooper, L. N., & Antosh, M. P. (2017). Gene Expression as a Dosimeter in Irradiated Drosophila melanogaster. *Journal of Computational Biology*, *24*(12), 1265–1274. https://doi.org/10.1089/cmb.2017.0170

Sieber, M. H., & Thummel, C. S. (2012). Coordination of triacylglycerol and cholesterol homeostasis by DHR96 and the drosophila lipa homolog magro. *Cell Metabolism*, *15*(1), 122–127. https://doi.org/10.1016/j.cmet.2011.11.011

Simon, A., Kullberg, B. J., Tripet, B., Boerman, O. C., Zeeuwen, P., Van Der Ven-Jongekrijg, J., … Netea, M. G. (2008). Drosomycin-like defensin, a human homologue of Drosophila melanogaster drosomycin with antifungal activity. *Antimicrobial Agents and Chemotherapy*, *52*(4), 1407–1412. https://doi.org/10.1128/AAC.00155-07

Skorobagatko, D. A., Mazilov, A. A., & Strashnyuk, V. Y. (2018). Endoreduplication in Drosophila melanogaster progeny after exposure to acute γ-irradiation. *BioRxiv*. https://doi.org/10.1101/376145

Ślosarek, K., Konopacka, M., Rogolinski, J., & Sochanik, A. (2014). Effect of dose-rate and irradiation geometry on the biological response of normal cells and cancer cells under radiotherapeutic conditions. *Mutation Research - Genetic Toxicology and Environmental Mutagenesis*, *773*, 14–22. https://doi.org/10.1016/j.mrgentox.2014.07.005

Smith, M., Craig, D., Herrmann, N., Mahoney, E., Krezel, J., McIntyre, N., & Goodliff, K. (2020). The Artemis Program: An Overview of NASA's Activities to Return Humans to the Moon. *IEEE Aerospace Conference Proceedings*, 1–10. https://doi.org/10.1109/AERO47225.2020.9172323

Soares, H. P., Kumar, A., Daniels, S., Swann, S., Cantor, A., Hozo, I., … Djulbegovic, B. (2012). Evaluation of New Treatments in radiation oncology. *JAMA*, *293*(8).

Straub, J. M., New, J., Hamilton, C. D., Lominska, C., Shnayder, Y., & Thomas, S. M. (2015). Radiation-induced fibrosis: mechanisms and implications for therapy. *Journal of Cancer Research and Clinical Oncology*, *141*(11), 1985–1994. https://doi.org/10.1007/s00432-015-1974-6

Strilbytska, O. M., Semaniuk, U. V., Storey, K. B., Yurkevych, I. S., & Lushchak, O. (2020). Insulin Signaling in Intestinal Stem and Progenitor Cells as an Important Determinant of Physiological and Metabolic Traits in Drosophila. *Cells*, *9*(4). https://doi.org/10.3390/cells9040803

Stuschke, M., & Thames, H. D. (1997). Hyperfractionated radiotherapy of human tumors: Overview of the randomized clinical trials. *International Journal of Radiation Oncology Biology Physics*, *37*(2), 259–267. https://doi.org/10.1016/S0360-3016(96)00511-1

Sudmeier, L. J., Howard, S. P., & Ganetzky, B. (2015). A Drosophila model to investigate the neurotoxic side effects of radiation exposure. *Disease Models & Mechanisms*, *8*(7), 669–677. https://doi.org/10.1242/dmm.019786

225

Sudmeier, L. J., Samudrala, S. S., Howard, S. P., & Ganetzky, B. (2015). Persistent activation of the innate immune response in adult Drosophila following radiation exposure during larval development. *G3: Genes, Genomes, Genetics*, *5*(11), 2299–2306. https://doi.org/10.1534/g3.115.021782

Tanaka, K. M., Takahashi, A., Fuse, N., & Takano-Shimizu-Kouno, T. (2014). A novel cell death gene acts to repair patterning defects in Drosophila melanogaster. *Genetics*, *197*(2), 739–742. https://doi.org/10.1534/genetics.114.163337

Tatar, M., Post, S., & Yu, K. (2014). Nutrient control of Drosophila longevity. *Trends in Endocrinology and Metabolism*, *25*(10), 509–517. https://doi.org/10.1016/j.tem.2014.02.006

Taylor, A. M. R., Harnden, D. G., Arlett, C. F., Harcourt, S. A., Lehmann, A. R., Stevens, S., & Bridges, B. A. (1975). Ataxia telangiectasia: a human mutation with abnormal radiation sensitivity. *Nature*, *258*, 427–429.

Trost, M., Blattner, A. C., & Lehner, C. F. (2016). Regulated protein depletion by the auxin-inducible degradation system in Drosophila melanogaster. *Fly*, *10*(1), 35–46. https://doi.org/10.1080/19336934.2016.1168552

Vaisnav, M., Xing, C., Ku, H.-C., Hwang, D., Stojadinovic, S., Pertsemlidis, A., & Abrams, J. M. (2014). Genome-Wide Association Analysis of Radiation Resistance in Drosophila melanogaster. *PLoS ONE*, *9*(8), e104858. https://doi.org/10.1371/journal.pone.0104858

Wang, H. D., Kazemi-Esfarjani, P., & Benzer, S. (2004). Multiple-stress analysis for isolation of Drosophila longevity genes. Proceedings of the National Academy of Sciences, 101(34), 12610-12615.

Wang, X., Fang, H., Huang, Z., Shang, W., Hou, T., Cheng, A., & Cheng, H. (2013). Imaging ROS signaling in cells and animals. *Journal of Molecular Medicine*, *91*(8), 917–927. https://doi.org/10.1007/s00109-013-1067-4

Wang, Y., Liu, L., Pazhanisamy, S. K., Meng, A., & Zhou, D. (2009). Total Body Irradiation Causes Residual Bone Marrow Injury by Induction of Persistent Oxidative Stress in Murine Hematopoietic Stem Cells. *Blood*, *114*(22), 3209–3209. https://doi.org/10.1182/blood.v114.22.3209.3209

Wangler, M. F., Hu, Y., & Shulman, J. M. (2017). *Drosophila* and genome-wide association studies: a review and resource for the functional dissection of human complex traits. *Disease Models & Mechanisms*, *10*(2), 77–88. https://doi.org/10.1242/dmm.027680

Weavers, H., Wood, W., & Martin, P. (2019). Injury Activates a Dynamic

Cytoprotective Network to Confer Stress Resilience and Drive Repair. *Current Biology*, *29*(22), 3851-3862.e4. https://doi.org/10.1016/j.cub.2019.09.035

Wei, J., Wang, B., Wang, H., Meng, L., Zhao, Q., Li, X., … Jiang, X. (2019). Radiation-Induced Normal Tissue Damage: Oxidative Stress and Epigenetic Mechanisms. *Oxidative Medicine and Cellular Longevity*, *2019*. https://doi.org/10.1155/2019/3010342

Wijtten, P. J. A., Meulen, J. Van Der, & Verstegen, M. W. A. (2011). Intestinal barrier function and absorption in pigs after weaning: A review. *British Journal of Nutrition*, *105*(7), 967–981. https://doi.org/10.1017/S0007114510005660

Xu, P., Damschroder, D., Zhang, M., Ryall, K. A., Adler, P. N., Saucerman, J. J., … Yan, Z. (2019). Atg2, Atg9 and Atg18 in mitochondrial integrity, cardiac function and healthspan in Drosophila. *Journal of Molecular and Cellular Cardiology*, *127*, 116–124. https://doi.org/10.1016/j.yjmcc.2018.12.006

Yang, W. Y., Wen, S. Y., Huang, Y. D., Ye, M. Q., Deng, X. J., Han, D., … Cao, Y. (2006). Functional divergence of six isoforms of antifungal peptide Drosomycin in Drosophila melanogaster. *Gene*, *379*(1–2), 26–32. https://doi.org/10.1016/j.gene.2006.03.017

Yushkova, E. (2019). Effects of ionizing radiation at Drosophila melanogaster with differently active hobo transposons. *International Journal of Radiation Biology*, *95*(11), 1564–1572. https://doi.org/10.1080/09553002.2019.1642534

Zaidman-Rémy, A., Poidevin, M., Hervé, M., Welchman, D. P., Paredes, J. C., Fahlander, C., … Lemaitre, B. (2011). Drosophila immunity: Analysis of PGRP-SB1 expression, enzymatic activity and function. *PLoS ONE*, *6*(2). https://doi.org/10.1371/journal.pone.0017231

Zainullin, V. G., Shevchenko, V. A., Mjasnjankina, E. N., Generalova, M. V., & Rakin, A. O. (1992). The mutation frequency of Drosophila melanogaster populations living under conditions of increased background radiation due to the Chernobyl accident. *Science of the Total Environment, The*, *112*(1), 37–44. https://doi.org/10.1016/0048-9697(92)90236-L

Zang, Y., Wan, M., Liu, M., Ke, H., Ma, S., Liu, L. P., … Pastor-Pareja, J. C. (2015). Plasma membrane overgrowth causes fibrotic collagen accumulation and immune activation in Drosophila adipocytes. *ELife*, *4*(JUNE2015), 1–23. https://doi.org/10.7554/eLife.07187

Zhang, S., Wimmer-Schweingruber, R. F., Yu, J., Wang, C., Fu, Q., Zou, Y., … Quan, Z. (2020). First measurements of the radiation dose on the lunar surface. *Science Advances*, *6*(39), 1–6. https://doi.org/10.1126/sciadv.aaz1334

Zugazagoitia, J., Guedes, C., Ponce, S., Ferrer, I., Molina-Pinelo, S., & Paz-Ares, L. (2016). Current Challenges in Cancer Treatment. *Clinical Therapeutics*, *38*(7), 1551–1566. https://doi.org/10.1016/j.clinthera.2016.03.026

Appendix

1   Guide on how to use the MultiFlipper

Components of the MultiFlipper system

MultiFlipper

Rack
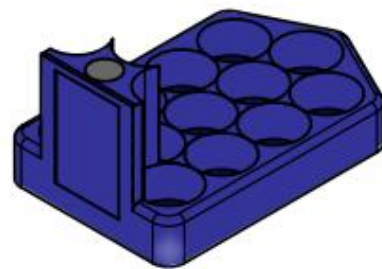
Lid
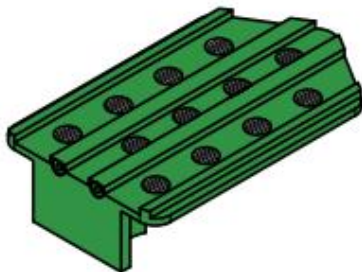
Depositor

Slider
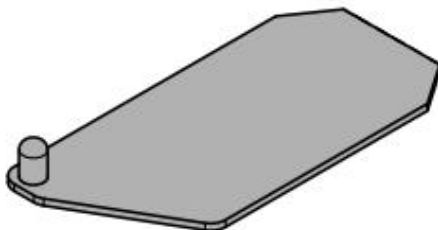
Guide to construction

Depositing *Drosophila* into the rack

Anathetise experimental *Drosophila* ready for pootering into MultiFlipper
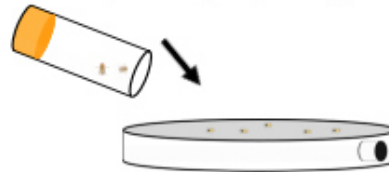
Video demonstration

Tip - Sort into piles ready to be placed into individual vials e.g. 10 per vial

Insert the Depositor into the MultiFlipper

Transfer *Drosophila* into the MultiFlipper

Tip - Ensure Pooter is fully inserted into each valve before transferring *Drosophila*

Insert Rack containing fresh food onto the MultiFlipper
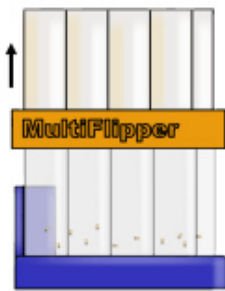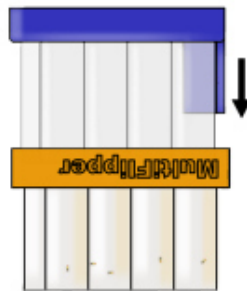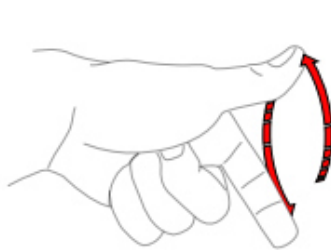
Remove Depositor whilst pressing down on the Rack

Turn over and bang *Drosophila* into Rack

Quickly replace MultiFlipper with Lid

Rack is now ready to be stored, ready for next flip

Page 2

230

Transferring *Drosophila* to fresh media

Quickly replace Lid with MultiFlipper

Video demonstration

Transfer *Drosophila* into MultiFlipper

Insert Slider and remove old Rack

Insert fresh Rack and remove Slider

Transfer *Drosophila* into fresh Rack
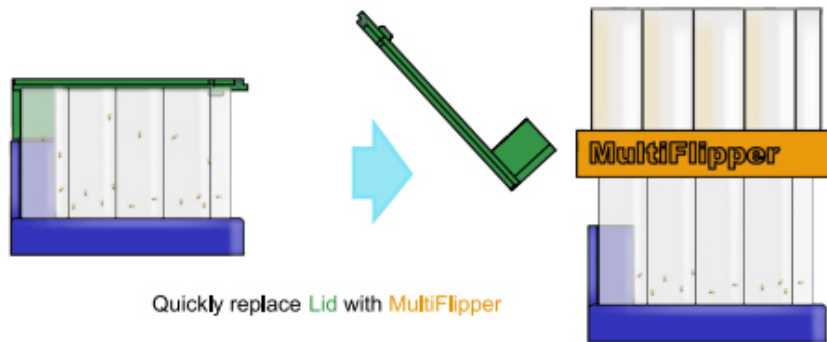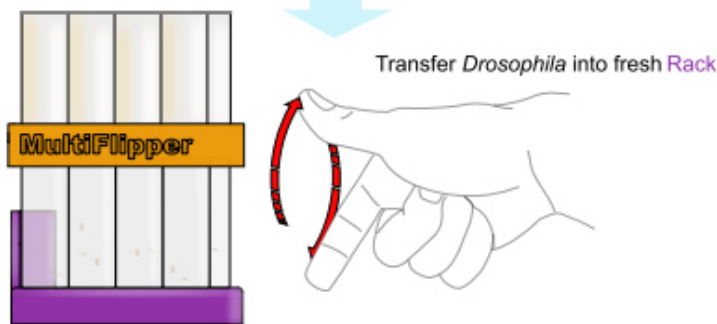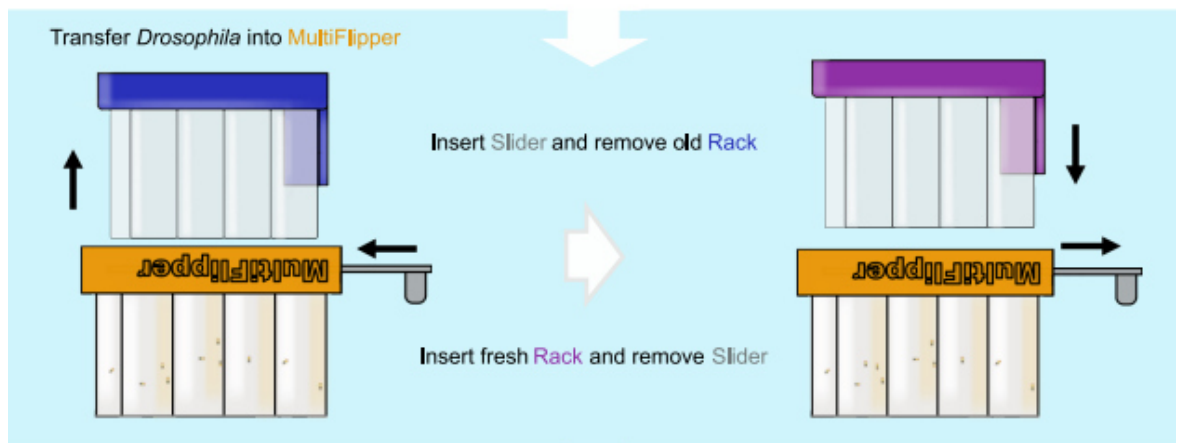
Tip - Make sure to have the Lid at hand

Quickly replace MultiFlipper with Lid

Rack is now ready to be stored, ready for next transfer

231
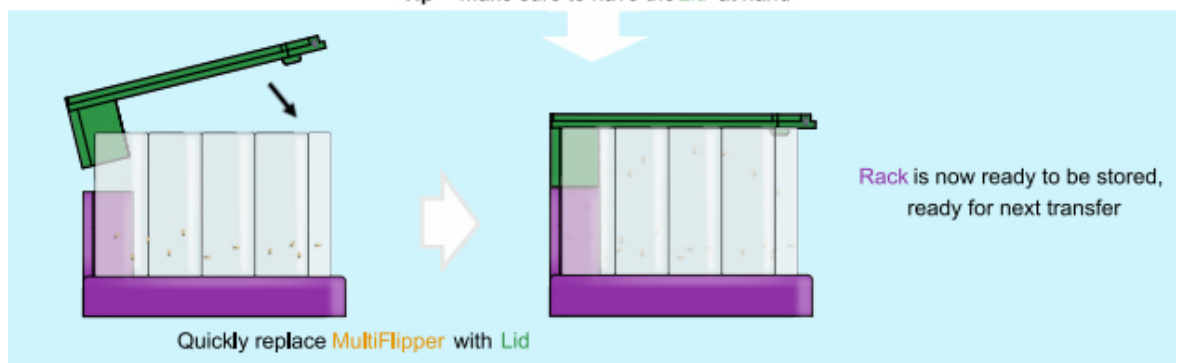
Data logging

Rack containing used food

Turn the Rack to get a bird's-eye view of the food

Colour legend
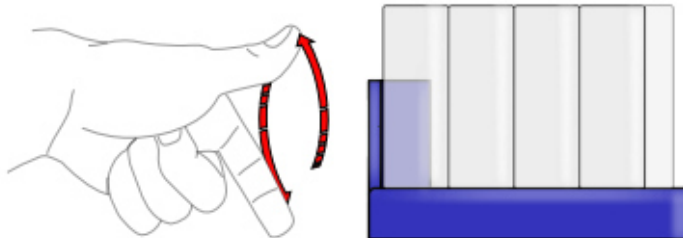
Dead	🔴
Carried over	🔵
Censored	🟢

Colours must correspond to colour legend

Check that *Drosophila* left within vials are dead

Date: *20/03/2020*

Days since last flip

1	2	3	4	5	6	7
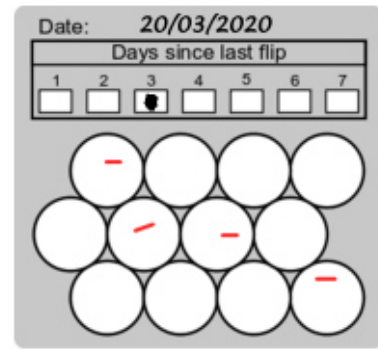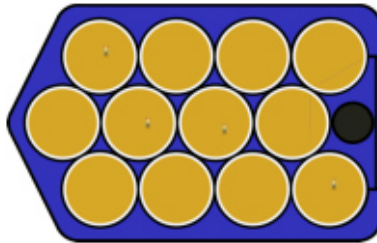
Fill in date and days since last flip as shown above

Drosophila that are alive but stuck it is recommended to censor

Tip - Ensure not to draw over a vial perimeter, or the boxes for days since last flip

Data logging of Anonymised experiments

Code: for sheet number

Genotype:

Treatment:

Start date:

Date:

Days since last flip

Scan data sheet QR code to find number

Scan QR code of racks to find corresponding rack

2   Output of automated lifespan statistical analysis R script

Survival analysis of Drosophila survival data

Created by Trinca & deNavascues (2019)

Generated on 18 December, 2019

About this document

Please use caution when using this documnet, it was created by biologists as oppose to statisitician, and therefore inteprete at your own risk.

This document will use Kaplan-Meier (KM) plots to visualise and Cox Proportional Hazard (CoxPH) modelling to analyse datasets. First it will check for equal distribution of replicates within each cohort and will suggest triming of outlier replicates if needed, it will then generate a CoxPH which will model each replicate, followed by modelling interactions between models. Finally, the assumptions of CoxPH modelling will be tested. Detailed explanations on how to best inteprete statsitical and graphical outputs can be found in section - Results in more detail.

Caution - this documment assumes that the experimental is well versed in suvival data types, e.g. censoring. If this is not the case then a detailed explanation of CoxPH modelling and its implementation in R can be found at sthda_modelling. The two main R packages which this script depends on are Survival (Therneau, T.M, 2019) and Survminers (Kassambara, A, 2019).

Summary of Results

Dataset

```
## # A tibble: 6 x 6
##     Day Event Replicate  Dose Genotype Batch
##   <dbl> <dbl>     <dbl> <dbl> <chr>    <dbl>
## 1    42     1         1   150 w1118        2
## 2    54     1         1   150 w1118        2
## 3    54     1         1   150 w1118        2
## 4    57     1         1   150 w1118        2
## 5    62     1         1   150 w1118        2
## 6    62     1         1   150 w1118        2
```

The dataset contains data for 4 variables. Variables include: Replicate, Dose, Genotype.

Note - Please ensure correct ordering of columns as follows; column 1 = Day, column 2 = Event, column 3 = Replicate, column 4 = Variable 1, column 5 = Variable 2.

Replicates

Data is subsetted to analyse replicates of individual cohorts.

Replicates for: Variable_1 - 150 and Variable_2 - w1118
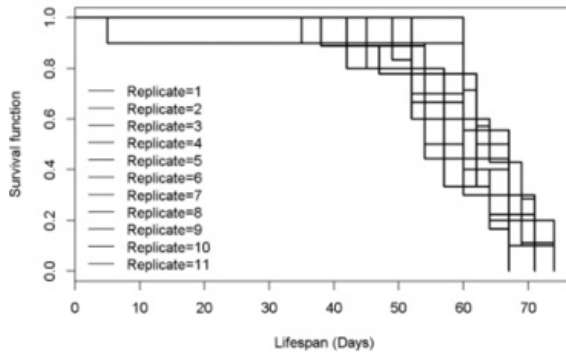
Replicates for: Variable_1 - 0 and Variable_2 - w1118
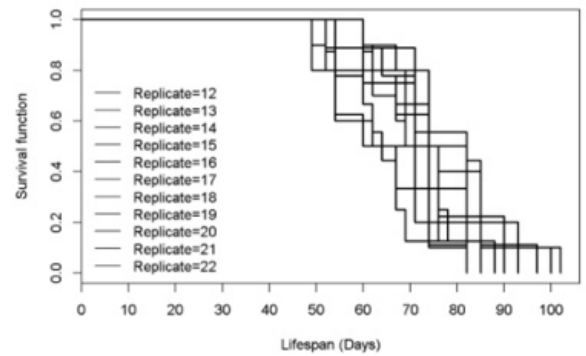
Replicates for: Variable_1 - 150 and Variable_2 - jafrac
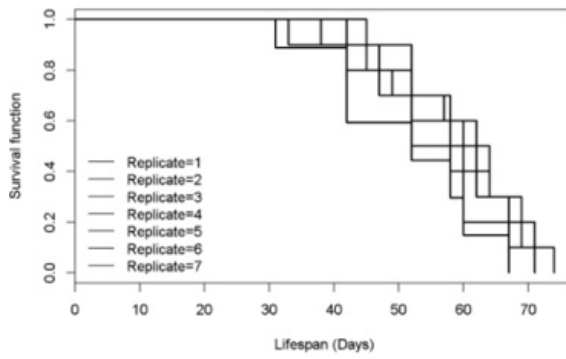
Replicates for: Variable_1 - 0 and Variable_2 - jafrac
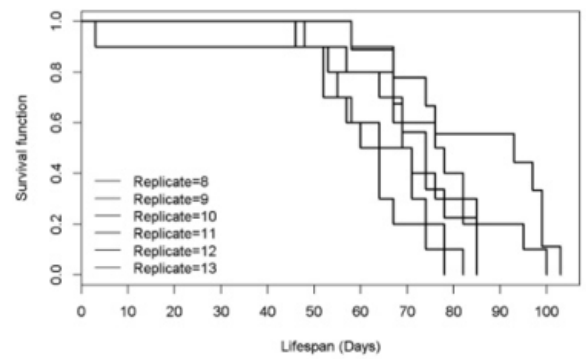
Analysing variables - Dose and Genotype

This contains CoxPH analysis of variables, interactions (significant or not, it will state), and tests for the assumptions of the CoxPH model.

CoxPH model

```
## Call: survfit(formula = mySurv ~ LifespanData$Genotype + LifespanData$Dose)
##
##                                                      n events median 0.95LCL
## LifespanData$Genotype=jafrac, LifespanData$Dose=0    60     58     71      67
## LifespanData$Genotype=jafrac, LifespanData$Dose=150  70     67     60      58
## LifespanData$Genotype=w1118, LifespanData$Dose=0    110    100     71      71
## LifespanData$Genotype=w1118, LifespanData$Dose=150  110    100     62      60
##                                                      0.95UCL
## LifespanData$Genotype=jafrac, LifespanData$Dose=0        76
## LifespanData$Genotype=jafrac, LifespanData$Dose=150      60
## LifespanData$Genotype=w1118, LifespanData$Dose=0         74
## LifespanData$Genotype=w1118, LifespanData$Dose=150       64
```
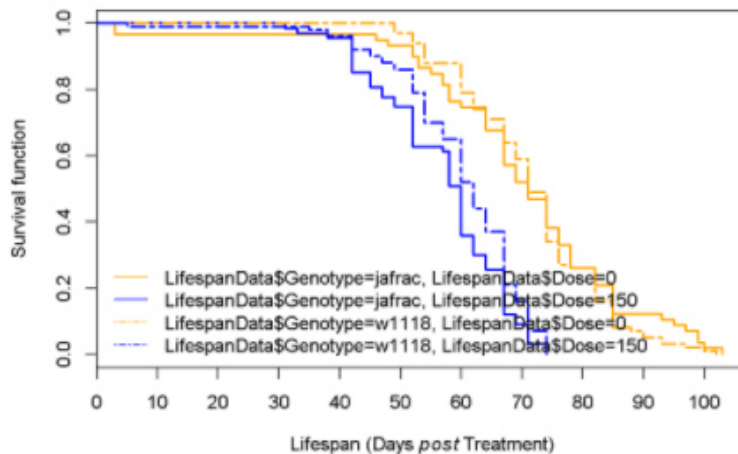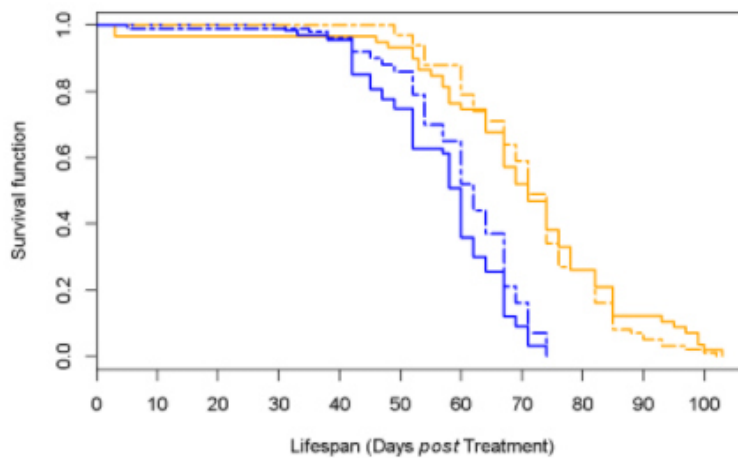


```
## [1] "The variable Dose has a signficant effect on survival, with an estimated HR of 0.0108329545652834 and a p valu
e of 9.5734779239 2207e-16"
```

```
## [1] "The variable Genotype has no signficant effect on survival, with a p value of 0.496013006550319"
```

```
## [1] "The interaction between Dose and Genotype does not have a signficant effect on lifespan, with a p value of 0.0
7019 71557984761"
```

Testing assumptions of Coxph model

Proportional hazards (PH) – scaled Schoenfeld residual plot. For details on how to inteprete the graphical output see next section.

```
##                                                    rho  chisq      p
## LifespanData$Dose                               0.0744  1.974  0.1600
## LifespanData$Genotypew1118                      0.0920  2.789  0.0949
## LifespanData$Dose:LifespanData$Genotypew1118   -0.0379  0.472  0.4920
## GLOBAL                                              NA  4.944  0.1760
```
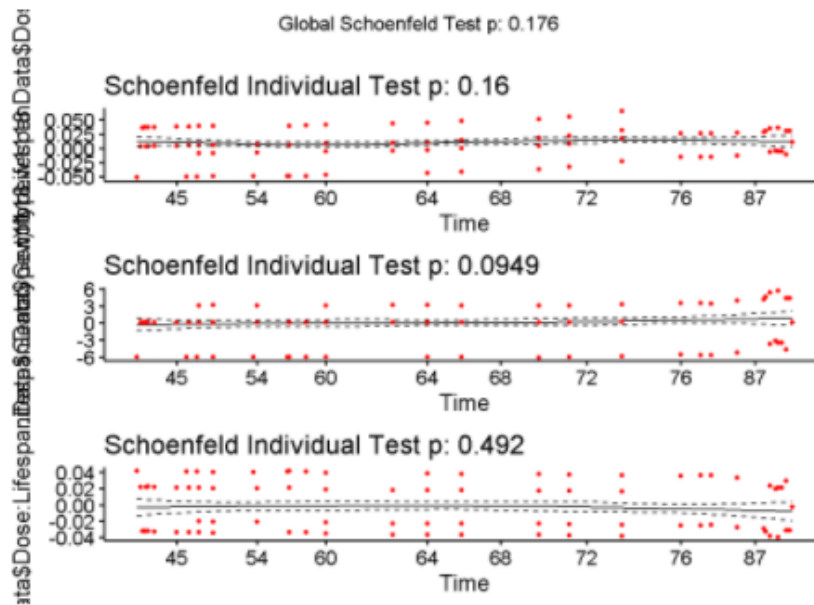


```
## [1] "For variable Dose , PH assumption was met, with a p value of 0.160029930732655"
```

```
## [1] "For variable Genotype , PH assumption was met, with a p value of 0.0949355610735956"
```

```
## [1] "For the interaction between the variables Dose and Genotype , PH assumption was met, with a p value of 0.49196
7671636379"
```

Useful Reading

- Us, github, paper etc

- Clark, T.G., Bradburn, M.J. & Altman, D.G. (2003) Survival Analysis Part I: Basic concepts and first analyses. British Journal of Cancer 89, 232 - 238. https://www.nature.com/articles/6601118

- Bradburn, M.J., Clark, T.G., Love, S.B. & Altman, D.G. (2003) Survival Analysis Part II: Multivariate data analysis - an introduction to concepts and methods. British Journal of Cancer 89, 431 - 436. https://www.nature.com/articles/6601119

- Bradburn, M.J., Clark, T.G., Love, S.B. & Altman, D.G. (2003) Survival Analysis Part III: Multivariate data analysis - choosing a model and assessing its adequacy and fit. British Journal of Cancer 89, 605 - 611. https://www.nature.com/articles/6601120

- Bradburn, M.J., Clark, T.G., Love, S.B. & Altman, D.G. (2003) Survival Analysis Part IV: Further concepts and methods in survival analysis. British Journal of Cancer 89, 781 - 786. https://www.nature.com/articles/6601117

- Therneau, T.M. (2019) R Package 'Survival'. https://cran.r-project.org/web/packages/survival/survival.pdf

- Kassambara, A., Kosinski, M., Biecek, P. & Fabian, S. (2019) https://cran.r-project.org/web/packages/survminer/survminer.pdf

3 Automated GstD1::GFP quantification crowning script

```python
from skimage.io import imread as imread
import os
import platform
from skimage.filters import threshold_otsu
import skimage.measure as skime
import skimage.morphology as skimo
import pandas as pd
import numpy as np
from skimage.morphology import disk
import matplotlib.pyplot as plt
import tifffile
import scipy
from skimage.morphology import watershed
from skimage.feature import peak_local_max
import math


######################################################################
############
def bwareaopen(bw, sz):
    '''BWAREAOPEN takes a b/w image and removes the connected areas
smaller than
    the specified size. The output is a boolean array.


    ================================================================
    ========
    INPUT DATA TYPE CHECKS NEED TO BE IMPLEMENTED

    ================================================================
    ========
    '''
    L = skime.label(bw)
    props = skime.regionprops(L)  # ,
['Area','BoundingBox','Coordinates','Image'])
    bw_open = np.zeros(bw.shape, dtype='int')
    for blob in props:
        if blob['Area'] >= sz:
            s = slice_boundingbox(blob['BoundingBox'])
            # check that the blob is not a background island:
            if np.sum(np.multiply(bw[s], blob['Image'])) > 0:
                # transfer the blob to the new image
                bw_open[blob['Coordinates'][:, 0],
blob['Coordinates'][:, 1]] = 1

    return normalize_img(bw_open, 1, True)



def slice_boundingbox(BoundingBox):
    '''SLICE_BOUNDINGBOX obtains a slice object from the
coordinates of a
    skimage.measure.regionprops Bounding Box'''

    s = np.s_[BoundingBox[0]:BoundingBox[2],
BoundingBox[1]:BoundingBox[3]]

    return s
```

```python
def normalize_img(img, bit_depth, bw=False):
    '''NORMALIZE_IMG takes a numpy array (intended to contain image
data) and
    normalizes the signal values between 0 and (2^bit_depth)-1, with
bit_depth
    taking the values 1, 8 or 16. Depending of the value of
bit_depth and the
    argument bw, the output will be:

    bit_depth  bw          Max value       Data type
    -------------------------------------------------
     1          False           1          float16
     1          True            1          boolean
     8          either        255          uint8
    16          either      65535          uint16'''

    if bit_depth not in [1, 8, 16]:
        raise ValueError('The bit depth must take one of the
values: 1, 8, 16')

    max_value = np.power(2, bit_depth) - 1

    img = img.astype('float64')

    if bit_depth == 1 and not bw:
        output = np.float32(((img - np.min(img)) * max_value) /
(np.max(img) - np.min(img)))
    elif bit_depth == 1 and bw:
        output = np.greater(((img - np.min(img)) * max_value) /
(np.max(img) - np.min(img)), 0)
    elif bit_depth == 8:
        output = np.uint8(((img - np.min(img)) * max_value) /
(np.max(img) - np.min(img)))
    elif bit_depth == 16:
        output = np.uint16(((img - np.min(img)) * max_value) /
(np.max(img) - np.min(img)))
    elif bit_depth == 32:
        output = np.uint32(((img - np.min(img)) * max_value) /
(np.max(img) - np.min(img)))

    return output


####################################################################
################

Operating_System = str(platform.system())
if Operating_System == 'Windows':
    img_folderpath =
"H:/Terrence/Images/Confocal/OxidativeStress/GSTGFP_sensor/All_image
s"
    imshow = plt.imshow
elif Operating_System == 'Darwin':
    pass

img_list = [x for x in os.listdir(img_folderpath) if
x.endswith('.lsm')]
```

238

```python
#####################################################################
################

import time

start = time.time()
col_names = ['Treatment',
             'Nuclei_Area',
             'H2AvD_sum',
             'H2AvDsum_AreaCorrected',
             'GstD1_cytoplasmic_mean',
             'Replicate',
             'Day',
             'Sex']


GstD1_H2AvD_df = pd.DataFrame(columns=col_names)
image = img_list[10]
for image in img_list:
    im = tifffile.imread(os.path.join(img_folderpath, image))
    im_max = np.max(im, axis=1)
    im_maxed = np.max(im_max, axis=0)
    print(image)
    print(im_maxed.shape)
    print(f"It has been: {time.time() - start} secs")


    if len(im_max.shape) == 3 or 4:
        dapi_img = im_maxed[2]
        dapi_img = np.int32(dapi_img)
        nuclei_img = dapi_img > threshold_otsu(dapi_img)
        img_eroded = skimo.binary_erosion(nuclei_img)
        threshold_area_lower = 10
        img_closed_filtered = bwareaopen(img_eroded,
threshold_area_lower)
        distance =
scipy.ndimage.distance_transform_edt(img_closed_filtered)
        local_maxi = peak_local_max(distance, indices=False,
footprint=np.ones((5, 5)), labels=img_closed_filtered)
        markers = scipy.ndimage.label(local_maxi)[0]
        labels = watershed(-distance, markers,
mask=img_closed_filtered)
        regions = skime.regionprops(skime.label(labels))
        for region in regions:
            if (region.filled_area) > 5:
                Sex = image.split('_')[-3][:-1]
                Treatment = image.split('_')[-2][:-2]
                Replicate = image.split('_')[-1][:-4]
                Day = image.split('_')[0][:-3]

                Area = region.filled_area
                new_img = np.zeros(labels.shape)  # blank image
                new_img[region.coords[:, 0], region.coords[:,
1]] = 1   # make mask for a single nucleus
                crowning_radius = math.sqrt(region.filled_area /
3.14159265359)

                # Adaptive crown in the GstD1 channel
                crown = skimo.binary_dilation(new_img,
```

```python
                    disk(crowning_radius))  # grow the nucleus 5-pixel wide (for
instance)
                    crown = crown - new_img  # remove the nucleus
to leave the crown around

                    GstD1_cytoplasmic = im_maxed[0, 1] * crown
                    GstD1_cytoplasmic =
GstD1_cytoplasmic[GstD1_cytoplasmic != 0]
                    GstD1_cytoplasmic_mean =
np.mean(GstD1_cytoplasmic)

                    H2AvD = im_maxed[0] * new_img
                    H2AvD_sum = np.sum(H2AvD)
                    H2AvDsum_AreaCorrected = H2AvD_sum / Area
                    expt_data = [Treatment, Area, H2AvD_sum,
H2AvDsum_AreaCorrected, GstD1_cytoplasmic_mean, Replicate, Day,
                                 Sex]
                    dummyDF = pd.DataFrame([expt_data],
columns=col_names)
                    GstD1_H2AvD_df = GstD1_H2AvD_df.append(dummyDF)

    elif len(im_max.shape) == 5: # redundency in case I had
multiple stacks in a single LSM file
        for stack in range(im_max.shape[0]):
            dapi_img = im_maxed[stack, 1]
            print(dapi_img.shape)
            dapi_img = np.int32(dapi_img)
            nuclei_img = dapi_img > threshold_otsu(dapi_img)
            img_eroded = skimo.binary_erosion(nuclei_img)
            threshold_area_lower = 10
            img_closed_filtered = bwareaopen(img_eroded,
threshold_area_lower)

                # Seperating 'touching' objects - seperating nuclei
using watershed
            distance =
scipy.ndimage.distance_transform_edt(img_closed_filtered)
            local_maxi = peak_local_max(distance, indices=False,
footprint=np.ones((5, 5)), labels=img_closed_filtered)
            markers = scipy.ndimage.label(local_maxi)[0]
            labels = watershed(-distance, markers,
mask=img_closed_filtered)

            regions = skime.regionprops(skime.label(labels))
            for region in regions:
                if (region.filled_area) > 5:
                    Treatment = image.split('_')[3]
                    Replicate = stack
                    Area = region.filled_area
                    new_img = np.zeros(labels.shape)  # blank
image
                    new_img[region.coords[:, 0],
region.coords[:, 1]] = 1  # make mask for a single nucleus

                    crowning_radius =
math.sqrt(region.filled_area / 3.14159265359)
                        # Adaptive crown in the GstD1 channel
                    crown = skimo.binary_dilation(new_img,
```

240

```python
disk(crowning_radius))  # grow the nucleus 5-pixel wide (for
instance)
                    crown = crown - new_img  # remove the
nucleus to leave the crown around
                    GstD1_cytoplasmic = im_maxed[0, 1] * crown
                    GstD1_cytoplasmic_mean =
np.mean(GstD1_cytoplasmic)

                    H2AvD = im_maxed[0] * new_img
                    H2AvD_sum = np.sum(H2AvD)
                    H2AvDsum_AreaCorrected = H2AvD_sum / Area

                    expt_data = [Treatment, Area, H2AvD_sum,
H2AvDsum_AreaCorrected, GstD1_cytoplasmic_mean, Replicate]
                    dummyDF = pd.DataFrame([expt_data],
columns=col_names)
                    GstD1_H2AvD_df =
GstD1_H2AvD_df.append(dummyDF)

end = time.time()
print(end - start)


import xlsxwriter
writer =
pd.ExcelWriter('H:/Terrence/Images/Confocal/OxidativeStress/GSTGFP_s
ensor/All_images/GstD1_H2AvD_df_1day.xlsx',
                        engine='xlsxwriter')
# Convert the dataframe to an XlsxWriter Excel object.
GstD1_H2AvD_df.to_excel(writer, sheet_name='Data')  # index=False
# Close the Pandas Excel writer and output the Excel file.
writer.save()
writer.close()
```

4 Automated nuclei size and 3D positioning script, with diagram (Figure S1).
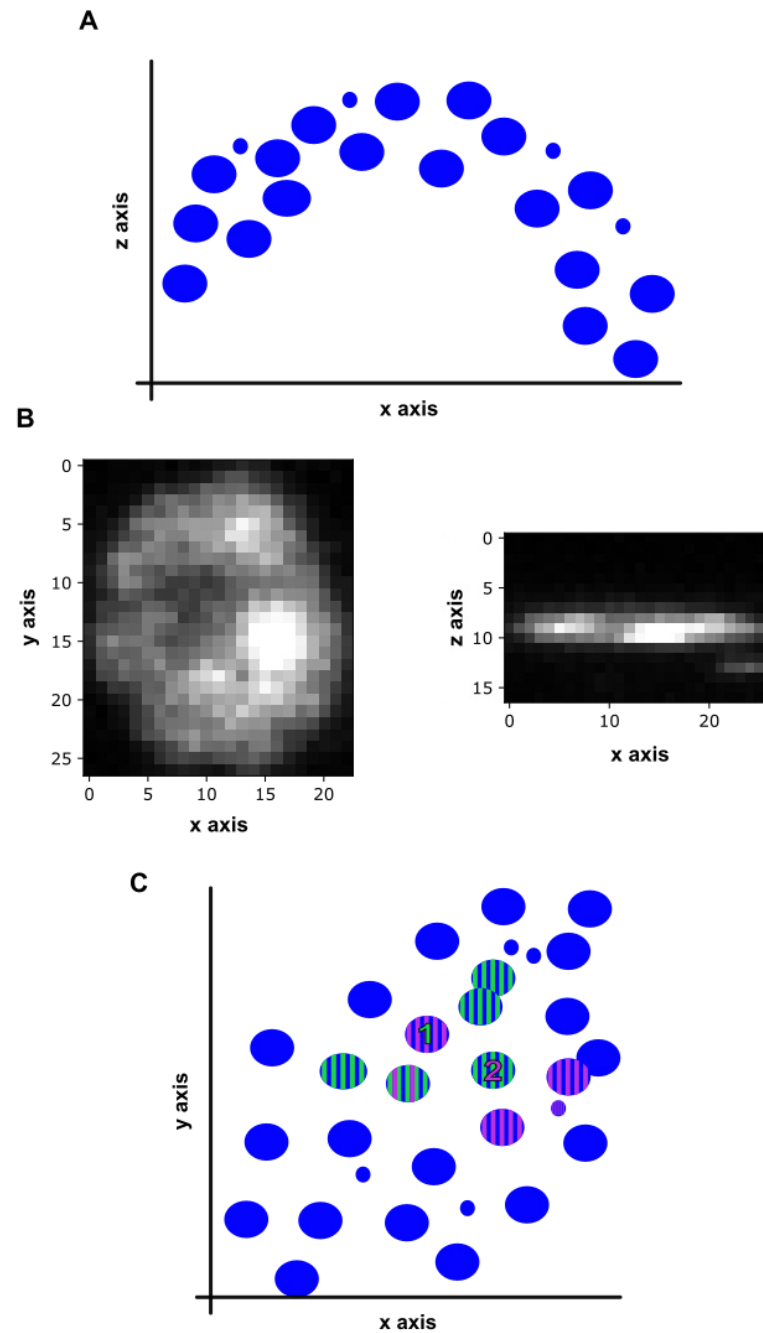
Figure S1: Determining each nucleus's closest neighbours via Euclidean distance (XYZ coordinates). **A** Typical representation of the *Drosophila* midgut stack in 405 channel showing the natural curvature. **B** individual segmented nucleus, in both y,x dimensions and z, x dimensions. **C** representation of the sequential algorithm that measures the 'closeness' of each nuclei to its neighbours, 1 representing the first cell and all nuclei that have green bars are determined to be its closest neighbours, the same for 2 and magenta.

```python
import os
import cv2
import matplotlib.pyplot as plt
from skimage.io import imread
import numpy as np
import pandas as pd
from skimage.filters import threshold_otsu
import scipy
from skimage.measure import label, regionprops
from skimage.feature import peak_local_max
from skimage.segmentation import watershed
import scipy.spatial
import skimage.morphology as skimo


################################################################
####
###                         Functions
###
################################################################
####


def bwareaopen(bw, sz):
    '''BWAREAOPEN takes a b/w image and removes the connected
areas smaller than
    the specified size. The output is a boolean array.



    ================================================================
===========
    INPUT DATA TYPE CHECKS NEED TO BE IMPLEMENTED


    ================================================================
===========
    '''


    L = label(bw)
    props = regionprops(L)   # ,
['Area','BoundingBox','Coordinates','Image'])
    bw_open = np.zeros(bw.shape, dtype='int')
    for blob in props:
        if blob['Area'] >= sz:
            s = slice_boundingbox(blob['BoundingBox'])
            # check that the blob is not a background island:
            if np.sum(np.multiply(bw[s], blob['Image'])) > 0:
                # transfer the blob to the new image
                bw_open[blob['Coordinates'][:, 0],
blob['Coordinates'][:, 1]] = 1


    return normalize_img(bw_open, 1, True)


def slice_boundingbox(BoundingBox):
    '''SLICE_BOUNDINGBOX obtains a slice object from the
coordinates of a
    skimage.measure.regionprops Bounding Box'''


    s = np.s_[BoundingBox[0]:BoundingBox[2],
BoundingBox[1]:BoundingBox[3]]
```

243

```python
    return s

def normalize_img(img, bit_depth, bw=False):
    '''NORMALIZE_IMG takes a numpy array (intended to contain
image data) and
    normalizes the signal values between 0 and (2^bit_depth)-1,
with bit_depth
    taking the values 1, 8 or 16. Depending of the value of
bit_depth and the
    argument bw, the output will be:

    bit_depth  bw            Max value       Data type
    -----------------------------------------------
    1          False                1        float16
    1          True                 1        boolean
    8          either             255        uint8
    16         either           65535        uint16'''

    if bit_depth not in [1, 8, 16]:
        raise ValueError('The bit depth must take one of the
values: 1, 8, 16')

    max_value = np.power(2, bit_depth) - 1

    img = img.astype('float64')

    if bit_depth == 1 and not bw:
        output = np.float32(((img - np.min(img)) * max_value)
/ (np.max(img) - np.min(img)))
    elif bit_depth == 1 and bw:
        output = np.greater(((img - np.min(img)) * max_value)
/ (np.max(img) - np.min(img)), 0)
    elif bit_depth == 8:
        output = np.uint8(((img - np.min(img)) * max_value) /
(np.max(img) - np.min(img)))
    elif bit_depth == 16:
        output = np.uint16(((img - np.min(img)) * max_value)
/ (np.max(img) - np.min(img)))
    elif bit_depth == 32:
        output = np.uint32(((img - np.min(img)) * max_value)
/ (np.max(img) - np.min(img)))

    return output

def otsu_close_fill(greyscale_image):
    '''
    Binarise, close and fill objects
    :param greyscale_image:
    :return img_closed:
    '''
    img_otsu = greyscale_image >
threshold_otsu(greyscale_image)
    img_dilated =
skimo.binary_dilation(skimo.binary_dilation(img_otsu))
```

```python
        img_dilated_filled =
scipy.ndimage.morphology.binary_fill_holes(img_dilated)
        img_closed = skimo.binary_erosion(img_dilated_filled)

        return img_closed


def watershed_nuclei(img_greyscale_cleaned):
        '''
        Watershed touching nuclei which have been already binarised
        :param img_greyscale_cleaned:
        :return:
        '''
        distance =
scipy.ndimage.distance_transform_edt(img_greyscale_cleaned)
        local_maxi = peak_local_max(distance, indices=False,
footprint=np.ones((3, 3)), labels=img_greyscale_cleaned)
        markers = scipy.ndimage.label(local_maxi)[0]
        img_watershed = watershed(-distance, markers,
mask=img_greyscale_cleaned)

        return img_watershed


#######################################################################
####
###                              Script
###
#######################################################################
####


img_folderpath ="H:/Terrence/Images/Confocal/DNA
damage/H2Avd/OregonR/day_20"
img_list = [x for x in os.listdir(img_folderpath) if
x.endswith('.lsm')]

col_names = ['Cell',
             'Tissue_location',
             'Gut',
             'Treatment',
             'Time',
             'X_coords',
             'Y_coords',
             'Z_coords',
             'DAPI_Area_XY',
             'DAPI_Area_YZ',
             'Nucleus_Volume',
             'H2AVD_Intensity',
             'H2AVD_XYAreaCorrected_Sum']
Nuclei_loci_df = pd.DataFrame(columns=col_names)

import time
start = time.time()
i = 1
for image in img_list:
        img = imread(os.path.join(img_folderpath,image),
plugin='tifffile')
```

245

```python
    img = img[0,:,:,:,:]
    img_max = np.max(img, axis = 0)
    img_grey = img_max[1,:,:]
    img_closed = otsu_close_fill(img_grey)


    threshold_area_lower = 40
    img_closed_filtered = bwareaopen(img_closed,
threshold_area_lower)

    img_closed_filtered_watershed =
watershed_nuclei(img_closed_filtered)


    nuclei = regionprops(label(img_closed_filtered_watershed))


    Treatment = image.split('_')[-3]
    Tissue_location = image.split('_')[-1][3:-4]
    Gut = image.split('_')[-2][3:]
    Time = image.split('_')[1][3:]


    for idx in range(0,len(nuclei)):

        y_coords = nuclei[idx].centroid[0]
        y_coords = y_coords/4.8177
        x_coords = nuclei[idx].centroid[1]
        x_coords = x_coords /4.8177


        slice = img[:, :,
nuclei[idx].bbox[0]:nuclei[idx].bbox[2],
nuclei[idx].bbox[1]:nuclei[idx].bbox[3]]


        slice_DAPI = slice[:,1,:,:]
        Nuclei_volume = 0
        for slice_idx in range(slice_DAPI.shape[0]):
            print(np.count_nonzero(slice_DAPI[slice_idx, :,
:]))
            #nuclei_volume += XY_area_micron * 1.97
            XY_area_pixel =
np.count_nonzero(slice_DAPI[slice_idx, :, :])
            XY_area_micron = XY_area_pixel / 4.8177
            Nuclei_volume += XY_area_micron * 1.97


        slice_max = np.max(slice, axis=-1)   # This should be
sum!
        slice_grey = slice_max[:, 1, :]
        slice_grey_otsu = slice_grey >
threshold_otsu(slice_grey)
        slice_regions = regionprops(label(slice_grey_otsu))


        DAPI_Area_XY = nuclei[idx].filled_area
        print(f"Nuclei XY area = {DAPI_Area_XY}, Nuclei volume
= {Nuclei_volume}")


        new_img = np.zeros(img_grey.shape)  # blank image
        new_img[nuclei[idx].coords[:, 0],
nuclei[idx].coords[:,1]] = 1   # make mask for a single nucleus
```

```python
            # Assuming channel is H2aVD
            H2AVD = img_max[0] * new_img
            H2AVD_sum = np.sum(H2AVD)
            H2AVD_XYAreaCorrected_Sum = H2AVD_sum / DAPI_Area_XY

            nucleus_label = []

            areas = [x.area for x in slice_regions]
            areas.sort()
            for ob in slice_regions:
                if ob.area == areas[-1]:
                    nucleus_label.append(ob)
                    DAPI_Area_YZ = ob.filled_area

            z_coords = nucleus_label[0].centroid[0]
            z_coords = z_coords/1.97 # need to automate
            print(f"y = {y_coords}, x = {x_coords}, z =
{z_coords}")
            Time = "day20"
            #append to DF
            cell_data = [idx, Tissue_location, Gut, Treatment,
Time, x_coords, y_coords, z_coords, DAPI_Area_XY,
DAPI_Area_YZ,Nuclei_volume, H2AVD_sum,
H2AVD_XYAreaCorrected_Sum]
            dummyDF = pd.DataFrame([cell_data], columns=col_names)
            Nuclei_loci_df = Nuclei_loci_df.append(dummyDF)

    print(i)
    i += 1


end = time.time()
print(f"took {end - start} seconds to run.")



import xlsxwriter

img_folderpath = "H:/Terrence/Tissue_remodelling/20day"
writer = pd.ExcelWriter(img_folderpath +
'/Nuclei_day20_characteristics.xlsx', engine='xlsxwriter')
# Convert the dataframe to an XlsxWriter Excel object.
Nuclei_loci_df.to_excel(writer, sheet_name= 'Data') #index=False
# Close the Pandas Excel writer and output the Excel file.

writer.save()
writer.close()



################################################################
####
###                    Euclidean distance
###
################################################################
####
```

```python
img_folderpath = "H:/Terrence/Tissue_remodelling/20day"
Nuclei_loci_df = pd.read_excel(img_folderpath +
'/Nuclei_day20_characteristics.xlsx', engine='openpyxl')



import time
start = time.time()

dist_dict = {}
for level in Nuclei_loci_df['Treatment'].unique():
    for gut in Nuclei_loci_df['Gut'].unique():
        for loci in
Nuclei_loci_df['Tissue_location'].unique():
            print(level, gut, loci)
            Nuclei_df_subset =
Nuclei_loci_df[(Nuclei_loci_df.Treatment == level) &

(Nuclei_loci_df.Gut == gut) &

(Nuclei_loci_df.Tissue_location == loci)]
            print(Nuclei_df_subset.head())


            for idx in range(0, len(Nuclei_df_subset)):
                ref_cell = (Nuclei_df_subset.iloc[idx][-3],
Nuclei_df_subset.iloc[idx][-2], Nuclei_df_subset.iloc[idx][-1])
                cell_dist = []
                for idxx in range(0, len(Nuclei_df_subset)):
                    exp_cell = (
                    Nuclei_df_subset.iloc[idxx][-3],
Nuclei_df_subset.iloc[idxx][-2], Nuclei_df_subset.iloc[idxx][-
1])
                    cell_dst =
scipy.spatial.distance.euclidean(ref_cell, exp_cell)
                    cell_dist.append(cell_dst)
                    cell_dist.sort()
                    # cell_dist =
statistics.mean(cell_dist[1:5])
                values =
[cell_dist[1],cell_dist[2],cell_dist[3],cell_dist[4], level,
gut, loci]
                dist_dict[idx] = values
                #print(f"ref = {idx}, other = {dist_dict}")

            x = pd.DataFrame.from_dict(dist_dict,
orient='index',

columns=["neighbour_1", "neighbour_2", "neighbour_3",
"neighbour_4", 'Treatment',

'Gut', 'Tissue_location'])
            col = x.loc[:, "neighbour_1":"neighbour_4"]
            x['neighbour_mean'] = col.mean(axis=1)
```

```python
            import xlsxwriter

            img_folderpath =
"H:/Terrence/Tissue_remodelling/20day/Distance_between_cells"
            writer = pd.ExcelWriter(img_folderpath +
f'/{level}_gut{gut}_loci{loci}.xlsx', engine='xlsxwriter')
            # Convert the dataframe to an XlsxWriter Excel
object.
            x.to_excel(writer, sheet_name='Data')   #
index=False
            # Close the Pandas Excel writer and output the
Excel file.

            writer.save()
            writer.close()


end = time.time()
print(f"took {end - start} seconds to run.")


# add metadata to each file
xlsx_folderpath
="H:/Terrence/Tissue_remodelling/1day/Distance_between_cells"
xlsx_list = [x for x in os.listdir(xlsx_folderpath) if
x.endswith('.xlsx')]


for xlsx in xlsx_list:
    df = pd.read_excel(os.path.join(img_folderpath, xlsx),
engine='openpyxl')
    df['Gut'] = xlsx.split('_')[-2][-1]
    df['Treatment'] = xlsx.split('_')[0]
    df['loci'] = xlsx.split('_')[-1][4]

df.to_excel(f"H:/Terrence/Tissue_remodelling/20day/Distance_betwe
en_cells/modified/{xlsx}")

# Make a master file

xlsx_folderpath
="H:/Terrence/Tissue_remodelling/20day/Distance_between_cells/mod
ified"
xlsx_list = [x for x in os.listdir(xlsx_folderpath) if
x.endswith('.xlsx')]


df_total = pd.DataFrame()
for xlsx in xlsx_list:
    df = pd.read_excel(os.path.join(img_folderpath, xlsx),
engine='openpyxl')
    df_total = df_total.append(df)


df_total.to_excel("H:/Terrence/Tissue_remodelling/20day/Distance_
between_cells/modified/combined_distances_20day.xlsx")
```

```python
#data analysis

img_folderpath =
"H:/Terrence/Tissue_remodelling/20day/Distance_between_cells"
Nuclei_loci_df = pd.read_excel(img_folderpath +
'/modified/combined_distances_20day.xlsx', engine='openpyxl')


Nuclei_loci_df["combined"] =
Nuclei_loci_df["Treatment"].astype(str) +
Nuclei_loci_df["Gut"].astype(str) +
Nuclei_loci_df['Tissue_location'].astype(str)


col_names = ['Treatment',
             'Gut',
             'Tissue_location',
             'neighbour_mean_mean']
Neighbour_df = pd.DataFrame(columns=col_names)


for level in Nuclei_loci_df['combined'].unique():
    Nuclei_df_subset = Nuclei_loci_df[(Nuclei_loci_df.combined
== level)]


    distance_mean = Nuclei_df_subset['neighbour_mean'].mean()
    # append to DF
    neighbour_data = [level[:-2], level[-2], level[-1],
distance_mean]
    dummyDF = pd.DataFrame([neighbour_data], columns=col_names)
    Neighbour_df = Neighbour_df.append(dummyDF)



Neighbour_df.to_excel("H:/Terrence/Tissue_remodelling/20day/Dista
nce_between_cells/Tissue_neighbour_mean.xlsx")



import seaborn as sns



g = sns.catplot(x="Treatment", y="neighbour_mean_mean",
            order=["0Gy", "200Gy"],kind="box",
data=Neighbour_df) # hue="Gut"

#g.set(ylim=(0, 8))





#ANOVA
from scipy.stats import ttest_ind, f_oneway

cat1 = Neighbour_df[Neighbour_df['Treatment']=='Control']
cat2 = Neighbour_df[Neighbour_df['Treatment']=='Biosci']
cat3 = Neighbour_df[Neighbour_df['Treatment']=='Heath']
```

```python
ttest_ind(cat1['neighbour_mean_mean'],
cat2['neighbour_mean_mean'])

f_oneway(cat1['neighbour_mean_mean'],cat2['neighbour_mean_mean'],
cat3['neighbour_mean_mean'])

from statsmodels.stats.multicomp import pairwise_tukeyhsd

tukey =
pairwise_tukeyhsd(endog=Neighbour_df['neighbour_mean_mean'],

groups=Neighbour_df['Treatment'],
                                  alpha=0.05)
print(tukey)




##################################################################
####
###                       Delauney - cell density
###
##################################################################
####

from scipy.spatial import Delaunay

def unique_rows(A):
    unique_idc = A.view(np.dtype((np.void, A.dtype.itemsize *
A.shape[1])))
    _, idx = np.unique(unique_idc, return_index=True)
    A_unique_rows = A[idx]

    return A_unique_rows

def wise_hull_vertices(vertices):
    # vertices is a numpy array
    import math
    import numpy as np
    centroid = np.mean(vertices,axis=0)
    hull_list = vertices.tolist()
    hull_list.sort(key=lambda p: math.atan2(p[1]-
centroid[1],p[0]-centroid[0])) # again it is quite simple!
    return np.array(hull_list)

def polygon_area(x,y):
    area = 0.5 * np.abs( np.dot(x,np.roll(y,1)) -
np.dot(y,np.roll(x,1)) )
    return area




img_folderpath = "H:/Terrence/Tissue_remodelling/20day"
Nuclei_loci_df = pd.read_excel(img_folderpath +
'/Nuclei_day20_characteristics.xlsx', engine='openpyxl')
```

```python
Nuclei_loci_df["combined"] =
Nuclei_loci_df["Treatment"].astype(str) +
Nuclei_loci_df["Gut"].astype(str) +
Nuclei_loci_df['Tissue_location'].astype(str)


col_names = ['Treatment',
             'Gut',
             'Tissue_location',
             'Density (10microns^2)']
Density_df = pd.DataFrame(columns=col_names)


for level in Nuclei_loci_df['combined'].unique():
    Nuclei_df_subset = Nuclei_loci_df[(Nuclei_loci_df.combined
== level)]
    coords_array = Nuclei_df_subset[['X_coords',
'Y_coords']].to_numpy()

    D = Delaunay(coords_array)   # D for Delaunay
    hull_vertices =
coords_array[np.unique(D.convex_hull.flatten()), :]
    hull_vsorted = wise_hull_vertices(hull_vertices)
    hull_area = polygon_area(hull_vsorted[:, 1],
hull_vsorted[:, 0])

    cells = len(coords_array) - len(hull_vsorted) * 0.5
    density = cells / hull_area
    print(f"cell density for treatment: {level[:-2]}, gut:
{level[-2]}, location: {level[-1]} was {density * 100} per
10microns^2")

    # append to DF
    tissue_data = [level[:-2], level[-2], level[-1], density *
100]
    dummyDF = pd.DataFrame([tissue_data], columns=col_names)
    Density_df = Density_df.append(dummyDF)



Density_df.to_excel("H:/Terrence/Tissue_remodelling/20day/Delaune
y_cell_density/Delauney_day10.xlsx")



import seaborn as sns

sns.catplot(x="Treatment", y="Density (10microns^2)",
            order=["0Gy", "200Gy"],kind="box",
data=Density_df) # hue="Gut"



from scipy.stats import ttest_ind, f_oneway

cat1 = Density_df[Density_df['Treatment']=='Control']
cat2 = Density_df[Density_df['Treatment']=='Biosci']
cat3 = Density_df[Density_df['Treatment']=='Heath']
```

```python
ttest_ind(cat1['Density (10microns^2)'], cat2['Density
(10microns^2)'])

#ANOVA
f_oneway(cat1['Density (10microns^2)'],cat2['Density
(10microns^2)'], cat3['Density (10microns^2)'])

from statsmodels.stats.multicomp import pairwise_tukeyhsd

tukey = pairwise_tukeyhsd(endog=Density_df['Density
(10microns^2)'],
                          groups=Density_df['Treatment'],
                          alpha=0.05)
print(tukey)




####################################################################
####
###          Non-zeros counting - Measuring Nuclei volume
###
####################################################################
####


img_folderpath ="Data_tmp"
img_list = [x for x in os.listdir(img_folderpath) if
x.endswith('.lsm')]

for image in img_list:
    img = imread(os.path.join(img_folderpath,image),
plugin='tifffile')
    img = img[0,:,:,:,:]
    img_max = np.max(img, axis = 0)
    img_grey = img_max[1,:,:]
    img_closed = otsu_close_fill(img_grey)


    threshold_area_lower = 40
    img_closed_filtered = bwareaopen(img_closed,
threshold_area_lower)
    img_closed_filtered_watershed =
watershed_nuclei(img_closed_filtered)
    nuclei = regionprops(label(img_closed_filtered_watershed))
    Treatment = image.split('_')[2]
    Tissue_location = image.split('_')[-1][3:-4]
    Gut = image.split('_')[-2][3:]
    Time = image.split('_')[1][3:]


    for idx in range(0,len(nuclei)):

        y_coords = nuclei[idx].centroid[0]
        y_coords = y_coords/4.8177
        x_coords = nuclei[idx].centroid[1]
        x_coords = x_coords /4.8177
```

253

```python
        slice = img[:, :,
nuclei[idx].bbox[0]:nuclei[idx].bbox[2],
nuclei[idx].bbox[1]:nuclei[idx].bbox[3]]
        # this loop will go through slice and count nuclei area
for each slice and convert to microns


        slice_DAPI = slice[:,1,:,:]
        nuclei_volume = 0
        for slice_idx in range(slice_DAPI.shape[0]):
            print(np.count_nonzero(slice_DAPI[slice_idx, :,
:]))
            #nuclei_volume += XY_area_micron * 1.97
            XY_area_pixel =
np.count_nonzero(slice_DAPI[slice_idx, :, :])
            XY_area_micron = XY_area_pixel / 4.8177
            nuclei_volume += XY_area_micron * 1.97
            print(nuclei_volume)



        slice_max = np.max(slice, axis=-1)   # This should be
sum!
        slice_grey = slice_max[:, 1, :]
        slice_grey_otsu = slice_grey >
threshold_otsu(slice_grey)
        slice_regions = regionprops(label(slice_grey_otsu))
```

5 Script for automated nuclei segmentation and watershedding for nuclei H2AvD quantification

```python
import pandas as pd
import numpy as np
from skimage.external.tifffile
import TiffFile
from skimage.morphology
import disk
import scipy
from skimage.morphology
import watershed
from skimage.feature
import peak_local_max
from scipy
import ndimage as ndi
from scipy
import ndimage
import xlsxwriter
import PyQt5
import matplotlib.pyplot as plt
plt.rcParams["figure.figsize"] = [35, 20]# % matplotlib inline
################################################################
################# Functions
################################################################
##################
def bwareaopen(bw, sz):
    ""
"BWAREAOPEN takes a b/w image and removes the connected areas
smaller than
the specified size.The output is a boolean array.
=== === === === === === === === === === === === === === ===
=== ===
=== === === === === === === === =
INPUT DATA TYPE CHECKS NEED TO BE IMPLEMENTED
    === === === === === === === === === === === === === ===
=== ===
    === === === === === === === === === =
    Taken from JQ tricks script ""
"
L = skime.label(bw)
props = skime.regionprops(L)#, ['Area', 'BoundingBox',
'Coordinates',
'Image'
])
bw_open = np.zeros(bw.shape, dtype = "int")
for blob in props:
    if blob["Area"] >= sz:
    s = slice_boundingbox(blob["BoundingBox"])# check that the
blob is not a background island:
    if np.sum(np.multiply(bw[s], blob["Image"])) > 0:
#transfer the blob to the new image
bw_open[blob["Coordinates"][: , 0], blob["Coordinates"][: , 1]]
= 1
return normalize_img(bw_open, 1, True)
def slice_boundingbox(BoundingBox):
    ""
```

```python
    "SLICE_BOUNDINGBOX obtains a slice object from the coordinates of
a
skimage.measure.regionprops Bounding Box ""
"
s = np.s_[BoundingBox[0]: BoundingBox[2], BoundingBox[1]:
BoundingBox[
    3]]
return s
def normalize_img(img, bit_depth, bw = False):
    ""
"NORMALIZE_IMG takes a numpy array (intended to contain image
data) and
normalizes the signal values between 0 and(2 ^ bit_depth) - 1,
with bit_depth
taking the values 1, 8 or 16. Depending of the value of
bit_depth and the
argument bw, the output will be:
    bit_depth bw Max value Data type
    -- -- -- -- -- -- -- -- -- -- -- -- -- -- -- -- -- -- -
- -- -- --
    -- -
    1 False 1 float16
1 True 1 boolean
8 either 255 uint8
16 either 65535 uint16
Taken from JQ tricks script
    ""
"
if bit_depth not in [1, 8, 16]:
    raise ValueError(
        "The bit depth must take one of the values: 1, 8, 16")
max_value = np.power(2, bit_depth) - 1
img = img.astype("float64")
if bit_depth == 1 and not bw:
    output = np.float32(
        ((img - np.min(img)) * max_value) / (np.max(img) -
np.min(img))
    )
elif bit_depth == 1 and bw:
    output = np.greater(
        ((img - np.min(img)) * max_value) / (np.max(img) -
np.min(img)),
        0
    )
elif bit_depth == 8:
    output = np.uint8(
        ((img - np.min(img)) * max_value) / (np.max(img) -
np.min(img))
    )
elif bit_depth == 16:
    output = np.uint16(
        ((img - np.min(img)) * max_value) / (np.max(img) -
np.min(img))
    )
elif bit_depth == 32:
    output = np.uint32(
        ((img - np.min(img)) * max_value) / (np.max(img) -
np.min(img))
```

```python
        )
return output
####################################################################
################## Loading
data################################################################
######################
Operating_System = str(platform.system())
if Operating_System == "Windows":
    img_folderpath = "G:/Terrence/Images/Confocal/DGRP"
imshow = plt.imshow
elif Operating_System == "Darwin":
    img_folderpath = "/Volumes/KESS2/Images"
import time
start = time.time()
col_names = [
    "Genotype",
    "Treatment",
    "Gut_Number",
    "Gut_Position",
    "Replicate",
    "H2AVD_Intensity",
    "DAPI_Area",
    "H2VD_DAPI_AreaCorrected",
]
H2AVD_df = pd.DataFrame(columns = col_names)
img_list = [x
    for x in os.listdir(img_folderpath) if x.endswith(".lsm")
]
image = img_list[2]
for image in img_list:
    im = imread(os.path.join(img_folderpath, image))
im_sum = np.sum(im, axis = 1)# This should be sum!
    im_summed = np.max(im_sum, axis = 0) # redundant channel
print(image)
# Cleaning image - closing objects and removing small objects
dapi_img = im_summed[1]
dapi_img = np.int32(dapi_img)
nuclei_img = dapi_img > threshold_otsu(dapi_img)
img_dilated = skimo.binary_dilation(
    skimo.binary_dilation(skimo.binary_dilation(nuclei_img))
)
img_eroded = skimo.binary_erosion(
    skimo.binary_erosion(skimo.binary_erosion(img_dilated))
)
img_closed =
scipy.ndimage.morphology.binary_fill_holes(img_eroded)
# Seperating 'touching'
objects - seperating nuclei using watershed algorithm
implemented in
    scikits - image package
dapi_img =
scipy.ndimage.morphology.binary_fill_holes(img_closed)
distance = ndi.distance_transform_edt(dapi_img)
local_maxi = peak_local_max(
    distance, indices = False, footprint = np.ones((3, 3)),
    labels = dapi_img
)
markers = ndi.label(local_maxi)[0]
```

```python
labels = watershed(-distance, markers, mask = dapi_img)
# Remove small objects presumed to be debri and non - specific
DAPI aggregates
threshold_area_lower = 10
img_closed_filtered = bwareaopen(img_closed,
threshold_area_lower)
regions = skime.regionprops(skime.label(img_closed_filtered))
for region in regions:
    Genotype = image.split("_")[0]
Treatment = image.split("_")[2]
Gut_Number = image.split("_")[5]
Gut_Position = image.split("_")[6]
Replicate = image.split("_")[5] + image.split("_")[6]
DAPI_Area = region.filled_area
print(DAPI_Area)
new_img = np.zeros(dapi_img.shape)# blank image
new_img[
    region.coords[: , 0], region.coords[: , 1]
] = 1# make mask
for a single nucleus
# Assuming channel is H2aVD
H2AVD = im_summed[0] * new_img
H2AVD_sum = np.sum(H2AVD)
H2AVD_AreaCorrected = H2AVD_sum / DAPI_Area
expt_data = [
    Genotype,
    Treatment,
    Gut_Number,
    Gut_Position,
    Replicate,
    H2AVD_sum,
    DAPI_Area,
    H2AVD_AreaCorrected,
]
dummyDF = pd.DataFrame([expt_data], columns = col_names)
H2AVD_df = H2AVD_df.append(dummyDF)
end = time.time()
print(end - start)
writer = pd.ExcelWriter("H2AVD_df.xlsx", engine =
"xlsxwriter")# Convert the dataframe to an XlsxWriter Excel
object
.
H2AVD_df.to_excel(writer, sheet_name = "Data")# index = False#
Close the Pandas Excel writer and output the Excel file
.
writer.save()
writer.close()
```

6 Script for automated compiling of literature search results

```python
### https://gist.github.com/bonzanini/5a4c39e4c02502a8451d
##https://marcobonzanini.wordpress.com/2015/01/12/searching-
pubmed-with-python/
#https://www.ncbi.nlm.nih.gov/books/NBK3837/#EntrezHelp.Entrez_Se
arching_Options


from Bio import Entrez

def search(query):
    Entrez.email = 'terrence.trinca@gmail.com'
    handle = Entrez.esearch(db='pubmed',
                            sort='relevance',
                            retmax='100',
                            retmode='xml',
                            term=query)
    results = Entrez.read(handle)
    return results


def fetch_details(id_list):
    ids = ','.join(id_list)
    Entrez.email = 'terrence.trinca@gmail.com'
    handle = Entrez.efetch(db='pubmed',
                           retmode='xml',
                           id=ids)
    results = Entrez.read(handle)
    return results



query = "(late OR long-term) AND (radiation OR radiotherapy OR
irradiation OR ionization) AND (response OR toxicity OR effect OR
reaction) AND (human OR Mammalian) NOT rat OR mouse"

if __name__ == '__main__':
    results = search(query)
    id_list = results['IdList']
    papers = fetch_details(id_list)
    for i, paper in enumerate(papers['PubmedArticle']):
        print((i + 1,
paper['MedlineCitation']['Article']['Abstract']))
    # Pretty print the first paper in full
    import json
    print(json.dumps(papers[0], indent=2, separators=(',',
':')))
```

7   UNIX scripts for RNA-seq analysis

Read quality control

```bash
#!/bin/bash
#SBATCH --partition=defq        # the requested queue
#SBATCH --nodes=1               # number of nodes to use
#SBATCH --tasks-per-node=1      # for parallel distributed jobs
#SBATCH --cpus-per-task=4       # for multi-threaded jobs
#SBATCH --mem-per-cpu=4G        # in megabytes, unless unit
explicitly stated
#SBATCH --error=logs/%J.err        # redirect stderr to this
file
#SBATCH --output=logs/%J.out       # redirect stdout to this
file


## Load some Modules
#module load fastqc-0.11.7-gcc-8.3.1-qhnnf6z
module load trimmomatic-0.38-gcc-8.3.1-kgerxgv
module load fastqc
export workingdir=/mnt/data/GROUP-sbipao/c1648025/RNA-
seq_experiments/Terrence_dataset



#list=(
#     A1_1.fq A1_2.fq A2_1.fq A2_2.fq \
#     A3_1.fq A3_2.fq A4_1.fq A4_2.fq \
#     A5_1.fq A5_2.fq A6_1.fq A6_2.fq \
#     A7_1.fq A7_2.fq A8_1.fq A8_2.fq \
#     A9_1.fq A9_2.fq A10_1.fq A10_2.fq \
#     A11_1.fq A11_2.fq A12_1.fq A12_2.fq \
#     A17_1.fq A17_2.fq A18_1.fq A18_2.fq \
#     A19_1.fq A19_2.fq A20_1.fq A20_2.fq \
#     A21_1.fq A21_2.fq A22_1.fq A22_2.fq \
#     A23_1.fq A23_2.fq A24_1.fq A24_2.fq )

list=(A25_1.fq A25_2.fq A26_1.fq A26_2.fq A27_1.fq A27_2.fq
A28_1.fq A28_2.fq )




for i in ${list[@]}
do

fastqc $workingdir/data/${i};



## The commands you want to run

#fastqc $workingdir/data/*.fastq.gz
```

Indexing genome

```bash
#!/bin/bash
#SBATCH --partition=defq        # the requested queue
#SBATCH --nodes=1               # number of nodes to use
#SBATCH --tasks-per-node=1      #
#SBATCH --cpus-per-task=8       #
#SBATCH --mem-per-cpu=8000      # in megabytes, unless unit
explicitly stated
#SBATCH --time=2:0:0
#SBATCH --error=logs/%J.err         # redirect stderr to this
file
#SBATCH --output=logs/%J.out        # redirect stdout to this
file


module load STAR/2.7.6a

export refdir=/mnt/data/GROUP-sbipao/c1648025/RNA-
seq_experiments/Terrence_dataset/genome_index

#STAR     --readFilesCommand zcat \
STAR       --runThreadN ${SLURM_CPUS_PER_TASK} \
      --runMode genomeGenerate \
      --genomeDir   $refdir/ \
      --genomeFastaFiles
$refdir/Drosophila_melanogaster.BDGP6.28.dna_sm.toplevel.fa \
      --sjdbGTFfile
$refdir/Drosophila_melanogaster.BDGP6.28.100.gtf \
      --sjdbOverhang 49
```

Read mapping

```bash
#!/bin/bash
#SBATCH --partition=defq        # the requested queue
#SBATCH --nodes=1               # number of nodes to use
#SBATCH --tasks-per-node=1      # for parallel distributed jobs
#SBATCH --cpus-per-task=8       # for multi-threaded jobs
#SBATCH --mem-per-cpu=4G        # in megabytes, unless unit explicitly
stated
#SBATCH --error=logs/%J.err        # redirect stderr to this file
#SBATCH --output=logs/%J.out       # redirect stdout to this file


## Load some Modules

module load STAR/2.7.6a
export workingdir=/mnt/data/GROUP-sbipao/c1648025/RNA-
seq_experiments/Terrence_dataset/data
export refdir=/mnt/data/GROUP-sbipao/c1648025/RNA-
seq_experiments/Terrence_dataset/genome_index

list=(
    A1 A2 A3 A4 A5 A6 A7 A8 \
    A9 A10 A11 A12 A17 A18 \
    A19 A20 A21 A22 A23 A24 \
    A25 A26 A27 A28 )


## The commands you want to run
#mkdir star

for i in ${list[@]}
do
# map forward and reverse reads to genome
#STAR   --readFilesCommand zcat \            ### If input data is
gzipped
STAR    --outMultimapperOrder Random \
        --outSAMmultNmax 1 \
        --runThreadN ${SLURM_CPUS_PER_TASK}  \
        --runMode alignReads \
        --outSAMtype BAM Unsorted \
        --quantMode GeneCounts \
        --outFileNamePrefix $workingdir/star/${i}-unsort. \
        --genomeDir $refdir \
        --readFilesIn $workingdir/${i}_1.fq $workingdir/${i}_2.fq
done
```

Duplicate read marking

```bash
#!/bin/bash
#SBATCH --partition=defq        # the requested queue
#SBATCH --nodes=1               # number of nodes to use
#SBATCH --tasks-per-node=1      #
#SBATCH --cpus-per-task=4       #
#SBATCH --mem-per-cpu=8G        # in megabytes, unless unit
explicitly stated
#SBATCH --error=logs/%J.err         # redirect stderr to this file
#SBATCH --output=logs/%J.out        # redirect stdout to this file


## Useful shortcuts
export workingdir=/mnt/data/GROUP-sbipao/c1648025/RNA-
seq_experiments/Terrence_dataset
#export refdir=/mnt/data/GROUP-sbipao/c1648025/RNA-
seq_experiments/Terrence_dataset

#module load picard/2.22.2
module load picard-2.20.8-gcc-8.3.1-empup7y
#module load samtools
module load bamtools/v2.5.1



list=(
    A1 A2 A3 A4 A5 A6 A7 A8 \
    A9 A10 A11 A12 A17 A18 \
    A19 A20 A21 A22 A23 A24 \
    A25 A26 A27 A28 )


#mkdir markdup

for i in ${list[@]}
do

#bamtools index  -in $workingdir/star/${i}-unsort.Aligned.out.bam
#bamtools sort -out $workingdir/star/${i}-sorted.bam -in
$workingdir/star/${i}-unsort.Aligned.out.bam

##  MARK DUPLICATES  ##
#picard MarkDuplicates I=$workingdir/star/${i}-sorted.bam
O=$workingdir/markdup/${i}.markdup.bam
M=$workingdir/markdup/${i}.metrics.markdup.txt
REMOVE_DUPLICATES=false VALIDATION_STRINGENCY=SILENT

bamtools stats -in $workingdir/markdup/${i}.markdup.bam >
$workingdir/markdup/${i}.markdup.dupstats.txt


## REMOVE DUPLICATES ##
#picard MarkDuplicates I=$workingdir/star/${i}-sorted.bam
O=$workingdir/markdup/${i}.rmdup.bam
M=$workingdir/markdup/${i}.metrics.rmdup.txt REMOVE_DUPLICATES=true
VALIDATION_STRINGENCY=SILENT

bamtools stats -in $workingdir/markdup/${i}.rmdup.bam >
$workingdir/markdup/${i}.rmdup.dupstats.txt


done
```

263

Read counting per gene

```bash
#!/bin/bash
#SBATCH --partition=defq        # the requested queue
#SBATCH --nodes=1               # number of nodes to use
#SBATCH --tasks-per-node=1      #
#SBATCH --cpus-per-task=8       #
#SBATCH --mem-per-cpu=4G        # in megabytes, unless unit
explicitly stated
#SBATCH --error=logs/%J.err        # redirect stderr to this file
#SBATCH --output=logs/%J.out       # redirect stdout to this file


## Make a list to iterate over
list=(
    A1 A2 A3 A4 A5 A6 A7 A8 \
    A9 A10 A11 A12 A17 A18 \
    A19 A20 A21 A22 A23 A24 \
    A25 A26 A27 A28 )

module load subread-2.0.0-gcc-8.3.1-l7x34bp

## Useful shortcuts
export workingdir=/mnt/data/GROUP-sbipao/c1648025/RNA-
seq_experiments/Terrence_dataset
export refdir=/mnt/data/GROUP-sbipao/c1648025/RNA-
seq_experiments/Terrence_dataset/genome_index



mkdir $workingdir/featureCounts

for i in ${list[@]}
do

cd $workingdir/featureCounts/ && featureCounts \
        -T 8 -p -F GTF -t exon -g gene_id \
        -a $refdir/Drosophila_melanogaster.BDGP6.28.100.gtf \
        -o $workingdir/featureCounts/${i}.markdup.featurecount \
        $workingdir/markdup/${i}.markdup.bam

cd $workingdir/featureCounts/ && featureCounts \
        -T 8 -p -F GTF -t exon -g gene_id \
        -a $refdir/Drosophila_melanogaster.BDGP6.28.100.gtf \
        -o $workingdir/featureCounts/${i}.rmdup.featurecount \
        $workingdir/markdup/${i}.rmdup.bam

done
```

R script for differential expression analysis

```
#####################################################################
############
### R script to compare several conditions with the SARTools and
DESeq2 packages
### Hugo Varet
### November 28th, 2019
### designed to be executed with SARTools 1.7.3
#####################################################################
############
# Only the first time ever to install
install.packages("devtools")
library(devtools)
devtools::install_github("PF2-pasteur-fr/SARTools", build_opts="--
no-resave-data")
library(SARTools)
library(dplyr)


#####################################################################
############
###                     parameters: to be modified by the user
###
#####################################################################
############
rm(list=ls())                                       # remove all
the objects from the R session

workDir <- "C:/path/to/your/working/directory/"      # *** working
directory for the R session

projectName <- "projectName"                         # *** name of
the project
author <- "Your name"                                # *** author of
the statistical analysis/report

targetFile <- "target.txt"                           # *** path to
the design/target file
rawDir <- "raw"                                      # *** path to
the directory containing raw counts files
featuresToRemove <- c("alignment_not_unique",        # names of the
features to be removed
                      "ambiguous", "no_feature",     # (specific
HTSeq-count information and rRNA for example)
                      "not_aligned", "too_low_aQual")# NULL if no
feature to remove

varInt <- "group"                                    # *** factor of
interest
condRef <- "WT"                                      # *** reference
biological condition
batch <- NULL                                        # blocking
factor: NULL (default) or "batch" for example

fitType <- "parametric"                              # mean-variance
relationship: "parametric" (default), "local" or "mean"
cooksCutoff <- TRUE                                  # TRUE/FALSE to
perform the outliers detection (default is TRUE)
independentFiltering <- TRUE                         # TRUE/FALSE to
perform independent filtering (default is TRUE)
```

265

```r
alpha <- 0.05                                            # threshold of
statistical significance
pAdjustMethod <- "BH"                                    # p-value
adjustment method: "BH" (default) or "BY"

typeTrans <- "VST"                                       #
transformation for PCA/clustering: "VST" or "rlog"
locfunc <- "median"                                      # "median"
(default) or "shorth" to estimate the size factors

colors <- c("#f3c300", "#875692", "#f38400",             # vector of
colors of each biological condition on the plots
            "#a1caf1", "#be0032", "#c2b280",
            "#848482", "#008856", "#e68fac",
            "#0067a5", "#f99379", "#604e97")

forceCairoGraph <- FALSE

#IDtoGene <-
read.delim("C:/path/to/your/working/directory/Homo_sapiens.GRCh38.97
.map.txt", header=T)  # *** BESPOKE For using common gene names

################################################################################
############
###                                running script
###
################################################################################
############
setwd(workDir)
library(SARTools)
if (forceCairoGraph) options(bitmapType="cairo")

# checking parameters
checkParameters.DESeq2(projectName=projectName,author=author,targetF
ile=targetFile,

rawDir=rawDir,featuresToRemove=featuresToRemove,varInt=varInt,

condRef=condRef,batch=batch,fitType=fitType,cooksCutoff=cooksCutoff,

independentFiltering=independentFiltering,alpha=alpha,pAdjustMethod=
pAdjustMethod,

typeTrans=typeTrans,locfunc=locfunc,colors=colors)

# loading target file
target <- loadTargetFile(targetFile=targetFile, varInt=varInt,
condRef=condRef, batch=batch)

# loading counts
counts <- loadCountData(target=target, rawDir=rawDir,
featuresToRemove=featuresToRemove)

# description plots
majSequences <- descriptionPlots(counts=counts,
group=target[,varInt], col=colors)

# analysis with DESeq2
out.DESeq2 <- run.DESeq2(counts=counts, target=target,
varInt=varInt, batch=batch,
```

266

```
                                locfunc=locfunc, fitType=fitType,
pAdjustMethod=pAdjustMethod,
                                cooksCutoff=cooksCutoff,
independentFiltering=independentFiltering, alpha=alpha)

# PCA + clustering
exploreCounts(object=out.DESeq2$dds, group=target[,varInt],
typeTrans=typeTrans, col=colors)

# summary of the analysis (boxplots, dispersions, diag size factors,
export table, nDiffTotal, histograms, MA plot)
summaryResults <- summarizeResults.DESeq2(out.DESeq2,
group=target[,varInt], col=colors,

independentFiltering=independentFiltering,
                                          cooksCutoff=cooksCutoff,
alpha=alpha)

# save image of the R session
save.image(file=paste0(projectName, ".RData"))

# generating HTML report
writeReport.DESeq2(target=target, counts=counts,
out.DESeq2=out.DESeq2, summaryResults=summaryResults,
                   majSequences=majSequences, workDir=workDir,
projectName=projectName, author=author,
                   targetFile=targetFile, rawDir=rawDir,
featuresToRemove=featuresToRemove, varInt=varInt,
                   condRef=condRef, batch=batch, fitType=fitType,
cooksCutoff=cooksCutoff,
                   independentFiltering=independentFiltering,
alpha=alpha, pAdjustMethod=pAdjustMethod,
                   typeTrans=typeTrans, locfunc=locfunc,
colors=colors)

# BESPOKE Add coulmmn to tables with gene name and filtering columns
#tables <- list.files(path="tables", pattern="*.txt",
full.names=TRUE, recursive=FALSE)
#lapply(tables, function(x) {
#  t <-read.table(x, header=TRUE)
#  t.cols <- select(t, Id, log2FoldChange, pvalue, padj)
#  t.annot <- merge(t.cols, IDtoGene, by='Id')
#  write.table(t.annot, file=paste(x, ".annot.csv", sep=""),
sep="\t", quote=FALSE, row.names=FALSE, col.names=TRUE)
#})
```